ECO-DWOR:
ECOlogical finishing agents for Durable Water&Oil-Repellent textiles with advanced functionalities

Amado Lacruz Cruz
May 2022
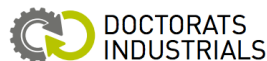
ECO-DWOR: ECOlogical finishing agents for Durable Water & Oil-Repellent textiles with advanced functionalities

Thesis by compendium of publications

Amado Lacruz Cruz

DOCTORATS INDUSTRIALS

Doctoral Thesis by compendium of publications

PhD program: Polymers and Biopolymers

Escuela Técnica Superior de Ingeniería Industrial de Barcelona (ETSEIB)

Departamento de Ingeniería Química

Polímeros Industriales Avanzados y Biopolímeros Tecnológicos (POL)

ECO-DWOR: ECOlogical finishing agents for Durable Water&Oil-Repellent textiles with advanced functionalities.

ECO-DWOR: agentes de acabado ECOlógicos para la obtención de textiles con Repelencia Duradera al Agua y los Aceites y con funcionalidades avanzadas.

Doctoral student: Amado Lacruz Cruz

Thesis director: Dr. Antxon Martínez de Ilarduya

Company supervisor: Josep Aliaga Parera

Filling date: May 2022

This work is dedicated to my parents

Table of contents

Acronyms and symbols

Acronym / Symbol	Description (units)
APTES	Aminopropyltriethoxysilane
CA	Contact angle
CAH	Contact angle hysteresis
D4	Octamethyl cyclotetrasiloxane
D5	Decamethyl cyclopentasiloxane
D6	Dodecamethyl cyclohexasiloxane
DDSC	Dynamic DSC
DLS	Dynamic light scattering
DOE	Design of experiments
DSC	Differential scanning calorimetry
DWOR	Durable water and oil repellency
DWR	Durable water repellency
E	Elastic modulus (MPa)
ε_b	Strain at break (%)
FtOH	Fluorotelomer alcohols
4:2 FTOH	1H,1H,2H,2H-Perfluorohexan-1-ol
6:2 FTOH	1H,1H,2H,2H-Perfluoro-1-octanol
8:2 FTOH	1H,1H,2H,2H-Perfluoro-1-decanol
GPC	Gel permeation chromatography
HDTMS	Hexadecyltrimethoxy silane
HMDSO	Hexamethyl disiloxane
HP	Hydrostatic pressure
LBL	Layer-by-layer
MDM	Octamethyl trisiloxane
MD2M	Decamethyl tetrasiloxane
MD3M	Dodecamethyl pentasiloxane
M_3T	3-[tris(trimethylsilyloxy)silyl]propyl methacrylate
NMR	Nuclear magnetic resonance
NPs	Nanoparticles
OCA	Oil contact angle
OTES	octyltriethoxy silane
O/W	Oil in water
$P_{breakthrough}$	Breakthrough pressure
PET	Poly(ethylen terephthalate)
PFASs	Per- and polyfluoroalkyl substances
PFCs	Per and polyfluorinated chemicals
PFHxA	2,2,3,3,4,4,5,5,6,6,6-undecafluorohexanoic acid Perfluorohexanoic acid
PFOA	2,2,3,3,4,4,5,5,6,6,7,7,8,8,8-pentadecafluorooctanoic acid Perfluorooctanoic acid
PFOS	1,1,2,2,3,3,4,4,5,5,6,6,7,7,8,8,8-Heptadecafluorooctane-1-sulfonic acid Perfluorooctanesulfonic Acid
POSS	Polyhedral oligomeric silsesquioxanes
P_{ref}	Reference pressure
PTFE	Polytetrafluoroethylene
PVDF	Polyvinylidene fluoride
RAFT	Reversible addition-fragmentation chain transfer polymerization
SA	Sliding angle (°)
SEM	Scanning electron microscopy
SMA	Stearyl methacrylate
SWCNT	Single-walled carbon nanotubes
TA	Tilt angle (°)

Acronyms and symbols

TEOS	Tetraethyl orthosilicate
T_g	Glass transition temperature (°C)
TGA	Thermogravimetric analysis
T_gH	T_g of hard segment (°C)
T_gS	T_g of soft segment (°C)
σ_b	Stress at break (MPa)
θ	Young's contact angle or equilibrium contact angle between a liquid and a smooth solid surface (°)
θ_w	Apparent contact angle according to Wenzel state (°)
θ_{CB}	Apparent contact angle according to Cassie-Baxter state (°)
θ_{adv}	Advancing contact angle (°)
θ_{rec}	Receding contact angle (°)
ϒ	Surface tension (mN m^{-1})
VOCs	Volatile organic compounds
WCA	Water contact angle (°)
WPU	Waterborne polyurethane
WPUD	Waterborne polyurethane-urea dispersion
WSA	Water shedding angle (°)
WSA	Water sliding angle (°)
WOR	Water and Oil Repellent

Abstract

Fluorinated chemicals, commonly known as per- and polyfluoroalkyl substances (PFASs), are widely used to obtain water-, oil- and stain-repellent textiles. The constant development and optimization of fluorochemicals for textile applications initiated more than five decades ago has resulted in a very efficient DWOR-technology and textiles with exceptional hydro- and oleo-phobic properties (DWOR acronym stands for Durable Water and Oil Repellent). However, PFASs' high mobility, persistence and harmful health effects, has been proved by numerous scientific studies and, therefore, regulation and phase-out of several PFASs is being implemented by governments. At the present time the textile industry lacks suitable alternatives to fluorochemicals with comparable material characteristics.

The Thesis' main goal is to design fluorine-free textile finishing agents based on sustainable polymers with low surface-tension functional groups in combination with (nano)materials to confer water- and oil-repellency to textiles as well as advanced multifunctionalities. Therefore, synergies of new available bio-based building-blocks, polymer synthesis and (nano)materials have been explored to develop new finishing agents able to provide water and oil repellence to fabrics, without using fluorine-containing chemicals.

Resumen

Los productos químicos fluorados, comúnmente conocidos como sustancias per- y polifluoroalquiladas (PFASs), se utilizan ampliamente para obtener textiles que repelen el agua, el aceite y las manchas. El constante desarrollo y optimización de los fluoroquímicos para aplicaciones textiles iniciado hace más de cinco décadas ha dado como resultado una tecnología DWOR (Durable Water and Oil Repellent) muy eficiente y textiles con propiedades hidrofóbicas y oleofóbicas excepcionales. Sin embargo, la alta movilidad, la persistencia y los efectos nocivos para la salud de las PFASs han sido corroborados por numerosos estudios científicos y, por lo tanto, los gobiernos están implementando la regulación y eliminación de varias PFAS. En la actualidad, la industria textil carece de alternativas adecuadas a los fluoroquímicos con características y prestaciones comparables.

El objetivo principal de la Tesis es diseñar agentes de acabado textil sin flúor, basados en polímeros sostenibles con grupos funcionales de baja tensión superficial en combinación con (nano)materiales, para conferir repelencia al agua y al aceite a los textiles, así como multifuncionalidades avanzadas. Por consiguiente, se han explorado las sinergias de nuevos monómeros bio-basados, la síntesis de polímeros y los (nano)materiales para desarrollar nuevos agentes de acabado capaces de proporcionar repelencia al agua y al aceite a los tejidos, sin utilizar productos químicos que contengan flúor.

Company profile

Color Center, S.A. (CC), is the company where most of this work has been carried out in

collaboration with the UPC. The company was founded in 1978, its core business focuses on the manufacture and marketing of chemical products for the textile industry. The company faces the new challenges by applying proactive strategies based on open innovation with customers, suppliers, partners, research centers and universities. Our staff treasures high technical skills with insight in market needs and new technologies. The company is committed with sustainability, social responsibility, quality and technical support to our customers. Therefore, all these values are part of the mission and vision of CC. The company has modern facilities in Terrassa, in the province of Barcelona. These facilities house one of the cornerstones of the company, its modern R&D laboratories, where they carry out activities such as: synthesis, chemical characterization, application and quality control of the product.

Throughout its history, Color Center has participated and carried out different R&D projects that have received funding from national and European entities (ACCIÓ - Catalonia-, CDTI -Spain-, H2020 -Europe-). CC has been accredited since 2016 with the INNOVATIVE SME seal of the Ministry of Economy and Competitiveness.

Motivation and objectives of the Thesis

Per- and polyfluoroalkyl substances are widely used to obtain water-, oil- and stain-repellent surfaces. PFASs are ubiquitously present in numerous daily life products like technical textiles, upholstery, medical devices, electronics, etc. As a consequence of this, PFASs are found in air, water, living organisms and soil at locations across the globe. The constant development and optimization of fluorochemicals for textile applications initiated more than five decades ago has resulted in a very efficient DWOR-technology and textiles with exceptional hydro- and oleo-phobic properties. However, numerous scientific studies show that exposure to PFASs may be linked to harmful health effects in humans and animals. This has led to the restriction or phase-out of an ever-increasing number of PFASs. At the present time, the textile industry lacks suitable alternatives to fluorochemicals with comparable performance. The motivations and objectives of the Thesis are summarized below.

Motivation of the Thesis:

- Due to PFASs widespread use, high mobility and persistence in the environment, many PFASs are found in water, land, and in the blood of people and animals all over the world.

- Fluorinated chemical finishing agents, which make it possible to obtain water and oil repellent fabrics, have adverse effects on human health and the environment. As a consequence, increasingly stringent ecotoxicological regulations are being implemented to reduce or phase-out several PFASs.

- Regulation of individual fluorinated substances is leading to a replacement with similar molecules not yet regulated but of similar concern; e.g., replacement of few fluorine atoms by hydrogens and/or chlorine, branching, etc. Thus, a huge ecosystem of new fluorinated organic substances of unknown toxicity is currently arising. The amount, identity, formation pathways, and degradation dynamics of these substitutive PFASs is largely unknown.

- The growing awareness of consumers and authorities about the harmful chemicals present in textiles is generating a significant trend towards the use of more sustainable materials in textile production.

- All actors involved in the textile supply chain have a responsibility to meet the growing interest in health and sustainability, providing consumers with ECO-designed and more sustainable products.

- Fluorine-free solutions, still a minority on the market, provide a lower technical performance than finishing agents based on fluorine chemistry.

Objectives of the Thesis:

The purpose of the Thesis is to obtain environmentally-friendly, fluorine-free, high-performance DWOR finishing agents, based on polymers with low surface-tension functional groups obtained from renewable sources and (nano)materials. The new developments are conceived to be applied to textiles in order to impart water, oil and dirt repellency. The specific objectives of the Thesis are summarized below.

- Development of new ECO-designed and fluorine-free finishing agents for textiles, based on partially biobased polymers with low surface tension functional groups and (nano)materials.

- Development of sustainable finishing systems to obtain durable water and oil repellent textiles (DWOR), with advanced functionalities, for application in the technical textiles sector.

- Design and optimization of the prototypes so that they can be applied using the standard machinery commonly used in the textile sector (padding, knife-coating), thus avoiding costly investments in new facilities that would represent an entry barrier for the new solutions.

1   Introduction

1.1   Theory of hydrophobic and oleophobic surfaces

1.1.1   Basic theoretical models

Liquid-repellent surfaces are present both in nature and in our daily lives, we also find them in many essential technical applications for modern life. In nature we find countless examples of water-repellent surfaces such as the feathers of many birds, the skin or fur of different animals and insects [1], etc. Also the leaves, stems and petals of a large number of plant species have an amazing ability to repel water, among them one of the most studied is the lotus leaf [2], which will be discussed in more detail later.

The wettability of a solid surface by polar and nonpolar liquids is one of the fundamental features that determines its properties, functionality and performance [3]. There are numerous reviews focused on the theoretical foundations of superhydrophobicity [4–6], in this work we will describe some basic theoretical models. One of the most used methodologies to quantify the wettability of a solid surface is the measurement of the contact angle θ of a drop of the liquid under study when it comes into contact with the surface that we want to characterize. This allows us to determine the surface free energy, also called surface tension at the solid-liquid-vapor interface (Figure 1).
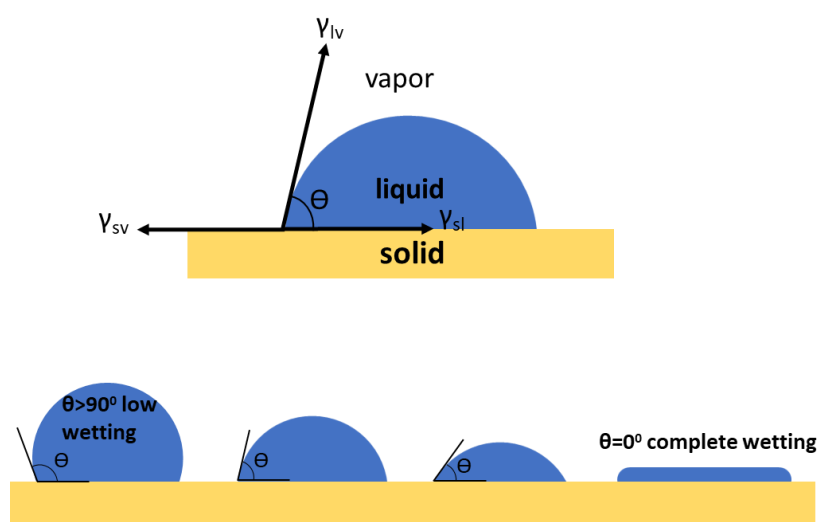
Figure 1. Top: Schematics of Young's model. Down: relationship between wettability and contact angle.

The relationship between the contact angle θ and the surface tensions of the interfaces of the solid, the liquid and the vapor phase was expressed for the first time through the Young relation [7] (Equation 1).

$$\gamma_{sv} = \gamma_{sl} + \gamma_{lv}cos\theta$$

Equation 1. Young's relation.

where γ_{sv}, γ_{sl}, γ_{lv} are the surface tensions between the interphases solid-vapor, solid-liquid and liquid-vapor, respectively.

Based on the above equation, a surface with a contact angle ≥150° is defined as superhydrophobic or superoleophobic, depending on whether the liquid is water or oil, respectively. Contact angles >90° denote low wettability and θ<90° indicates that the surface tends to be wetted by the liquid. However, Young's model makes a very important simplification, considering the surface of the solid as an "ideal" surface, completely flat and homogeneous, devoid of any roughness. Therefore, Equation 1 does not allow to predict the apparent contact angle in the case of rough surfaces. We know that the micro- and nano-roughness of a surface have a great impact on its wettability against any liquid, whether polar or nonpolar [8]. After Young's model, two models emerged that allowed us to explain wettability on rough surfaces: the Wenzel and Cassie-Baxter models, represented in Figure 2.
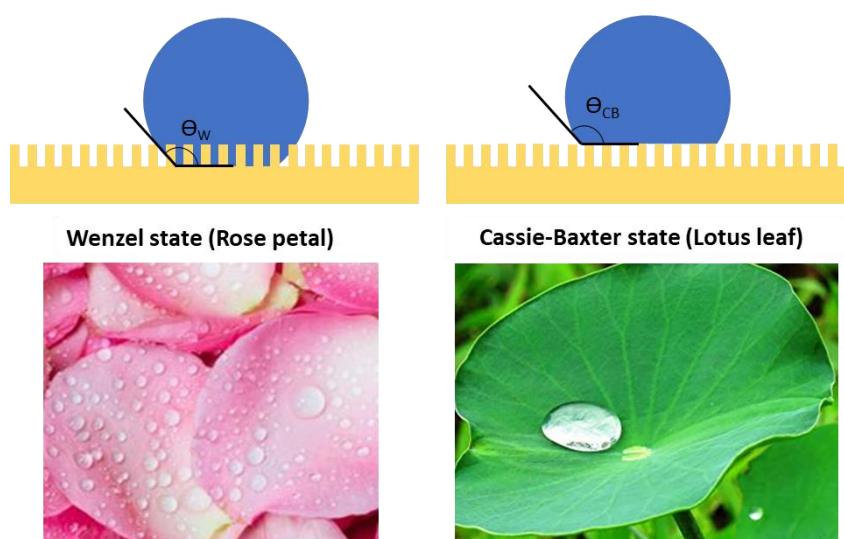
Figure 2. Top: schematics of Wenzel and Cassie-Baxter states. Down: examples of natural surfaces showing wettability under Wenzel and Cassie-Baxter state.

Wenzel [9,10] modified Young's equation by introducing the roughness factor of the surface under study (Equation 2) where θ_w is the Wenzel apparent contact angle and r is the roughness factor that is calculated as the ratio between the solid-liquid contact area and the projected area.

$$r(\gamma_{sv} - \gamma_{sl}) = \gamma_{lv} \cos \theta_w$$

Equation 2. Wenzel's model.

The Wenzel's equation is usually expressed as Equation 3 where θ is the contact angle formed between the liquid-air and the solid-liquid interfaces at equilibrium (Young's contact angle).

$$\cos \theta_w = r \cos \theta$$

Equation 3.

Equation 3 for a solid/water/air system indicates that, in the Wenzel state (i.e., a solid surface with all the gaps created by roughness filled with water) a hydrophobic surface will become more hydrophobic with increasing roughness, and a hydrophilic surface will become more hydrophilic with increasing roughness. As shown in Figure 2, the Wenzel's model assumes that the liquid drop completely occupies the "pockets" or gaps caused by the roughness and therefore remains anchored to the surface, not being able to slide when said surface is tilted. When the drops of water come into contact with the petals of the rose flower, they do not wet the surface but they do remain anchored, making it difficult for them to slide. The water repellency behavior of the rose petal is a good example of the Wenzel's state. However, the lotus leaf, in addition to having excellent water repellency, allows water drops to slide easily across its surface. Cassie's and Cassie-Baxter's models [11] were created after Wenzel's to explain this type of behavior. Cassie's relation describes the apparent contact angle adopted on a surface composed of multiple surface chemistries (Equation 4).

$$\text{(a) } \cos \theta_C = \Sigma f_i \, cos\theta_i; \; \Sigma_i^n f_i = 1 \quad \text{(b) } \cos \theta_C = f_1 \, cos\theta_1 + f_2 cos\theta_2$$

Equation 4. (a) Cassie's model and (b) Cassie's model for two surface chemistries.

In Equation 4 (a), θ_C is the apparent contact angle in the Cassie's model, and θ_i and f_i are the Young's contact angle and area fraction for surface chemistry i, respectively. The

Cassie-Baxter's model focuses on porous surfaces, where liquid does not penetrate the grooves on the rough surface and leaves air gaps. If the vapor phase is air and the liquid is water, then since the contact angle between water and air is approximately 180°, we can substitute θ_2=180° in Equation 4 (b) to obtain the Equation 5. In Figure 2 on the right we can see a schematic of Cassie-Baxter's state where the drop of liquid does not penetrate the pockets, which are filled with the vapor phase.

$$\cos \theta_{CB} = f_1 \, cos\theta_1 - (1 - f_1)$$

Equation 5. Cassie-Baxter's model for a system formed by water-solid-air.

Unlike the Wenzel's model, in the Cassie-Baxter's model the liquid droplets have a high mobility that allow them to slide across the surface.

For a solid smooth surface (r = 1) covered with hydrophobic functional groups polydimethyl siloxane (PDMS), -CH$_3$, -CF$_2$, -CF$_3$, respectively, the equilibrium (Young) contact angles with water are well above 100° in all the cases (105° = $\theta^w_{PDMS} < \theta^w_{-CH3} < \theta^w_{-CF2} < \theta^w_{-CF3}$ = 120°) [12]. When the roughness is gradually increased for all these hydrophobic surfaces, the apparent WCA in the Wenzel state progressively increases to values up to 180° [12] (Figure 3). Conversely, Wenzel's apparent WCA on a hydrophilic solid surface (i.e., glass or cotton which are materials with plenty of hydrophilic -OH groups on the surface) decreases as the surface roughness increases. Therefore, for water (γ_{lv}=72 mN m^{-1}), we are able to manufacture solid surfaces with a wide range of apparent contact angles and this is possible because, for a solid/water/air system, both hydrophilic (θ < 90°) and hydrophobic (θ > 90°) surface chemistries are available. According to [12] the equilibrium (Young) contact angles with hexadecane (θ^{HD}) and decane (θ^D) are below 80° for smooth solids with low surface energy (35° = $\theta^{HD}_{PDMS} < \theta^{HD}_{-CH3} < \theta^{HD}_{-CF2} < \theta^{HD}_{-CF3}$ = 78° and 13° = $\theta^D_{PDMS} < \theta^D_{-CH3} < \theta^D_{-CF2} < \theta^D_{-CF3}$ = 70°). Therefore, for liquids with low surface tension, such as decane or hexadecane (γ_{lv} = 23,83 mN m^{-1} and 27,47 mN m^{-1}, respectively [13]), hydrophobic surface chemistries (θ > 90°) do not exist and subsequent introduction of roughness will only decrease Wenzel's apparent contact angle (Figure 3). According to the data discussed above, it seems clear that the only way to achieve oleophobicity in front of low surface tension

liquids is to fabricate rough surfaces whose air gaps remain unwetted by the liquid droplets (Cassie-Baxter state).
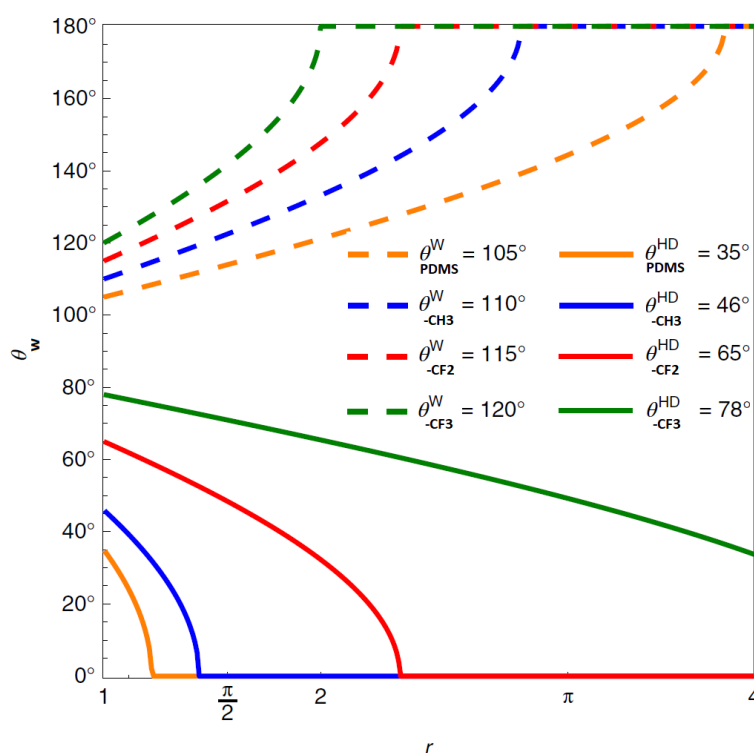
Figure 3. Apparent Wenzel contact angle (Θ_w) with water (dashed lines) and hexadecane (solid lines) in terms of the Wenzel roughness (r) for four different chemistries (PDMS, -CH₃, -CF₂, -CF₃). The legend shows the equilibrium contact angles with water (Θ^w) and hexadecane (Θ^HD). Reproduced with permission of Springer Nature [12].

In practice, for low surface-tension liquids it is common to observe irreversible transition from the metastable Cassie-Baxter state to the Wenzel state (Figure 4) due to changes in pressure, evaporation, among others [14]. The likeliness of this transition is also very dependent on the diameter, heigh, shape and spacing of the air pockets on the surface [15].
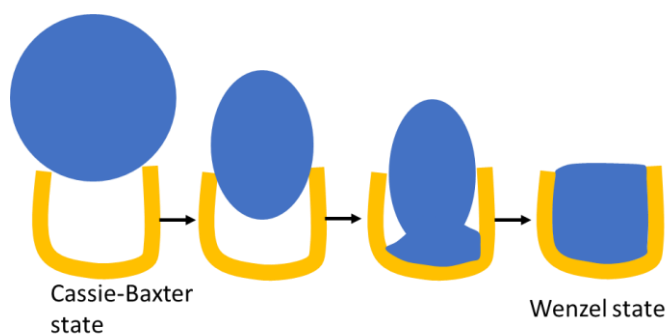
Figure 4. Simplified scheme of the transition between the Cassie–Baxter and Wenzel state.

1.1.2 Dynamic wettability, CAH, self-cleaning

What happens when we place a drop of liquid on a surface and then tilt the surface so that the drop is on top? In most cases, reaching a certain angle of inclination that we call sliding angle (SA) or roll-off angle, the drop will begin to descend (see Figure 5).
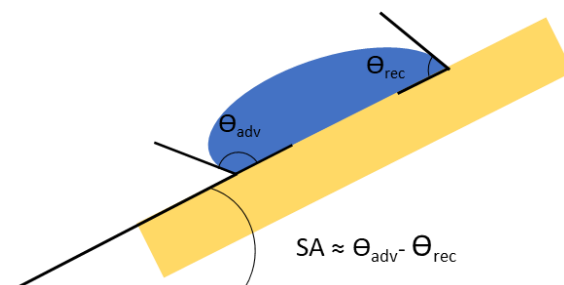
Figure 5. Representation of the contact angle hysteresis (known as sliding angle -SA- or roll-off angle).

At this point we must complete the definition of superhydrophobic surface that we have given at the beginning of this chapter: superhydrophobicity = $\theta \geq 150^o$ and SA<10°. Superolephobicity is defined exactly the same way, i.e., contact angles with oil of $\theta \geq 150^o$ and SA<10°. SA is related to contact angle hysteresis (CAH). CHA is essentially the displacement of a line of contact, either by expansion or retraction of the droplet. This phenomenon occurs because in a non-ideal solid there are different thermodynamically stable contact angles: the advancing contact angle is the highest stable angle, while the receding contact angle is the smallest possible stable angle. These states are known as metastable thermodynamic states [16]. CHA arises from chemical and topographical heterogeneity of the surface, or swelling, rearrangement, or alteration of the surface by a liquid. The value of CAH is determined experimentally through the measurement of the advancing contact angle (θ_{adv}) and receding contact angle (θ_{rec}), specifically CAH = θ_{adv}- θ_{rec}. Experimental measurement of θ_{adv} is done by gradually increasing the volume of the liquid droplet at a controlled speed until the solid-liquid-vapor contact line begins to expand, θ_{rec} is measured inversely (see Figure 6). The contact angle hysteresis is closely related to the adhesion forces between the surface and the liquid.
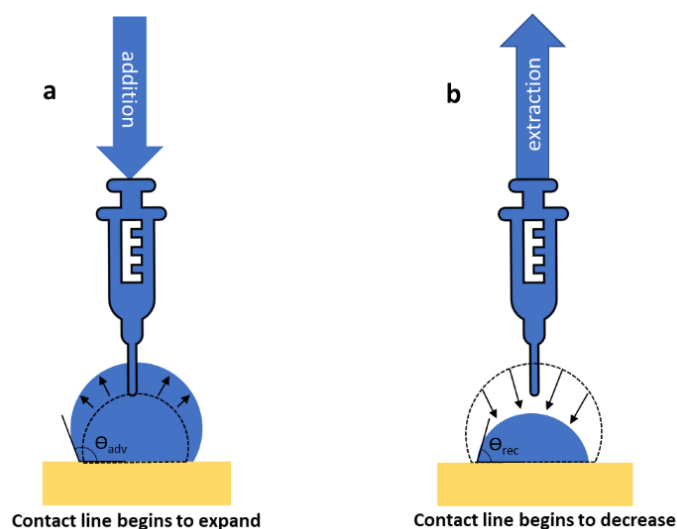
Figure 6. Experimental measurement of advancing contact angle (a) and receding contact angle (b).

The CAH concept gives rise to comment on another very important topic within DWOR finishes in the textile sector, the "self-cleaning effect" (see Figure 7). The lotus leaf (Nelumbo nucifera) is one of the most obvious natural examples of superhydrophobicity and self-cleaning effect. With contact angles with water of approximately 162° and very low CAH, the lotus leaf causes water droplets to roll almost freely on its surface (see Figure 7 (a)), without losing its spherical shape, being the surface tensions between leaf-water, leaf-dirt and water-dirt very low. Numerous studies of the surface of the lotus leaf have ended up confirming that all these properties have their origin in the positive synergy between a highly hydrophobic surface composed of vegetable waxes and a micro-nano surface roughness [17,18]. On the other hand, on most smooth surfaces, such as window and car glass, water droplets slide off and leave dirt particles behind, which remain on the surface (see Figure 7 (b)).
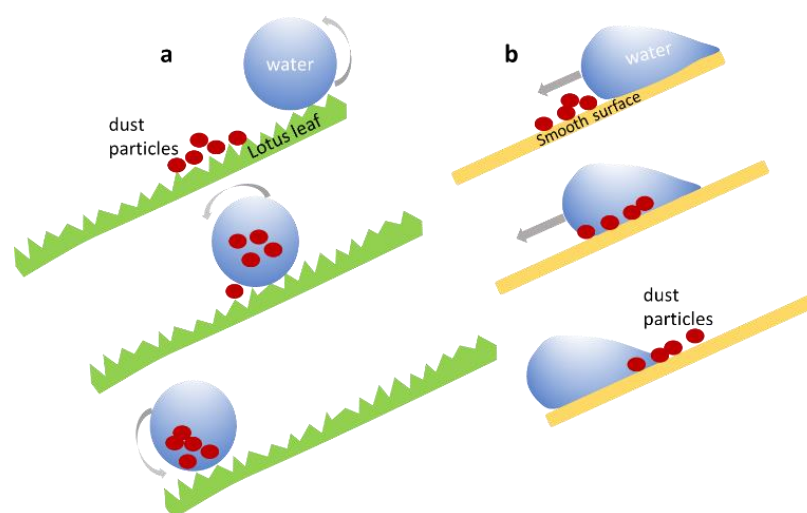
Figure 7. Schematic representation of a drop of water sliding on the lotus leaf -self-cleaning effect- (a) and on a smooth surface (b).

1.1.3   The specific case of textile surfaces

Having reviewed the basic models, we will focus in this section on the study of hydro- and oil-repellency in textile substrates. Most textiles are made from materials that have remarkable wettability (cotton, silk, polyester, nylon...) and therefore have a high tendency to absorb liquids. Textiles modified with DWOR treatments are highly valued in today's markets as they form part of advanced applications: medical textiles, protection workwear, technical garments for extreme outdoor sports, textiles for public buildings, automotive and aeronautics fabrics, membranes for water/oil separation, etc. Wenzel [10] carried out studies that pointed out that a textile can become hydrophobic by simply coating it with a hydrophobic chemical product, without the need to texturize its surface, since in most textiles said texturization already exists (surface roughness) due to the intrinsic structure and construction of the fabric itself (Figure 8). This statement, however, is not applicable when we talk about oleophobicity. If we consider hexadecane, we see that this liquid is capable of wetting most textiles instantly, and contact angles cannot be experimentally evaluated. In order to study the wettability of textile surfaces, Tuteja [19–23] and his collaborators have developed specific models that include two new dimensionless parameters: D* (spacing ratio) and A* (robustness factor), especially designed for liquids with low surface tension. D* is a function of the pore size and the distribution of pores in the fabric, it gives us an idea of the air that is trapped under a drop of liquid that remains on the fabric.
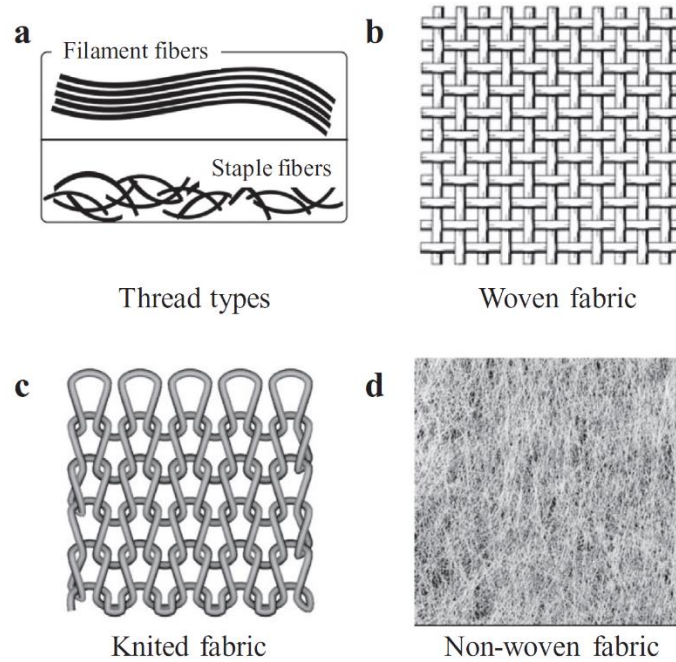
Figure 8. (a) types of textile filaments (short fiber, long fiber), (b) woven fabric with warp and weft, (c) knitted, (d) non-woven (short fibers bonded each other with resin or by mechanical or thermal procedures). Source: Zahid et al. [24].

In the case of a woven fabric (see Figure 8 (b)), and making the simplification that this fabric is made up of continuous cylindrical fibers of the same diameter (Figure 9 (a)), D* is defined as D*$_{fiber}$= (R$_{fiber}$+D$_{fiber}$)/ R$_{fiber}$ where R$_{fiber}$ is de fiber's radius and 2 D$_{fiber}$ is the gap between fibers (Figure 9 (a)). Large values of D*$_{fiber}$ indicate fabrics with high intrinsic porosity. In this case, the Cassie-Baxter equation is modified according to Equation 6 [19,20], where θ is Young's contact angle and θ*$_{fiber}$ is the observed contact angle on the fibers. It is worth to mention that, for woven fabrics, there are industrial limitations regarding the porosity that can be achieved, so that the typical values of D*$_{fiber}$ are comprised between 4 and 9 for most textiles [12]. Regarding hexadecane repellence, Figure 10 (a) shows that θ*$_{fiber}$ is clearly below 150° and reach 0° for D*$_{fiber}$ ≈ 1 for non-fluorinated chemistries, while fluorinated chemistries show 30° < θ*$_{fiber}$ ≤ 150° even for D*$_{fiber}$ = 1, thus confirming the excellent oil-repellent properties of fluorochemical-based finishes.

$$cos\theta^*_{fiber} = -1 + \frac{1}{D^*_{fiber}}[sin\theta + (\pi - \theta)cos\theta]$$

Equation 6.

If we consider a model based on a flat surface where nanospheres are deposited on the top, then D* would be defined as $D^*_{particle} = [(R_{particle}+D_{particle})/ R_{particle}]^2$, where $R_{particle}$ is the nanospheres radius and 2 $D_{particle}$ is the spacing between nanospheres. In this situation, the modified Cassie-Baxter equation adopts the expression of Equation 7, where $\theta^*_{particle}$ is the observed contact angle on a smooth surface decorated with spherical particles. Design diagram of Equation 7 is shown in Figure 10 (b).

$$cos\theta^*_{particle} = -1 + \frac{1}{D^*_{particle}}\left[\frac{\pi}{2\sqrt{3}} + (1 + cos\theta)\right]^2$$

Equation 7.

When the two situations that we have just described occur simultaneously, that is, a fabric composed of cylindrical fibers that are in turn decorated with spherical nanoparticles (see Figure 9 (b)), then the Cassie-Baxter expression is given by Equation 8 [19,23]. In Equation 8, $\theta^*_{hierarchical}$ is the observed contact angle on the fibers decorated with particles. Unlike bare fibers, there is no industrial limitation on the porosity of fabrics made of particle-decorated fibers.

$$cos\theta^*_{hierarchical} = -1 + \frac{1}{D^*_{fiber}}\left[sin\theta^*_{particle} + \left(\pi - \theta^*_{particle}\right) cos\theta^*_{particle}\right]$$

Equation 8.
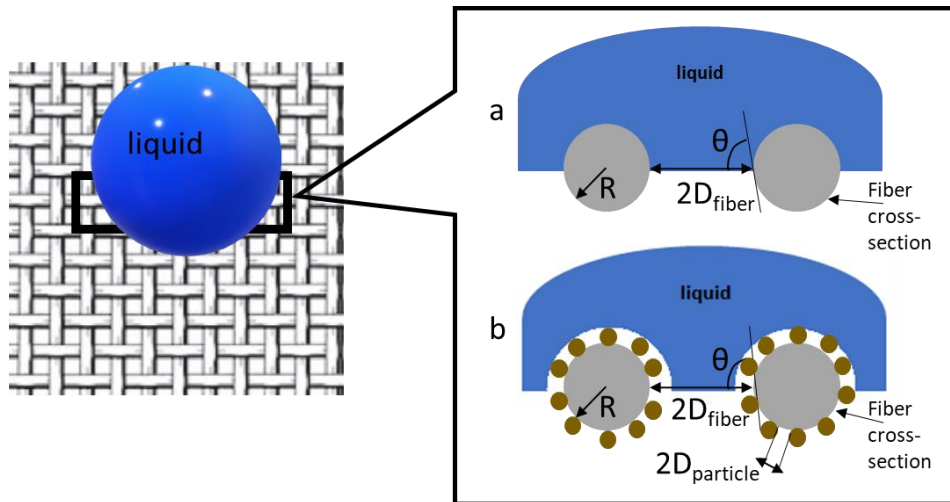
Figure 9. Scheme of a drop of liquid on the surface of a porous fabric, in Cassie-Baxter state (a) with the intrinsic structure of the fabric and (b) with additional nano/micro-roughness conferred by decorating particles. Θ is the equilibrium contact angle.

Figure 10 (c) shows that, independently of surface chemistry, for $1 \leq D^*_{fiber} < \pi/2$ there is a minimum required value of $\theta^*_{particle}$ to achieve $\theta^*_{hierarchical} > 0$. For instance, $\theta^*_{particle}$ should be $\geq 56°$ for $D^*_{fiber} = 1$ to have $\theta^*_{hierarchical} > 0°$. On the other hand, for a fiber with porosity $D^*_{fiber} \geq \pi$, then $\theta^*_{hierarchical}$ will be $\geq 90°$ regardless the value of $\theta^*_{particle}$.

Another key parameter is A* [20–22], the robustness factor, which is determined by the breakthrough pressure ($P_{breakthrough}$) or pressure from which the liquid would fill the pores of the fabric allowing transition from a Cassie-Baxter state to a Wenzel state. Thus, we define the robustness factor as $A^* = P_{breakthrough} / P_{ref}$, where P_{ref} is defined as the Laplace pressure of a droplet whose radius is equal to the capillarity length of the liquid and it can be understood as the pressure that the liquid droplets would exert on the fabric in the absence of external forces. P_{ref} is a function of the liquid surface tension, its density, and capillarity constant, according to Equation 9. Membranes or fabrics with A*>>1 will not be permeable to the liquid while membranes with A*<1 will be permeated by the liquid.

$$P_{ref} = 2 \frac{\gamma_{lv}}{l_{cap}} \quad \{l_{cap} = (\gamma_{lv}/\rho g)^{1/2}\}$$

Equation 9. γ_{lv} is the liquid surface tension, l_{cap} is the capillary length of the liquid, ρ is the liquid density and g the gravity acceleration.
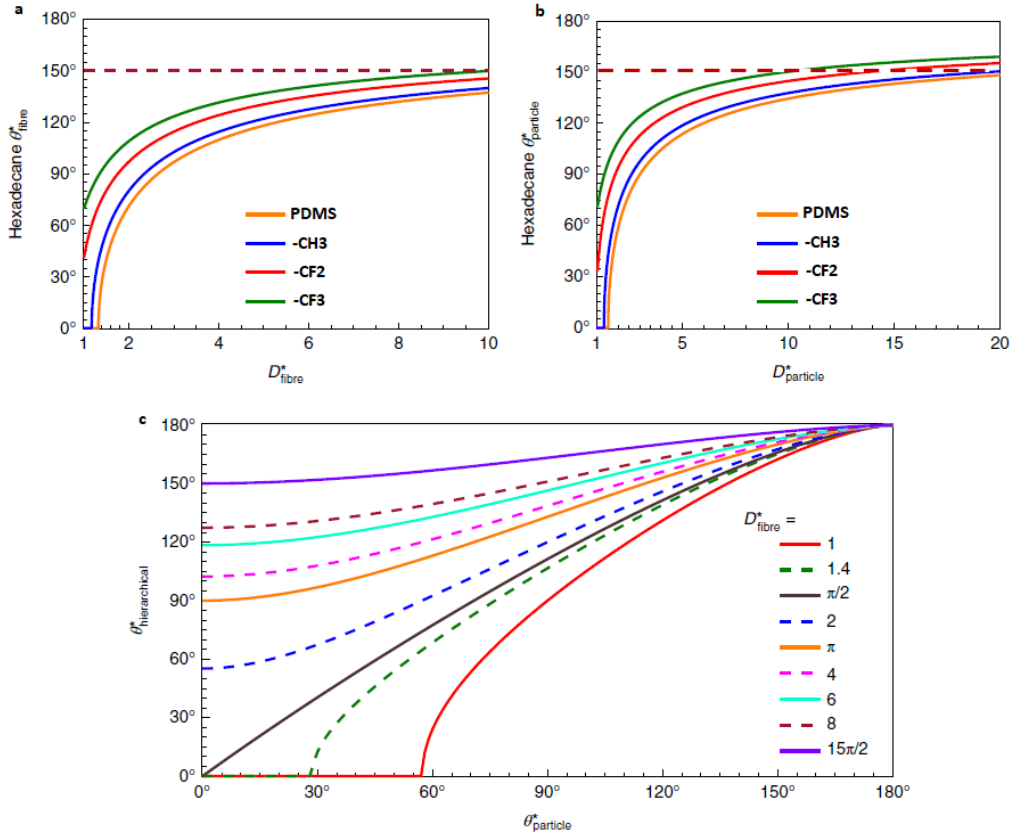
*Figure 10. **a** Design diagram of Equation 6: apparent contact angle of hexadecane on bare (non-decorated) fibers as a function of fiber porosity, for four different surface chemistries. **b** Design diagram of Equation 7: apparent contact angle of hexadecane on particles as a function of particle porosity, for four different surface chemistries. **c** Design diagram of Equation 8: apparent contact angle on hierarchical fabrics of varying porosity as a function of apparent contact angle of the particles, for nine different values of D*$_{fiber}$. Whereas **a** and **b** are specific for hexadecane, **c** holds for any liquid. Reproduced with permission of Springer Nature [12].*

Equation 10 and Equation 11 show the expression of the robustness factor for woven cylindrical fibers and flat surface covered with nanoparticles, respectively [21,25,26] (see also Figure 9 (a) and (b) for an schematic representation).

$$A^*_{fiber} = \frac{P_{breakthough}}{P_{ref}} = \frac{l_{cap}}{R_{fiber}\left(D^*_{fiber} - 1\right)} \frac{(1 - cos\theta)}{(D^*_{fiber} - 1 + 2sin\theta)}$$

Equation 10. Expression of the robustness factor in the case of interwoven cylindrical fibers.

$$A^*_{particle} = \frac{P_{breakthough}}{P_{ref}} = \frac{2\pi l_{cap}}{R_{particle}\left(2\sqrt{3}D^*_{particle} - \pi\right)} \frac{(1 - cos\theta)}{(D^*_{particle} - 1 + 2sin\theta)}$$

Equation 11. Expression of the robustness factor in the case of a flat surface decorated with nanospheres.

In Figure 11, the plots of θ*$_{fiber}$ and A*$_{fiber}$ versus D*$_{fiber}$ are represented for four different surface chemistries (design diagram of Equation 6 and Equation 10, respectively). Non-fluorinated chemistries allow permeation (A*$_{fiber}$ < 1) well before reaching apparent

contact angles of θ^*_{fiber} = 150° which means that superoleophobicity in front of hexadecane cannot be achieved only by fabric porosity and non-fluorinated chemistry.
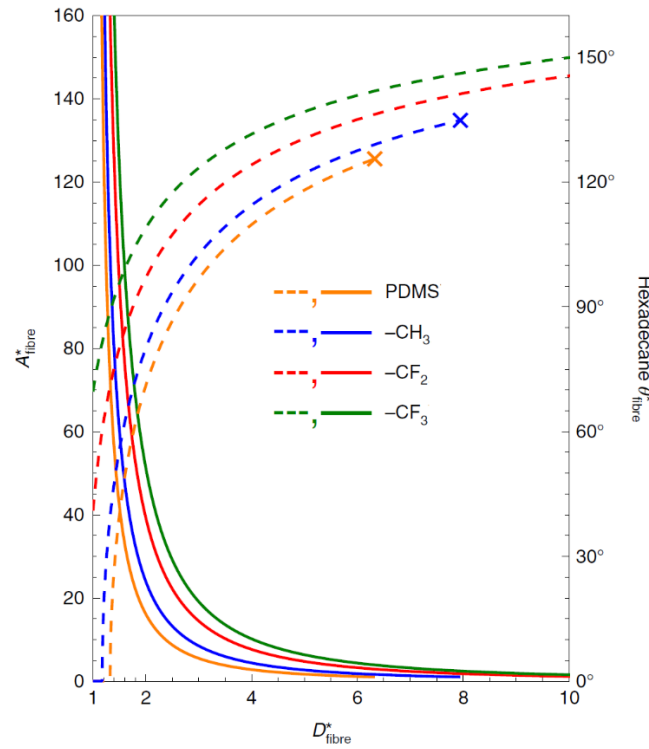
Figure 11. Robustness factor (solid lines) and apparent contact angle (dashed lines) of hexadecane for four different surface chemistries as a function of the porosity of the fibers. The "X" indicates when $A^*<1$ has been reached. Reproduced with permission of Springer Nature [12].

In the case of a fabric made up of woven cylindrical fibers that are decorated with nanospheres (hierarchical system, see Figure 9 (b)) it can be assumed that $R_{particle}$ << D_{fiber} [21], resembling the robustness factor of said hierarchical system to A^*_{fiber} ($A^*_{hierarchical}$ = A^*_{fiber}). In other words, the addition of particles on the top of a woven fabric do not impact the robustness of the non-wetted interface. However, according to Shabanian et al. [12], for decorating particles that are not wetted by the liquid, θ should be substituted by $\theta^*_{particle}$ on Equation 10 as far as the meniscus on the fibers will sit at $\theta^*_{particle}$ and not θ, giving place to Equation 12.

$$A^*_{hierarchical} = \frac{P_{breakthough}}{P_{ref}} = \frac{l_{cap}}{R_{fiber}\left(D^*_{fiber} - 1\right)} \frac{\left(1 - cos\theta^*_{particle}\right)}{\left(D^*_{fiber} - 1 + 2sin\theta^*_{particle}\right)}$$

Equation 12. Expression of the robustness factor in the case of interwoven cylindrical fibers.

21

If the restriction of A*>1 is imposed, then Equation 12 can be rewritten as Equation 13 [12], where porosity of fibers and particles adopts restricted values for a given apparent contact angle. Thus, Equation 13 gives de maximum D^*_{fiber} for a given $\theta^*_{particle}$.

$$D^*_{fiber\_max} = 1 - sin\theta^*_{particle} - \sqrt{sin^2\,\theta^*_{particle} + \frac{l_{cap}(1 - cos\,\theta^*_{particle})}{A^*_{hierarchical}R_{fiber}}}$$

Equation 13.

Equation 13 is useful to realize that different fabric constructions may need different finishes to achieve the same level of oil repellency. For instance, a fluorine-free finish that gives a $\theta^*_{particle}$ = 60° with hexadecane when coated on a smooth surface will lead to a value of $D^*_{fiber\_max}$ = 10 when applied on a fabric with R_{fiber} = 10 µm and A^* = 1. If we do the same calculation but considering a more robust fabric (A^* = 10), then $D^*_{fiber\_max}$ = 3.3.

In addition, by combining Equation 7, Equation 8 and Equation 13, a phase diagram of D^*_{fiber} versus $D^*_{particle}$ can be constructed under defined values of $\theta^*_{hierarchical}$ and $A^*_{hierarchical}$. Phase diagram for a robust oleophobic fabric ($\theta^*_{hierarchical}$ ≥ 90° and $A^*_{hierarchical}$ ≥ 1) in front of hexadecane is shown in Figure 12, where the curves for the four finish chemistries displayed are curves of constant apparent contact angle ($\theta^*_{hexadecane}$ = 90°).
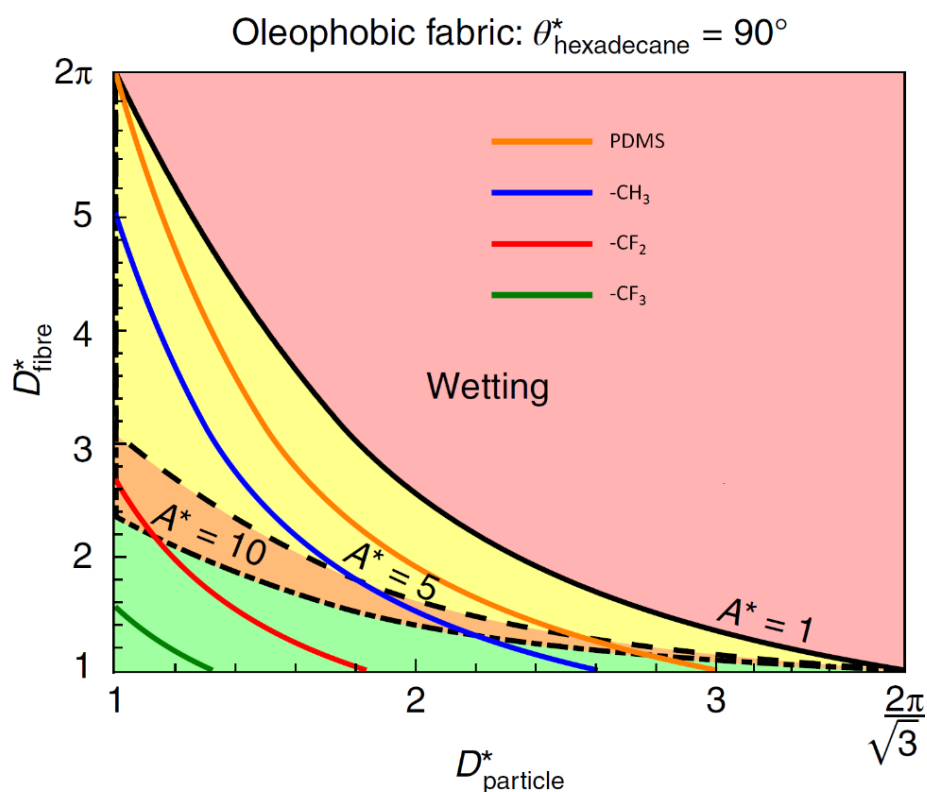
Figure 12. Phase diagram for the design of robust and oleophobic fabrics in front of hexadecane as a function of the fiber and particle porosity (assuming R_{fiber} = 10 µm) for four different chemistries. Reproduced with permission of Springer Nature [12].

In Figure 12, for a given D^*_{fibre} (specific of the fabric construction), moving to the right of the desired finish chemistry curve indicates fabrics with higher contact angles but lower robustness, until wetting region is reached. For example, a fabric with D^*_{fibre} = 3.4 and a paraffin finish (-CH$_3$) will be oleophobic only for values of $D^*_{particle}$ comprised between 1.25 and 1.68. Therefore, phase diagram from Figure 12 shows how for a given fabric (constant value of D^*_{fiber}), achieving robust (A*$_{hierarchical}$ ≥ 1) oleophobic ($\theta^*_{hierarchical}$ ≥ 90°) properties with fluorine-free finishes is only possible for a limited range of $D^*_{particle}$. Accordingly, $\theta^*_{hierarchical}$ and A*$_{hierarchical}$ are considered fundamental parameters for the design of (super)oleophobic fabrics.

From what has been depicted above, it can be deduced that the main strategy to achieve robust, omniphobic, self-cleaning and low-adhesion fabrics is to conveniently design the fabric construction, the additional roughness provided by the decorating nanoparticles and the surface chemistry.

In textile substrates, it should be noted that the measurement of static contact angles always entails an error as a result of the intrinsic structure of the fabric itself (fibers that protrude from the surface and that do not allow the baseline to be established correctly). Therefore, the characterization of hydrophobicity on textile surfaces should be done based not only on the contact angle, but also complemented with dynamic measurements such as SA, the residence time of liquid droplets on the surface or hydrostatic pressure tests (water column).

1.2   The PFASs' ecosystem and its regulation

Highly fluorinated aliphatic substances are commonly referred to as perfluoroalkyl and polyfluoroalkyl substances (PFASs). Due to PFASs widespread use, high mobility and persistence in the environment, many PFASs are found in water, land, and in the blood of people and animals all over the world. According to Buck et al. [27] we can divide PFASs in two classes: non-polymeric and polymeric PFASs, most commonly used fluorinated chemicals in textile industry fall within the last class. Polymeric PFASs have been for several decades valuable, widely used coatings for textile substrates as they are inert, low surface energy materials, extremely stable and very little bio-degradable, therefore providing coated fabrics with exceptional durable water and oil repellence (DWOR) as well as outstanding weatherability and durability.

Non-polymeric PFASs can be divided into two subcategories: non-polymeric perfluoroalkyl substances and non-polymeric polyfluoroalkyl substances, both contain the perfluoroalkyl moiety $C_nF_{n+1}-$ (n≥1) although the first have exclusively perfluorinated carbon atoms (except those C that are part of functional groups) while the latter contain saturated and/or unsaturated hydrocarbon moieties (e.g. $-C_nH_{2n}-$, $C_nH_{2n+1}-$, $CH_2=CH-$) and at least one perfluoroalkyl moiety $C_nF_{n+1}-$ (n≥1). On the other hand, the class of polymeric PFASs encompasses the following subcategories: fluoropolymers, side-chain fluorinated polymers (commonly known in the textile industry as fluorocarbons), and perfluoropolyethers. As defined by Buck et al. [27], fluoropolymers differ from side-chain fluorinated polymers in that they are based on a backbone made up exclusively of carbon atoms with F atoms directly attached to it, e.g., polytetrafluoroethylene (PTFE), although some fluoropolymers may also contain H, Cl or O atoms directly attached to the backbone. Conversely, side-chain fluorinated polymers contain a non-fluorinated polymer backbone and (per)fluorinated side-chains.

Non-polymeric PFASs possess harmful effects on health and the environment. Some of them, such as perfluorooctanoic acid (PFOA) and perfluoroctane sulfonic acid (PFOS) are considered bioaccumulative compounds, suspected of being carcinogenic [28,29], they affect lipid metabolism, and also hormonal and reproductive systems [30,31], and are persistent in nature [32]. In 2000, the United States Environmental Protection Agency

(EPA), aware of the scientific studies that pointed out that the PFOA was present in the blood of the entire world population [33], began leading actions for the progressive elimination of the PFOA (2010/15 Stewardship Program). The European Union is also taking initiatives in this same direction, culminating in Regulation (EU) 2017/1000 that prohibits the manufacture and marketing of PFOA and related substances (including any polymer that has linear or branched perfluoroheptyl and/or perfluorooctyl groups) by the year 2020 (except for a few exceptions that have extensions). Shorter homologues like perfluorohexanoic acid (PFHxA) and 1H, 1H, 2H, 2H -Perfluorooctanol (6:2 FTOH), are currently under study to better understand their environmental and human health effects [34–37] and it is likely that restriction proposals recently posted by some EU countries will come into force in the near future. In fact, European Chemicals Agency (ECHA) is considering a 2019 proposal from Germany to restrict the manufacture, sale, and use of PFHxA, its salts, and related substances.

It is well known that polymers have very different physical, chemical, and biological properties than discrete molecules. Fluoropolymers like PTFE, regarded accordingly to the Organization for Economic Cooperation and Development criteria (OECD-PLC [38]), could be considered as PLC (Polymers of Low Concern) [39]. However, polymers have been recently under increased regulatory scrutiny according to the Conceptual Framework for Polymer Risk Assessment (CF4Polymers [40]) run by the European Centre for Ecotoxicology and Toxicology of Chemicals (ECETOC) which uses a more realistic scenario for polymers, considering potential chemical hazards at each life stage of a polymer. Accordingly, it cannot be concluded in any way that polymeric PFASs are chemicals of low concern. In fact, PTFE and PVDF (Polyvinylidene fluoride) emulsions or fine powders are manufactured using non-polymeric PFASs as processing aids that can be released to the environment during their manufacture, application (manufacture of finished articles), use and disposal [41]. Furthermore, many fluoropolymer substances are commercialised in the form of fine suspensions ranging the sub-micron particle size that can give rise to bioavailable fluoropolymer particles and oligomers not exempt from possible harmful effects on health [42,43]. In addition, side-chain fluorinated polymers can release and / or degrade to non-polymeric PFASs to the environment [44] and therefore present similar challenges as fluoropolymers. Thus, despite their excellent

performance, polymeric PFASs are a potential source of non-polymeric PFASs, small particles and oligomers, that can be released into the environment during their manufacturing process and, subsequently, by degradation during life-cycle and disposal [45,46]. Regulation of individual fluorinated substances (e.g., PFOA, PFOS, 8:2 FTOH) is leading to a replacement with similar molecules not yet regulated but of similar concern, e.g., shortening of perfluorinated chains, replacement of few fluorine atoms by hydrogens and/or chlorine, branching, etc. Thus, a huge ecosystem of new fluorinated organic substances of unknown toxicity is currently arising. The amount, identity, formation pathways, and degradation dynamics of these substitutive PFASs is largely unknown. Some examples of non-polymeric and polymeric PFASs as well as their interrelationships are illustrated in Figure 13.
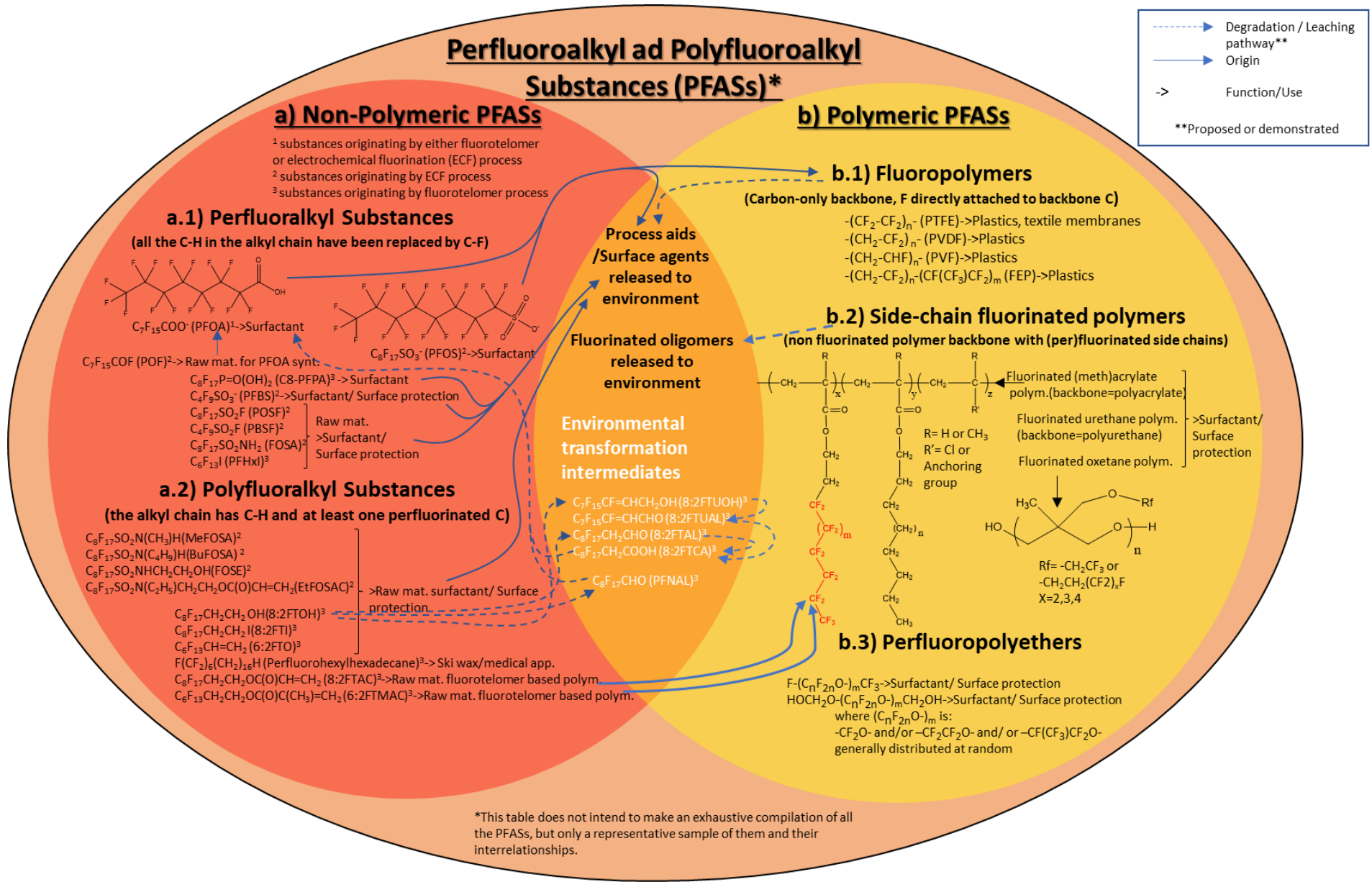
Figure 13. Simplified scheme of PFASs ecosystem and their interrelationships.

As already mentioned, polymers with (per)fluorinated side chains are widely used in the textile industry. They are commonly known as fluorocarbons and belong to the group of polymeric PFASs, more specifically to the family of side-chain fluorinated polymers. Fluorocarbons generally respond to the chemical structure represented in Figure 14. If the side chains are made up of 8 perfluorinated carbon atoms then they are called C8-fluorocarbons. These C8-fluorocarbons have been widely used for decades in the textile industry as DWOR finishing agents.
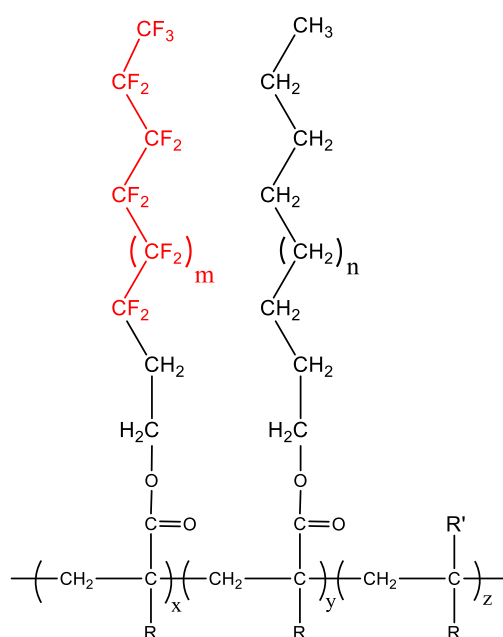
Figure 14. Chemical structure of a fluorocarbon for DWOR finishing of textiles. Generally, R= H, CH3 and R' is Cl or a reactive crosslinking group to confer durability.

Currently in Europe, C8-fluorocarbons are strongly regulated by the abovementioned Regulation (EU) 2017/1000 from European Commission. Short-chain fluorocarbons, mainly C6-fluorocarbons (side chains are made up of 6 perfluorinated carbon atoms), are being used as the logical replacement for long-chain fluorocarbons. However, C6-fluorocarbons have comparatively lower mechanical and chemical resistance as well as worse performance [47]. Short-chain fluorocarbons contain and could generate PFHxA, 6:2 FTOH and related substances that, as mentioned above, are currently under toxicological study.

It should be noted that commercial textile articles may contain multiple types of fluorinated polymers, which means that the PFASs found in these articles are diverse and come from different origins [48]. For instance, multiple layered materials used in all-weather clothing are the result of a laminate commonly composed of three layers: outer layer made of polyester or polyamide fibers coated by a side-chain fluorinated polymer to confer water and oil repellence, middle layer which typically is a PTFE or polyurethane membrane that confers hydrostatic pressure, and finally an inner layer of hydrophilic nature that allows the transport of sweat and moisture to the outside. See Figure 15 for a schematic of a typical multi-layered fabric for outdoor clothing.
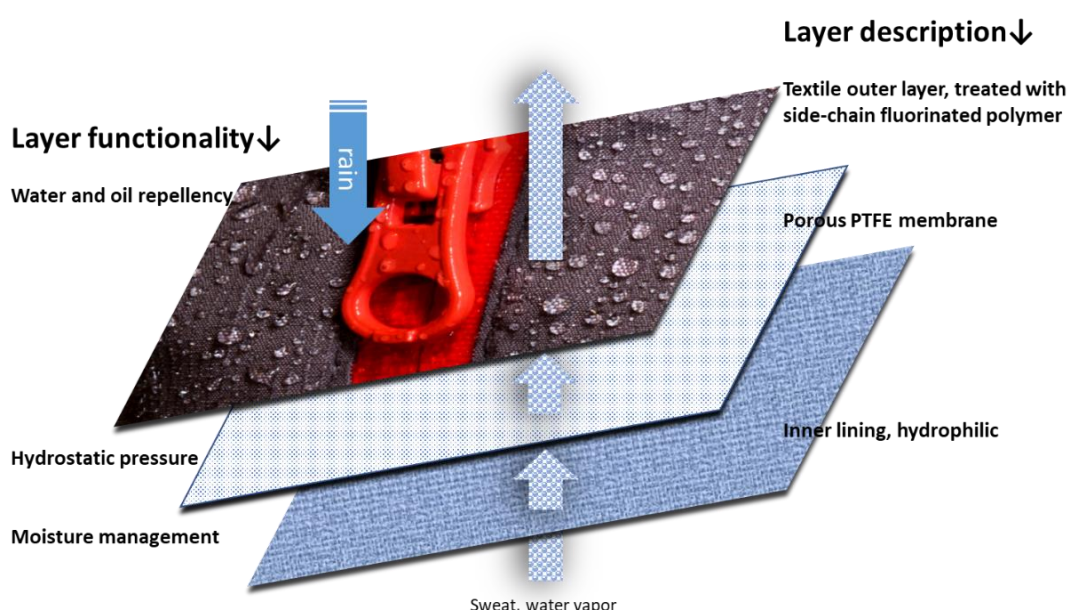
Figure 15. Scheme of a typical multi-layered fabric for outdoor clothing where a multitude of PFASs from different origins can be found.

All the above-mentioned concerns regarding PFASs are leading to intensive research and high market demand of fluorine-free alternatives for DWOR finishing.

1.3 Estate of the art of DWOR chemistry

In recent years there has been a growing interest in the development of surfaces that are highly repellent to water (superhydrophobic), oils (superoleophobic), or both (superomniphobic or superamphiphobic). Numerous researchers and companies are investing efforts and resources in this field. If we perform a search by topic in the ISI Web of Science database (core collection), we can obtain quantitative data about academic interest in this field. Thus, we have interrogated the database in the time span from 2000 to 2021. The results of the query are shown in Figure 16, 19.476 references on this topic have been retrieved, also observing a progressive increase in the number of publications within the last decade.
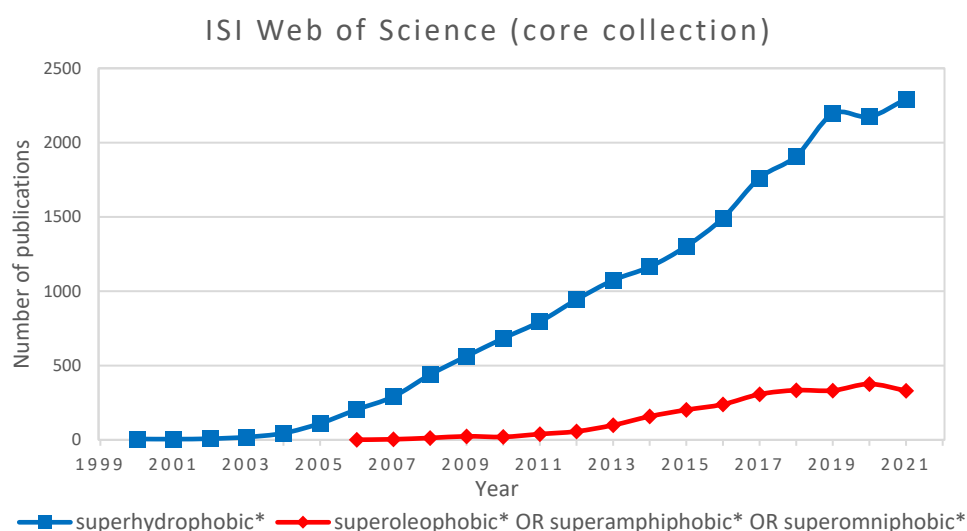
Figure 16. Query of the ISI Web of Science database (core collection) with the following search strategies: (1) TS= (superhydrophobic*), and (2) TS= (superoleophobic* OR superamphiphobic* OR superomniphobic*), in the time span from 2000 to 2021.

If we perform a more specific search in ISI Web of Science (core collection) on hydro/oleo-repellent textiles in the time span 2000-2021, we retrieve 2.379 references and we also see a clear increase in the number of publications issued in the last 5 years, see Figure 17. Therefore, within the textile sector, the study of WOR finishes is a highly demanded topic, monopolizing approximately 12% of the publications on this subject. In addition, it should be noted that this increase in the number of publications in the last decade is not only motivated by a purely technical interest but also by the growing demand for technical alternatives to traditional fluorocarbons, caused by the current

regulations and restrictions on the use of long-chain perfluorinated chemicals (≥C8) as well as the growing social awareness and pressure that NGOs such as Greenpeace [48] put on important outdoor apparel brands to find more sustainable alternatives to fluorine chemistry.
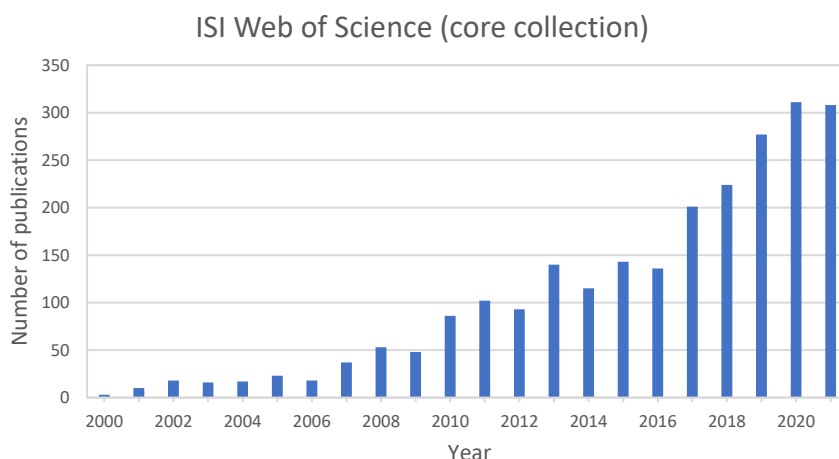
Figure 17. search strategy TS=((hydrophobic* OR oleophobic* OR omniphobic* OR amphiphobic* OR superhydrophobic* OR superoleophobic* OR superomniphobic* OR superamphiphobic*) AND textile*), time span: 2000-2021.

To get a general idea of the types of chemicals that are currently emerging as alternatives to long-chain fluorocarbons (≥C8), the following search in ISI Web of Science (core collection) has been carried out: TS=(superhydrophobic* AND textile*), in the period 2016-2021. 510 references were retrieved and manually classified into 8 different chemical families (see list below).

- **Fluorinated ≥C8**: treated textiles with log chain (≥C8) fluorocarbons or fluorosilanes.
- **Fluorinated ≤C6**: treated textiles with short chain (≥C6) fluorocarbons or fluorosilanes.
- **Silica NPs/silanes**: textiles treated with nanoparticles based on silica and/or (alkyl) silanes, which may contain polymers of different nature as binders. Fluorine-free.
- **PDMS**: textiles treated with hydrophobizers based on polydimethylsiloxanes, which may contain nanoparticles as additives to increase roughness. Fluorine-free.

- **Other NPs**: textiles treated with other types of nanoparticles (ZnO, TiO$_2$, other metal oxides and salts, POSS, etc.), which may contain polymers of different nature as binders and silica nanoparticles as additives. Fluorine-free.

- **Waxes/Paraffins**: textiles treated with e.g., fats, fatty acids, waxes, paraffins, that may contain polymers and/or nanoparticles as additives to increase binding and roughness, respectively. Fluorine-free.

- **Ac/PU**: textiles coated with acrylic polymers/monomers or polyurethanes, optionally containing nanoparticles as additives to increase roughness. Fluorine-free.

- **Others:** chemical etching, laser-etching, plasma-treatment, chemical vapor deposition (CVD), etc.

Figure 18 shows the result of the manual indexing of the retrieved references following the above criteria, it also shows the growing interest in the development of DWOR textile finishes and the progressive decrease in the number of scientific works that use long-chain fluorocarbons (strongly regulated), in favor of more sustainable alternatives.
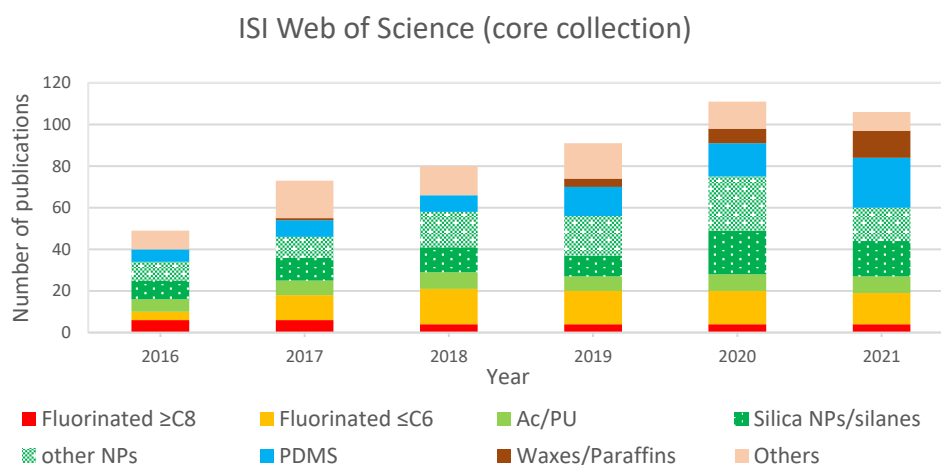
Figure 18. Search strategy TS=(superhydrophobic AND textile*), time span: 2016-2021. 510 references have been retrieved and manually indexed within the following categories: Fluorinated ≥C8, Fluorinated ≤C6, Ac/PU, Silica NPs/silanes, other NPs, PDMS, Waxes/Paraffins, Others.*

Long- and short-chain fluorochemicals belong to PFASs and have already been addressed in the previous section. Next, we will describe with some examples the families based on fluorine-free chemicals. It should be noted that it is often difficult to assign a publication clearly and unequivocally under one of the established categories.

This is because chemical products of a different nature are often combined in the same work (e.g., nanoparticles and polymers), taking advantage of the synergies generated between them. In these cases, the assignment has been made taking into consideration the main claims of the publication.

Silica NPs/silanes: textiles treated with nanoparticles based on silica and/or (alkyl) silanes, which may contain polymers of different nature as binders are attracting growing interest as superhydrophobic finishes for textiles generally made of cellulosic fibers like cotton. The majority of the coatings within this category are applied by dip-coating or spray which are not common methods in textile finishing industry. Moreover, long-term stability of these coating formulations is not usually assessed in view of industrial implementation. Manatunga et al. [49] functionalized a cotton fabric with sol-gel technology, where silica nanoparticles were used to increase the roughness of the surface and further hydrophobized with different hydrophobic agents such as hexadecyltrimethoxy silane (HDTMS), stearic acid (SA), octyltriethoxy silane (OTES) and hybrid mixtures of HDTMS/SA and HDTMS/OTES; silica nanoparticles were prepared by alkaline hydrolysis of tetraethyl orthosilicate (TEOS) in ethanol (Stöber method); hydrophobic silanes were prepared in ethanolic medium and acidic pH, cotton fabrics were first immersed in ethanolic silica, followed by drying and washing to remove unfixed silica; in a second step, fabrics were treated with the silane sols followed by drying and curing. WCA between 140 and 160° were achieved on the treated cotton fabrics. There are many works that describe similar approaches based on a combination of silica nanoparticles and hydrophobic silanes, using several steps of sol-gel coating assisted by solvents [50–53].

Other works use one-step solvent-based methods, for instance Li et al. [54] treated cotton fabrics with an ethanolic solution of octadecyltrimethoxysilane and TEOS while Guo et al. [55] developed a polydopamine/SiO_2/trimethylsilyl coating made from dopamine, TEOS and hexamethyl disilazane.

Few waterborne silane-based coatings are reported in literature. For instance, Wang et al. [56] developed a dispersion of HDTMS in aqueous (poly)dopamine solution. Rahman et al. [57] made a coating solution based on HDTMS and octadecylamine. Guo

et al. [51] developed a TEOS hydrosol using sodium dodecylbenzene as emulsifier and adding different silanes as hydrophobizing agents (OTES, dodecyltriethoxysiliane and isooctyltriethoxysiliane) in combination of silane-coupling agent γ-mercaptopropyltriethoxysilane; this hydrosol was applied by electrocoating. Zhao et al. [58] developed a dispersion of silica nanoparticles (Aeroxide LE2) functionalized with 3-aminopropyltriethoxy silane and HDTMS that was coated by spray on different substrates achieving WCA above 150°.

Urata et al. have reported sol-gel methods [59,60] to achieve dynamically oleophobic but statically oleophillic coatings; tetramethoxysilane and several alkyltriethoxysilanes have been used as a sol-gel precursors in solvent-based formulations; low CAH and tilt angles have been achieved with n-hexadecane; these coatings have not been applied on fabrics but on silicon wafers, however, we consider them worth mentioning because they deal with the concept of dynamic oleophobicity.

PDMS: textiles treated with reactive or non-reactive polydimethylsiloxanes (PDMS) as hydrophobizers, which may contain nanoparticles as additives to increase roughness are quite common in literature. Ma et al. [61] applied a linear PDMS with side-chain epoxy functional groups dissolved in isopropyl alcohol on a cotton fabric by a pad-dry-cure method, conferring water column to fabrics while keeping breathability. Liu et al. [62] prepared a dispersion of hydrophobic silica particles, PDMS precursor and PDMS curing agent dispersed in n-hexane; the treated cotton fabrics display good hydrophobicity with WCA of 161° and SA below 5°. Xue et al. [63] used padding as a conventional textile finishing method to coat polyester fabric (previously impregnated in ethanol) with a solution of two-component elastic silicone rubber in THF; WCA close to 167° were obtained. A similar approach was used by Guo et al. [64] to achieve multifunctional hydrophobic polyester fabrics by dip-coating using a two-component elastomeric PDMS dissolved in THF; in this case two previous steps were performed to incorporate poly(dimethyldiallylammonium chloride) and carbon nanotubes as positive-charged layer and negative-charged electrically-conductive layer, respectively, conducting several cumulative layer-by-layer (LBL) depositions; WCA of 166.9° and SA of 4.2° were achieved. Hao et al. [65] hydrophobized silica nanoparticles using a crosslinked polysiloxane bearing end-capped epoxy groups and aminopropyltriethoxysilane (APTES)

as a adhesion promoter between SiO_2 and PDMS; several solvents were employed as isopropanol, benzene, ethanol and ethyl acetate; the nanocomposite was applied on cotton fabric conferring roughness and low surface energy to the fabric with WCA of 158°. Zhu et al. [66] used a LBL deposition technique to coat a cotton fabric by dip-coating; the inner layer was a PDMS which acted as a adhesion promoter, the middle layer was made of ZnO nanoparticles and finally an outer layer of PDMS was deposited; THF was used as a solvent to dissolve PDMS; a multifunctional fabric was obtained with UV-blocking properties, WCA of 160° and SA of 5°. Cheng et al. [67] described brush-like PDMS coatings to confer dynamic oleophobicity (low CAH) but static oleophilicity with decane and hexadecane (OCA < 40°); in this work fabrics have not been used, but silicon wafers have been employed as a substrate for coating; complex coating systems including vapor deposition and many solvents were employed. Shabanian et al. [12] coated a nylon fabric previously activated with oxygen plasma with ethanolic solution of TEOS applied by dip-coating and subsequent contacting se silanized fabric with vaporized 1,3-dichlorotetramethyldisiloxane during 1h; WCA > 120° and OCA of 108° and 110° with olive and canola oil, respectively, were achieved on nylon fabric. Khatir et al. [68] reports a similar multistep solvent-based approach also based on 1,3-dichlorotetramethyldisiloxane; here WCA of 106-108° and hexadecane CA of 34-36° were obtained on nylon fabric; the authors claim that this surface treatment can confer dynamic omniphobicity to any surface because the obtained CAH values are extremely low, allowing liquids to roll-off when the treated surface is tilted; however, OCA < 90° denotes wettability and therefore treated surfaces should be considered as dynamically oleophobic but statically oleophilic.

Other NPs: textiles finished with nanoparticles different from silica (ZnO, TiO_2, other metal oxides and salts, POSS, etc.) are also described in several publications, which may contain polymers of different nature as binders and silica nanoparticles as additives. Tissera et al. [69] reported the grafting of graphene oxide nanosheets on a cotton fabric by dip-dry method, obtaining adhesive-type hydrophobicity with WCA up to 143°. Attia et al. [70] described the coating of different fabrics with TiO_2 and ZnO nanoparticles using a commercial binder to fix them to the surface, toluene was used as a solvent; WCA of 160° were obtained as well as additional features (UV-barrier). Mai et al. [71]

coated pristine cotton fabrics combining ZnO nanoparticles and polyvinylsilsesquioxane binder dispersed in ethanol; UV shielding, durable superhydrophobic (WCA of 160°) and antimicrobial properties were obtained. Xu et al. [72] obtained superhydrophobic cotton textiles with ultraviolet-blocking and photocatalytic multifunctionalities by in situ generation of flower-like copper sulfide which was deposited on cotton fabric to generate a hierarchical mesoporous microstructure; PDMS was used as a binder and low-surface-tension polymeric coating; isopropyl alcohol was used as a solvent during the dip-cure process that also involved ultrasonication; WCA close to 158° and WSA of 7.2° were obtained. Fu et al. [73] reported the use of Fe_3O_4 nanoparticles generated in situ in combination with polydopamine as a precoating and HDTMS; first, aqueous solution of PDA was applied on cotton by dip-coating at raw temperature for 16 hours and, secondly, aqueous dispersion of Fe_3O_4 and HDTMS was applied by dip-coating at 60 °C for 16 hours; superhydrophobic fabric was obtained with added magnetic properties (displacement under magnetic field) that can be of interest for enhanced oil recovery.

Polyhedral oligomeric silsesquioxanes (POSS) have a rigid cage-like structure made of Si-O-Si bonds, which resembles that of silica, and organic substituents (R) on outer corners. They respond to the composition $R_n(SiO1.5)_n$ where n is an even integer ≥ 4 (n = 8 being the most common) and R substituents range from H to non-reactive and / or reactive organic groups. POSS have nanoscale dimensions, with silicon-silicon distance of 0.53 nm, and an average diameter of 1–3 nm [74,75], however, particles are often aggregated in the 1–100 μm [76]. POSS can be incorporated into common polymers via copolymerization, grafting, or blending. Sun et al. [77] derivatized methacrylheptaisobutyl POSS by reaction with 1-dodecanethiol and 3-mercaptopropyltriethoxysilane under UV-irradiation, then grafted the reactive POSS to cotton fabric; dichloromethane and acetone were used as a solvents; WCA of 146° and low roll-off angles were obtained. Hou et al. [78] grafted methacrylheptaisobutyl POSS to cotton fabrics using 3-mercaptopropyltriethoxysilane as a coupling agent; ethanol and dichloromethane were used as a solvents in a multi-step coating method that includes UV irradiation; WCA of 159° and SA of 7° were obtained.

Waxes/Paraffins: within this family we find textiles treated with e.g., fats, fatty acids, waxes, paraffins, that may contain polymers and/or nanoparticles as additives to increase binding and roughness, respectively. Most natural hydrophobic surfaces are based on hierarchical waxy structures. We find numerous examples of waterproof and self-cleaning surfaces in nature; a well-known example is the lotus leaf [1,2]. Waxes can be classified into natural and synthetic. Within natural waxes we find plant-derived waxes (carnauba wax, candelilla wax, soy wax, sunflower wax, berry wax, rice bran wax, castor wax, etc.), animal-derived waxes (beeswax, wool wax, shellac, spermaceti, etc.) and mineral waxes (paraffin, microcistalline wax, montan wax, lignite, ozocerite, ceresin, utah, peat, etc.). Synthetic waxes are very varied: fatty alcohols and acids (e.g., stearyl alcohol, stearic acid, palmitic acid, myristic acid), fatty acid esters and glycerides (glyceryl stearates, glycol fatty-acid stearates, sorbitol stearates, etc.), hydrogenated oils, ketones, amines, amides, (e.g., stearone, laurone, aliphatic amines, aliphatic amides), chloronaphthalenes, synthetic mineral waxes (e.g., Fisher-Tropsch, duroxon), etc. Guan et al. [79] reported an ethyl acetate suspension containing polyethylene wax, silica nanoparticles (to increase roughness), hexamethylenediisocyanate and hydroxyl acrylic polymer (binder system); WCA up to 163° were obtained. Forsman et al. [80] coated cellulose substrate by LBL deposition of aqueous cationic poly-L-lysine and anionic carnauba wax; deposition of two bilayers was found to be enough to attain the complete surface coverage with the desired roughness; WCA up to 156° were obtained. Zhao et al. [81] finished a polyester fabric by waterborne combination of a paraffin wax and hydroxyl-terminated PDMS condensed with TEOS using a organotin catalyst; WCA of 156.7° were achieved and the authors demonstrated the self-cleaning ability of the treated fabrics as well as its feasibility to be employed as a water/oil separation membranes. Liu et al. [82] fabricated polydopamine nanocapsules containing octadecylamine and octadecanethiol in the core; capsules were fabricated and coated on fabrics via in-situ polymerization; the coating showed self-healing hydrophobic properties thanks to the release of core hydrophobic molecules triggered by mechanical and shear forces. Mohshin et al. [83] polymerized stearic acid with citric acid and triethanolamine under various conditions and temperatures; the obtained polymers were dissolved in water/isopropanol and applied onto cotton fabrics by pad-dry-cure method; WCA up to 145° were achieved.

Ac/PU: textiles coated with acrylic polymers/monomers or polyurethanes, optionally containing nanoparticles as additives to increase roughness have also been extensively investigated.

Grafting of acrylic monomers onto the fiber surface using irradiation, chemical catalysis or plasma-induced methods is a common approach reported in several works. Wu et al. [84] immersed cotton fabrics in methanolic solutions of different alkyl methacrylates (methyl methacrylate, ethyl methacrylate, n-propyl methacrylate, n-butyl methacrylate, n-hexyl methacrylate and n-lauryl methacrylate) and afterwards performed γ-ray induced polymerization to graft the monomers to the cotton surface; treated cotton fabrics achieved superhydrophobicity and showed a characteristic degree of grafting that decreased with the length of the alkyl chain from the acrylate. Wang et al. [85] described hydrophobic finishing of cotton by treatment with ethanolic lauryl methacrylate in presence of crosslinking agent glycol dimethacrylate; first, ammonium ceric nitrate was dissolved in ethanol and atomized onto fabrics, second, the monomer solution was also atomized onto the fabric surface, dried and heated at 60 °C overnight; acrylic solutions were also coated by immersion method; the modified cotton fabrics exhibit laundering-durable and mechanically stable superhydrophobicity. Li et al. [86] studied the plasma-induced graft polymerization of stearyl methacrylate on cotton substrates; fabric was pre-impregnated with an ethanolic solution of stearyl methacrylate, dried, placed in the plasma chamber where glow discharge of the helium low temperature plasma was applied to induce graft polymerization; WCAs up to 140° were reached.

Finishing of fabrics with waterborne polyacrylates or polyurethanes is gaining special interest in recent years due to its ease of application, low VOCs content, economic affordability and, ultimately, a differentiation in terms of sustainability with respect to many of the approaches provided in most scientific works. As a matter of fact, the papers presented in this Thesis fall within this scope. Zhang et al. [87] used a commercial waterborne polyurethane binder combined with polysiloxane-modified palygorskite nanorods to coat glass substrates and render them hydrophobic; nanorods are 20–40 nm in diameter and a few hundreds of nanometers to one micrometer in length; superhydrophobic PU/nanorods coatings were prepared by layer-by-layer spray-coating

onto glass slides pre-heated at 150 °C; two layers were applied and WCA up to 157.9° and SA of 7.2° were obtained; the coating of textile surfaces was not reported in this work. Dai et al. [88] reported the synthesis of a waterborne PDMS-polyurethane hybrid bearing terminal hydroxyl groups that was combined with nanofillers to get nanocomposites; graphene and multiwalled carbon nanotubes were selected as a nanofillers and dispersed in water using a high pressure microfluidizer and subsequently mixed with the PDMS-PU dispersion to obtain nanocomposites; the nanocomposites were added with polyisocyanate as a curing agent and coated onto cotton/polyester fabrics (70:30 wt. %) by a dipping/ultrasonic method; WCA of 153.6° on coated fabrics were achieved and also electrical and thermal conductivity was conferred by the fillers. Rutkevicius et al. [89] synthesized a waterborne PDMS-polyurethane hybrid with and without grafted hydrophobic fumed silica particles; the synthesis was performed by the prepolymer method, with the concourse of solvents (acetone, DMF) and copper chloride as a catalyst; the best values of WCA (169°) were achieved from the fabrics coated by the waterborne PDMS-PU polymer without grafted silica plus a second layer of the hydrophobic silica dispersed in isopropanol. Liu et al. [90] synthesized a waterborne branched cationic PDMS-polyurethane hybrid from toluene diisocyanate, glyceryl monostearate and hydroxypropyl-terminated PDMS; dibutyltin dilaurate, acetone and butanone oxime were used as a catalyst, co-solvent and blocking agent, respectively; WCA up to 148° were achieved on coated fabrics. Biobased waterborne polyurethane [91], polyurethane-urea [92], and UV curable polyurethane-acrylate dispersions [93] are gaining relevance as a sustainable extremely versatile coatings for different sectors. Within the framework of this Thesis, we have explored the synthesis of a series of fluorine-free waterborne polyurethane-ureas for the textile sector, obtained from isophorone diisocyanate and three different commercially-available biobased building blocks. This research work led to three published papers. One of our published works described the synthesis of a polyurethane series obtained from a biobased polyether-polyol [94]; the other two published works focused on the synthesis of polyurethanes from semi-crystalline [95] and fully amorph [96] biobased polyester-polyols that, in turn, were combined with SWCNT and reactive POSS, respectively, to obtain nanocomposites. The novelty of these three works lies in, on the one hand, obtaining biobased polyurethanes as a hydrophobic textile finishing agents, and, on the other hand, their

application by the knife coating method, which allowed obtaining single-face coated fabrics with high resistance to water-permeation (water column or hydrostatic head). Finally, the combination of the polyurethane-ureas with nanomaterials led to interesting synergies like the improvement in hydrophobicity for POSS or electrical conductivity for SWCNT.

Lei et al. [97] synthesized a series of copolymers from 3-[tris(trimethylsilyloxy)silyl]propyl methacrylate (M$_3$T), trimethoxysilylpropyl methacrylate, hydroxyethyl methacrylate and propyl methacrylate; toluene was used as a polymerization media; obtained copolymers were diluted in white spirit and applied on several substrates (masonry and cotton fabric) by spray and dip-coating; coated substrates were subjected to additional isocyanate curing; the authors claim that also waterborne emulsions of M$_3$T, triethoxysilylpropyl methacrylate and propyl methacrylate has been prepared but they do not give details about the polymerization procedure; coated surfaces displayed surface-energy values as low as 13 dyn cm^{-1} and a certain resistance to olive oil wetting. Within the framework of this Thesis and inspired by the previous work of Lei et al. [97], we have explored the synthesis of a series of fluorine-free (co)polymethacrylates obtained from M$_3$T and bio-based stearyl methacrylate (SMA) [98]; the (co)polymers were obtained by miniemulsion polymerization and applied to textiles substrates by one-step simple padding-curing method; the novelty of this development lies in the fact that, for the first time, waterborne copolymers of M$_3$T and a bio-based comonomer (SMA) have been obtained, which provided remarkable repellency to water, olive oil and different types of dirt, as will be discussed later.

Others: chemical etching, laser-etching, plasma-treatment, chemical vapor deposition (CVD), among others, are sophisticated techniques reported in several works to obtain liquid-repellent fabrics. These approaches involve the use of machinery and devices that are very different from the finishing methods used in the textile sector and, in general, they are not fully available on an industrial scale. Therefore, there is a high barrier to entry to their implementation. Despite this, some plasma treatments can currently be found in some niche applications in the textile sector [99]. Li et al. [100] conducted an aerosol-assisted chemical vapour deposition using a TEOS and PDMS as a roughness

precursor and hydrophobic coating, respectively; ethanol and ethyl acetate were used as a solvents and film deposition was carried out in a cold-walled horizontal-bed CVD reactor; WCA > 160° and SA < 1° were obtained on glass surfaces and the authors claim the viability of this method for coating flexible substrates like fabrics. Caschera et al. [101] used plasma enhanced chemical vapor deposition (PECVD) to obtain superhydrophobic surface on one of the faces of a cotton fabric; in this work nano-etched morphology was achieved by plasma pre-treatment followed by diamond-like carbon coating chemical deposition (DLC); high vacuum and different gases (O_2, Ar, H_2) were employed during plasma pre-treatment and a mixture of CH_4, H_2 and Ar was used for DLC; O_2 plasma pre-treated fabrics and subsequently coated by DLC displayed the highest contact angle at 146.4°. Oh et al. [102] reported a method to render PET fabric superhydrophobic without using chemical finishing agents; oxygen plasma etching for 60 min created hierarchical structures on the surface, and the heating process at 130 °C for 24 h accelerated the hydrophobic ageing effect; static WCA of 174° was reported.

It is worth to note that the fluorine-free alternatives to achieve DWOR finishes are diverse, being based on very heterogeneous chemistries. Most of the indexed publications provide complex solutions, which require several steps for their application on fabrics, which makes them unattractive for industrial implementation. The use of materials with low availability and high price is also quite frequent, in addition to the use of solvents and additives with a high environmental impact.

Despite some works claim dynamic oleophobicity by applying fluorine-free complex treatments [59,60,67,68], or certain degree of static repellency towards vegetable oils [12,97], none of the retrieved alternatives to PFASs provides static oil repellency to low surface tension liquids such as dodecane or hexadecane. For all these reasons, the need to continue investing resources in this field of research becomes evident, especially when the textile industry is under the spotlight for being one of the most polluting sectors at a global level [103]. In this sense, the novelty of this work lies in the fact that totally fluorine-free products have been developed for the DWOR finish on textiles. In addition, the new polymers developed are partially bio-based and the use of VOCs and harmful additives has been minimized. Finally, the developed prototypes can be applied

by finishing methods commonly used in the textile sector (i.e., padding, and knife-coating), thus ensuring its industrial and market interest.

1.4 Thesis' framework, methodology and research lines

This Thesis has been performed under the framework of the project "*E!11894*" that has been funded by the Eurostars-2 joint program with co-financing from CDTI (Spain), Ministry of Education and Youth (Czech Republic) and from the Horizon 2020 Research and Innovation Framework Program of the European Union. Additional financial support has been received from the AGAUR (Doctorats Industrials: 2018 DI 093).

Project *E!11894* has been possible thanks to the joint work of a consortium of companies, universities, and research centers, namely: Color Center, S.A. as project leader; Inotex spol. s. r.o., as industrial partner; Tekniker and UPC as a research center and university, respectively.

In this work we have focused on the development of polymeric coatings to confer hydro- and oil repellency to fabrics. Specifically, waterborne polyacrylates and polyurethane-ureas have been developed, combined in some cases with (nano)materials to optimize performance and/or confer multifunctionality to coated fabrics. The choice of these lines of research and not others such as sol-gel chemistry, surface modification by plasma, or chemical vapor deposition (CVD), is motivated by several factors. On the one hand, the design of waterborne polymers allows their application on fabrics through standard textile finishing machinery (padding, knife coating) and avoiding intensive use of volatile organic substances (VOCs), which eliminates a barrier to entry in textile market. On the other hand, these polymers (acrylic and polyurethane) can be obtained from a wide range of commercially available building-blocks. In addition, the synthesis strategies for obtaining said (co)polymers allow us to obtain polymeric coatings whose properties are finely tunable according to the selection of monomers and synthesis conditions. Finally, among the commercially available building-blocks for polyurethanes and polyacrylates, there is a growing number of monomers from renewable sources [104], some of them containing functional groups of very low surface tension in their chemical structure, which makes them especially attractive for the development of highly hydrophobic polymers.

The general methodology followed is shown in Figure 19. Much of the experimental work has been structured through the design of experiments (DOE) of ternary mixtures.

DOE has allowed us to systematically explore the ratio between the different building-blocks, revealing itself as a good methodology to establish a correlation between structure and properties that enables fine-tuning of polymer properties as a function of the relationship between the different components of the mixture.
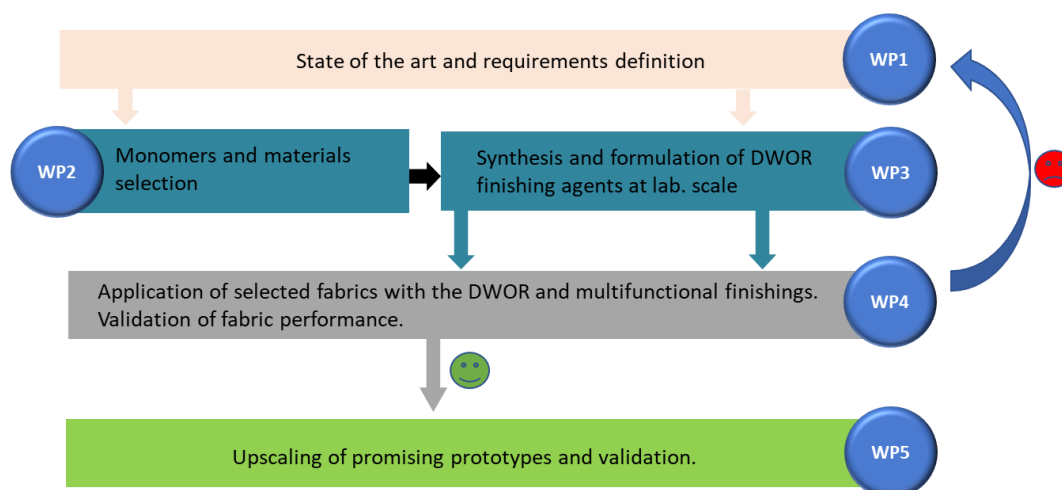

Figure 19. Thesis Workflow (WP stands for Work Package).

The Thesis consists of two research lines. For each line, innovative polymers have been successfully synthesized from bio-based building-blocks carefully selected with eco-design criteria. Research line 1 focuses on the development of fluorine-free hydrophobic polyurethane-ureas while in research line 2 the synthesis of polymethacrylates with ultra-low surface tension functional groups have been addressed. Both lines of research have been selected due to the increasing availability of bio-based building blocks with (ultra)low surface tension both in the range of acrylic monomers, polyols and chain extenders. In addition, a correct design of the synthesis strategies as well as monomer and (nano)materials composition, has allowed the obtention of polymers and nanocomposites with a controlled microstructure, according to the requirements of the project. All the synthesis and formulation work has been conducted without the use of fluorinated chemicals, harmful additives or catalysts based on heavy metals. In all cases, the biobased polymers obtained have been dispersed in water (waterborne polymeric dispersions) and subsequently applied on selected fabrics, alone or in combination with (nano)materials, with the aim of conferring DWOR and advanced functionalities to the textile substrates. The development of these two lines of research has given rise to

publications in different scientific journals. The research lines are summarized below, the papers published within each line are also referenced.

- Research line 1: Development of fluorine-free bio-based waterborne polyurethane-urea dispersions (WPUD) and combination with (nano)materials for DWOR finishings.

In this research line three sets of experiments have been performed. In the first set (set 1) [94] Fully bio-based poly(1,3-propylene glycol), fatty dimer-diol (Pripol 2033, fully biobased) and ethylenediamine (EDA) were used as polyol and chain extenders, respectively. In the second set (set 2) [95], semi-crystalline polyester-polyol (Priplast 3294, 100 % biobased) was used as polyol and 1,3-propanediol (1,3-PDO, 100% biobased) and EDA were used as chain extenders. The obtained WPUD were doped with single-walled carbon nanotubes and surface properties as well as electrical conductivity were assessed. In the third set (set 3) [96], amorphous polyester-polyol (Priplast 3238, 100 % biobased) was used and a combination of functionalized nanomaterial trans-cyclohexanediol isobutyl POSS (POSS-OH), 1,3-PDO and EDA was used as extender system. In all the experiments, isophorone diisocyanate (IPDI) was used as polyurethane-urea precursor, dimethylolbutanoic acid (DMBA) as internal emulsifier, triethylamine (TEA) as neutralizing agent and bismuth neodecanoate as tin-free catalyst. Figure 20 shows the chemical structure and simplified structure of the bio-based polyols and the main chain extenders. Particle size and stability for all of the developed WPUD have been studied. Finally, the WPUD have been applied on PET fabrics by Knife-coating and the repellence to liquids, and water permeation resistance (head pressure) of treated textiles has been assessed.
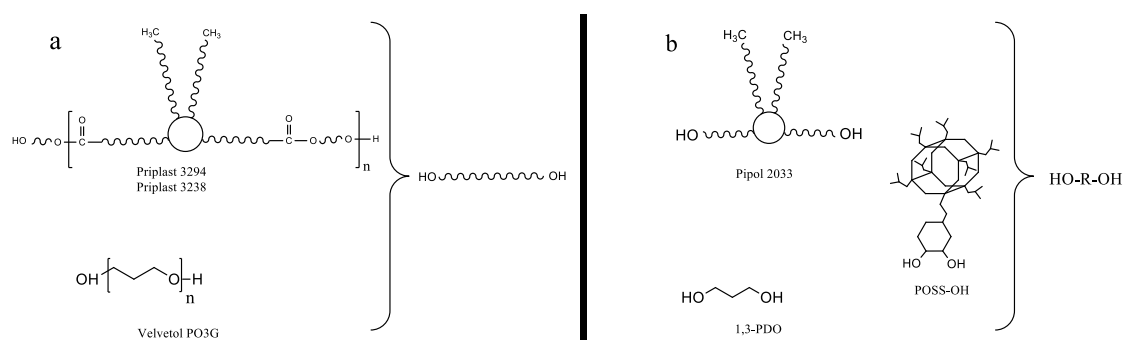

Figure 20. Chemical structure and simplified structure of a: the bio-based polyols, b: the main extenders used.

Figure 21 exemplifies the synthesis strategy for the obtention of the WPUD.

1) 80ºC, 2h
2) Prepolymer neutralization with NEt₃
3) Phase inversion in water
4) Chain extension with EDA
5) Co-solvent elimination
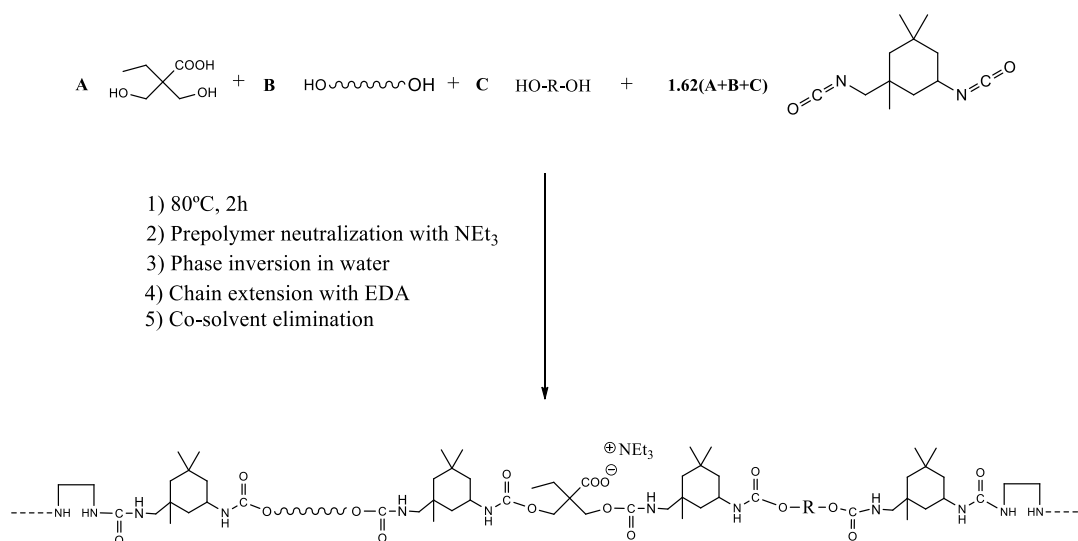
Figure 21. Synthesis strategy of waterborne polyurethane-urea dispersions.

In addition, a review summarizing the abovementioned published works has been published in the journal "*Revista de Plásticos Modernos*" [105].

• Research line 2: Development of fluorine-free bio-based (co)polymethacrylate waterborne emulsions for DWOR finishings

In this work, a series of fluorine-free, low surface-energy and partially bio-based (co)polymethacrylates based on 3-[tris(trimethylsilyloxy)silyl]propyl methacrylate (M3T) and stearyl methacrylate (SMA) (Figure 22) have been successfully synthesized by miniemulsion polymerization and characterized by different spectroscopic and thermal methods [98].

SMA   M3T

Figure 22. Chemical structure of monomers used for the synthesis of PM3TxSMAy (co)polymethacrylates.

Particle size, particle size distribution and stability of developed waterborne emulsions have been assessed. Finally, the fluorine-free M3T/SMA

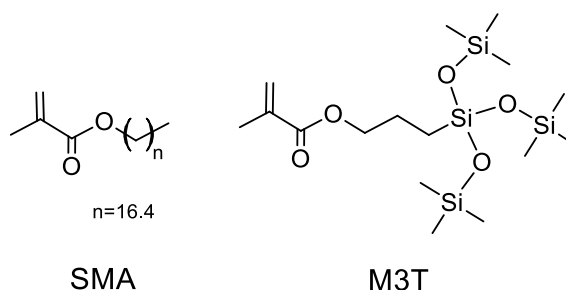(co)polymethacrylates have been applied on cotton fabrics by padding and the performance to water and oil repellence of treated textiles has been assessed.

2   Overall discussion of results and conclusions

Main results obtained from the two research lines are summarized below.

- Research line 1: Development of fluorine-free bio-based waterborne polyurethane-urea dispersions (WPUD) and combination with (nano)materials for DWOR finishings.

The WPUD obtained were stable with particle sizes determined by DLS between 50 and 220 nm and Z potentials between -23 and -56 mV. The films obtained after drying and curing the dispersions presented a transparent and homogeneous appearance suitable for the textile coating sector. Films were used for structural characterization by FTIR and NMR and for the determination of thermal, mechanical and swelling properties.

Essay PUD_VI5 (set 1) presents the lowest glass transition temperature (T_g) and the essay 3238-3POSS (set 3) has the highest T_g and also presents another second order transition at 76.6 °C which could be attributed to the thermal mobility of the hard segments of the polymer. Figure 23 shows the stress-strain curves of some essays belonging to sets of experiments 1, 2 and 3, as well as of several non-bio-based commercial polyurethanes used in the textile coatings sector (C80, C85, RD27). In Figure 23 it can be seen how the essay PUD_VI5 (set 1) has the highest strain at break, while the essay 3238-3POSS (set 3) has the highest elastic modulus and the lowest elongation at break. The essay 3294IPDI-2 (set 2) has intermediate mechanical properties. We can conclude that, in general terms, the thermal and mechanical properties of the synthesized polyurethane-ureas were similar and in some cases superior to those of the films obtained from non-bio-based commercial polyurethanes. Therefore, the synthesized bio-based polyurethane-ureas meet the necessary requirements to be applied in the field of coatings in technical textiles, namely: low T_g, low crystallinity (to guarantee transparency), decomposition temperatures higher than industrial application temperatures, remarkable flexibility, resilience and sufficient elongation at break.
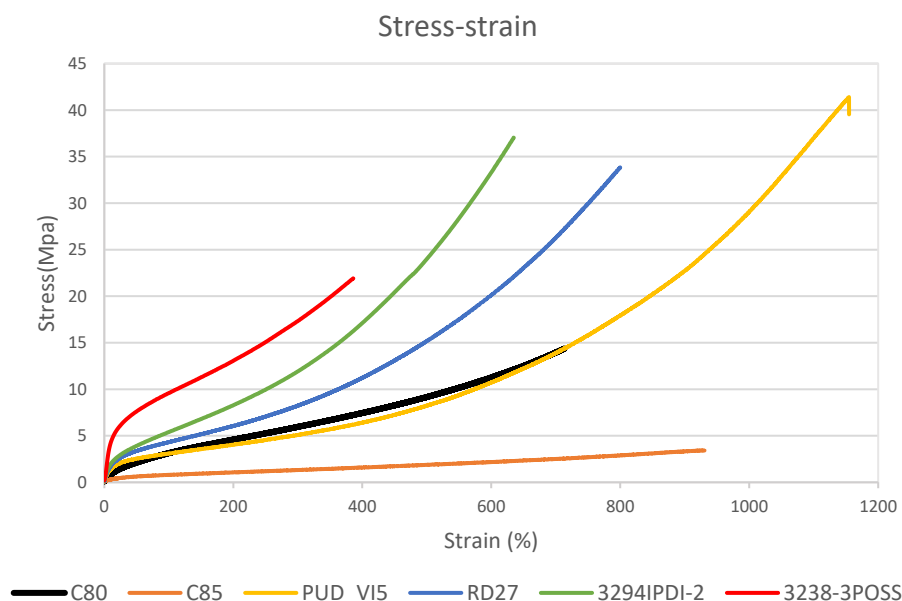
Figure 23. Stress-strain graphs obtained by standardized test BS ISO 37:2005.

The performance of the coated fabrics was evaluated through various standardized tests such as the determination of static contact angles, measurement of the water column (EN 20811:1992), air permeability (ISO 9237:1995), weft- and warp-stiffness (ČSN 80 0858) and electrical conductivity (EN 1149). The static WCAs of the coated polyester fabrics are between 107 and 135°, which means low wettability but not superhydrophobicity (>150°). Comparative example RD27 provides a slightly lower WCA and therefore lower performance in terms of water repellency. The essay 3238-3POSS (set 3) presents the best WCA value (135°), this essay incorporates POSS-OH covalently bound in the structure of the polyurethane-urea thus indicating that the incorporation of heptaisobutyl POSS side groups, highly hydrophobic and bulky, create an additional nano-roughness that favors the hydro-repellency of the coating. Figure 24 (a) shows SEM image of the fabric coated with the essay 3238-7POSS and the inset (Figure 24 (b)) is a picture of the drop of water deposited on said fabric during the WCA measurement. It is important to note that the WCAs of coated glass slides are markedly lower than the WCAs measured on the coated fabrics. Therefore, the inherent roughness of the textile substrate contributes to increasing these values. Hydrostatic pressure was assessed after coating the WPUD on polyacrylonitrile fabric for set 1 and polyester fabric for set 2 and set 3. Within set 1, essay PUD_VI5 and commercial non-bio-based polyurethane RD27 showed head pressure values of 177

and 171 cm after double-layer coating, respectively, which are good values, both above 1 m of hydrostatic pressure. Some formulations in set 2 were dopped with small amounts of SWCNT giving rise to coatings that, in addition to having good hydrophobicity and water column properties, confer electrical conductivity. In this way, multifunctional finishes could be obtained in technical fabrics suitable for work protection apparel. Figure 24 (c) shows the SEM photograph corresponding to a fabric coated with the nanocomposite obtained from the essay 3294IPDI-2 (set 2) doped with 0.05% SWCNT.
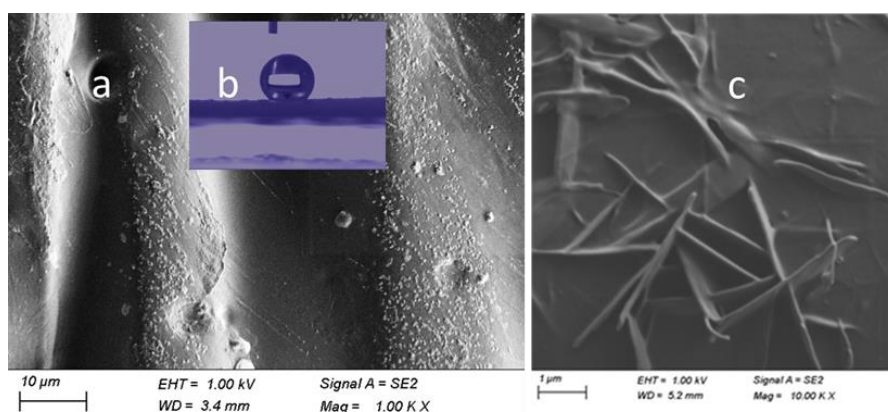

Figure 24. (a) SEM image of the fabric coated with the essay 3238-7POSS, (b) image of the drop of water deposited on said fabric during the WCA measurement, (c) SEM image corresponding to a fabric coated with the nanocomposite obtained from essay 3294IPDI-2 (set 2) doped with 0.05% SWCNT.

- Research line 2: Development of fluorine-free bio-based (co)polymethacrylate waterborne emulsions for DWOR finishings

PM3T$_x$SMA$_y$ (co)polymers displayed high molar masses as revealed by GPC. ^{1}H and ^{13}C NMR spectra of all copolymers were recorded, thus confirming chemical structure, (co)polymer composition and tacticity. Thermal properties and stability of the developed polymers were evaluated by DSC and TGA. TGA thermograms demonstrated that these copolymers were stable up to 250 °C. DSC thermograms of (co)polymers with SMA content ≥ 50 molar% (PM3T$_{50}$SMA$_{50}$ and PM3T$_{25}$SMA$_{75}$) showed the presence of melting and crystallization peaks, their enthalpies decreasing, and their melting and crystallization temperatures shifting to lower values as M3T content increases, suggesting that both comonomers are randomly incorporated in the chain during the polymerization.

Polymethacrylate emulsions were applied on cotton fabrics by padding and SEM micrographs of untreated and treated fabrics were recorded. The untreated cotton fibres showed smooth surface and cylindrical structures. After fabric was coated by polymeric emulsions, an evident roughness was generated on the surface (Figure 25). Treated fabric with 60g/L of prototype PM3T$_{50}$SMA$_{50}$ achieved WCA of 133° and OCA (olive oil) of 120°; the same fabric treated with same dosage of C6-fluorocarbon gave a WCA of 132° and OCA of 122°.

| (a) | (b) |
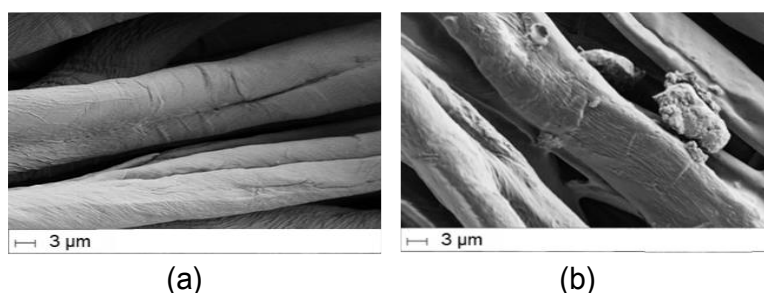
Figure 25. SEM micrographs for: (a) untreated cotton and (b) PM3T coated cotton fabric.

The anti-stain performance of PM3T$_x$SMA$_y$ (co)polymers was assessed (Figure 26). For untreated cotton, all the liquids quickly spread and penetrated. However, the cotton substrates coated with PM3T$_x$SMA$_y$ emulsions at 60 g/L retained the drop of water-based liquids on the surface. Moreover, the drop of olive oil was also maintained on the surface for PM3T and PM3T$_{75}$SMA$_{25}$ for more than 5 min.

Anti-stain performance	water	coffee	red wine	Juice + milk	Olive oil
Untreated fabric					
PM3T$_{75}$SMA$_{25}$ (60 g/L)					

Figure 26. Image of a drop of liquid after 5 min. on untreated and coated cotton textiles.

From all the experimental work carried out in this Thesis, we can draw some general conclusions.

In this work two different chemistries to confer water- and oil-repellence to textiles have been studied. In research line 1, biobased polyurethane-ureas have been developed.

Obtained WPUD show good mechanical and thermal properties and therefore were chosen to be coated onto fabrics by knife-coating. In this way we were able to coat one side of the fabrics with a continuous polyurethane-urea film, capable of drastically reducing the permeability of the textiles to water and thus conferring remarkable hydrostatic pressure values to the treated fabrics; HP values were of the same order as those obtained with non-biobased polyurethanes. Therefore, ease of filming of the obtained WPUD make them good candidates to substitute PTFE inner membranes in technical fabrics (see Figure 15) by more sustainable fluorine-free alternatives. Air permeability dramatically decreased, and stiffness increased in all of the coated fabrics compared to untreated fabrics. This is logical when considering that a polymer layer was applied on top of one of the fabric's faces. Reduced air permeability and stiffness can be a positive feature when it comes to technical fabrics with wind-stopper functionality (awnings and tents). However, water vapor breathability is highly appreciated in sports outdoor apparel, therefore new lines of research will have to be initiated to improve the breathability of these polyurethane-urea membranes without affecting their barrier properties to liquids.

In research line 2, new fluorine-free waterborne (co)polymethacrylates have been developed. These polyacrylates offer excellent performance when applied to fabric by the padding method, i.e., by total immersion of the fabric in the finishing liquor, squeezing at controlled speed and pressure, and subsequent drying and curing. Unlike research line 1, here the coatings obtained do not significantly increase the stiffness of the fabrics nor significantly reduce their air permeability. This is due to the fact that the polymethacrylate creates a thin coating on the surface of each individual fibre, giving rise to "jacketed fibres" instead a continuous film on one of the fabric's faces. Thanks to this, highly hydrophobic breathable fabrics with reasonably good oleophobic properties against fatty triglycerides have been achieved. Therefore, these polymethacrylates are good candidates to substitute side-chain perfluorinated polymers in fabric's outer layer (see Figure 10) by more sustainable fluorine-free alternatives. However, for the developed prototypes, olive oil's drops only remained on the fabrics' surface for a limited time and therefore further efforts must be devoted to achieving a more robust oil repellence.

It is important to highlight that all the developments reported in this work are stable waterborne formulations able to be applied by standard procedures and facilities in large-scale textile production, thus reducing its entry barrier to textile finishing industry. Finally, it is worth emphasizing the complementarity of the two developed lines of research, providing the textile sector with an open window to valid, sustainable, and fluorine-free solutions to achieve high-performance DWOR finishes.

3 Scientific production during the Thesis

Published papers that form part of this Doctoral Thesis
Lacruz, A.; Salvador, M.; Aliaga, J.; de Ilarduya, A.M. Síntesis, caracterización y validación aplicativa de un poliuretano bio-basado en dispersión acuosa para el sector de recubrimientos textiles. *Rev. química e Ind. téxtil* **2019**, 32–36.
Lacruz, A.; Salvador, M.; Blanco, M.; Vidal, K.; Martínez de Ilarduya, A. Development of fluorine-free waterborne textile finishing agents for anti-stain and solvent-water separation based on low surface energy (co)polymers. *Prog. Org. Coatings* **2021**, *150*, 105968, doi:10.1016/J.PORGCOAT.2020.105968.
Lacruz, A.; Salvador, M.; Blanco, M.; Vidal, K.; Goitandia, A.M.; Martinková, L.; Kyselka, M.; de Ilarduya, A.M. Biobased waterborne polyurethane-urea/SWCNT nanocomposites for hydrophobic and electrically conductive textile coatings. *Polymers (Basel).* **2021**, *13*, doi:10.3390/POLYM13101624.
Lacruz, A.; Salvador, M.; Blanco, M.; Vidal, K.; Goitandia, A.M.; Martinková, L.; Kyselka, M.; de Ilarduya, A.M. Biobased waterborne polyurethane-ureas modified with POSS-OH for fluorine-free hydrophobic textile coatings. *Polymers (Basel).* **2021**, *13*, doi:10.3390/POLYM13203526.
Lacruz, A.; Salvador, M.; Aliaga, J.; Camps, J.; de Ilarduya, A.M. Poliuretano-ureas bio-basados en dispersión acuosa para el sector de recubrimientos textiles. *Rev. plásticos Mod. Cienc. y Tecnol. polímeros* **2021**, *122*, 3.

Oral communication in congress
Oral communication at GEP-SLAP2022 Congress. Lacruz, A.; Salvador, M.; Blanco, M.; Vidal, K.; Martínez de Ilarduya, A. Fluorine-free waterborne textile finishing agents for anti-stain and solvent-water separation based on low surface energy (co)poly(methacrylate)s.

4 Scale-up in pilot plant

4.1 Laboratory and industrial pilot plants

Once successful prototypes were obtained on a small scale (up to 150 g), to continue advancing with the project and to be able to manufacture them in larger quantities, we have set-up a laboratory and an industrial pilot plant that allows the manufacture of up to 2 kg and up to 50 kg of polymer emulsion, respectively. All the prototypes from research lines 1 and 2 have been manufactured in an amount ranging from 0.5 to 1.5 kg in the laboratory pilot plant. At the present time, only some prototypes from research line 2 have been manufactured in the industrial pilot plant. More specifically, two batches of 50 kg of a prototype similar to PSMA described in research line 2 [98] have been manufactured in the industrial pilot plant. Both, laboratory and industrial pilot plants have the same main elements as shown in Figure 27. Ultrasonication unit is only necessary for acrylic prototypes.
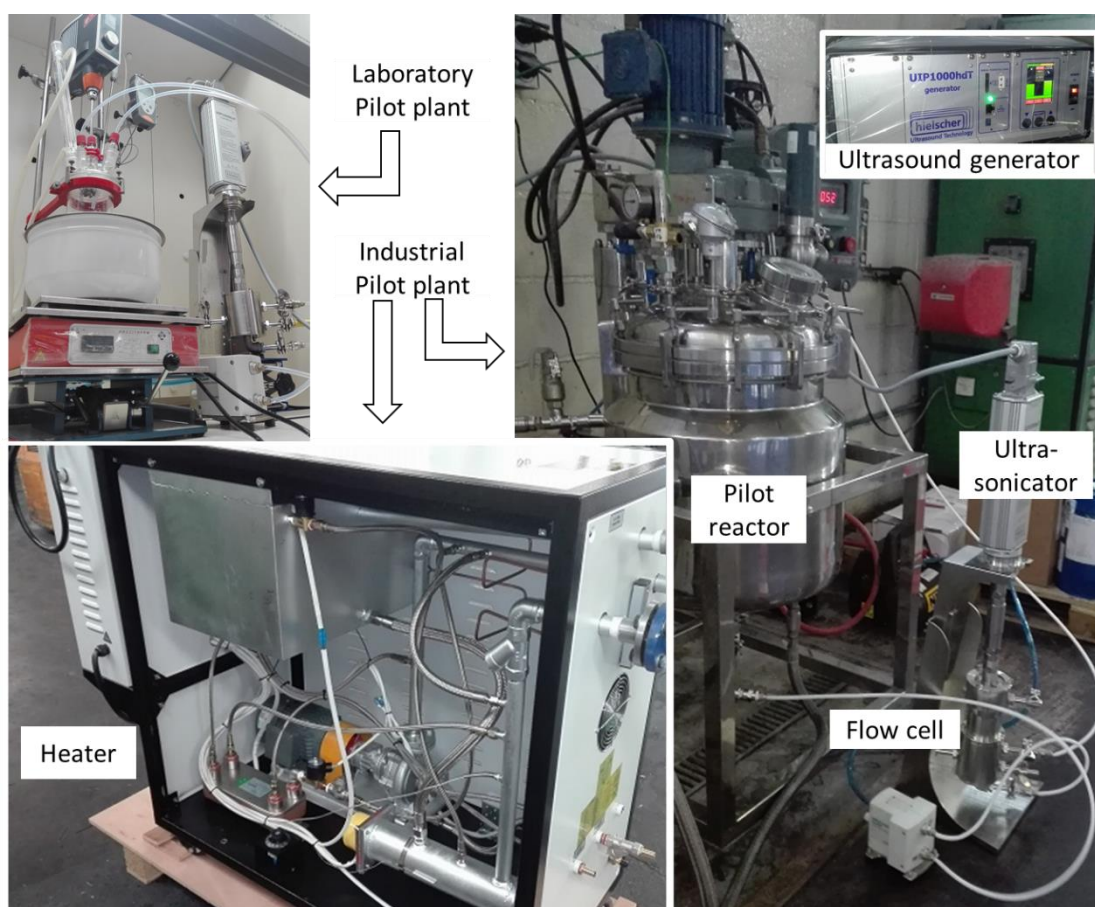

Figure 27. Pictures of the laboratory and industrial pilot plant.

The laboratory and industrial pilot plants are mainly made up of three units, the pilot reactor, the thermal oil heater & temperature controller, and the sonication unit. The rest of elements such as pumps, compressor, nitrogen blanketing, etc. are auxiliary elements that allow the correct operation of the installation and process (see Figure 28).

The industrial pilot reactor is a mobile and vertical equipment. It is made up of two enclosures, the body and the heating/cooling jacket, and it is entirely made of mirror-polished stainless steel. The body is a hermetically sealable vessel, it is equipped with a two-heights impeller system and can be fully opened and accessed by elevating the top Klopper lid by means of a hydraulic piston. The lid is closed and adjusted with the eyebolts distributed around the perimeter. The raw materials are loaded into the tank manually or by pumping through the specific nozzles. The industrial pilot reactor has auxiliary nozzles for adding raw materials or additives, nitrogen blanketing, sample withdraw and to unload the final product.

The main technical characteristics of the pilot industrial reactor are summarized below:
- 60 liters of capacity.
- Inspection hatch with a Pyrex-glass window.
- 6 service nozzles with clamp type connection.
- Impeller agitation system with variable-speed drive.
- Interior vessel with two baffles.
- Double temperature control with PT100.
- Relief valves.
- Heating / cooling jacket for thermal fluid recirculation
- Top Klopper lid with hydraulic piston.
- Bottom valve.

Acrylic (co)polymers in research line 2 were obtained by miniemulsion polymerization. Emulsification of highly hydrophobic monomers in water using low amounts of external emulsifiers requires a high-energy emulsification method in order to obtain stable emulsions before, during and after polymerization. In this work, an industrial ultrasonicator model Hielscher UIP 1000hdT has been used, which allows both, batch

sonication of small quantities and continuous sonication of larger quantities using a flow-cell (industrial scale).

Acoustic cavitation is the driving force behind ultrasonic processing. When a liquid is ultrasonicated, micro-bubbles grow, oscillate extremely fast, and eventually collapse. Extreme conditions inside the bubbles (about 5000 K, 2000 atm.) generate powerful micro-jets and shock waves upon its implosion that hit the matrix, generating fragmentation. UIP 1000hdT ultrasonic processor operates at the lower edge of ultrasonic spectrum, 20 kHz, to maximize mechanical shear forces induced by cavitation, and has a power of 1000 W. It is equipped with a booster model B4-1.4 for mechanical increase (1:1.4) or decrease (1:0.71) of the amplitude at the sonotrode. Two sonotrode probes are available to be coupled to the booster: model BS4d22 (tip diameter 22 mm, effective work surface approx. 3.8 cm² and amplitude ratio 1:2.4) and model CS4d40L2 (tip diameter 40 mm, effective work surface approx. 33 cm² and amplitude ratio 1:1.4), for small and large volumes, respectively. This device allows to control the sonication amplitude (A) which is a parameter that measures the distance between the horn's fully extended and fully contracted positions, measured in microns (μm). Amplitude is set to a certain level in %, which corresponds to a value in microns that can be identified using the horn's calibration certificate. Once the amplitude is set, it will remain at the same level throughout the sonication process. The amplitude and the intensity of cavitation are directly related (A α Cavitation). The power conveyed from the generator to the sonicated sample is displayed in real-time on the generator's screen in watts (W), this power cannot be set directly because it depends on several parameters like A, horn immersion depth (for batch configurations), pressure (for closed-flow-cell configurations), sample viscosity, etc. The generator automatically adjusts the power to keep the default value of A. At the end of the sonication process, the software from Hielscher provides the total energy supplied to the sample in Watts second (W·s) or Joules (J), this value can be divided by the total weight of sonicated sample to obtain the specific energy (kJ kg⁻¹) conferred to the sample after the sonication process.
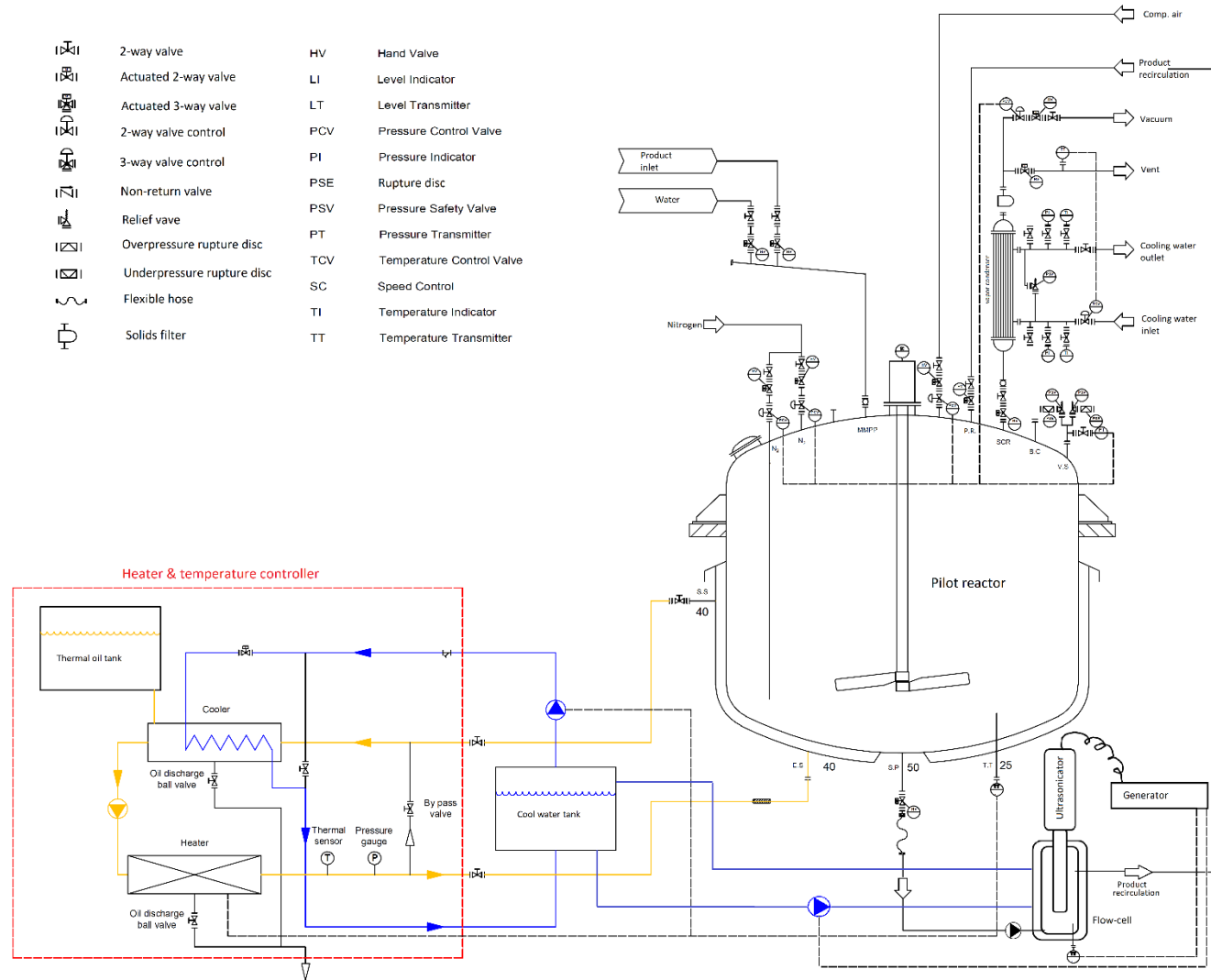
Figure 28. Scheme of the main elements of the laboratory and industrial pilot plants.

4.2 Industrial scale-up in research line 2. Emulsion characterization

The advantage of ultrasonic emulsification is its scalability. The optimum specific energy to be conferred to the sample to get the desired properties can be determined with batch essays at lab scale, afterwards the up-scale is quite simple and basically has to ensure that the same level of specific energy is reached for larger batch sizes. The scale-up work of the acrylic prototypes consisted of investigating the variation of the particle size (PS), determined by dynamic light scattering (DLS), and the stability of the emulsions (Z-potential) before polymerization (monomer emulsions) with the sonication conditions (amplitude and time). For this purpose, a 3^2 factorial design of experiments (DOE) was proposed where 2 factors were considered, which are the time and the amplitude of sonication, at 3 levels each factor (1, 2 and 3 min. and 55, 65 and 75 % for time and amplitude, respectively), performing a total of 9 essays. Additionally, the emulsions subjected to 3 min. of sonication were polymerized and the PS and the Z-potential of the final latexes were also measured.

All of the essays have been named beginning with "TD" and followed by the applied sonication amplitude and time. For instance, essay TD55-1 was sonicated at A = 55 % for 1 min. All of the "TD" essays had identical monomer composition, water content and emulsifying system. Monomer composition and emulsifying system from "TD" essays cannot be discussed in detail here due to confidentiality reasons. Suffice it to say that composition of "TD" essays is similar to that described for essay named "PSMA" in research line 2 [98] but stearyl methacrylate has been replaced by a mixture of stearyl acrylate (main co-monomer) and crosslinking acrylic monomers (minor co-monomers); emulsifying system has also been slightly modified with respect to "PSMA" essay by incorporation of a proprietary cationic co-surfactant. All of the experiments have been performed by sonication of 130 g of sample with a sonotrode model BS4d22 and keeping temperature between 60 – 65 °C. All of the PS and the Z-potential measurements were performed at 20°C using a Malvern Zetasizer ZS and previously diluting all of the emulsions with deionized water to 30 g/L. Table 1 summarizes PS and ZP results from experimental design.

Table 1. Particle size, Z potential and polydispersity index measured from the monomer emulsions subjected to different amplitudes and sonication times.

Essay	A (%)	t (min.)	Average power (W)	Specific energy (kJ/kg)	PS (nm)[a] / PdI	Z-pot. (mv)[a]	PS (nm)[b] / PdI	Z-pot. (mV)[b]
TD55-1	55	1	133.0	61.4	206 ± 2	-	-	-
TD55-2	55	2	133.0	123.1	186 ± 1	-	-	-
TD55-3	55	3	133.5	185.2	161 ± 1 / 0.168	+52 ± 1	84 ± 2 / 0.144	+51 ± 3
TD65-1	65	1	156.4	72.3	201 ± 1	-	-	-
TD65-2	65	2	154.6	144.0	175 ± 1	-	-	-
TD65-3	65	3	151.4	214.3	159 ± 3 / 0.189	+50 ± 1	86 ± 1 / 0.149	+51 ± 2
TD75-1	75	1	182.6	84.2	199 ± 3	-	-	-
TD75-2	75	2	180.2	167.5	164 ± 3	-	-	-
TD75-3	75	3	177.6	249.9	154 ± 3 / 0.183	+52 ± 5	90 ± 1 / 0.153	+53 ± 2

[a] *before polymerization,* [b] *after polymerization*

Within the range of amplitudes studied, it was observed that after 1 min. of sonication, all the monomer emulsions presented an appreciable amount of non-emulsified monomer, which immediately tended to separate on the surface. This can also be seen in the size distribution by intensity graphs (Figure 29) where a bimodal distribution is observed with a main peak around 200 nm and a small peak around 5000 nm. Some monomer emulsions at sonication time of 2 min. still present a very mall peak around 5000 nm while all the emulsions at sonication time of 3 min. were monomodal. This is an indication that a sonication time of 1 min. is not sufficient for stable droplet formation while 3 min. is a safe sonication time to ensure complete homogenization. Figure 30 shows the surface plot of PS versus sonication time and A, generated by de DOE software Minitab. From surface plot can be inferred that sonication time has more influence in reduction of PS than A.
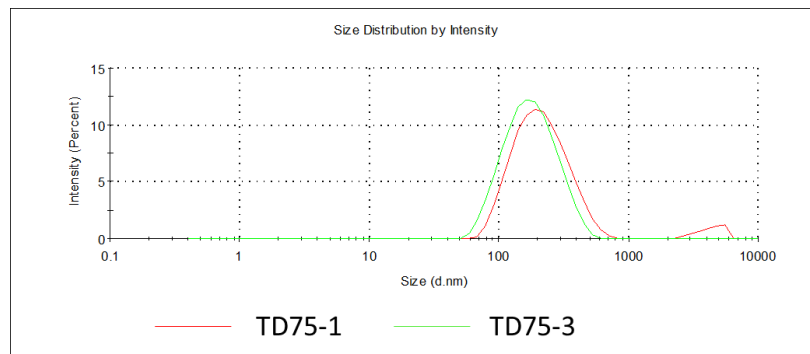
Figure 29. Size distribution by intensity graphs of monomer emulsions sonicated with A= 75% for 1 min (red) and 3 min. (green).
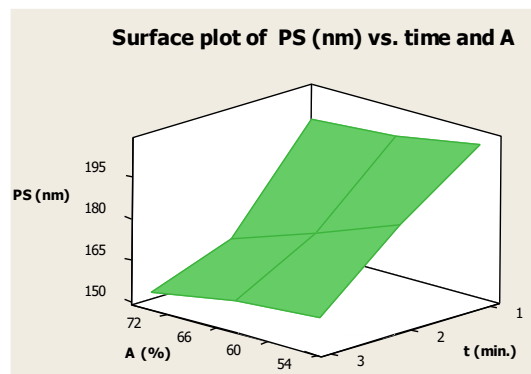

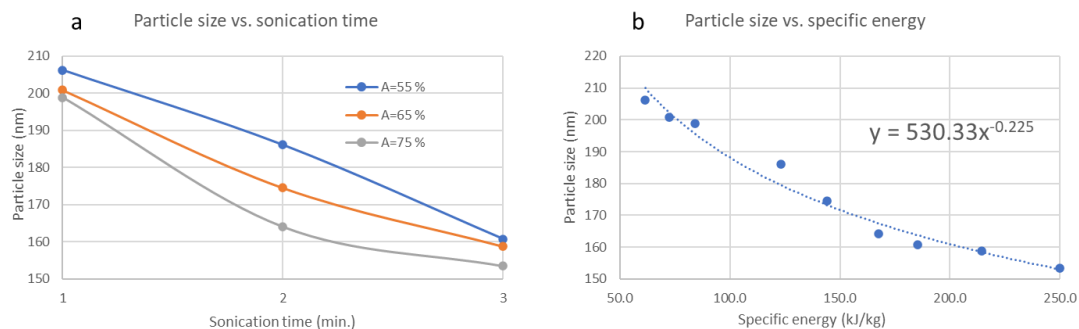*Figure 30. Surface plot of PS vs. sonication time and amplitude generated from DOE Minitab software.*

Figure 31. (a) Particle size vs. sonication time at A = 55, 65, and 75% for monomer emulsions. (b) Particle size vs. specific energy for monomer emulsions; blue dots are the experimental points and dot line is the fitting function.

In Figure 31 (a) and Table 1 can be seen how PS decreases with A at a fixed time, being this effect more evident after two min. of sonication. Particle size greatly decreases with time at a given amplitude. This is consistent with the fact that cavitation is proportional to amplitude and that it is a cumulative phenomenon. During the first minute of sonication, cavitation has been mainly employed in forming oil in water emulsion from

the two immiscible phases (monomers and water), giving rise to monomer droplets with PS around 200 nm. During the second min. of sonication the formed droplets are further impacted by cavitation bubbles, with a reduction in PS of 10%, 13% and 18% for A = 55, 65 and 75%, respectively. After 3 min. of sonication a total reduction of PS is around 22% with respect the first min. of sonication, reaching a particle size around 160 nm, for all the amplitudes. Figure 31 (b) is a plot of particle size vs. specific energy, which is proportional to A and sonication time for a given batch size. The experimental points fit reasonably well to an exponential function (R^2 = 0.97) which suggests that, under the experimental conditions studied, applying specific energies above 250 kJ kg^{-1} will not lead to further drastic reductions in particle size. Accordingly, experiment TD55-3 with a total applied specific energy of 185 kJ kg^{-1} for batch processing, seems to have a good compromise between sonication A, sonication time and energy consumption to get monomer droplets with particle size ranging 160 nm. Therefore, essay TD55-3 was selected for scaling-up in the pilot industrial plant. Before performing the 50 kg batch, 1 kg the of the same monomer emulsion was sonicated using the in-line process from the laboratory pilot plant which consist of continuous sonication at a flow rate of 0.4 kg min^{-1} using the flow cell equipped with the sonotrode BS4d22, working at A = 55 % (average power 135 W). Under these conditions, 1 kg of emulsion takes 2.5 min. to pass through the sonication chamber, therefore, PS was measured every 2.5 min. and recirculation was stopped when PS ≈ 160 nm. The time necessary to reach PS ≈ 160 nm was 12.5 min. and total applied specific energy for in-line system under the specified working conditions was 101 kJ kg^{-1}. As can be seen, continuous sonication allows us to further decrease specific energy due to optimized geometry of flow-cell's sonication chamber; the pre-emulsification work performed by the impeller blades from the 1 L reactor and the shear conferred by the pumping system also led to further reduction of sonication specific energy. With the value of 101 kJ kg^{-1} in mind, to process 50 kg of monomer emulsion in 3 h, a power of 0.47 kW will be required. To achieve a sonication power of 0.47 KW, the sonotrode BS4d22 (small volumes) must be replaced by the cascatrode CS4d40L2 (big volumes) which has a higher working surface. According to the manufacturer's technical parameters, the sonotrode BS4d22 working at A = 55 % has a mechanical amplitude of 44 μm. Cascatrode CS4d40L2 has a maximum mechanical amplitude of 42 μm (A = 100 %). However, we decided not to work at the maximum

amplitude to maximize the durability of the cascatrode and instead we chose to set A = 85 % (36 μm) because under this amplitude an average power of 0.5 kW was supplied by the sonicator. Finally, 50 kg of monomer emulsion were sonicated using the cascatrode CS4d40L2 with the in-line configuration at A = 85 % (average power of 0.5 kw), a processing time of 3h and a flow rate of 2 kg min^{-1}, reaching a PS of 156 nm. A second batch with the same processing conditions was performed, obtaining a PS value of 154 nm and thus confirming operating settings of the industrial pilot plant.

Our polymerization system is consistent with the definition of miniemulsion polymerization described in the literature [106–108], where the monomer droplets at the onset of polymerization usually have a PS between 80 and 200 nm [106]. As interfacial area of monomer droplets in miniemulsion systems is very large, most of the surfactant is adsorbed at the droplet surface and therefore free emulsifier molecules are below its critical micellar concentration (CMC). Consequently, there are no surfactant micelles within the continuous phase (water) and only a low concentration of molecularly dissolved surfactant is present. As a consequence of that, mechanism of miniemulsion polymerization is simpler than conventional emulsion polymerization. In miniemulsion polymerization all the monomer droplets are hit by radicals and become latex particles, i.e., the reaction proceeds by polymerization of the monomer within the miniemulsion droplets. Therefore, in miniemulsion polymerization, droplet nucleation is the dominant particle nucleation process, unlike emulsion polymerization where homogeneous and micellar nucleation dominate. Z-potential (ZP) has been assessed for all of the monomer emulsions after 3 min. of sonication finding absolute values of ZP above 50 mV for all the studied amplitudes, which suggests a good stability of the monomer emulsions [109,110]. To support that, the monomer emulsions sonicated for 3 min. at A = 55, 65 and 75% were polymerized for 6 h at 65°C and PS and ZP values were measured for the emulsions after polymerization (see Table 1). PS values for all the polymerized emulsions are between 90 and 84 nm which means a decrease of more than 40% in the particle size after complete polymerization of the monomer emulsions. Therefore, the resulting latex emulsions can be classified as nano emulsions (PS < 100 nm). It is also worth to mention that ZP has been measured for all of the polymerized emulsions and absolute values of ZP above 50 mV for all of the studied amplitudes were

found. Therefore, emulsion stability during and after polymerization is good and shows ZP values similar to those of the emulsions before polymerization. Moreover, our work shows that the addition of traditional co-stabilizers like cetyl alcohol or hexadecane to prevent Ostwald ripening [111] is not necessary here because the employed acrylic monomers are highly hydrophobic and act as a reactive co-stabilizers as reported in previous works [112,113]. As reported above, a mixture of non-ionic and cationic surfactants has been employed in all the essays at the same concentration to enhance colloidal stability and retard droplet coalescence, creaming and settling. Cationic surfactant confers electrostatic stabilization to monomer droplets while non-ionic surfactant act as a steric stabilizer [114]. According to several authors [106,115], for miniemulsion polymerization, PS of the latex particles after polymerization should be similar to the PS of the precursor monomer droplets. However, for the system studied here, PS of the final latex particles is 40% smaller than that of the monomer droplets before polymerization, as it can be seen from PSD curves in Figure 32 for essay TD55-3 (before polymerization) and TD55-3P (polymerized latex).
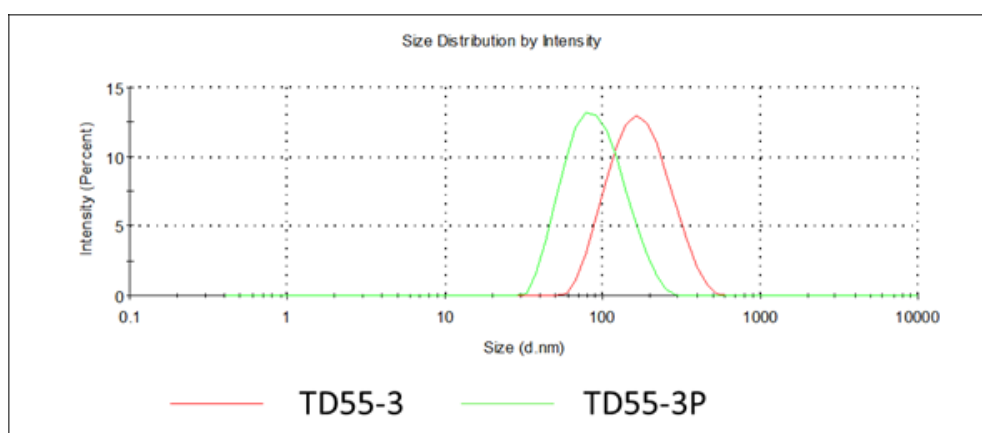

Figure 32. PSD curves of essays TD55-3 (before polymerization) and TD55-3P (polymerized latex).

Also, it is important to highlight that polydispersity index (PdI), that gives an indication of the broadness of the PSD curve, is always lower in the final latex in comparison to the initial monomer emulsion (Table 1). Huang et al. [107] reported for miniemulsion copolymerization of styrene and butyl acrylate a reduction of particle size of about 35% between the initial stage (0% conversion) and an intermediate stage (20% conversion), however, as conversions progressed to higher values, PS also increased reaching PS values at 90% conversion only 11% lower than that of the initial monomer droplets. For

our studied system, one possible explanation for the observed decrease in PS in the final latex with respect to the initial monomer emulsion could be that some extent of micellar nucleation could co-exist together with droplet nucleation [116]. This could occur due to the desorption of some surfactant molecules from the droplet interface. This desorption would occur during the 6 h of polymerization at 65ºC, giving rise to the formation of surfactant micelles in the continuous medium (water), smaller in diameter than the monomer droplets. Within these micelles, micellar nucleation could take place, giving rise to a population of particles of smaller diameter than the monomer droplets of the initial emulsion, thus shifting PS to lower values. Other possibility is that particle nucleation takes place predominantly within the smallest monomer droplets (<100 nm), while larger monomer droplets (>100 nm) act as a monomer reservoir that slowly migrates to surfactant micelles and/or to small droplets where eventually polymerization takes place. It is worth considering that the density of the resulting polymer (polystearyl acrylate, 0.94 g cm^{-3} at 20 °C) is higher than that of the monomer (0.80 g cm^{-3} at 20 °C), this could partially explain the decrease in PS after polymerization. However, these differences in density would surely not explain the 40% decrease in PS observed after polymerization [108]. Finally, it is important to highlight that PS measurements of the initial monomer emulsions have been performed 24 hours after sonication. This is due to the fact that the sonicator and the DLS are placed in different locations and it is not possible to carry out the measurements just after sonication. Consequently, some aggregation of monomer droplet could have taken place during this time, leading to higher PS values with respect to the freshly sonicated monomer emulsions. Therefore, more research needs to be done to clarify this point.

4.3   Application of the prototypes on fabrics using pilot and industrial facilities

Prototypes obtained in the framework of this Thesis have been manufactured in sufficient quantity to be applied on fabrics using (semi)industrial machinery.

In this section, two application methods are going to be differentiated: impregnation (padding), and knife coating. Polyurethane-ureas from research line 1 are specifically designed to be applied by knife coating while acrylic prototypes from research line 2 are intended to be applied by padding or exhaustion.

4.3.1   Methods for fabric characterization

The durability of the DWOR finishing applied onto fabrics has been assessed by measuring certain properties before and after repeated washings. The washings have been carried out according to ISO 6330, 4N which reproduces domestic laundry conditions.

The treated fabrics were tested to measure different properties as water column, stain-release, water-vapor resistance (R_{et}), spray test, absorptivity and water drop test.

Water column has been assessed according to standard EN 20811:1992. Briefly, the fabric is subjected to a steadily increasing pressure of water on one face, under standard conditions, until penetration occurs in three places (three drops passing through the fabric). The water pressure may be applied from below or from above the test specimen. The hydrostatic head supported by a fabric is a measure of the resistance to the passage of water through the fabric.

Figure 33. Device used to the measurement of resistance to water penetration -water column or hydrostatic pressure test-. (a) General view, (b) pressure unit, (c) the fabric begins to yield to the water pressure, as denoted by the appearance of water droplets.

To check the performance of a stain-resistant finish we have developed a personalized variant of the so-called Tchibo test developed by Huntsman, a chemical company that markets stain-resistant finishes. Briefly, soiling products have been selected for the test: coffee, juice & milk, red wine, olive oil, motor oil, mustard and ketchup. Then the treated fabric with the anti-stain finishing is stained with a drop of each product and assessed initially, after 5 min. and after wiping of the product. The same testing procedure is repeated but replacing the treated fabric with a treated fabric that has been subjected to 5 washes at 40 °C. The assessment is made according to a 5-points criteria that allow to assign the anti-stain rate for each product, see Table 2.

Table 2. Guidelines to assign the anti-stain performance.

Rating	Appearance of the textiles
4	drop remains on the fabric's surface after 5 min., no wetting is observed, no stain residue remains after removing the drop
3	drop remains on the fabric's surface after 5 min., no wetting is observed, slight stain residue remains after removing the drop
2	partial wetting of the fabric surface by the drop after 5 min., stain residue remains after removing the drop
1	partial wetting of the fabric surface by the drop after 5 min., clear visible stain residue remains after removing the drop
0	complete wetting of the fabric surface by the drop after 5 min

In ISO 11092, the water vapor resistance of the fabric (R_{et}) refers to the ratio of the water vapor pressure difference on both sides of the fabric (P1, P2) to the heat flux evaporated

vertically (Q) per unit area of the fabric (S), see Equation 14. The units of R_{et} are square meters pascal per watt, m²·Pa W^{-1}, the lower this value, the greater the breathability to water vapor and the greater the comfort of the garment. The schematics of the device to measure R_{et} according to ISO 11092 is shown in Figure 34. Briefly, the samples (26 x 26 cm) are placed onto an electrically heated porous plate (thermoregulation model of the human skin). The plate is placed in a climatic chamber and a fan blows air with defined temperature, humidity and velocity tangentially onto the surface of the sample. In order to avoid heat loss, the measuring plate is surrounded (underneath and on the sides) by a guard which is heated to the same temperature as the plate (35°C). The measuring surface is covered by a foil permeable to water vapor but impermeable to liquid water. Water is supplied to the plate to allow a water vapor flow from the surface. The water vapor resistance is assessed using the heating power supplied to the surface under steady-state conditions (as a measure of the amount of vaporized water), the pressure difference between the atmosphere and the plate, and the size of the plate.

$$R_{et} = \frac{s(P1 - P2)}{Q}$$

Equation 14. R_{et}
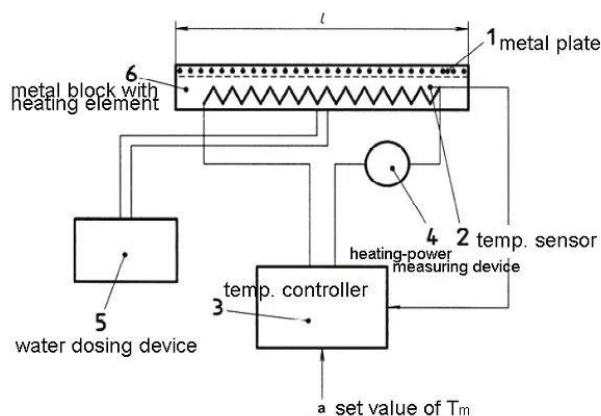
Figure 34. schematics of the device to measure R_{et} according to ISO 11092.

Spray test method (ISO 4920:2012) has been used for determining the resistance of a fabric to surface wetting by water. The determination of the spray test has been carried out using the ISO 4920:2012 standard. Briefly, this standard consists of arranging a fabric

at 45° under a funnel that has a perforated shower of standardized dimensions and size as discharge, located at a height specified by the standard. A measured amount of water at 25ºC is introduced into the funnel, the liquid discharges onto the fabric impacting on it. Depending on the fabric's water repellency and impact resistance, water is repelled to a greater or lesser degree, the result being rated with the help of reference images (Figure 35).
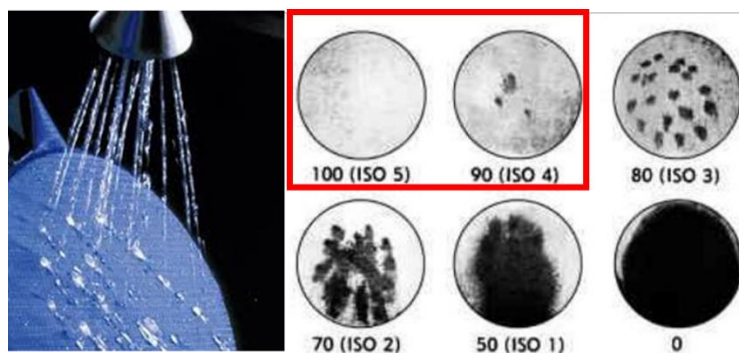

Figure 35. Spray test according to ISO 4920:2012. On the right reference images to assign the ratings.

Absorbability according to standard ČSN 80 0831:1970 Method 7 measures the capacity of a fabric to absorb water. Briefly, a fabric sample of 10 x 10 cm is cut and weighted (W_0). Afterwards the specimen is immersed in distilled water at 24 °C for 1 min. avoiding swim-up, then the sample is pulled out, hinged vertically for 5 min. to remove the excess of water and weighted again (W_i). The absorbability is measured as the wt. % of water absorbed by the fabric (Abs = [W_i-W_0] 100/W_0). The test is performed by triplicate.

Water drop test consists of carefully depositing a drop of water of known volume, 100 μL in our experiment, on the surface of the fabric and measuring the time it takes for the drop to wet the fabric. It is also a measure of hydrophobicity.

Air permeability was measured according to ISO 9237. Briefly, the rate of air flow passing perpendicularly through a given area of fabric is measured at a given pressure difference across the fabric test area over a given time period. The air permeability of a fabric is a measure of how well it allows air to pass through a fabric. The parameters affecting the air permeability of the fabric are the spacing between the warp and weft yarns, the weave structure and the porosity of the yarn.

Tensile strength was determined according to ISO 13934-1 STRIP. It is a procedure to determine the maximum force and elongation at maximum force of textile fabrics using a strip method. The machine measures the force applied to the test specimen in stretching it to rupture and the corresponding extension of the test specimen.

4.3.2 Application results

For research line 1 (polyurethane-ureas) we have been able to manufacture up to 1.5 kg of the prototypes described in [95] and [96] using Color Center's laboratory pilot plant. With these amounts, application trials have been performed using INOTEX coating facilities.

In the case of research line 2 (polyacrylates), 100 kg of prototype TD55-3P have been manufactured, mixed with paraffin emulsion and waterborne blocked isocyanate and renamed as compound ARK/ICL-1. Paraffin and isocyanate have been added to improve spray test rating and increase wash fastness, respectively. ARK/ICL-1 has been applied onto different fabrics using the laboratory and pilot plant from INOTEX. Also, industrial trials using standard industrial machinery have been performed. A summary of the most representative application results is provided below.

4.3.2.1 Pilot trials with polyurethane-ureas carried out at INOTEX

Polyurethane-urea prototypes from published works [95] and [96] have been manufactured in quantities up to 1.5 kg, formulated as a printing pastes as described in [95] and [96], and face-coated onto Upron fabric using knife-coating machine and drying/curing oven from INOTEX. Industrial applicability and runnability of the printing pastes has been confirmed using INOTEX coating pilot plant. In Figure 36 can be seen the pilot knife-coating process for prototypes 3294IPDI-2 and 3294IPDI-2/SWCNT-0.1 wt. %. Water column values between 33 and 45 cm and tilt angles with water ranging from 24 to 29° have been obtained for single coatings onto Upron fabrics, respectively, thus indicating more than acceptable hydrophobicity values. Water vapor resistance (R_{et}) of prototype *3294IPDI-2* (63 mol. % semicrystalline polyol Priplast 3294) has been measured, being 1629 and 1458 m^2 Pa W^{-1} for face side and back side to unit, respectively. This value is 2 times higher that R_{et} measured for the polyurethane-urea prototype *3238-2* from our published work [96] (63 mol. % fully amorph polyol Priplast 3238). Thus, the higher crystallinity of soft segments seems to limit the moisture transfer efficiency. This behavior has also been reported by Shu-Yi Chen et al. [117].
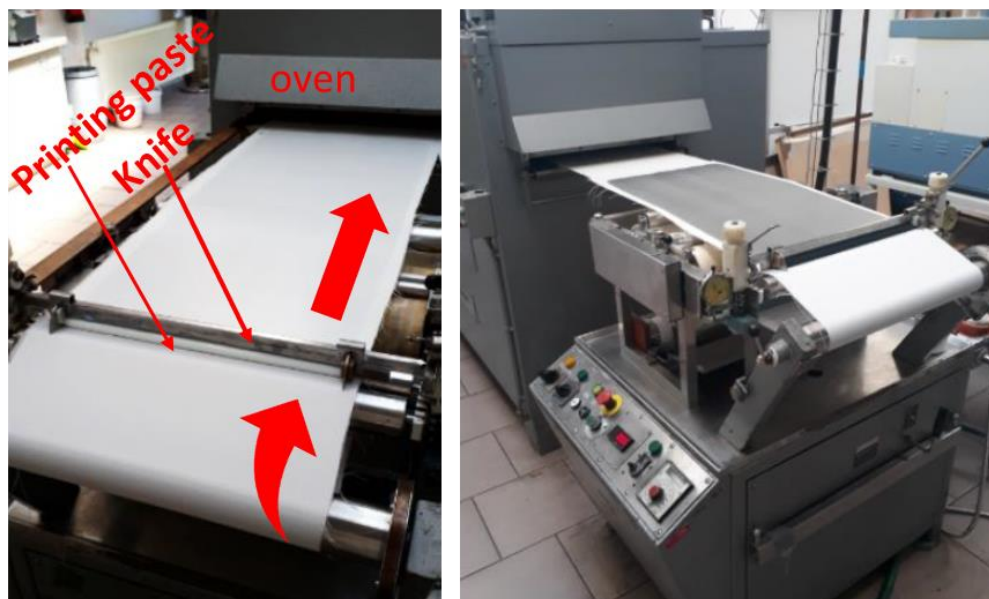
Figure 36. Knife coating process for prototypes 3294IPDI-2 (left) and 3294IPDI-2/SWCNT-0.1 wt. % (right). Coating conditions: air-knife single coating on one of the fabric faces, followed by drying 2 min. at 110 °C and curing 3 min. at 150 °C. Average dry add-on for all of the coated fabrics was 25 g m^{-2}.

Soil resistant properties have been assessed for Upron fabrics face-coated with selected polyurethane-urea prototypes, see Figure 37. Upron fabrics coated with polyurethane-ureas present very good stain-release properties, especially for water-based stains (coffee, milk & juice, red wine), but also for mustard and ketchup. Pure oils (olive oil and motor oil) spread on the coated surface and leave some mark after wiping out the drop (not fully appreciated in the pictures). However, olive oil does not penetrate to the other side of the coating, thus the polymeric layer confers a good barrier to vegetal triglycerides despite it is not hydrophobic. Stain release properties seems to be slightly better for polyurethane-ureas based on semicrystalline polyol (3294 series), this could be attributed to a tighter packing of the alkyl chains from the polymer.

3294IPDI-2								
100 % PES Upron	water	coffee	milk & juice	red wine	olive oil	motor oil	mustard	ketchup
0 min.								
5 min								
drop removed								
Score	4	3-4	4	3-4	1*	1	4	4

3294IPDI-2/SWCNT 0.05%								
100 % PES Upron	water	coffee	milk & juice	red wine	olive oil	motor oil	mustard	ketchup
0 min.								
5 min								
drop removed								
Score	4	4	4	4	1*	1	4	4

3238-3POSS								
100 % PES Upron	water	coffee	milk & juice	red wine	olive oil	motor oil	mustard	ketchup
0 min.								
5 min								
drop removed								
Score	4	3	3-4	3-4	1*	0-1	3	3

Figure 37. Stain-release tests for selected polyurethane-ureas: 3294IPDI-2 (top left), 3294IPDI-2/SWCNT-0.05 wt. % (top right) and 3238-3POSS (down). Prototypes named beginning by 3294 are based on semicrystalline polyol while prototype 3238-3POSS is based on fully amorph polyol and contains a 27 mol. % of POSS.
*olive oil spreads the coated layer but does not penetrate the fabric.

4.3.2.2 Pilot trials with prototype ARK/ICL-1 carried out at INOTEX

Four pilot trials were performed with the compound ARK/ICL-1 by padding, each trial was carried out using a selected fabric widely used in the textile market. Padding was performed in a continuous Benz line from INOTEX (Figure 38) equipped with padding unit and drying/curing oven. The main application parameters for pilot trials are summarized in Table 3.

Figure 38. Continuous Benz line from INOTEX.

Table 3. Summary of the main application parameters for pilot trials with prototype ARK/ICL-1.

	Pilot trial 1	Pilot trial 2	Pilot trial 3	Pilot trial 4
Technology / Machinery	Impregnation-Dry-Curing /Continuous Benz line-INOTEX Fabric width 50 cm, fabric length 3.2 m.			
Fabric characteristics	Cotton 100% (**ref. GABRIELLA**) 158.3 g/m² Threads/cm (EN 1049-2) warp = 50 / weft = 29	Cotton / PET 50/50 wt. % (**ref. GOLEM**) 138.8 g/m² Threads/cm (EN 1049-2) warp = 27 / weft = 27	PET 100% Tech. Textiles (**ref. UPRON**) 168.9 g/m² Threads/cm (EN 1049-2) warp = 40 / weft = 16	PET 100% Outdoor (**ref. UTEX**) 73.0 g/m² (rip-stop) Threads/cm (EN 1049-2) warp = 39 / weft = 38
Wet pick-up[a]	75%	78%	63%	28%
Processing conditions	80 g/L ARK/ICL-1 Drying 120 °C, 2 min (1 m/min.) Curing: 120 °C, 2 min (1.2 m/min.)			

[a] *Wet pick-up is expressed by the following equation:* $Wet\ pickup = \frac{W_2 - W_0}{W_0} * 100$ *, where W_2 is the weight of fabric after impregnation and W_0 is the initial weight of the fabric before impregnation.*

Water vapor resistance for the fabrics finished with ARK/ICL-1 at 80g/L were measured and compared to the values of the untreated fabrics, see Table 4. Water vapor resistance

of the untreated fabrics and treated fabrics is very similar which means that finishing with prototype ARK/ICL-1 do not alter the water vapor permeability of the fabrics. In addition, R_{et} values are low for all of the fabrics and therefore the comfortability (sweat evacuation) is very good, this is important if fabrics are intended for garment. Spray test rate for the fabrics treated with ARK/ICL-1 at 80g/L were measured and compared to the values of the untreated fabrics and treated fabrics with 5 and 10 washes; three measurements have been performed on each fabric, see Table 4. Regarding spray test, it is important to highlight that values obtained from unwashed fabrics are lower than values obtained after 5 washes (except for Gabriella which remain unchanged). A possible explanation to this behavior is that, after 5 washes, the emulsifying system used in the synthesis of the polymer is removed from the fabric and therefore hydrophobicity is enhanced. For Gabriella, a fabric made of 100 % cotton, we do not see this effect, this could be explained because emulsifiers, especially cationic ones, are more strongly adsorbed on the cotton fibers in comparison to PET fibers. In Figure 39 average spray test is shown for the untreated, treated and washed fabrics. After 10 washes only a slight decrease in spray test is observed, which means that the durability of the hydrophobic treatment in good. Also, it is important to note that 100 % PET fabrics (Upron, Utex) reach higher spray test than 100 % cotton (Gabriella) or cotton / PET (Golem), this could be ascribed to the intrinsic hydrophilicity of the cellulosic fibers which bear hydroxyl groups thus being more difficult to render them hydrophobic. Air permeability values before and after hydrophobic treatment are of the same order, which leads us to think that the treatment does not affect the fabric structure or the size of the pores. A similar behavior is observed when measuring the tensile strength. Mechanical properties at break before and after the treatment are very similar, thus indicating that the treatment does not debilitate the fibers.

Table 4. Summary of the main properties of the treated fabrics from Trial 1 and Trial 2.

			Obtained values			
Property	Unit	Comments to the measurements	Gabriella pilot trial 1	Golem pilot trial 2	Upron pilot trial 3	Utex pilot trial 4
Water-vapor resistance (R_{et})	m²·Pa W⁻¹	Face / back[a], untreated	2.69 / 2.67	1.90 / 1.87	3.23 / 3.28	1.27 / 1.25
		Face / back[a], finished	2.71 / 2.61	2.10 / 2.13	3.62 / 3.60	1.59 / 1.57
Hydrophobicity (spray test)	Rate ISO	Untreated	wets	wets	wets	wets
		Treated unwashed	3.5, 3.0, 3.5	3.0, 3.0, 3.0	2.5, 2.5, 2.5	2.5, 2.5, 2.5
		Washed 5x40 °C [b]	3.0, 3.5, 3.5	3.5, 3.5, 3.5	3.5, 4.0, 3.5	4.0, 3.5, 3.5
		Washed 10x40 °C [b]	3.0, 3.0, 3.0	3.0, 3.0, 3.0	3.5, 3.5, 3.5	3.5, 3.5, 3.5
Air permeability	mm s⁻¹	Untreated	119	595	71	28
		Treated	178	593	112	67
Tensile strength	N	warp/weft, untreated	890 / 544	686 / 558	1804 / 794	640 / 515
		warp/weft, treated	881 / 530	611 / 581	1753 / 821	597 / 538

[a] Measurement of water vapor resistance under steady-state conditions (sweating guarded-hotplate test), face side to unit / back side to unit. [b] Washing tests have been performed according to ISO 6330, 4N.
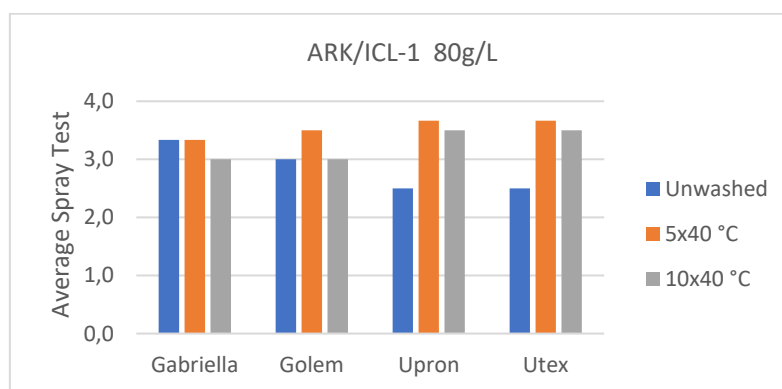
Figure 39. Average spray test obtained from four different fabrics (Gabriella, Golem, Upron, Utex), unwashed, after 5 washes and after 10 washes.

The four fabrics treated with ARK/ICL-1 have also been assessed for anti-stain performance (Tchibo test). Pictures and score of unwashed and washed fabrics can be seen in Figure 40 and Figure 41.

ARK/ICL-1 80g/L

100 % cotton Gabriella	water	coffee	milk & juice	red wine	olive oil	motor oil	mustard	ketchup
Score	4	3-4	3-4	3	0	0	2-3	2-3
washed 5x40 °C ↓								
Score	4	3-4	4	3-4	0	0	3	3

ARK/ICL-1 80g/L

50/50 CO/PES Golem	water	coffee	milk & juice	red wine	olive oil	motor oil	mustard	ketchup
Score	4	3	4	3	0	0	3	3
washed 5x40 °C ↓								
Score	4	4	4	3-4	0	0	3-4	3

Figure 40. Anti-stain performance of treated Gabriella (left) and Golem (right) fabrics with 80 g/L ARK/ICL-1. Anti-stain tests have been performed before (up) and after 5x40 °C washes (down). Score for anti-stain performance is also provided.

ARK/ICL-1 80g/L

100 % PES TT Upron	water	coffee	milk & juice	red wine	olive oil	motor oil	mustard	ketchup
Score	4	2	4	2	0	0	2-3	2
washed 5x40 °C ↓								
Score	4	3	4	2-3	0	0	3	2

ARK/ICL-1 80g/L

100 % PES Outdoor Utex	water	coffee	milk & juice	red wine	olive oil	motor oil	mustard	ketchup
Score	3	2-3	3	3	1	1	2-3	2-3
washed 5x40 °C ↓								
Score	4	4	4	3-4	1	1	3-4	3

Figure 41. Anti-stain performance of treated Upron (left) and Utex (right) fabrics with 80 g/L ARK/ICL-1. Anti-stain tests have been performed before (up) and after 5x40 °C washes (down). Score for anti-stain performance is also provided.

From Figure 40 and Figure 41 can be derived that stain-release properties improved after washing, thus confirming durability of the ARK/ICL-1 finishing and also elimination of polymerization emulsifiers during washing, that further improves stain-release performance. Good stain-release properties to water-based liquids have been obtained

for all of the fabrics finished with ARK/ICL-1, specially for coffee and milk & juice. Protection against red wine is also reasonably good except for Upron fabric, this could be attributed to the fabric structure of this fabric that makes more difficult to wipe out the stain. Stain-release for fatty stains like mustard and ketchup is also reasonably good (except for Upron fabric), specially for washed fabrics. Regarding olive and motor oil, the treated fabrics with ARK/ICL-1 do not provide any stain-release effect because the surface energy conferred to the fabrics its well below the surface tension of these pure oils. For comparison purposes, anti-stain performance has been assessed on Gabriella fabric treated with prototype PM$_3$T obtained from [98], see Figure 42. For PM$_3$T treated fabrics the stain-release is very good, even for pure oils (olive and motor oil). Therefore, PM$_3$T offers better stain-release against pure oils than ARK7ICL-1 prototype. However, wash-fastness of treated fabrics with PM$_3$T is not good (see Figure 42 down) and more research will be required on the crosslinking system to confer more durability.

100 % cotton Gabriella	PM$_3$T 80g/L							
	water	coffee	milk & juice	red wine	olive oil	motor oil	mustard	ketchup
0 min.								
5 min								
drop removed								
Score	4	3-4	3-4	3	3-4	2-3	3-4	3-4
washed 5x40 °C ↓								
0 min.								
5 min								
drop removed								
Score	2	1-2	1	0	0	0	2-3	2-3

Figure 42. Anti-stain performance of treated Gabriella fabric with 80 g/L PM$_3$T. Anti-stain tests have been performed before (up) and after 5x40 °C washes (down). Score for anti-stain performance is also provided.

4.3.2.3 Industrial trials with prototype ARK/ICL-1 carried out at JITEX-comfort s.r.o.

Two industrial trials were performed with the compound ARK/ICL-1 in an industrial mill from Czech Republic, JITEX-comfort s.r.o., on March 9 and 10, 2021, and April 25, 2021, with the supervision of INOTEX. Results are reported in this section. Details about the application process, machinery are summarized in Table 5.

Table 5. Summary of the main application parameters for industrial trials with prototype ARK/ICL-1.

	Trial 1	Trial 2
Factory	Jitex Comfort s.r.o	
Material	Polyamide66 / Lycra 95/5 wt. %, knit, single jersey (No. 7071), 190 g/m^2, black. For functional wear.	Viscose / Lycra 95/5 wt. %, knit, single jersey, 203 g/m^2, black. For functional wear.
Required properties	Water drop must not be soaked by the knit, remaining completely on the fabric surface for minimum 10 min., this effect must be stable after 5 washings at 40 °C.	
Technology / machinery	Application by: 1. Exhaustion - winch POLDI ALTICORRO machine 2. Hydroextraction - centrifugue H KRANZ, GmbH 3. Drying – stenter frame BRÜCKNER 4. Curing - stenter frame BRÜCKNER (6 chambers)	

Processing conditions	1. Exhaustion
	   a. Finishing bath concentration: 40 g/L ARK/ICL-1
	   b. Small winch: 10 kg knit, 250 L bath (L.R.^{a}: 1:16.7)
	   c. Big winch: 90 kg knit, 1500 L bath (L.R.^{a}: 1:16.7)
	   d. Temperature 40 °C
	   e. Time: 30 min.
	2. Hydroextraction
	   a. 750 r.p.m, 2 min.
	   b. Wet pick-up^b: 101 wt. % (for **Trial 1**), 95 wt. % (for **Trial 2**)
	3. Drying: 120 °C, frame speed 10 m/min.
	   Curing: 160 °C, frame speed 12 m/min.	

[a] L.R. is the Liquor Ratio and defines de ratio: weight of fabric : weight of finishing bath. [b] Wet pick-up is expressed by the following equation: $Wet\ pickup = \frac{W_2 - W_0}{W_0} * 100$ *, where W_2 is the weight of fabric after hydroextraction and W_0 is the initial weight of the fabric before impregnation.*

Figure 43.Pictures of the industrial facilities of JITEX-comfort s.r.o., where trials with ARK/ICL-1 were performed. With permission of INOTEX.

Table 6 shows the main properties conferred to the treated the fabrics. Water-vapor resistance values remain practically unchanged with respect to the untreated fabrics, which means that the hydrophobic finish does not affect the comfort of the fabric, i.e., treated fabrics still have good sweat evacuation. Duplicate measurements of Spray test for Trial 1 give values close to the maximum score (4.5 - 5) while for Trial 2 the values are slightly lower but still have a good score. Spray test values are maintained after 5 washes, thus indicating a good durability of the finishings. The Water drop test shows that a drop of water remains on the surface of the treated fabrics for more than 1 h, this effect is maintained after 5 washes, thus far exceeding customer requirements, see Figure 44. Also, it is worth to mention than the hydrophobic effect of Viscose/Lycra reached its maximum after 24h of room temperature conditioning after the finishing process. Therefore, Viscose/Lycra in Trial 2 is a more difficult substrate to be hydrophobized than Polyamide/Lycra in Trial 1 as can be also derived from the lower Spray test obtained and higher absorbability. Finally, air permeability values before and after hydrophobic treatment are of the same order, which leads us to think that the treatment does not affect the fabric structure or the size of the pores. Tensile strength before and after the treatment has been measured for Trial 1, similar values have been obtained, thus indicating that the treatment does not substantially debilitate the fibers.

Table 6. Summary of the main properties of the treated fabrics from Trial 1 and Trial 2.

Property	Unit	Obtained values		
		Comments to the measurements	Trial 1	Trial 2
Water-vapor resistance (R$_{et}$)	m^2·Pa W^{-1}	Face / back[a], untreated	2.66 / 2.64	2.33 / 2.01
		Face / back[a], finished	2.73 / 2.62	2.28 / 1.94
Hydrophobicity (spray test)	Rate ISO	Untreated	wets	wets
		Unwashed	4.5, 5	3.5, 4
		Washed 5x40 °C [b]	4.5, 4.5	3.5, 4
Absorbability	%	Untreated	206	224
		Unwashed	1.56	6.2
		Washed 5x40 °C [b]	0.99	5.3
Water drop test	min.	Untreated	wets	wets
		Unwashed	>60	>60
		Washed 5x40 °C [b]	>60	>60
Air permeability	mm s^{-1}	Untreated	410	378
		Treated	309	324
Tensile strength	N	wale/course, untreated	306 / 338	265 / 487
		wale/course, treated	274 / 307	Not measured

[a] *Measurement of water vapor resistance under steady-state conditions (sweating guarded-hotplate test), face side to unit / back side to unit.* [b] *Washing tests have been performed according to ISO 6330, 4N.*
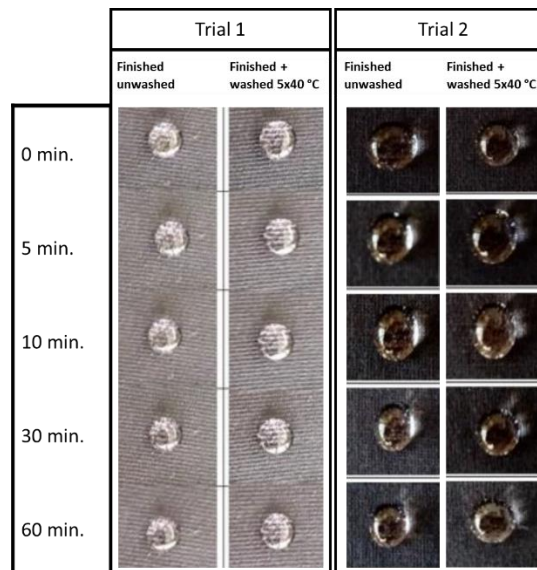
Figure 44. Pictures taken from water drop test at different times.

5   Market overview

In this section a review of the fluorine-free waterproofing products currently present in the textile market with noticeable market shares has been done. This summary has been made on the basis of an study published by The Danish Environmental Protection Agency [118] and the current market knowledge from Color Center. The alternatives to PFASs that cope the current DWR textile finishing market are reported and can be grouped into seven families each of them having advantages and drawbacks (see Table 7), only four of the reported products claim biobased content (Jintexguard BIO DWR, Zelan R3, Unidyne XF-5003 and Unidyne XF-5007).

Table 7. Alternatives to PFASs textile finishings according to Lassen et al. [118].

Commercial alternatives to PFASs	Comments (Market price estimate[a])	Comercial name (Manufacturer)	Oil repellency
Paraffin/wax/fatty acid emulsions	Water-based. May contain VOCs. Usually contain Zn or Al ions. (1/3 to 1/4 of the price of C6-fluorocarbons)	Phobotex APK (Huntsman) Phobotex ZAN (Huntsman) Arkophob NPK liq (Archroma)	NO
Fat-modified melamine resins	Water-based. May contain VOCs. May release formaldehyde. (1/3 of the price of C6-fluorocarbons)	Ecorepel® (Schoeller Technologies AG) Schoeller protec-FF (Schoeller Technologies AG) Phobotex®JVA (Huntsman) Phobotex®RHP (Huntsman) Phobotex®RSH (Huntsman) Phobotex®RHW (Huntsman)	NO
Polyacrylate-based	Water-based. Can be marketed as a mixture of polyacrylates and paraffin/wax or fat-modified melamine. May contain blocked polyisocyanates. (Half the price of C6-fluorocarbons)	Phobotex® RCO (Huntsman) Arkophob FFR[b] (Archroma) Arkophob 2150[b] (Archroma) Arkophob 2198[b] (Archroma) Jintexguard BIO DWR[b] (Jintex Corp.) Unidyne XF-5005[b] (Daikin) Unidyne XF-5007[b] (Daikin)	NO
Polydimethylsiloxane emulsions (PDMS)	Water-based. Siloxanes are persistent and are widespread in the environment. May contain VOCs both cyclic (D4, D5, D6) and/or linear	Phobotex WS Conc (Huntsman) Phobotex Cat. BC (Huntsman) Rhodorsil TCS 7001 (Bluestar Silicones)	NO

	(HMDSO, MDM, MD2M and MD3M) and also solvents. (Price of the same order as C6-fluorocarbons)	Tegotex RT 2033[b] (Evonik) Advalon HO 111[b] (Wacker)	
Dendrimer emulsions	Water-based. The product compositions were not specified sufficiently for an assessment, but some of the products contain unknown siloxanes, cationic polymers, blocked isocyanates or irritating organic acids. Its penetration rate in the textile market is low. (Price of the same order as C6-fluorocarbons)	Ruco-Dry ECO (Rudolf) OC-aquasil Tex W™ (OrganoClick) OC-aquasil Tex N™ (OrganoClick)	NO
Polyurethane-based	Water-based. The product compositions were not specified sufficiently for an assessment. Suspected to contain blocked isocyanates, that makes products potentially hazardous to skin and mucous membranes. (Price of the same order as C6-fluorocarbons)	Purtex® WR (Purtex) Zelan™ R3[b] (Hunstman)	NO
Nano-material based	Its penetration rate in the textile market is low. (Equal or higher price than C6-fluorocarbons)	At the present time no marketed products based on nanomaterials have been detected that claim to be free of fluorochemicals.	-

[a] *Estimation of the market price referenced to the price of C6-fluorocarbon with a solid content about 25-30 wt. %, which ranges between 12 and 16 €/kg according to Color Center's estimates for first quarter of 2022.* [b] *Added references that do not appear in the original work of Lassen et al.* [118] *or have been relocated within the classification because more information is currently available.*

The prototypes developed in research line 1 falls within the classification "Polyurethane-based", however, our developments are intended for application by knife-coating while all the referenced products in Table 7 are designed to be applied by padding. Therefore, the polyurethane-ureas developed in this work should be compared with hydrophobic anionic polyurethanes commercialized by manufacturers as Lamberti, Cromogenia or Covestro, among others, and specifically designed to confer water column to face-coated textiles. The average market price for commercially non-biobased polyurethanes

for water column is about 4 to 8 €/kg for waterborne dispersions with a dry content ranging from 35 to 50 wt. %. We have no evidence of commercial polyurethanes specifically designed for water column where (partially) biobased origin is claimed. It is difficult to estimate the price of the developed WPUD since they are not yet in the industrialization stage. A rough economic estimate of the prototypes developed in this work, with 35 wt. % solid content and a bio-based content of 55-65 %, indicates that they will fall within the same price range, although versions doped with SWCNT and POSS can reach significant higher market prices depending on the percentage of nanomaterials in the formulation.

The prototypes developed in research line 2 falls within the classification "Polyacrylate-based". Most commercial polyacrylate-based alternatives to PFAs have a solid content ranging from 25 to 35 wt. %. The estimated market price for our developed prototypes, with a solid content of 29 wt. %, greatly depends on the monomer composition. Those prototypes with highest content in SMA and the up-scaled prototypes based on polystearyl acrylate and paraffin, will have approximately half the price of C6-fluorocarbons while for those prototypes with medium to high M_3T content the market price will equal and even surpass the average price of C6-fluorocarbons. For instance, PM_3T, the prototype with higher M_3T content, could reach a market price of 2.6 times higher than a standard C6-fluorocarbon. PM_3T prototype has a very high market price because M_3T monomer is very expensive since it is a monomer used in other sectors very different from textiles (contact lenses, medical sector) and that, at present, it is not implanted in the sector of textile auxiliaries. However, it must be considered that PM_3T prototype is totally free of fluorine and that it offers repellency to triglyceride-type oils (soil-release), something totally new on the market. As long as the use of fluorocarbons based on the C6 chemistry is still allowed, it is to be expected that the PM_3T prototype will not have a relevant market penetration. However, due to growing concern about the sustainability of C6-fluorocarbons, it is expected that these will be greatly restricted in the coming years. This situation makes us think that, if we continue working on the optimization of this PM_3T prototype, in the coming years we may have a good market opportunity for this prototype.

Bibliography

[1]   B. Bhushan, Biomimetics: Lessons from nature - an overview, Philos. Trans. R. Soc. A Math. Phys. Eng. Sci. 367 (2009) 1445–1486. https://doi.org/10.1098/rsta.2009.0011.

[2]   W. Barthlott, C. Neinhuis, Purity of the sacred lotus, or escape from contamination in biological surfaces, Planta. 202 (1997) 1–8. https://doi.org/10.1007/s004250050096.

[3]   T. Sun, G. Qing, B. Su, L. Jiang, Functional biointerface materials inspired from nature, Chem. Soc. Rev. 40 (2011) 2909–2921. https://doi.org/10.1039/c0cs00124d.

[4]   S. Wang, K. Liu, X. Yao, L. Jiang, Bioinspired surfaces with superwettability: New insight on theory, design, and applications, Chem. Rev. 115 (2015) 8230–8293. https://doi.org/10.1021/cr400083y.

[5]   B. Wang, Y. Zhang, L. Shi, J. Li, Z. Guo, Advances in the theory of superhydrophobic surfaces, J. Mater. Chem. 22 (2012) 20112–20127. https://doi.org/10.1039/c2jm32780e.

[6]   E. Bormashenko, Progress in understanding wetting transitions on rough surfaces, Adv. Colloid Interface Sci. 222 (2015) 92–103. https://doi.org/10.1016/j.cis.2014.02.009.

[7]   T. Young, An essay on the cohesion of fluids, Philos. Trans. R. Soc. London. 95 (1805) 65–87.

[8]   L. Duta, A.C. Popescu, I. Zgura, N. Preda, I.N. Mihailescu, Wettability of nanostructured surfaces, in: Wetting and Wettability, InTech, 2015. https://doi.org/10.5772/60808.

[9]   R.N. Wenzel, Surface roughness and contact angle, J. Phys. Colloid Chem. 53 (1949) 1466–1467. https://doi.org/10.1021/j150474a015.

[10]   R.N. Wenzel, Resistance of solid surfaces to wetting by water, Ind. Eng. Chem. 28 (1936) 988–994. https://doi.org/10.1021/ie50320a024.

[11]   A.B.D. Cassie, S. Baxter, Wettability of porous surfaces, Trans. Faraday Soc. 40 (1944) 546–551. https://doi.org/10.1039/tf9444000546.

[12]   S. Shabanian, B. Khatir, A. Nisar, K. Golovin, Rational design of perfluorocarbon-free oleophobic textiles, Nat. Sustain. 3 (2020) 1059–1066. https://doi.org/10.1038/s41893-020-0591-9.

[13]   J.J. Jasper, The Surface Tension of Pure Liquid Compounds, J. Phys. Chem. Ref. Data. 1 (2009) 841. https://doi.org/10.1063/1.3253106.

[14]   R. Chunbo, D. Guqiao, L. Weichang, D. Yan, H. Wentao, Wetting on Nanoporous Alumina Surface: Transition between Wenzel and Cassie States Controlled by Surface Structure, Langmuir. 24 (2008) 9952–9955. https://doi.org/10.1021/LA801461J.

[15]   P. Lv, Y. Xue, H. Liu, Y. Shi, P. Xi, H. Lin, H. Duan, Symmetric and asymmetric meniscus collapse in wetting transition on submerged structured surfaces, Langmuir. 31 (2015) 1248–1254. https://doi.org/10.1021/LA503465Q/SUPPL_FILE/LA503465Q_SI_001.ZIP.

[16]   Wettability. John C. Berg (ed.)., Marcel Dekker, New York (N.Y.), 1993.

[17]   Z. Guo, W. Liu, Biomimic from the superhydrophobic plant leaves in nature: Binary structure and unitary structure, Plant Sci. 172 (2007) 1103–1112. https://doi.org/10.1016/j.plantsci.2007.03.005.

[18]   Z. Wang, J. Gong, J. Ma, J. Xu, In situ growth of hierarchical boehmite on 2024 aluminum alloy surface as superhydrophobic materials, RSC Adv. 4 (2014) 14708–14714. https://doi.org/10.1039/c4ra00160e.

[19]   A.K. Kota, Y. Li, J.M. Mabry, A. Tuteja, Hierarchically Structured Superoleophobic Surfaces with Ultralow Contact Angle Hysteresis, Adv. Mater. 24 (2012) 5838–5843. https://doi.org/10.1002/adma.201202554.

[20]   A. Tuteja, W. Choi, G.H. McKinley, R.E. Cohen, M.F. Rubner, Design parameters for superhydrophobicity and

superoleophobicity, MRS Bull. 33 (2008) 752–758. https://doi.org/10.1557/mrs2008.161.

[21]   W. Choi, A. Tuteja, S. Chhatre, J.M. Mabry, R.E. Cohen, G.H. McKinley, Fabrics with tunable oleophobicity, Adv. Mater. 21 (2009) 2190–2195. https://doi.org/10.1002/adma.200802502.

[22]   A. Tuteja, W. Choi, J.M. Mabry, G.H. McKinley, R.E. Cohen, Robust omniphobic surfaces, Proc. Natl. Acad. Sci. U. S. A. 105 (2008) 18200–18205. https://doi.org/10.1073/pnas.0804872105.

[23]   A. Tuteja, W. Choi, M. Ma, J.M. Mabry, S.A. Mazzella, G.C. Rutledge, G.H. McKinley, R.E. Cohen, Designing superoleophobic surfaces, Science (80-.). 318 (2007) 1618–1622. https://doi.org/10.1126/science.1148326.

[24]   M. Zahid, G. Mazzon, A. Athanassiou, I.S. Bayer, Environmentally benign non-wettable textile treatments: A review of recent state-of-the-art, Adv. Colloid Interface Sci. 270 (2019) 216–250. https://doi.org/10.1016/j.cis.2019.06.001.

[25]   A.K. Kota, G. Kwon, W. Choi, J.M. Mabry, A. Tuteja, Hygro-responsive membranes for effective oil-water separation, Nat. Commun. 3 (2012). https://doi.org/10.1038/ncomms2027.

[26]   S.S. Chhatre, W. Choi, A. Tuteja, K.C. Park, J.M. Mabry, G.H. McKinley, R.E. Cohen, Scale dependence of omniphobic mesh surfaces, Langmuir. 26 (2010) 4027–4035. https://doi.org/10.1021/la903489r.

[27]   R.C. Buck, J. Franklin, U. Berger, J.M. Conder, I.T. Cousins, P. De Voogt, A.A. Jensen, K. Kannan, S.A. Mabury, S.P.J. van Leeuwen, Perfluoroalkyl and polyfluoroalkyl substances in the environment: Terminology, classification, and origins, Integr. Environ. Assess. Manag. 7 (2011) 513–541. https://doi.org/10.1002/ieam.258.

[28]   J.P. Giesy, K. Kannan, Global distribution of perfluorooctane sulfonate in wildlife, Environ. Sci. Technol. 35 (2001) 1339–1342. https://doi.org/10.1021/es001834k.

[29]   J.W. Martin, S.A. Mabury, K.R. Solomon, D.C.G. Muir, Progress toward understanding the bioaccumulation of perfluorinated alkyl acids, Environ. Toxicol. Chem. 32 (2013) 2421–2423. https://doi.org/10.1002/etc.2376.

[30]   B.J. Apelberg, F.R. Witter, J.B. Herbstman, A.M. Calafat, R.U. Halden, L.L. Needham, L.R. Goldman, Cord serum concentrations of perfluorooctane sulfonate (PFOS) and perfluorooctanoate (PFOA) in relation to weight and size at birth, Environ. Health Perspect. 115 (2007) 1670–1676. https://doi.org/10.1289/ehp.10334.

[31]   C. Fei, J.K. McLaughlin, R.E. Tarone, J. Olsen, Perfluorinated chemicals and fetal growth: A study within the Danish national birth cohort, Environ. Health Perspect. 115 (2007) 1677–1682. https://doi.org/10.1289/ehp.10506.

[32]   L. Vierke, A. Möller, S. Klitzke, Transport of perfluoroalkyl acids in a water-saturated sediment column investigated under near-natural conditions, Environ. Pollut. 186 (2014) 7–13. https://doi.org/10.1016/j.envpol.2013.11.011.

[33]   K.J. Hansen, L.A. Clemen, M.E. Ellefson, H.O. Johnson, Compound-specific, quantitative characterization of organic fluorochemicals in biological matrices, Environ. Sci. Technol. 35 (2001) 766–770. https://doi.org/10.1021/es001489z.

[34]   A.L. Luz, J.K. Anderson, P. Goodrum, J. Durda, Perfluorohexanoic acid toxicity, part I: Development of a chronic human health toxicity value for use in risk assessment, Regul. Toxicol. Pharmacol. 103 (2019) 41–55. https://doi.org/10.1016/j.yrtph.2019.01.019.

[35]   J.E. Klaunig, M. Shinohara, H. Iwai, C.P. Chengelis, J.B. Kirkpatrick, Z. Wang, R.H. Bruner, Evaluation of the chronic toxicity and carcinogenicity of perfluorohexanoic acid (PFHxA) in Sprague-Dawley Rats, Toxicol. Pathol. 43 (2015) 209–220. https://doi.org/10.1177/0192623314530532.

[36]   P.A. Rice, J. Aungst, J. Cooper, O. Bandele, S. V. Kabadi, Comparative analysis of the toxicological databases for 6:2 fluorotelomer alcohol (6:2 FTOH) and perfluorohexanoic acid (PFHxA), Food Chem. Toxicol. 138 (2020) 111210. https://doi.org/10.1016/J.FCT.2020.111210.

[37]   L. Serrano, L.M. Iribarne-Durán, B. Suárez, F. Artacho-Cordón, F. Vela-Soria, M. Peña-Caballero, J.A. Hurtado, N. Olea, M.F. Fernández, C. Freire, Concentrations of perfluoroalkyl substances in donor breast milk in Southern Spain and their potential determinants, Int. J. Hyg. Environ. Health. 236 (2021) 113796. https://doi.org/10.1016/J.IJHEH.2021.113796.

[38]   Joint meeting of the Chemicals Commitee and The Working Party on Chemicals, Pesticides and Biotechnology: Data analysis of the identification of correlations between polymer characteristics and potential for health or ecotoxicological concern JT03258707 D, 2009. https://www.oecd.org/.

[39]   B.J. Henry, J.P. Carlin, J.A. Hammerschmidt, R.C. Buck, L.W. Buxton, H. Fiedler, J. Seed, O. Hernandez, A critical review of the application of polymer of low concern and regulatory criteria to fluoropolymers, Integr. Environ. Assess. Manag. 14 (2018) 316–334. https://doi.org/10.1002/ieam.4035.

[40]   The ECETOC Conceptual Framework for Polymer Risk Assessment (CF4Polymers) EUROPEAN CENTRE FOR ECOTOXICOLOGY AND TOXICOLOGY OF CHEMICALS, Brussels, 2019. https://www.ecetoc.org/publication/tr-133-the-ecetoc-conceptual-framework-for-polymer-risk-assessment-cf4polymers/.

[41]   R. Lohmann, I.T. Cousins, J.C. DeWitt, J. Glüge, G. Goldenman, D. Herzke, A.B. Lindstrom, M.F. Miller, C.A. Ng, S. Patton, M. Scheringer, X. Trier, Z. Wang, Are Fluoropolymers Really of Low Concern for Human and Environmental Health and Separate from Other PFAS?, Environ. Sci. Technol. (2020). https://doi.org/10.1021/acs.est.0c03244.

[42]   M. Geiser, S. Schürch, P. Gehr, Influence of surface chemistry and topography of particles on their immersion into the lung's surface-lining layer, J. Appl. Physiol. 94 (2003) 1793–1801. https://doi.org/10.1152/japplphysiol.00514.2002.

[43]   K.J. Groh, B. Geueke, J. Muncke, Food contact materials and gut health: Implications for toxicity assessment and relevance of high molecular weight migrants, Food Chem. Toxicol. 109 (2017) 1–18. https://doi.org/10.1016/j.fct.2017.08.023.

[44]   J.W. Washington, T.M. Jenkins, K. Rankin, J.E. Naile, Decades-scale degradation of commercial, side-chain, fluorotelomer-based polymers in soils and water, Environ. Sci. Technol. 49 (2015) 915–923. https://doi.org/10.1021/es504347u.

[45]   M.L. Brusseau, R.H. Anderson, B. Guo, PFAS concentrations in soils: Background levels versus contaminated sites, Sci. Total Environ. 740 (2020) 140017. https://doi.org/10.1016/j.scitotenv.2020.140017.

[46]   T. Stoiber, S. Evans, O. V. Naidenko, Disposal of products and materials containing per- and polyfluoroalkyl substances (PFAS): A cyclical problem, Chemosphere. 260 (2020) 127659. https://doi.org/10.1016/j.chemosphere.2020.127659.

[47]   J. Williams, Waterproof and water repellent textiles and clothing, Elsevier Inc., 2017. https://doi.org/10.1016/c2015-0-06037-3.

[48]   M. Cobbing, C. Campione, M. Kopp, PFC Revolution in the Outdoor Sector, Zürich, Switzerland, 2017. https://www.greenpeace.org/international/publication/7150/pfc-revolution-in-outdoor-sector/.

[49]   D.C. Manatunga, R.M. De Silva, K.M.N. De Silva, Double layer approach to create durable superhydrophobicity on cotton fabric using nano silica and auxiliary non fluorinated materials, Appl. Surf. Sci. 360 (2016) 777–788. https://doi.org/10.1016/J.APSUSC.2015.11.068.

[50]   Y. Wu, H. Qi, B. Li, H. Zhanhua, W. Li, S. Liu, Novel hydrophobic cotton fibers adsorbent for the removal of nitrobenzene in aqueous solution, Carbohydr. Polym. 155 (2017) 294–302. https://doi.org/10.1016/J.CARBPOL.2016.08.088.

[51]   N. Guo, Y. Chen, Q. Rao, Y. Yin, C. Wang, Fabrication of durable hydrophobic cellulose surface from silane-functionalized silica hydrosol via electrochemically assisted deposition, J. Appl. Polym. Sci. 132 (2015) 42733. https://doi.org/10.1002/APP.42733.

[52]   X.W. Cheng, C.X. Liang, J.P. Guan, X.H. Yang, R.C. Tang, Flame retardant and hydrophobic properties of novel sol-gel derived phytic acid/silica hybrid organic-inorganic coatings for silk fabric, Appl. Surf. Sci. 427 (2018) 69–80. https://doi.org/10.1016/J.APSUSC.2017.08.021.

[53]   Y. Wu, X. Tan, Y. Wang, F. Tao, M. Yu, X. Chen, Colloids and Surfaces A : Physicochemical and Engineering Aspects Nonfluorinated , transparent , and antireflective hydrophobic coating with self-cleaning function, Colloids Surfaces A Physicochem. Eng. Asp. 634 (2022) 127919. https://doi.org/10.1016/j.colsurfa.2021.127919.

[54]   J. Li, L. Yan, Y. Zhao, F. Zha, Q. Wang, Z. Lei, One-step fabrication of robust fabrics with both-faced superhydrophobicity for the separation and capture of oil from water, Phys. Chem. Chem. Phys. 17 (2015) 6451–6457. https://doi.org/10.1039/C5CP00154D.

[55]   F. Guo, Q. Wen, Y. Peng, Z. Guo, Simple one-pot approach toward robust and boiling-water resistant superhydrophobic cotton fabric and the application in oil/water separation, J. Mater. Chem. A. 5 (2017) 21866–21874. https://doi.org/10.1039/c7ta05599d.

[56]   H. Wang, H. Zhou, S. Liu, H. Shao, S. Fu, G.C. Rutledge, T. Lin, Durable, self-healing, superhydrophobic fabrics from fluorine-free, waterborne, polydopamine/alkyl silane coatings, RSC Adv. 7 (2017) 33986–33993. https://doi.org/10.1039/C7RA04863G.

[57]   A. Rahman, S. Lee, C.H. Park, A Facile and Non-toxic Approach to Develop Superhydrophobic Cotton Fabric Using Octadecylamine and Hexadecyltrimethoxysilane in Aqueous System, Fibers Polym. 22 (2021) 131–140. https://doi.org/10.1007/s12221-021-9645-5.

[58]   Q. Zhao, L.Y.L. Wu, H. Huang, Y. Liu, Ambient-curable superhydrophobic fabric coating prepared by water-based non-fluorinated formulation, Mater. Des. 92 (2016) 541–545. https://doi.org/10.1016/j.matdes.2015.12.054.

[59]   C. Urata, D.F. Cheng, B. Masheder, A. Hozumi, Smooth, transparent and nonperfluorinated surfaces exhibiting unusual contact angle behavior toward organic liquids, RSC Adv. 2 (2012) 9805–9808. https://doi.org/10.1039/c2ra21360e.

[60]   C. Urata, B. Masheder, D.F. Cheng, A. Hozumi, How to reduce resistance to movement of alkane liquid drops across tilted surfaces without relying on surface roughening and perfluorination, Langmuir. 28 (2012) 17681–17689. https://doi.org/10.1021/la303829p.

[61]   Y. Ma, D. Zhu, Y. Si, G. Sun, Fabricating durable, fluorine-free, water repellency cotton fabrics with CPDMS, J. Appl. Polym. Sci. 135 (2018) 46396. https://doi.org/10.1002/app.46396.

[62]   Q. Liu, J. Huang, J. Zhang, Y. Hong, Y. Wan, Q. Wang, M. Gong, Z. Wu, C.F. Guo, Thermal, waterproof, breathable, and antibacterial cloth with a nanoporous structure, ACS Appl. Mater. Interfaces. 10 (2018) 2026–2032. https://doi.org/10.1021/acsami.7b16422.

[63]   C.H. Xue, Y.R. Li, J.L. Hou, L. Zhang, J.Z. Ma, S.T. Jia, Self-roughened superhydrophobic coatings for continuous oil-water separation, J. Mater. Chem. A. 3 (2015) 10248–10253. https://doi.org/10.1039/c5ta01014d.

[64]   X.J. Guo, C.H. Xue, M. Li, X. Li, J.Z. Ma, Fabrication of robust, superhydrophobic, electrically conductive and UV-blocking fabrics via layer-by-layer assembly of carbon nanotubes, RSC Adv. 7 (2017) 25560–25565. https://doi.org/10.1039/C7RA02111A.

[65]   L. Hao, T. Gao, W. Xu, X. Wang, S. Yang, X. Liu, Preparation of crosslinked polysiloxane/SiO2 nanocomposite via in-situ condensation and its surface modification on cotton fabrics, Appl. Surf. Sci. 371 (2016) 281–288. https://doi.org/10.1016/J.APSUSC.2016.02.204.

[66]   T. Zhu, S. Li, J. Huang, M. Mihailiasa, Y. Lai, Rational design of multi-layered superhydrophobic coating on cotton fabrics for UV shielding, self-cleaning and oil-water separation, Mater. Des. 134 (2017) 342–351. https://doi.org/10.1016/J.MATDES.2017.08.071.

[67]   D.F. Cheng, C. Urata, M. Yagihashi, A. Hozumi, D.F. Cheng, C. Urata, A. Hozumi, M. Yagihashi, A Statically Oleophilic but Dynamically Oleophobic Smooth Nonperfluorinated Surface, Angew. Chemie Int. Ed. 51 (2012) 2956–2959. https://doi.org/10.1002/ANIE.201108800.

[68]   B. Khatir, S. Shabanian, K. Golovin, Design and High-Resolution Characterization of Silicon Wafer-like Omniphobic Liquid Layers Applicable to Any Substrate, ACS Appl. Mater. Interfaces. 12 (2020) 31933–31939. https://doi.org/10.1021/acsami.0c06433.

[69]   N.D. Tissera, R.N. Wijesena, J.R. Perera, K.M.N. De Silva, G.A.J. Amaratunge, Hydrophobic cotton textile surfaces using an amphiphilic graphene oxide (GO) coating, Appl. Surf. Sci. 324 (2015) 455–463. https://doi.org/10.1016/j.apsusc.2014.10.148.

[70]   N.F. Attia, M. Moussa, A.M.F. Sheta, R. Taha, H. Gamal, Effect of different nanoparticles based coating on the performance of textile properties, Prog. Org. Coatings. 104 (2017) 72–80. https://doi.org/10.1016/j.porgcoat.2016.12.007.

[71]   Z. Mai, Z. Xiong, X. Shu, X. Liu, H. Zhang, X. Yin, Y. Zhou, M. Liu, M. Zhang, W. Xu, D. Chen, Multifunctionalization of cotton fabrics with polyvinylsilsesquioxane/ZnO composite coatings, Carbohydr. Polym. 199 (2018) 516–525. https://doi.org/10.1016/j.carbpol.2018.07.052.

[72]   L. Xu, X. Zhang, Y. Shen, Y. Ding, L. Wang, Y. Sheng, Durable Superhydrophobic Cotton Textiles with Ultraviolet-blocking Property and Photocatalysis Based on Flower-Like Copper Sulfide, Ind. Eng. Chem. Res. 57 (2018) 6714–6725. https://doi.org/10.1021/ACS.IECR.8B00254/SUPPL_FILE/IE8B00254_SI_001.AVI.

[73]   S. Fu, H. Zhou, H. Wang, J. Ding, S. Liu, Y. Zhao, H. Niu, G.C. Rutledge, T. Lin, Magnet-responsive, superhydrophobic fabrics from waterborne, fluoride-free coatings, RSC Adv. 8 (2018) 717–723. https://doi.org/10.1039/c7ra10941e.

[74]   W. Hu, T. Hong, X. Gao, Y. Ji, Applications of nanoparticle-modified stationary phases in capillary electrochromatography, TrAC Trends Anal. Chem. 61 (2014) 29–39. https://doi.org/10.1016/J.TRAC.2014.05.011.

[75]   D.B. Cordes, P.D. Lickiss, F. Rataboul, Recent Developments in the Chemistry of Cubic Polyhedral Oligosilsesquioxanes, Chem. Rev. 110 (2010) 2081–2173. https://doi.org/10.1021/CR900201R.

[76]   K. Song, Micro- and nano-fillers used in the rubber industry, Prog. Rubber Nanocomposites. (2017) 41–80. https://doi.org/10.1016/B978-0-08-100409-8.00002-4.

[77]   D. Sun, W. Wang, D. Yu, Highly hydrophobic cotton fabrics prepared with fluorine-free functionalized silsesquioxanes, Cellulose. 24 (2017) 4519–4531. https://doi.org/10.1007/S10570-017-1388-5.

[78]   K. Hou, Y. Zeng, C. Zhou, J. Chen, X. Wen, S. Xu, J. Cheng, P. Pi, Facile generation of robust POSS-based superhydrophobic fabrics via thiol-ene click chemistry, Chem. Eng. J. 332 (2018) 150–159. https://doi.org/10.1016/j.cej.2017.09.074.

[79]   Y. Guan, C. Yu, J. Zhu, R. Yang, X. Li, D. Wei, X. Xu, Design and fabrication of vapor-induced superhydrophobic surfaces obtained from polyethylene wax and silica nanoparticles in hierarchical structures, RSC Adv. 8 (2018) 25150–25158. https://doi.org/10.1039/C8RA01666F.

[80]   N. Forsman, A. Lozhechnikova, A. Khakalo, L.-S. Johansson, J. Vartiainen, M. Österberg, Layer-by-layer assembled hydrophobic coatings for cellulose nanofibril films and textiles, made of polylysine and natural wax particles, Carbohydr. Polym. 173 (2017) 392–402. https://doi.org/10.1016/j.carbpol.2017.06.007.

[81]   Y. Zhao, E. Liu, J. Fan, B. Chen, X. Hu, Y. He, C. He, Superhydrophobic PDMS/wax coated polyester textiles with self-healing ability via inlaying method, Prog. Org. Coatings. 132 (2019) 100–107. https://doi.org/10.1016/J.PORGCOAT.2019.03.043.

[82]   Y. Liu, Y. Liu, H. Hu, Z. Liu, X. Pei, B. Yu, P. Yan, F. Zhou, Mechanically induced self-healing superhydrophobicity, J. Phys. Chem. C. 119 (2015) 7109–7114. https://doi.org/10.1021/jp5120493.

[83]   M. Mohsin, N. Ramzan, S.W. Ahmad, Synthesis and Application of Fluorine-free Environment-friendly Stearic Acid-based Oil and Water Repellent for Cotton Fabric, J. Nat. Fibers. 00 (2020) 1–16. https://doi.org/10.1080/15440478.2020.1787918.

[84]   J. Wu, J. Li, Z. Wang, M. Yu, H. Jiang, L. Li, B. Zhang, Designing breathable superhydrophobic cotton fabrics, RSC Adv. 5 (2015) 27752–27758. https://doi.org/10.1039/c5ra01028d.

[85]   L. Wang, G.H. Xi, S.J. Wan, C.H. Zhao, X.D. Liu, Asymmetrically superhydrophobic cotton fabrics fabricated by mist polymerization of lauryl methacrylate, Cellulose. 21 (2014) 2983–2994. https://doi.org/10.1007/s10570-014-0275-6.

[86]   Y. Li, Y. Zhang, C. Zou, J. Shao, Study of plasma-induced graft polymerization of stearyl methacrylate on cotton fabric substrates, Appl. Surf. Sci. 357 (2015) 2327–2332. https://doi.org/10.1016/j.apsusc.2015.09.236.

[87]   J. Zhang, Z. Gao, L. Li, B. Li, H. Sun, Waterborne Nonfluorinated Superhydrophobic Coatings with Exceptional Mechanical Durability Based on Natural Nanorods, Adv. Mater. Interfaces. 4 (2017) 1700723. https://doi.org/10.1002/ADMI.201700723.

[88]   M. Dai, Y. Zhai, Y. Zhang, A green approach to preparing hydrophobic, electrically conductive textiles based on waterborne polyurethane for electromagnetic interference shielding with low reflectivity, Chem. Eng. J. 421 (2021) 127749. https://doi.org/10.1016/j.cej.2020.127749.

[89]   M. Rutkevičius, T. Pirzada, M. Geiger, S.A. Khan, Creating superhydrophobic, abrasion-resistant and breathable coatings from water-borne polydimethylsiloxane-polyurethane Co-polymer and fumed silica, (2021). https://doi.org/10.1016/j.jcis.2021.02.072.

[90]   X. Liu, X. Zou, Z. Ge, W. Zhang, Y. Luo, Novel waterborne polyurethanes containing long-chain alkanes: Their synthesis and application to water repellency, RSC Adv. 9 (2019) 31357–31369. https://doi.org/10.1039/c9ra06462a.

[91]   L. Poussard, J. Lazko, J. Mariage, J.M. Raquez, P. Dubois, Biobased waterborne polyurethanes for coating applications: How fully biobased polyols may improve the coating properties, Prog. Org. Coatings. 97 (2016) 175–183. https://doi.org/10.1016/j.porgcoat.2016.04.003.

[92]   A. Santamaria-Echart, I. Fernandes, F. Barreiro, M.A. Corcuera, A. Eceiza, Advances in Waterborne Polyurethane and Polyurethane-Urea Dispersions and Their Eco-friendly Derivatives: A Review, Polym. 2021, Vol. 13, Page 409. 13 (2021) 409. https://doi.org/10.3390/POLYM13030409.

[93]   I. Etxaniz, O. Llorente, J. Aizpurua, L. Martín, A. González, L. Irusta, Dispersion Characteristics and Curing Behaviour of Waterborne UV Crosslinkable Polyurethanes Based on Renewable Dimer Fatty Acid Polyesters, J. Polym. Environ. 27 (2019) 189–197. https://doi.org/10.1007/s10924-018-1334-0.

[94]   A. Lacruz, M. Salvador, J. Aliaga, A.M. de Ilarduya, Síntesis, caracterización y validación aplicativa de un poliuretano bio-basado en dispersión acuosa para el sector de recubrimientos textiles, Rev. Química e Ind. Téxtil. (2019) 32–36. https://upcommons.upc.edu/handle/2117/174200.

[95]   A. Lacruz, M. Salvador, M. Blanco, K. Vidal, A.M. Goitandia, L. Martinková, M. Kyselka, A.M. de Ilarduya, Biobased Waterborne Polyurethane-Urea/SWCNT Nanocomposites for Hydrophobic and Electrically Conductive Textile Coatings, Polymers (Basel). 13 (2021) 1624. https://doi.org/10.3390/polym13101624.

[96]   A. Lacruz, M. Salvador, M. Blanco, K. Vidal, A.M. Goitandia, L. Martinková, M. Kyselka, A.M. de Ilarduya, Biobased Waterborne Polyurethane-Ureas Modified with POSS-OH for Fluorine-Free Hydrophobic Textile Coatings, Polymers (Basel). 13 (2021). https://doi.org/10.3390/POLYM13203526.

[97]   H. Lei, M. Xiong, J. Xiao, L. Zheng, Y. Zhu, X. Li, Q. Zhuang, Z. Han, Fluorine-free low surface energy organic coating for anti-stain applications, Prog. Org. Coatings. 103 (2017) 182–192. https://doi.org/10.1016/j.porgcoat.2016.10.036.

[98]   A. Lacruz, M. Salvador, M. Blanco, K. Vidal, A. Martínez de Ilarduya, Development of fluorine-free waterborne textile finishing agents for anti-stain and solvent-water separation based on low surface energy (co)polymers, Prog. Org. Coatings. 150 (2021). https://doi.org/10.1016/j.porgcoat.2020.105968.

[99]   E. Eslami, R. Jafari, G. Momen, A review of plasma-based superhydrophobic textiles: theoretical definitions, fabrication, and recent developments, J. Coatings Technol. Res. 18 (2021) 1635–1658. https://doi.org/10.1007/s11998-021-00523-8.

[100]   S. Li, K. Page, S. Sathasivam, F. Heale, G. He, Y. Lu, Y. Lai, G. Chen, C.J. Carmalt, I.P. Parkin, Efficiently texturing hierarchical superhydrophobic fluoride-free translucent films by AACVD with excellent durability and self-cleaning ability, J. Mater. Chem. A. 6 (2018) 17633–17641. https://doi.org/10.1039/c8ta05402a.

[101]   D. Caschera, A. Mezzi, L. Cerri, T. de Caro, C. Riccucci, G.M. Ingo, G. Padeletti, M. Biasiucci, G. Gigli, B. Cortese, Effects of plasma treatments for improving extreme wettability behavior of cotton fabrics, Cellulose. 21 (2014) 741–756. https://doi.org/10.1007/S10570-013-0123-0/FIGURES/8.

[102]   J.H. Oh, T.J. Ko, M.W. Moon, C.H. Park, Nanostructured fabric with robust superhydrophobicity induced by a thermal hydrophobic ageing process, RSC Adv. 7 (2017) 25597–25604. https://doi.org/10.1039/C7RA03801A.

[103]   N. Šajn, Environmental impact of textile and clothes industry. European Parliamentary Research Service., 2019. http://www.europarl.europa.eu/RegData/etudes/BRIE/2019/633143/EPRS_BRI(2019)633143_EN.pdf.

[104]   R. Chinthapalli, P. Skoczinski, M. Carus, W. Baltus, D. De Guzman, H. Käb, A. Raschka, J. Ravenstijn, Biobased Building Blocks and Polymers - Global Capacities, Production and Trends, 2018-2023, Ind. Biotechnol. 15 (2019) 237–241. https://doi.org/10.1089/ind.2019.29179.rch.

[105]   A. Lacruz, M. Salvador, J. Aliaga, J. Camps, A.M. de Ilarduya, Poliuretano-ureas bio-basados en dispersión acuosa para el sector de recubrimientos textiles, Rev. Plásticos Mod. Cienc. y Tecnol. Polímeros. 122 (2021) 3. https://dialnet.unirioja.es/servlet/articulo?codigo=8203152&info=resumen&idioma=ENG.

[106]   P.A. Lovell, F.J. Schork, Fundamentals of Emulsion Polymerization, Biomacromolecules 2020 21 (11),. 21 (2020) 4396–4441. https://doi.org/10.1021/acs.biomac.0c00769.

[107]   H. Huang, H. Zhang, F. Hu, Z. Ai, B. Tan, S. Cheng, J. Li, Miniemulsion copolymerization of styrene and butyl acrylate initiated by redox system at lower temperature: Reaction kinetics and evolution of particle-size distribution, J. Appl. Polym. Sci. 73 (1999) 315–322. https://doi.org/10.1002/(SICI)1097-4628(19990718)73:3<315::AID-APP2>3.0.CO;2-4.

[108]   J.M. Asua, Miniemulsion polymerization, Prog. Polym. Sci. 27 (2002) 1283–1346. https://doi.org/10.1016/S0079-6700(02)00010-2.

[109]   Y. Sun, X. Zhao, R. Liu, G. Chen, X. Zhou, Synthesis and characterization of fluorinated polyacrylate as water and oil repellent and soil release finishing agent for polyester fabric, Prog. Org. Coatings. 123 (2018) 306–313. https://doi.org/10.1016/j.porgcoat.2018.07.013.

[110]   Q. An, Q. An, W. Xu, W. Xu, L. Hao, L. Hao, L. Huang, L. Huang, Cationic fluorinated polyacrylate core-shell latex with pendant long chain alkyl: Synthesis, film morphology, and its performance on cotton substrates, J. Appl. Polym. Sci. 127 (2013) 1519–1526. https://doi.org/10.1002/APP.37553.

[111]   J. Delgado, M.S. El-Aasser, Kinetic and thermodynamic aspects of miniemulsion copolymerization, Makromol. Chemie. Macromol. Symp. 31 (1990) 63–87. https://doi.org/10.1002/MASY.19900310108.

[112]   C.S. Chern, Y.C. Liou, Effects of mixed surfactants on the styrene miniemulsion polymerization in the presence of an alkyl methacrylate, Macromol. Chem. Phys. 199 (1998) 2051–2061. https://doi.org/10.1002/(SICI)1521-3935(19980901)199:9<2051::AID-MACP2051>3.0.CO;2-0.

[113]   J. Reimers, F.J. Schork, Miniemulsion Copolymerization Using Water-Insoluble Comonomers as Cosurfactants, Http://Dx.Doi.Org/10.1080/10543414.1996.10744471. 4 (2013) 135–152. https://doi.org/10.1080/10543414.1996.10744471.

[114]   N. Lazaridis, A.H. Alexopoulos, E.G. Chatzi, C. Kiparissides, Steric stabilization in emulsion polymerization using oligomeric nonionic surfactants, Chem. Eng. Sci. 54 (1999) 3251–3261. https://doi.org/10.1016/S0009-2509(98)00336-4.

[115]   K. Landfester, N. Bechthold, S. Förster, M. Antonietti, Evidence for the preservation of the particle identity in miniemulsion polymerization, Macromol. Rapid Commun. 20 (1999) 81–84.

[116]   B. Sæthre, P.C. Mørk, J. Ugelstad, Preparation of poly(vinyl chloride) latexes by polymerization of stabilized monomer droplets, J. Polym. Sci. Part A Polym. Chem. 33 (1995) 2951–2959. https://doi.org/10.1002/POLA.1995.080331713.

[117]   S.Y. Chen, C.W. Chen, L.C. Cheng, F.S. Chuang, S.P. Rwei, A breathable waterborne poly-(urethane/urea) coating containing PO-EO-PO triblock copolymer, Mater. Res. Express. 7 (2020). https://doi.org/10.1088/2053-1591/abba50.

[118]   C. Lassen, A.A. Jensen, M. Warming, Alternatives to perfluoroalkyl and polyfluoroalkyl substances (PFAS) in

textiles., The Danish Environmental Protection Agency, Copenhagen, 2015. www.mst.dk/english.

Acknowledgments

I'd like to express my deepest thanks to Yensa Rodríguez, the colleagues who made possible the Eurostars *E!11894* project and to my Thesis Director, Antxon Martínez, for their patience and understanding.

Annex: Complete copy of the papers that are part of the compendium. Supplementary information

Development of fluorine-free waterborne textile finishing agents for anti-stain and solvent-water separation based on low surface energy (co) polymers

Amado Lacruz [a,c,*], Mireia Salvador [a], Miren Blanco [b], Karmele Vidal [b], Antxon Martínez de Ilarduya [c]

[a] *Color Center, S.A. Ptge. Marie Curie, 3 Nau 6, 08223, Terrassa, Spain*
[b] *Tekniker, Basque Research and Technology Alliance (BRTA), Surface Chemistry and Nanotechnology Unit, Iñaki Goenaga 5, 20600, Gipuzkoa, Spain*
[c] *Departament d'Enginyeria Química, Universitat Politècnica de Catalunya, ETSEIB, Diagonal 647, 08028 Barcelona, Spain*

ABSTRACT

Fabric functionalization to obtain omniphobic textiles is an increasing trend due to science and technology push in our current society. Fluorochemicals dominate the water and oil-repellent textile finishing market because of their excellent performance. However, fluorinated chemicals release harmful substances giving rise to serious damage to ecosystems worldwide. In this paper, a series of fluorine-free, low surface energy and partially bio-based (co)polymethacrylates based on 3-[Tris(trimethylsilyloxy)silyl]propyl methacrylate (M3T) and stearyl methacrylate (SMA) have been successfully synthesized and characterized by Fourier-transform infrared spectroscopy (FTIR), nuclear magnetic resonance (NMR), differential scanning calorimetry (DSC), thermogravimetric analysis (TGA) and Energy-Dispersive X-ray Spectroscopy (EDS). Moreover, the particle size, particle size distribution and stability of developed emulsions have been assessed by laser diffraction spectrometry (LDS) and Z-potential measurements. The fluorine-free M3T/SMA (co)polymethacrylates have been applied on cotton fabrics by padding at several product dosages and coated textiles have been characterized by scanning electron microscopy (SEM), EDS element mapping, X ray fluorescence (XRF) and water and olive oil static contact angle measurements, WCA and OCA, respectively. Finally, performance of the fabrics treated with the new M3T/SMA (co)polymethacrylates has been evaluated and compared with textiles finished with conventional fluorinated chemicals. All the synthetized (co)polymethacrylates provide the coated substrates with high static water contact angles as well as excellent solvent-water separation efficiencies. However, only the textiles coated with the (co)polymethacrylates with higher M3T contents showed good repellence to olive oil, being able to keep the drop of oil on the surface for longer times. This time-dependent olive oil's wettability observed for the copolymers with low contents on M3T units may be ascribed to: i) the evolution with time of the surface free energy of the coatings due to a reorientation over time of stearyl side chains of SMA during contact with the olive oil; and ii) the reduced barrier properties of the coatings with lower content of the bulky tris(trimethylsilyloxy)silyl side chains.

1. Introduction

Most textiles are manufactured from materials that have a remarkable wettability (cotton, silk, linen, polyester…) and therefore have a high tendency to absorb liquids. Modified textiles with treatments that give them hydrophobic and oleophobic properties are highly valued in textile industry not only on clothing, but also in technical textiles: medical fabrics, military uniforms and work protection, technical garments for extreme outdoor sports, textiles for public buildings, automotive, aeronautical, membranes for oil-water separation, etc. [1].

Currently, C8 fluorocarbons dominate the finishing agents' market, as they provide the fabrics with exceptional durable water and oil repellence (DWOR) properties as well as breathability. It is believed that the electronegativity of fluorine atom [2] and the orientation of the perfluorinated chains perpendicular to the textile fibres, helps the fabrics to form a "protective sheath" against fluids. Apart from the
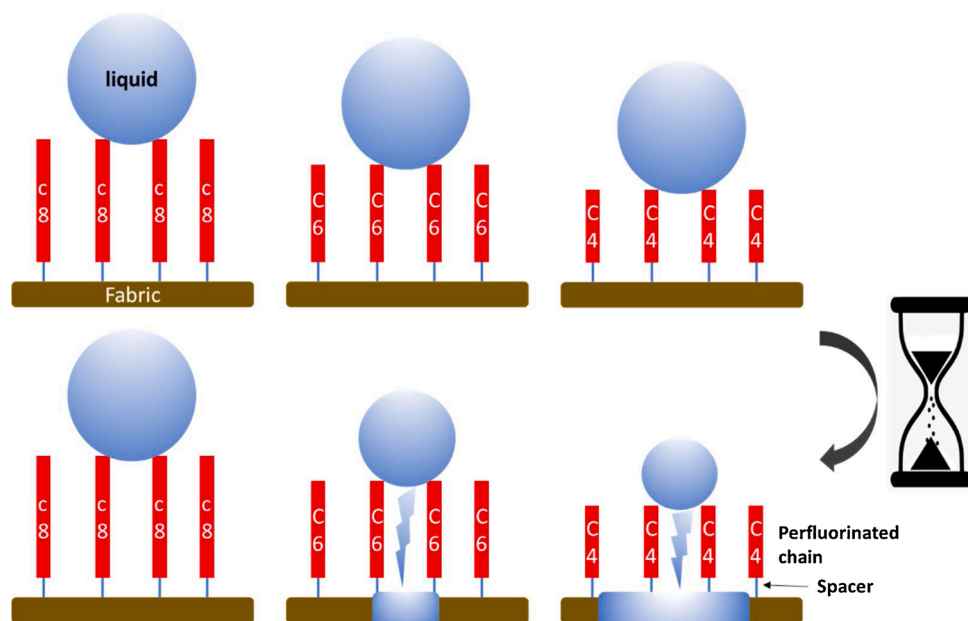
Fig. 1. Long-term wettability of the textiles treated with C8, C6 and C4 fluorocarbons. Adapted from ref. [1].

distribution of C8 fluorocarbons at surface and the generated roughness, low interchain forces, close pack of perfluorinated side chains of polymers and rigidity of the chains, contribute to their low surface energy that can reach values as low as 18 mN/m [3]. These finishing agents offer water contact angles of more than 150° and sliding angles of less than 10°, thus conferring superhydrophobicity, and also provide oil repellence (to a greater or lesser extent depending on the application dosage and the chemical structure of the fluorocarbon) [4,5]. However, despite their excellent performance, C8 fluorocarbons are a source of toxic chemicals that are released into the environment both in their manufacturing process (by-products) and subsequently, by degradation. These toxic substances, known as per- and polyfluorinated chemicals (PFCs), possess harmful effects on health and the environment. Some of them, such as perfluorooctanoic acid (PFOA) and perfluoroctane sulfonic acid (PFOS) are considered bioaccumulative compounds, suspected of being carcinogenic [6], they affect lipid metabolism, and also hormonal and reproductive systems [7,8], and are persistent in nature [9]. In 2000, the United States Environmental Protection Agency (EPA), aware of the scientific studies that pointed out that the PFOA was present in the blood of the entire world population [10], began leading actions for the progressive elimination of the PFOA (2010/15 Stewardship Program). The European community is also taking initiatives in this same direction, culminating in Regulation (EU) 2017/1000 that prohibits the manufacture and marketing of PFOA and related substances (including any polymer that has linear or branched perfluoroheptyl and/or perfluorooctyl groups) by the year 2020 (except for a few exceptions that have extensions).

The most logical alternative to replace C8 fluorocarbons (polymers containing lateral chains with 8 perfluorinated carbon atoms, also known as long-chain fluorocarbons) is the use of polymers with shorter perfluoroalkyl chains (from four to six perfluorinated carbons, also known as C4 and C6 fluorocarbons, respectively, or short-chain fluorocarbons generally speaking), that are not considered bioaccumulative [1,11–13]. However, short-chain fluorocarbons have comparatively lower mechanical and chemical resistance and worse performance [14] and therefore must be applied at higher doses. They have worse repellence to oils, and after a certain time, a drop of liquid ends up wetting the fabric. The Fig. 1 explains the long-term wettability of the textiles treated with C8, C6 and C4 fluorocarbons. The low wettability of textile surfaces treated with C8 fluorocarbon is not a time-dependent

mechanism while there is an increase in wettability over time as we move to short-chain fluorocarbons. The worse performance can be ascribed to the shorter length of the perfluorinated chains which, once in contact to the liquid drop, lose the ability to orient themselves perpendicularly to the fabric surface over time. In addition, C6 and C4 fluorocarbons generate PFCs, including perfluorohexanoic acid (PFHxA) and 1H, 1H, 2H, 2H -Perfluorooctanol (6:2 FTOH), which are currently under study to better understand their environmental and human health effects [5,15,16]. Fluorinated silicones and silanes are able to render oil-repellent surfaces but they fall in the same eco-toxicological drawbacks as fluorocarbons as far as they also have perfluorinated alkyl chains. All these concerns regarding fluorinated chemicals are leading to intensive research and high market demand of fluorine-free alternatives for DWOR finishing, as the textile industry lacks suitable alternatives with comparable material characteristics.

The fluorine-free finishing agents explored in bibliography to achieve DWOR finishes are very diverse, based on very heterogeneous types of chemicals [1]. Fluorine-free long chain alkylamines [17], poly/mono-acrylates [18,19] or silicon containing monomers/polymers [20–23] are being highly studied as (super)hydrophobic finishing for textiles and are commonly blended with nanoparticles such as silica [18, 24–28], polydopamine nanoparticles [17,29], Fe_3O_4 [30], TiO_2 [19,31], montmorillonite [32] to achieve surface roughness and impart superhydrophobic properties in textile fabrics. Apart from polymeric hydrophobic treatments for textiles, fabrics coated with graphene oxides [33], water-repellent textiles obtained by plasma induced surface roughness [34], and textiles functionalized with nanoparticles with or without binding polymers [35] have been intensively investigated. Most of them provide complex approaches, which require several steps for their application on fabrics, which make them unattractive for their industrial implementation. The use of materials such as silanes or polysilsesquioxanes (POSS) with low availability and high price is also quite frequent, in addition to the use of solvents and additives with high environmental impact.

Among the explored alternatives, silicon-based polymers are becoming popular because fabrics treated with them exhibit low surface energy, water repellence, stain resistance, and they also confer high thermal stability as well as softness to the treated goods due to the flexibility of the Si-O-Si bonds. However, most silicon based polymers have poor mechanical properties and bad adhesion to the treated

substrates. By contrast, acrylate polymers display good mechanical properties and good adhesion performance, but poor water resistance and thermal stability. In this context, many attempts for the preparation of silicon-containing acrylate polymers have been conducted with the aim of achieving positive synergies. Lei et al. [2] designed a series of copolymers by combining 3-[Tris(trimethylsilyloxy)silyl]propyl methacrylate (hereafter M3T) and different silicon-free (meth)acrylates to form copolymethacrylates with high silicon content. Side chain of M3T has three Si-$(CH_3)_3$ groups which prevents from easily hydrolysing and gain good alignment on film surface after curing. Moreover, the umbrella-like structure of the Si(OSi$(CH_3)_3)_3$ functional groups confers low surface energy to the treated fabrics allowing them to not only repel water but also fatty acid triglycerides like olive oil, as well as heavy oils (motor oil or mineral oil). These authors demonstrated that M3T-containing (co)polymethacrylates can provide omniphobic surfaces with good anti-stain properties when white spirit is used as solvent for the coating procedure, being the performance of the product reduced when using other organic solvents. However, no studies have been found regarding the synthesis and textile application of waterborne emulsions of M3T and bio-based methacrylic copolymers. As most silicon-containing acrylates, M3T is a prohibitively expensive material. Thus, M3T copolymerization with bio-based acrylates could be an interesting option to reduce price and at the same time investigate synergies while increasing sustainability. As it is well known, the most ideal solvent for chemical reactions is water, which is green and nontoxic. Academic and industrial areas have a strong desire for waterborne coatings. However, water is rarely used as a carrier for low surface tension chemicals because of the poor dispersibility of these materials which makes it very difficult to obtain stable emulsions or dispersions [36–38].

This paper reports the synthesis of a series of waterborne fluorine-free M3T-containing (co)polymethacrylates with remarkable water and oil repellence (WOR) properties. The (co)polymers were obtained by emulsion polymerization using stearyl methacrylate (SMA), a methacrylic comonomer with high bio-content. The conversion degree of the (co)monomers has been qualitatively verified by Fourier-transform infrared spectroscopy (FTIR). Structure and properties of the obtained (co)polymers has been assessed by nuclear magnetic resonance (NMR), differential scanning calorimetry (DSC), thermogravimetric analysis (TGA) and energy-dispersive X-ray spectroscopy (EDS). Moreover, the particle size, particle size distribution and stability of the developed emulsions have been tested by laser diffraction spectrometry (LDS) and Z-potential measurements. Afterwards, the M3T-containing copolymethacrylates were applied onto a hydrophilic cotton fabric by padding method at several product dosages and the textile surface and WOR performance was then characterized by scanning electron microscopy (SEM), EDS element mapping, X-ray fluorescence (XRF) and contact angle measurements with water and olive oil. Results were evaluated against conventional C6 fluorinated textiles. The effect of M3T content in the copolymer and the copolymer dosage in the padding liquor has been studied and related to the textile's WOR performance. Based on the obtained results, the application of the new coated textiles for anti-stain finishing and solvent separation processes have been proposed and demonstrated.

2. Experimental

2.1. Materials

3-[Tris(trimethylsilyloxy)silyl]propyl methacrylate (M3T) is a silicone-based methacrylate with a molecular weight of 422.8 g/mol and it has been supplied by Wacker Chemie AG. Fatty alcohol methacrylic ester Visiomer Terra C17,4-MA (SMA) is a methacrylic compound with a bio-content of 81 % (calculated as ratio of C-number alcohol to C-number methacrylate) and an average molecular weight of 330 g/mol, it has been purchased from Evonik Industries AG. Chemical structures of
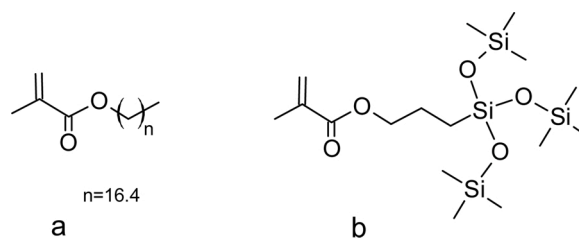
Fig. 2. Chemical structure of: a) SMA and b) M3T monomers.

Table 1
Series of methacrylic copolymers obtained from fluorine-free hydrophobic monomers.

Sample	Amount of M3T (molar %)	Amount of SMA (molar %)
PM3T	100	0
PM3T$_{75}$SMA$_{25}$	75	25
PM3T$_{50}$SMA$_{50}$	50	50
PM3T$_{25}$SMA$_{75}$	25	75
PSMA	0	100

the two monomers are shown in Fig. 2. Isotridecyl alcohol ethoxylated (IAEO) with HLB = 16.5, required to obtain stable emulsions of these monomers, was purchased from BASF (Lutensol TO 20, isotridecyl alcohol condensed with 20 mol of ethylene oxide). 2,2′-Azobis(2-methylpropionamidine)dihydrochloride (V-50) was supplied by Fujifilm. All the chemicals were used without further purification. CENTERGARD C6 PS is a C6 fluorocarbon commercialised by COLOR CENTER, S.A.; it is a waterborne fluorocarbon with an active content around 29 % and it is widely employed in the textile finishing sector as a high-performance fluorinated water and oil repellence (WOR) agent for technical textiles.

Cotton fabric, desized, alkaline scoured and peroxide pre-bleached to remove all the impurities was supplied by INOTEX spol. s r.o. and was used as a substrate to perform the coatings without further (pre)treatment. The main characteristics of the cotton fabric are summarized as follows: composition 100 % cotton; width (EN 1773) 150 cm; set (threads/cm, EN 1049−2) warp = 53.5 / weft = 28.5; weave twill 280; yard count (ISO 1144) warp/weft: 20 tex, cotton ring spun-combed; square weight =158 g/m^2.

2.2. Synthesis of M3T based copolymers and emulsions

(Co)polymers of M3T and SMA were synthesized by emulsion polymerization using the water-soluble azo initiator V-50. A typical process for the emulsion polymerization of the two components copolymer is described as follows: 21.0 g (50 mmol) M3T, 16.8 g of SMA (50 mmol), V-50 0.25 g (0.66 % weight ratio based on total monomer), 3.8 g of IAEO (10.0 % weight ratio based on total monomer) and 88.5 mL of deionized water were charged into a 250 mL three-neck round bottom flask equipped with a reflux condenser. The mixture was heated to 40 °C and stirred with mechanical impeller at 1500 rpm for 15 min.

Afterwards the mixture was ultrasonicated until a homogeneous Tindall emulsion was achieved, then the monomer emulsion was degassed with nitrogen using two vacuum/N$_2$ cycles. The temperature of the mixture was raised to 65 °C and held for 6 h at 500 rpm under nitrogen blanketing to ensure complete monomer conversion. The obtained waterborne (co)polymer emulsions, with a polymer content of 29 %, are summarized in Table 1 and were used without further purification to perform all the application tests on textile fabrics. On the other hand, a small amount of each waterborne emulsion was purified for chemical characterization purposes. The following purification procedure was followed: a small amount of the obtained polymer emulsion was precipitated by adding ethanol and washed several times with ethanol/

acetone 50/50 v/v to wash-off the emulsifying system, then the obtained pure (co)polymer was dried in an oven at 60 °C for 24 h to completely remove traces of water and solvents.

2.3. Application of M3T based copolymers on cotton fabrics

As a substrate, a highly hydrophilic woven cotton fabric, previously bleached and cleaned to remove impurities, has been employed. The cotton fabric is immersed in the bath liquor containing the WOR finishing agent (original copolymer emulsion diluted with deionized water at the indicated dosage), the excess of liquor absorbed by the fabric is removed by squeezing between two rotating rollers at controlled pressure and speed (Foulard Mathis operating at a pressure of 2 bar), the measured average wet pick-up of the impregnated fabrics was within 65 and 67 %. Finally, the impregnated fabric at the exit of the foulard is placed horizontally in a drying oven (Mathis Labcoater), at a drying temperature of 120 °C for 2 min, with a subsequent curing step at 160 °C for 1 min. As a reference, cotton fabrics have been also coated with C6 fluorocarbon CENTERGARD C6 PS.

2.4. Characterization techniques

2.4.1. Characterization of synthesized copolymers and emulsions

A small amount of each waterborne emulsion was precipitated to isolate the polymer which was further purified for subsequent chemical characterization. Fourier transform infrared spectroscopy (FTIR) was employed to qualitatively assess monomer conversion during polymerization. FTIR spectra were obtained using a Perkin Elmer Spectrum Two infrared equipment equipped with an ATR accessory. Forty scans were taken for each sample with a resolution of 8 cm^{-1}. A small portion of the reaction sample was previously treated at mild temperature under IR lamp to evaporate water, before performing FTIR spectra. Structural characterization of (co)polymers was performed by nuclear magnetic resonance (^{1}H NMR and ^{13}C NMR), using a Bruker AMX-300 spectrometer at 25.0 °C operating at 300.1 and 75.5 MHz, respectively. Samples were dissolved in deuterated chloroform, and spectra were internally referenced to tetramethylsilane (TMS). About 10 and 50 mg of sample dissolved in 1 mL of solvent were used for ^{1}H and ^{13}C NMR, respectively. Sixty-four scans were acquired for ^{1}H and 1000 − 10 000 for ^{13}C with 32 K and 64 K data points as well as relaxation delays of 1 and 2 s, respectively. Molecular weight analysis was performed by gel permeation chromatography (GPC) on a Waters equipment provided with RI and UV detectors. 100 μL of 0.1 % (w/v) sample solution was injected and chromatographed with a flow of 0.5 mL/min using as solvent THF. PL1110−1520 and PL1110−6500 Agilent linear PLgel columns (7.5 mm × 300 mm, pore size 10^3–10^4 Å) packed with cross-linked polystyrene and protected with a precolumn were used. Molecular weight averages and distributions were calculated against PMMA standards. Differential scanning calorimetry (DSC) studies of the obtained (co)polymers have been carried out to determine their melting temperature (T_m), crystallization temperature (T_c), melting enthalpy (ΔH_m) and crystallization enthalpy (ΔH_c) as well as possible second-order transitions such as glass transition temperature. Samples were heated from -70 to 150 °C at a constant heating rate of 10 °C/min in a Perkin Elmer model Pyris I under nitrogen atmosphere (50 mL/min), working with 5 mg samples placed in sealed aluminium pans. Second order transitions (T_g) were determined by the StepScan DSC technique that yields enhanced characterization information by separating out the reversible and irreversible thermal events. Measurements were run from -100 °C to 100 °C at a heating and cooling rate of 4 and 2 °C/min respectively, a modulation of amplitude of 1 °C and a period of 60 s. The thermal stability of the synthetized (co)polymers have been studied by thermogravimetric analysis (TGA) under nitrogen and oxidative conditions, using a Mettler Toledo TGA2 equipment. The thermogravimetric analysis consisted of recording the weight loss of the samples subjected to a temperature gradient from 25 °C to 600 °C at 10 °C/min in a furnace

Table 2
Surface tension of liquids employed for anti-stain test (literature values for 20-25 °C).

Liquid	Surface tension (mN/m)
Water [2]	71.4–72.9
Juice [40]+milk [41]	52.0–54.0
coffee [42]	46.2–48.7
red wine [43]	43.6–47.6
olive oil [1]	32.0–33.1

Table 3
Anti-stain performance rating scale.

Rating number	Appearance of the textiles
4	drop remains on the fabric's surface after 5 min, no wetting is observed, no stain residue remains after removing the drop
3	drop remains on the fabric's surface after 5 min, no wetting is observed, slight stain residue remains after removing the drop
2	partial wetting of the fabric surface by the drop after 5 min, stain residue remains after removing the drop
1	partial wetting of the fabric surface by the drop after 5 min, clear visible stain residue remains after removing the drop
0	complete wetting of the fabric surface by the drop after 5 min

with nitrogen or air atmospheres. Finally, the elemental composition of the copolymers has been analysed by Energy-Dispersive X-ray Spectroscopy (EDS), depositing a drop of each emulsion on a silicon wafer.

Moreover, the particle size and the particle size distribution (PSD) of developed aqueous polymeric emulsions have been characterized by Laser Diffraction Spectrometry (LDS). PSD is usually determined over a list of particle size ranges that covers nearly all sizes present in the sample. Polymer dispersity index (PdI) is used to evaluate the dispersion of PSD. LDS measurements were done in a Malvern Mastersizer 2000 instrument (Worcestershire, UK), using water as the dispersion media. A particle Refractive Index of 1.55 was considered for the analysis and 3 measurements were done for each sample. The stability of the dispersions was determined by Z-potential measurements using a Malvern Zetasizer ZS equipment.

2.4.2. Characterization of coated textiles

The surface morphologies of the cotton fibres were observed by scanning electron microscopy (SEM) using an Ultra Gemini-II microscope from Carl Zeiss SMT, also equipped with Energy-Dispersive X-ray Spectroscopy (EDS) which has been employed for element mapping analysis on textile surface. Moreover, X-ray Fluorescence (XRF) was used to perform a semi-quantitative measurement of certain elements on the surface of the treated fabrics using a Bruker S8 TIGER wavelength dispersive X-ray fluorescence spectrometer using vacuum for the analysis.

Water and oil-repellence of the treated cotton fabrics has been tested by a goniometer (SURFTENS Universal) by measuring the contact angle (θ) of a droplet of water (WCA) and olive oil (OCA) placed on the surface of the coated textile. The volume of each liquid droplet was 5 μL and the average value of five measurements, made at different positions of the textile surface, was adopted as the value of WCA or OCA. The sliding angle was measured by manually tilting the stage table of the goniometer. Finally, surface free energies of the copolymethacrylates were determined according to the method developed by Owens and Wendt [39].

Anti-stain performance of the cotton fabrics treated with the (co) polymer emulsions at a dosage of 60 g/L has been evaluated. Five low viscosity liquids were chosen (water, coffee, red wine, juice + milk, olive oil). The surface tension of these liquids is shown in Table 2.

The treated fabrics were first allowed to rest for 48 h and 60 % relative humidity, then 50 μL drops of each liquid were carefully placed
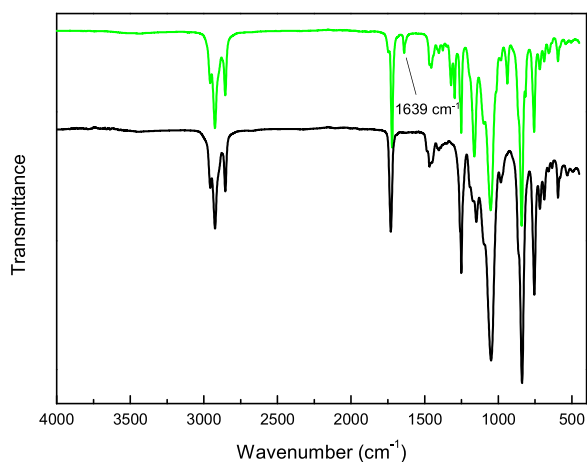
Fig. 3. FTIR spectra in the MIR region for PM3T$_{50}$SMA$_{50}$ sample before (top, green) and after polymerization (bottom, black).

on the substrate's surface via a pipette. The staining agents were allowed to remain on the surface for 5 min, afterwards the remaining drops were removed carefully by absorbent towel and the anti-stain performance was evaluated by 5 level ratings (Table 3).

Air permeability, tensile strength and elongation of the treated and untreated fabrics have been tested. Air permeability was tested using a POLYMERTEST (Zlín, CR) using a pressure difference of 200 Pa and a sample area of 20 cm^2 according to EN ISO 9237. Tensile strength and elongation were tested using the strip method in a SDL M350−10kN (TESTOMETRIC ROCHDALE, England), with a test speed of 100 mm/min according to EN ISO 13934−1.

The solvent-water separation efficiency of the fabrics coated with all the finishing agents at a dose of 60 g/L was measured by a filtration process of a mixture of water and a solvent which is immiscible with water. Water has a high surface tension (72.86 mN/m at 25 °C) while the selected solvent, chloroform, has a surface tension as low as 26.67 mN/m at 25 °C. A mixture containing 25 g of chloroform and 25 g of water was employed to investigate the separation efficiency of the hydrophobic fabrics. The mixture was slowly poured into the filtering equipment (see Fig. 12) where there is already placed the fabric. The hydrophobic fabric was reused 10 times. In each test, the amount of

chloroform is adjusted as it evaporates during the process. The mass of water recovered in each filtration cycle has been recorded. Moreover, the treated fabrics were also employed for solvent-water separation employing a mixture of n-hexadecane (surface tension of 27.30 mN/m at 25 °C) and water. A different test configuration has been employed as n-hexadecane is a light oil which floats on top of the water. The fabrics were employed to prepare a bag in which pristine polyurethane (PU) sponges were filled to achieve high oil absorption capacity. A mixture containing 20 g of n-hexadecane and 60 g of water was employed. The weight of water was measured after the separation cycle.

3. Results and discussion

3.1. Characterization of the synthetized polymeric emulsions

(Co)polymers of M3T and SMA were synthesized by emulsion polymerization using water as a polymerization media. Monomer conversion during polymerization was qualitatively assessed by ATR-FTIR spectroscopy in the MIR region. Fig. 3 shows the FTIR spectra of PM3T$_{50}$SMA$_{50}$ for the initial monomer emulsion of and after polymerization for 6 h at 65 °C. The peaks that clearly disappear during polymerization are: 1639 cm^{-1} (C═C stretching), 935 cm^{-1} (out of plane bending of C–H from the double bond). Also the peaks at 1320 and 1294 cm^{-1} assigned to asymmetric and symmetric stretching vibrations of the C—O bond from the ester groups of methacrylate monomers disappear, shifting to lower frequencies, once the monomers are polymerized. The disappearance of the peak at 1639 cm^{-1} has been specifically taken as a reference for qualitative assessment of monomer conversion. Similar spectra were obtained after polymerization of all the (co)polymers. FTIR spectra of monomers, emulsifier and catalyst employed in the synthesis has been also recorded and reported in Supplementary Information (Figures S1 and S2).

^{1}H and ^{13}C NMR spectra of all PM3T$_x$SMA$_y$ copolymers were recorded, thus confirming chemical structure, tacticity and (co)polymer composition. ^{1}H and ^{13}C NMR spectra of PM3T$_{50}$SMA$_{50}$ with peak assignments are depicted in Fig. 4. Full spectral width ^{1}H NMR spectrum is depicted in Figure S3. Spectra of all the series are included in the Supplementary Information (Figure S4 and S5, for ^{1}H NMR and ^{13}C NMR, respectively). Copolymer composition was determined by integration of signals corresponding to the Si−CH$_3$ and Si−CH$_2$ protons of M3T units appearing at 0.1 and 0.4 ppm respectively (peaks 8 and 7) and the
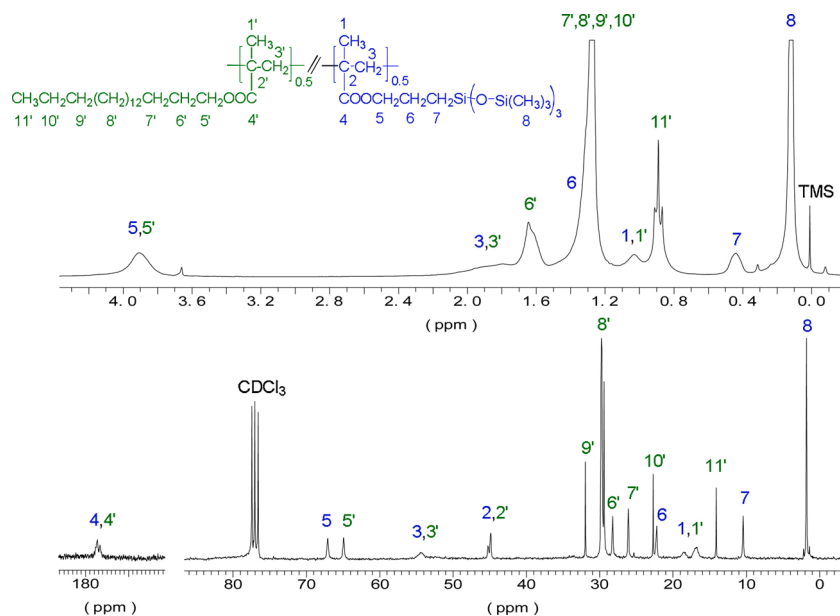
Fig. 4. ^{1}H NMR (top) and ^{13}C NMR (bottom) spectra of PM3T$_{50}$SMA$_{50}$ with peak assignments.

Table 4

Molecular weights, composition and tacticity of PM3T, PSMA and M3T-containing copolymethacrylates.

Polymer	Feed composition[a] [M3T]/[SMA]	Copolymer composition[b] [M3T]/[SMA]	Tacticity[c] m/r	M_n[d]	Đ[d]
PM3T	100/0	100/0	16.6/83.4	248,100	1.4
PM3T$_{75}$SMA$_{25}$	75/25	73.8/26.3	17.1/82.9	326,750	1.5
PM3T$_{50}$SMA$_{50}$	50/50	49.2/50.8	18.4/81.6	295,960	1.6
PM3T$_{25}$SMA$_{75}$	25/75	27.0/73.0	19.9/80.1	244,564	1.3
PSMA	0/100	0/100	17.1/82.9	425,389	1.5

[a] Molar ratio in the initial feed.

[b] Molar ratio in the (co)polymer determined from ^{1}H NMR spectra.

[c] Tacticity determined by integration and averaging of CH$_3$ (1,1′ peaks) and C (2,2′ peaks) which are sensitive to stereoregularity (m: meso or isotactic dyads and r: racemic or syndiotactic dyads).

[d] Number average molecular weights (M_n) and dispersities (Đ) determined by GPC.

signals due to the rest of the protons of both M3T and SMA units (Figure S3). A good correlation between M3T/SMA feed molar ratio and the determined by ^{1}H NMR was observed, indicating that both monomers were fully incorporated in the final copolymer (Table 4). On the other hand, ^{13}C NMR signals due to main chain carbons were used to determine the tacticity of the (co)polymers. These signals were observed to split into different peaks due to stereoregularity effects (Fig. 5). As an example, each of the signals due to CH$_3$ and C carbons were observed to split into two broad peaks corresponding to syndiotactic (rr) and heterotactic (mr/rm) triads. Signals due to isotactic (mm) triads were almost not detected because these copolymers were observed to be predominantly syndiotactic. By integration of these peaks the degree of syndiotacticity was determined, which was around 80 % for all (co)polymers studied (Table 4).

Copolymers of high molecular weights were achieved with M_n values between 244,000 and 425,400 and dispersities between 1.3–1.6 (Table 4).

The thermal properties of the developed (co)polymers have been analysed by DSC and TGA. The non-isothermal DSC thermograms for PM3T, M3T-containing copolymethacrylates and PSMA are shown in Fig. 6. The crystallization and melting temperatures and enthalpies and glass transition temperatures taken from these thermograms are shown in Table 5. The DSC thermogram of PSMA displayed a clear melting peak at 32.6 °C, and a crystallization peak at 19.9 °C, with fusion and crystallization enthalpies of 50.0 and 45.4 J/g, respectively, indicating its crystalline nature and attributed to lamellar packing of paraffinic side chains. The glass transition temperature (T_g) of PSMA has not been observed, not by DSC, not by StepScan DSC, that could be associated to a low content of amorphous phase on this polymer. On the other hand, the homopolymer PM3T only showed a second order transition at 2.0 °C, shown in Supplementary Information (Figure S6), ascribed to the T_g of the sample, which indicates the completely amorphous structure of the material. This can be assigned to the bulkiness of the M3T side groups that doesn't allow them to arrange in a crystalline structure. DSC thermograms of copolymers with SMA content ≥ 50 M% (PM3T$_{50}$SMA$_{50}$ and PM3T$_{25}$SMA$_{75}$) showed the presence of a melting and a crystallization peak, their enthalpies decreasing, and their melting and crystallization temperatures shifting to lower values as M3T content increases, suggesting that both comonomers are randomly incorporated in the chain during the emulsion polymerization. On the other hand, PM3T$_{75}$SMA$_{25}$ does not show first order transitions and a second order transition at -31 °C (Figure S6) due to T_g was observed for this copolymer. The incorporation of the M3T comonomer at random into the polymer chain restricts the packing of the paraffinic side chains reducing the observed melting temperature or preventing its crystallization.
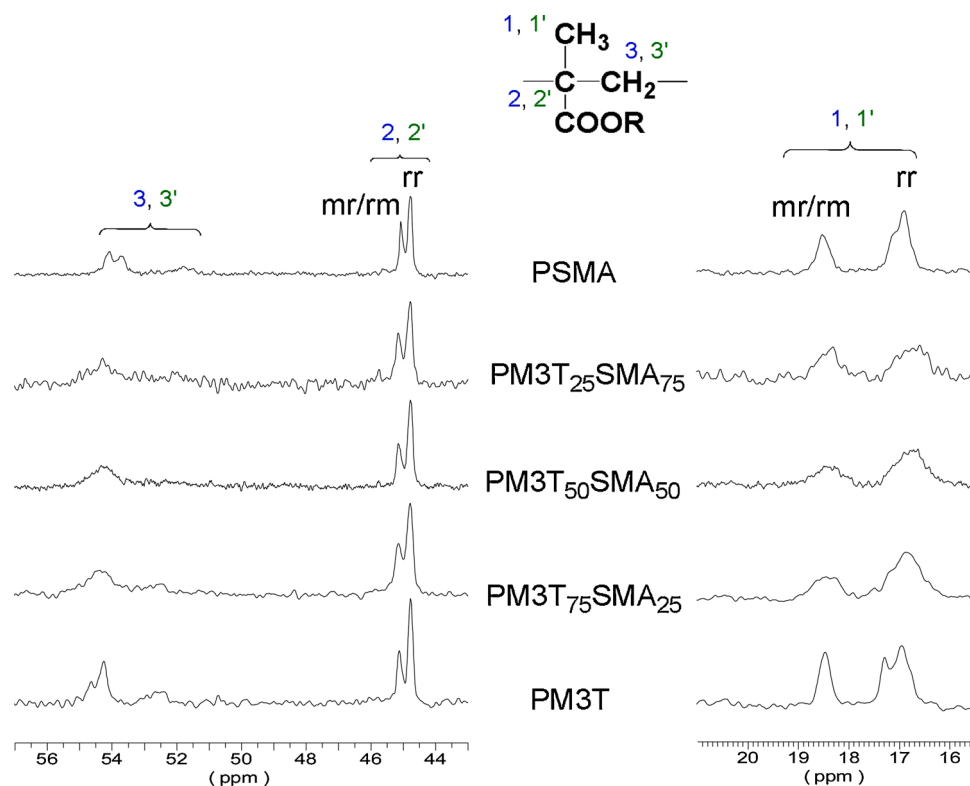
Fig. 5. Expanded ^{13}C NMR spectra of PM3T, PSMA and M3T-containing copolymethacrylates in the region of the main chain CH$_2$ (3,3′), C (2,2′) and CH$_3$ (1,1′) carbons with peak assignments to different stereosequences.

(a)

(b)
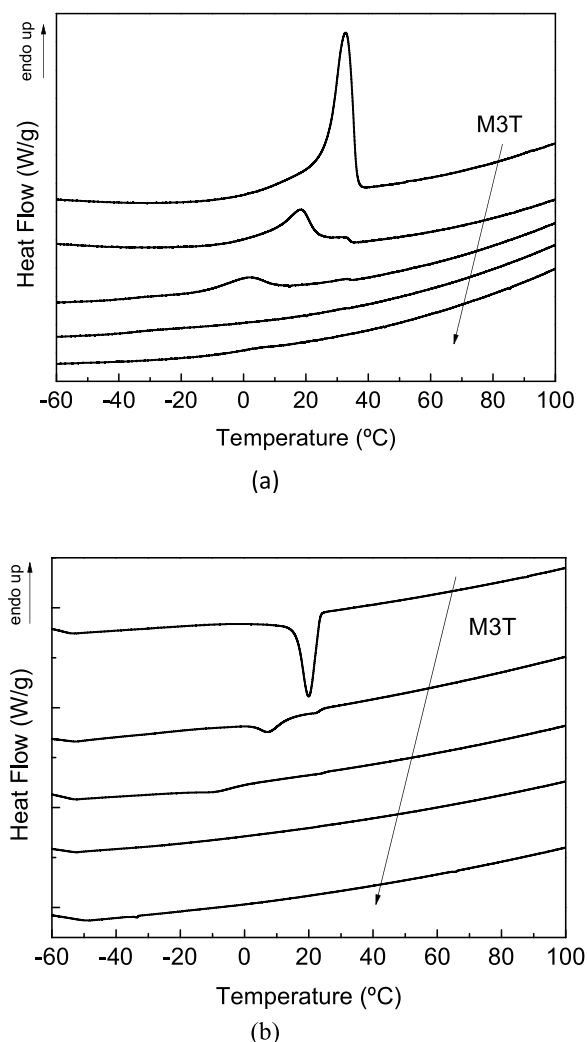
Fig. 6. Second heating (a) and cooling (b) DSC thermograms of the methacrylic (co)polymer. From top to bottom PSMA, PM3T$_{25}$SMA$_{75}$, PM3T$_{50}$SMA$_{50}$, PM3T$_{75}$SMA$_{25}$, PM3T.

The thermal stability of the synthetized (co)polymers has been studied by TGA and curves are collected in Figure S7. The degradation temperatures corresponding to a weight loss of 10 % and the temperatures of the maximum degradation rate are collected in Table 5. All the (co)polymers have sufficient thermal stability to withstand without degradation the temperature conditions that are required to be applied on the fabrics (drying at 120 °C followed by curing at 160 °C for 1 min).

The qualitative elemental composition for the synthetized

polymethacrylates and reference C6 fluorocarbon, obtained by EDS, is shown in Table 6. A drop of each concentrated emulsion has been analysed. EDS values, although they are semiquantitative, show a good correlation with the expected values from the theoretical ratio of monomers in the feed during the synthesis. As it is expected, silicon content determined by EDS decreases as the molar content in M3T in the copolymer decreases. All the samples in the PM3T$_x$SMA$_y$ series are fluorine-free, therefore showing no detectable fluorine. By contrast, fluorocarbon CENTERGARD C6 PS presents a high elemental fluorine content and also some chlorine content arising from the C6-perfluorinated methacrylate and vinylidene chloride monomers, respectively, both employed in the synthesis.

Finally, the emulsion stability, the particle size and particle size distribution of emulsions derived from M3T-containing copolymethacrylates have been investigated. Particle size distribution (PSD) curves of all developed aqueous polymeric emulsions analysed by LDS are shown in Figure S8 and particle size and PdI values are summarized in Table 7. As an example, Fig. 7 collects the particle size distribution curve of PM3T$_{50}$SMA$_{50}$ copolymer and C6 PS product. It is found that particle size distribution curves are unimodal for PM3T, PSMA and all M3T-containing copolymethacrylates, whereas C6 fluorocarbon product presented some agglomerates at higher particle sizes. The average particle sizes (d$_{50}$) were around 180 nm for all the emulsions in the PM3T$_x$SMA$_y$ series and polymer dispersity indexes (PdI) are close to 0.1, indicating that products had satisfactory stability and good dispersibility. The smaller the value of PdI, the better the homogeneity of emulsion [44].

The stability of the dispersions was determined by Z-potential. Measurements have been carried out diluting samples at 40 g/L with sample matrix solution. The Z potential curves of the samples are shown in Supplementary Information (Figure S9) and Z potential values are collected in Table 7. As expected, the zeta potential of C6 fluorocarbon product is higher than +30 mV, indicating their good stability and adhesion to anionic substrates [44,45]. For all the PM3T$_x$SMA$_y$ series, the zeta potential presented similar or even higher positive values indicating their high stability. These positive values could be ascribed to the ammonium chain ends produced by the initiating species which are supposed to be placed in the shell of the micelles.

3.2. Characterization of textiles coated with the PM3T$_x$SMA$_y$ emulsions

To test the performance of synthetized emulsions as WOR finishing agents for textiles, they have been applied on cotton fabrics by padding. SEM micrographs of untreated and treated cotton with PM3T$_x$SMA$_y$ emulsions are illustrated in Fig. 8. The untreated cotton fibres showed smooth surface and cylindrical structures with diameters between 5−20 μm. After the cotton fabric was coated by PM3T and PM3T$_{75}$SMA$_{25}$ at a dose of 60 g/L, an evidently roughness was generated on the surface. However, when the SMA content is increased in the copolymers it was observed that the coating became more smooth. Good film-forming

Table 5
Thermal properties of PM3T, PSMA and M3T-containing copolymethacrylates.

Polymer	DSC Second Heating[b]				DSC Cooling[b]	TGA (N$_2$)		(Air)	
	T_g[a] (°C)	T_m (°C)	ΔH_m (J/g)	T_c (°C)	ΔH_c (J/g)	T_d[c] (°C)	T_d[d] (°C)	T_d[c] (°C)	T_d[d] (°C)
PM3T	2.0	–	–	–	–	286.5	343.3	260.8	287.0
PM3T$_{75}$SMA$_{25}$	−31.0	–	–	–	–	266.6	323.5	246.2	299.1
PM3T$_{50}$SMA$_{50}$	–	2.5	5.5	−9.0	6.5	276.2	340.9	254.8	295.2
PM3T$_{25}$SMA$_{75}$	–	18.5	23.5	7.5	28.0	299.6	341.5	257.6	312.3
PSMA	–	32.5	50.0	20.0	45.5	278.5	325.5	266.6	332.2

[a] Glass-transition temperature taken as the inflection point of the heating step scan DSC.
[b] Melting (T_m) and crystallization (T_c) temperatures and their respective enthalpies (ΔH_m, ΔH_c) measured by DSC at heating / cooling rates of 10 °C min^{-1}.
[c] Temperature at which a 10 % weight loss was observed in the TGA traces recorded at 10 °C min^{-1}.
[d] Temperature of maximum degradation rate.

Table 6

Elemental analysis (wt.%) carried out by EDS for PM3T, M3T-containing copolymethacrylates and reference C6 fluorocarbon.

Element	PM3T	PM3T$_{75}$SMA$_{25}$	PM3T$_{50}$SMA$_{50}$	PM3T$_{25}$SMA$_{75}$	PSMA	C6_PS
C	52.8	57.8	65.5	77.3	85.0	43.1
O	22.9	21.7	19.3	14.5	14.1	8.2
Si	24.3	20.5	15.2	8.2		
F						41.0
Cl						7.7

Table 7

Particle size, PdI and Z-potential obtained by LDS for PM3T, PSMA, M3T-containing copolymethacrylates and reference C6 fluorocarbon.

Sample	d(10) (nm)	d(50) (nm)	d(90) (nm)	PdI	Z potential (mV)
PM3T	133	180	252	0.102	+ 33
PM3T$_{75}$SMA$_{25}$	134	182	256	0.104	+ 41
PM3T$_{50}$SMA$_{50}$	139	192	288	0.111	+ 48
PM3T$_{25}$SMA$_{75}$	137	177	224	0.114	+ 43
PSMA	128	162	194	0.132	+ 41
C6_PS	139	212	363	0.357	+ 33
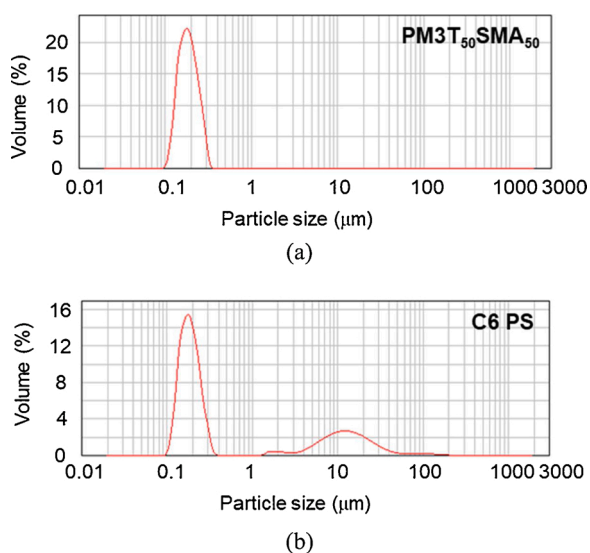
Fig. 7. Particle size distribution obtained by LDS for: a) PM3T$_{50}$SMA$_{50}$ and b) reference C6 fluorocarbon.

properties were observed from SEM images for all the (co)polymers, similar to the film-forming properties of C6 fluorocarbon. Moreover, three dosages of PM3T and PM3T$_{75}$SMA$_{25}$ finishing agent have been applied on cotton fibres. SEM images, collected in Fig. 9, showed that a dose of 100 g/L is too high as the fibres begin to stick together.

The homogeneous distribution of the product on the cotton fabric has been assessed by EDS mapping analysis of elemental silicon, fluorine and chlorine, as can be seen in Fig. 10.

To quantitatively characterize the distribution of elements of interest like Si and F on the fabrics' surface, XRF technique has been applied, obtaining consistent results. Table 8 shows the elemental analysis of the cotton fabrics coated with the (co)polymethacrylate series. The analysis of the different fabrics applied with 60 g/L of the corresponding finishing agent showed a decreasing content of silicon with the decrease in M3T content in the (co)polymer. In addition, silicon content is in a good agreement with EDS analysis. Some other elements such as Ca, S and Fe were also detected in similar amounts on all the fabrics (treated and untreated), indicating that these elements were present on the fibre as impurities. Chlorine, however, comes from the radical initiators used in

the synthesis process. XRF analysis of the fabric coated with C6 fluoropolymer showed also a high content of fluorine and chlorine elements on the samples. Differences in the element content between EDS and XRF can be ascribed to the fact that EDS directly analyses the polymers while XRF analyses the surface of the coated fabrics. The different measuring depth of X ray of both techniques could also contribute to this difference. When different doses of PM3T and PM3T$_{75}$SMA$_{25}$ finishing agents have been applied on cotton fibres, the amount of silicone on the surface increased proportionally.

Water and oil-repellence of the textile surfaces has been characterized by using de-ionized water and olive oil to determine the surface wettability of coatings. Table 9 lists the values of the static water and oil contact angles and the tilt angles, obtained for all samples with the different product doses and the time that a droplet of water and olive oil remained on surface for the fabrics impregnated with the WOR agents at a dose of 60 g/L. It is well known that untreated cotton quickly absorbs water and olive oil and therefore, droplets do not remain on the surface time enough to measure the contact angle. When the cotton fabric was coated by M3T-containing (co)polymethacrylates, these values were dramatically improved and revealed a good repellence towards water and olive oil, at some extent.

Fig. 11 shows the images of the water and oil drops on cotton textile coated with PM3T$_{75}$SMA$_{25}$ as an example. WCA is quite stable with SMA content and remain on surface more than 3600 s with an angle around 127−133°. OCA increases slightly as the SMA content increases to certain extent, going from 110° for 0% SMA, reaching a plateau for SMA content between 25 and 50 % and decreasing again for SMA content ≥75 %. WCA and OCA are also similar to those obtained with the C6 fluoropolymer at this initial time. The similarity of all the values indicates a great contribution of the surface texture/porosity of the fabric [1]. The roughness generated on the surface of these cotton fabrics by the coating, shown in Fig. 8, could contribute to this behaviour.

To better understand the role of copolymethacrylate's composition on WCA and OCA measurements, a control experiment applying these products on smooth glass slides was carried out. The surface free energy of the coated surfaces has been measured showing that PM3T has a surface free energy (around 21 mN/m) whereas the surface free energy of the PSMA is higher (around 26 mN/m). The surface energy of copolymethacrylates are even lower and only slightly higher than the slide covered with the C6 fluoropolymer. These values are in good agreement with previous results [2], but in our study the surface free energy of the polyacrylates is lower than previous reported values due to the different chemical structure.

During the contact angle measurements, a decrease with time of the initial olive oil's contact angle on some glass slide surfaces has been observed. The Table 10 collects the surface free energies calculated from deionized water and olive oil contact angles obtained at time 0, 2, 10, 30 and 60 min. Values at time 0 are in good agreement with the values obtained by Lei et al. for M3T containing copolymethacrylates [2]. For the coatings with higher M3T content, the surface free energy remains constant with time, whereas the coatings with higher SMA content undergo an increase with time. At the molecular level, this trend can be reasoned on the basis that, as the SMA content increases in the coating, the stearyl side chains once in contact with the olive oil reorient themselves over time due to the Van der Waals interactions with the oil. Moreover, the reduction in M3T content causes an increase in the

(a)

(b)

(c)

(d)

(e)

(f)

(g)
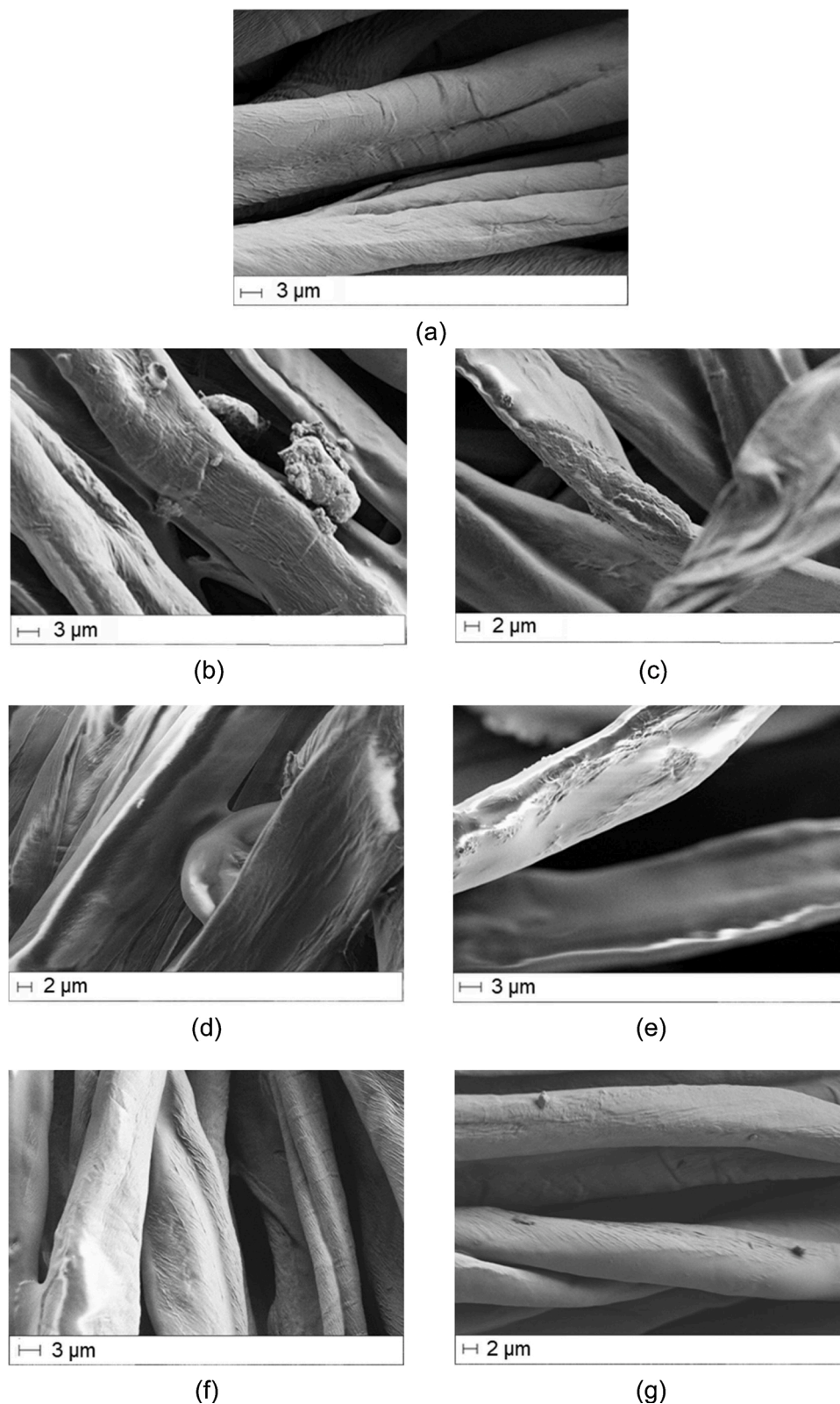
Fig. 8. SEM micrographs for: (a) untreated cotton and coated cotton fabrics: (b) PM3T, (c) PM3T$_{75}$SMA$_{25}$, (d) PM3T$_{50}$SMA$_{50}$, (e) PM3T$_{25}$SMA$_{75}$, (f) PSMA and (g) C6 PS with a dosage of 60 g/L. Micrographs have been obtained with a magnification of x2000 and 3.3 mm of working distance.

distance between bulky tris(trimethylsilyloxy)silyl side chains, thus reducing the barrier protection of the coating to olive oil.

In the case of the coated cotton fabrics, significant differences are observed in the time that the droplets of olive oil remain on fabric's surfaces, due to the coating composition. Whereas the olive oil is immediately absorbed by the fabric coated with PSMA, the olive oil droplet remains initially on the surface of the fabrics with copolymethacrylates and PM3T and thereafter, it is progressively absorbed. This can be related to the evolution of the surface free energy of the product. The time that an olive oil droplet remains on the surface increases with
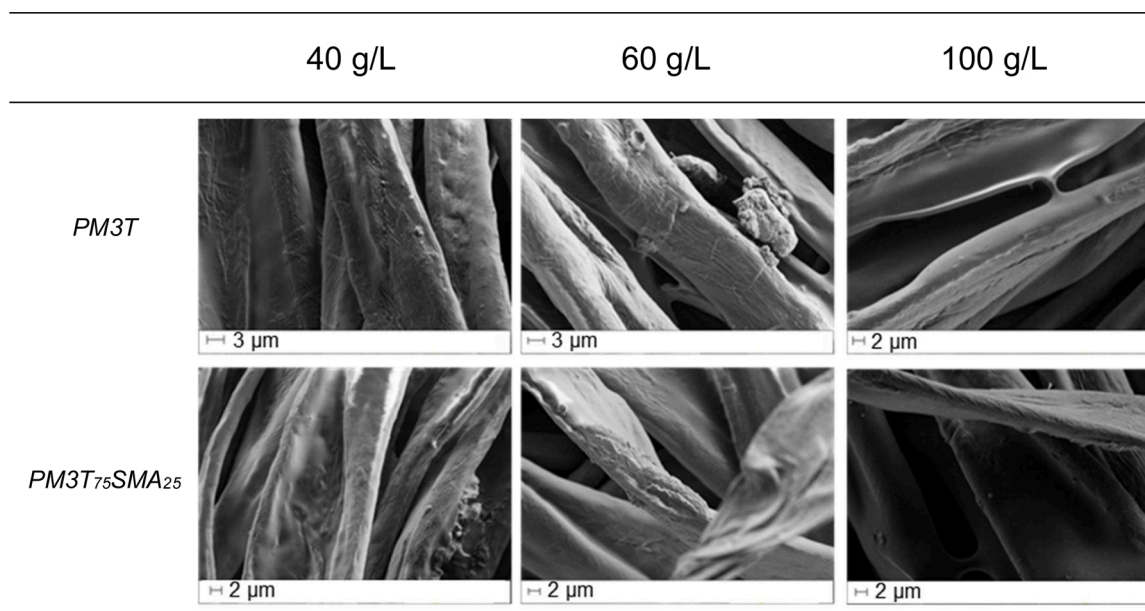
Fig. 9. SEM micrographs for PM3T and PM3T$_{75}$SMA$_{25}$ coated cotton textiles with a dosage of 40, 60 and 100 g/L. Micrographs have been obtained with a magnification of x2000 and 3.3 mm of working distance.
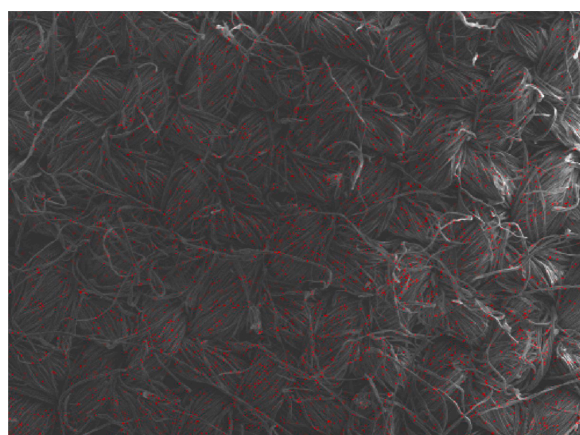
(a)
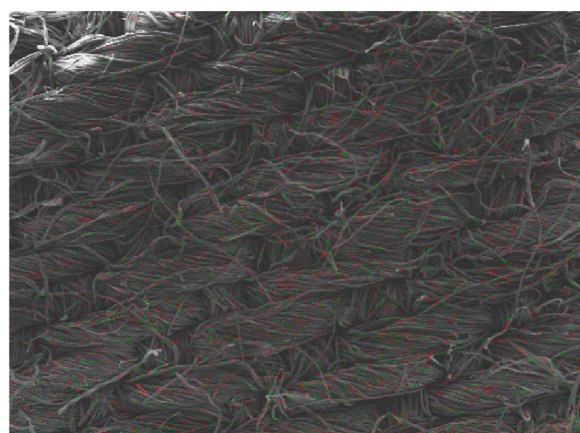
(b)

Fig. 10. EDS mapping of coated cotton textiles with doses of 60 g/L of: a) PM3T$_{75}$SMA$_{25}$ emulsion (silicon in red) and b) C6 PS fluorocarbon (fluorine in green and chlorine in red).

Table 8
Atomic concentration (%) by XRF for untreated and coated cotton textiles.

Product applied on cotton fabric per(dose)	XRF (%)					
	Si	Cl	Ca	S	Fe	F
Untreated cotton	0.01	0.04	0.22	0.01	0.02	–
PM3T (40 g/L)	0.87	0.07	0.20	0.03	0.04	–
PM3T (60 g/L)	1.43	0.08	0.21	0.04	0.03	–
PM3T (100 g/L)	2.27	0.07	0.21	0.03	0.03	–
PM3T$_{75}$SMA$_{25}$ (40 g/L)	0.81	0.07	0.21	0.03	0.02	–
PM3T$_{75}$SMA$_{25}$ (60 g/L)	1.11	0.07	0.21	0.03	0.06	–
PM3T$_{75}$SMA$_{25}$ (100 g/L)	1.67	0.08	0.20	0.03	0.04	–
PM3T$_{50}$SMA$_{50}$ (60 g/L)	0.74	0.08	0.21	0.03	0.08	–
PM3T$_{25}$SMA$_{75}$ (60 g/L)	0.39	0.08	0.23	0.03	0.09	–
PSMA (60 g/L)	0.01	0.09	0.25	0.03	0.04	
C6 PS (60 g/L)	0.02	0.79	0.22	0.05	0.03	0.91

M3T content, reaching a maximum around 2100 s for the M3T homo-polymer. The tilt angle for water and olive oil is quite similar for all the samples but higher than C6 PS fluorocarbon, indicating the higher surface free energy of cotton fabrics treated with PM3T$_x$SMA$_y$ emulsions, as previously observed in Table 9. Moreover, for the three doses of PM3T and PM3T$_{75}$SMA$_{25}$ finishing agent that have been applied on cotton fibres, only slight changes in static and tilt angle measurements for water and oil were observed. It can be concluded that 60 g/L is an optimum dosage and dosages of 100 g/L do not lead to better results.

Overall, the coatings showed good hydrophobicity but limited oleophobic properties, as olive oil drops remained on the surfaces and thereafter, they soaked. The best results in terms of oleo-repellence are obtained for PM3T and PM3T$_{75}$SMA$_{25}$, while PSMA presented the worse results. However, it is important to highlight that PM3T$_x$SMA$_y$ emulsions are able to confer oil-repellence against fatty triglycerides without using fluorine, this paves the way for the use of these new polymers for different applications, such as anti-stain finishing and solvent-water separation.

The anti-stain performance of PM3T$_x$SMA$_y$ emulsions is shown in Tables 11, Table 1212 and Table 1313 . For untreated cotton, all the liquids quickly spread and penetrated, leaving a marked stain after removing the liquid and cleaning the substrate. However, the cotton substrates coated with PM3T$_x$SMA$_y$ emulsions at 60 g/L retain the drop

Table 9

Values of water and olive oil static contact angles and water and olive oil tilt angles for untreated and coated cotton textiles.

Product applied on cotton fabric (dose)	Water static contact angle (θs) (°)	Time that the water's droplet remains (s)	Tilt angle for water (°)	Olive oil static contact angle (°)	Time that the olive oil's droplet remains (s)	Tilt angle for olive oil (°)
Untreated cotton	absorbed	absorbed	absorbed	absorbed	absorbed	absorbed
PM3T (40 g/L)	119 ± 1	–	30 ± 3	101 ± 1	–	49 ± 3
PM3T (60 g/L)	128 ± 1	> 3600	36 ± 3	110 ± 1	~2100	45 ± 3
PM3T (100 g/L)	123 ± 1	–	32 ± 2	114 ± 1	–	47 ± 2
PM3T$_{75}$SMA$_{25}$ (40 g/L)	126 ± 1	–	42 ± 3	115 ± 1	–	43 ± 4
PM3T$_{75}$SMA$_{25}$ (60 g/L)	127 ± 2	> 3600	47 ± 2	120 ± 1	~720	42 ± 4
PM3T$_{75}$SMA$_{25}$ (100 g/L)	129 ± 2	–	39 ± 5	116 ± 1	–	43 ± 3
PM3T$_{50}$SMA$_{50}$ (60 g/L)	133 ± 1	> 3600	41 ± 3	120 ± 1	~100	48 ± 3
PM3T$_{25}$SMA$_{75}$ (60 g/L)	129 ± 1	> 3600	45 ± 2	117 ± 3	~45	48 ± 3
PSMA (60 g/L)	130 ± 3	> 3600	42 ± 2	absorbed	0	absorbed
C6 PS (60 g/L)	132 ± 1	> 3600	27 ± 3	122 ± 2	> 3600	40 ± 3
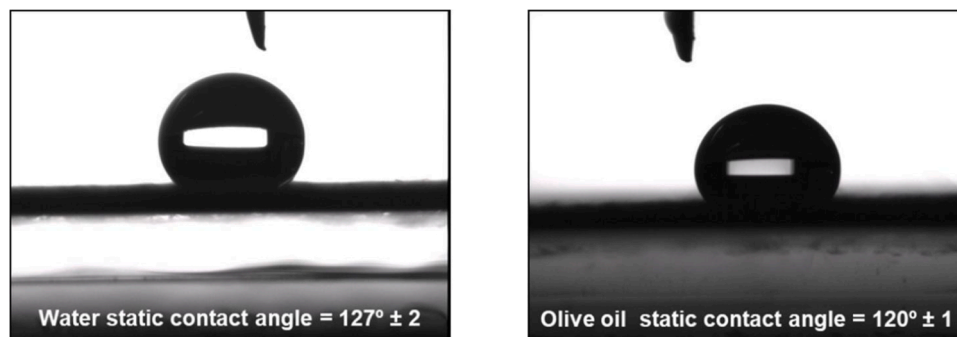
Fig. 11. Image of a drop of: water (left) and olive oil (right) on cotton textile coated with PM3T$_{75}$SMA$_{25}$ at 60 g/L.

of water-based liquids on the surface for 5 min and much longer time. Moreover, the drop of olive oil is also maintained on the surface for PM3T and PM3T$_{75}$SMA$_{25}$ for 5 min (thereafter, drop soaked). After carefully removing the remaining drop, it can be observed that drops of liquids with higher surface tensions, such as water, coffee and juice + milk drops, do not leave any mark on textiles. Wine left a small mark on all surfaces, even in the C6 fluorocarboned substrate. Finally, the drop of liquid with the lowest surface tension, the olive oil, left a noticeable mark on textiles which have absorbed the drop, but only a slight mark is observed for PM3T coated textile and the mark on PM3T$_{75}$SMA$_{25}$ coated textile is almost undetectable. As it was expected the oil repellence of the textiles increases with the M3T content in copolymer.

The solvent-water separation performance of the treated fabrics was validated by a filtering process of a mixture of two immiscible liquids with different surface tensions: water and chloroform in a weight ratio of 1:1 [46,47]. The chloroform-water mixture was slowly poured into the filtration equipment where the treated fabric is already placed and acts as a filtration membrane. Because of its higher density, chloroform comes immediately into contact with the fabric membrane and passes throughout it while water is retained. The filtration process is very fast and it takes less than 30 s for all the experiments. The hydrophobic fabrics have been reused 10 times. The mass of water has been weighted after each cycle. As it can be observed in Fig. 12, the water amount remained almost constant for the filtration recycling processes for all the textiles indicating their high efficiency in chloroform-water separation. A video has been included in supporting information showing the

performance of a cotton fabric coated with PM3T$_{75}$SMA$_{25}$ at 60 g/L (see Video1).

Moreover, the fabrics have been also employed for solvent-water separation employing a mixture of n-hexadecane/water in a weight ratio 3:1. The fabrics were employed to prepare a bag in which pristine polyurethane (PU) sponges were filled to achieve high oil absorption capacity (Fig. 13) [48]. The weight of water was measured after the separation process showing that all n-hexadecane has been absorbed by the bags. A n-hexadecane:water separation performance between 95 and 98 % has been achieved for all the textiles (Table 14).

Finally, air permeability, tensile strength and elongation of some of the finished cotton fabrics were measured and compared with the values from the untreated fabric. As can be seen in Table 15, the cotton fabrics finished with 60 g/L of PM3T and PM3T$_{75}$SMA$_{25}$ does not result in significant change of air permeability, tensile strength and elongation with respect to the untreated fabric.

4. Conclusions

A series of waterborne PM3T$_x$SMA$_y$ emulsions have been successfully synthesized by emulsion free radical polymerization of M3T and SMA, being the latter a bio-based monomer, with the aim of obtaining eco-friendly WOR finishing agents for textile applications. Monomer conversion was qualitatively assessed by FTIR and chemical structure, tacticity and copolymer composition was studied by NMR. DSC results corroborated the random polymerization of the comonomers as well as

(a)

(b)
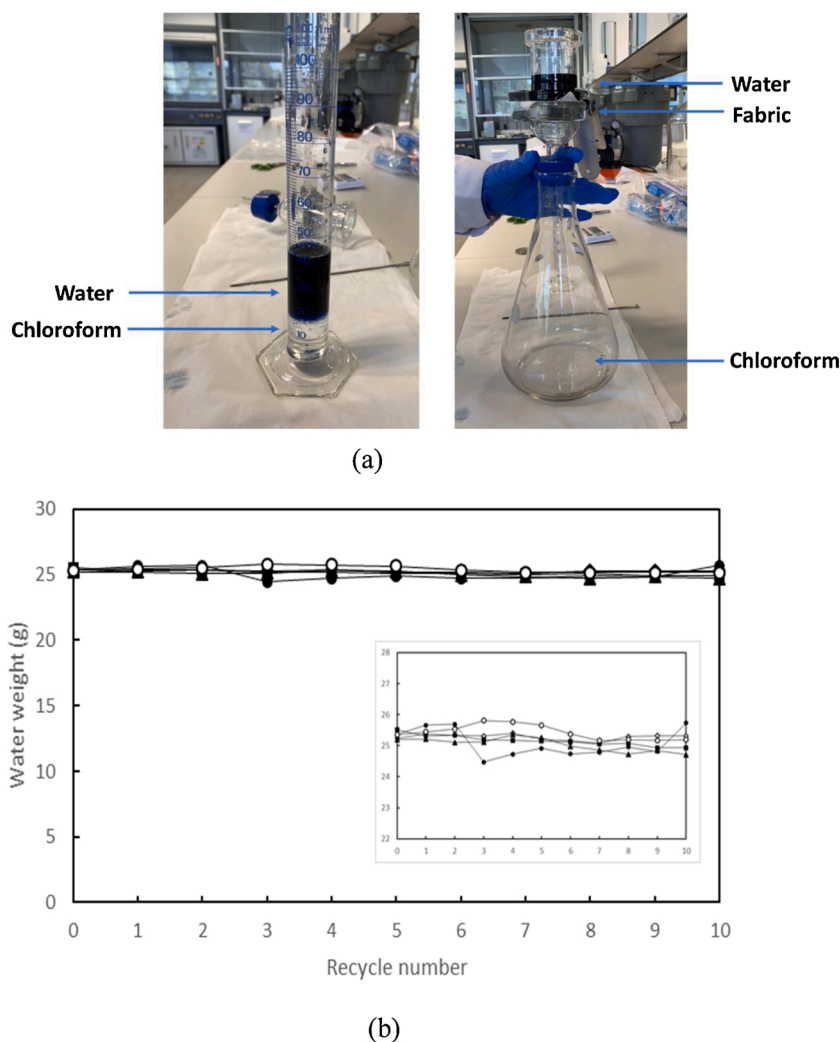
Fig. 12. (a) Pictures of the chloroform-water separation process and (b) variation of the water weight after each filtering cycle for (●) PM3T, (■) PM3T$_{75}$SMA$_{25}$, (▲) PM3T$_{50}$SMA$_{50}$, (○) PM3T$_{25}$SMA$_{75}$ and (◇) PSMA.

Table 10
Evolution of surface free energies with time for the coatings applied on glass slides.
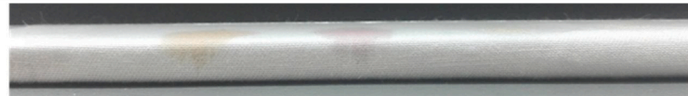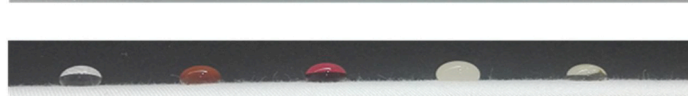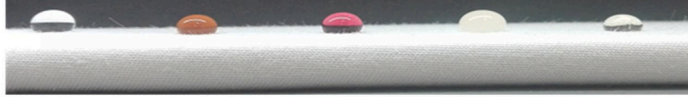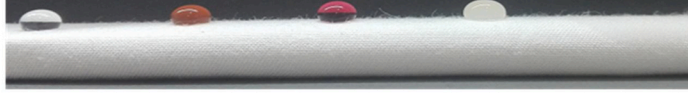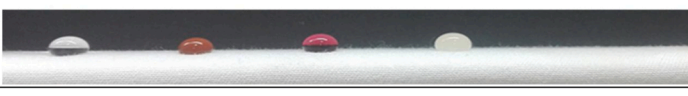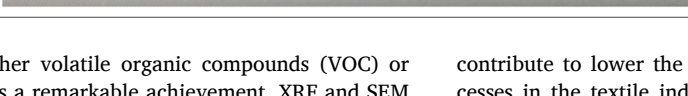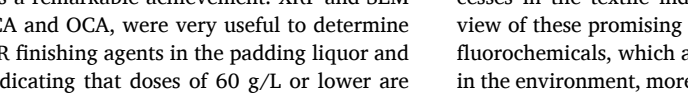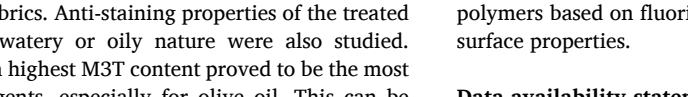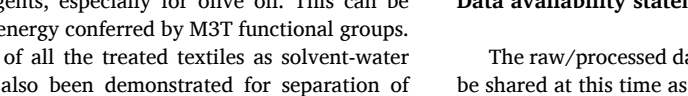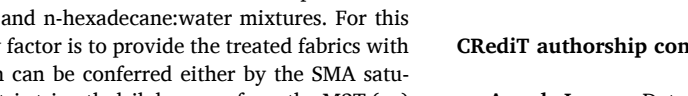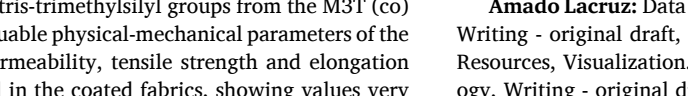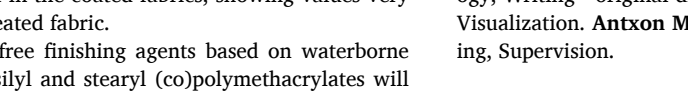
Product (dose)	Surface free energy (mN/m)				
	t =0 min	t =2 min	t =10 min	t =30 min	t =60 min
PM3T (60 g/L)	21.5	22.2	22.3	22.6	22.1
PM3T$_{75}$SMA$_{25}$ (60 g/L)	16.4	15.9	18.7	15.9	15.8
PM3T$_{50}$SMA$_{50}$ (60 g/L)	14.3	17.8	22.4	25.0	26.4
PM3T$_{25}$SMA$_{75}$ (60 g/L)	16.2	18.8	21.4	22.0	22.4
PSMA (60 g/L)	26.0	26.8	26.9	33.1	32.7
C6 PS (60 g/L)	13.4	13.5	13.6	13.3	13.4

first and second order thermal transitions, whereas EDS confirmed an increasing content of silicon with the increase of M3T in the obtained copolymers. TGA was used to determine the thermal stability of the (co)polymers. Moreover, particle size, particle size distribution and zeta potential of the (co)polymethacrylate emulsions have been analysed. The results showed that (co)polymethacrylate emulsions had good stability, all of them showing a particle size below 200 nm (d(50)) as well as narrow unimodal particle size distribution.

Thereafter, the PM3T$_x$SMA$_y$ emulsions were applied onto cotton fabric by padding method and the textile surface and performance were then characterized and compared against conventional C6 fluorocarbon. SEM and XRF analysis confirmed that (co)polymethacrylates had been successfully applied onto the surface of cotton fabric. As expected, a decreasing content of elemental silicon is observed in the textiles with the decrease of M3T molar ratio in the copolymer. EDS mapping analysis of silicon indicated a homogeneous distribution of the finishing agents on the fabric's surface. Static contact angle measurements, WCA and OCA, showed that all the studied finishing agents provided cotton with good hydrophobicity with WCA around 127−133º, and acceptable oleophobic properties in front of olive oil. OCA between 101° and 120° were obtained for all the treated substrates except for the fabrics treated with PSMA where olive oil soaked immediately due to the absence of tris-trimethylsilyl functional groups. Olive oil's drops only remained on the fabrics' surface for a limited period (from a few seconds for (co)polymers with low M3T content to several minutes for (co)polymers with higher M3T ratio) and thereafter they soaked. This time-dependent wettability may be ascribed to the evolution with time of the surface free energy of the coatings with lower M3T contents due to a reorientation over time of stearyl side chains of SMA once in contact with the olive oil and to the lower barrier properties of the coatings with lower contents of the bulky tris-trimethylsilyl side-chains.

In any case, it is important to highlight that PM3T$_x$SMA$_y$ emulsions can confer oil-repellence against fatty triglycerides without using

Table 11
Image of a drop of liquid after 5 min. on untreated and coated cotton textiles.

Anti-stain performance	water	coffee	red wine	Juice + milk	Olive oil
Untreated fabric					
PM3T (60 g/L)					
PM3T$_{75}$SMA$_{25}$ (60 g/L)					
PM3T$_{50}$SMA$_{50}$ (60 g/L)					
PM3T$_{25}$SMA$_{75}$ (60 g/L)					
PSMA (60 g/L)					
C6 PS (60 g/L)					

fluorinated chemicals, neither volatile organic compounds (VOC) or harmful chemicals, which is a remarkable achievement. XRF and SEM micrographs, as well as WCA and OCA, were very useful to determine the optimum dosage of WOR finishing agents in the padding liquor and therefore on the fabrics, indicating that doses of 60 g/L or lower are optimum for the selected fabrics. Anti-staining properties of the treated fabrics against liquids of watery or oily nature were also studied. PM3T$_x$SMA$_y$ emulsions with highest M3T content proved to be the most efficient as anti-staining agents, especially for olive oil. This can be ascribed to the low surface energy conferred by M3T functional groups. The excellent performance of all the treated textiles as solvent-water separation membrane has also been demonstrated for separation of chloroform:water mixtures and n-hexadecane:water mixtures. For this specific application, the key factor is to provide the treated fabrics with high hydrophobicity, which can be conferred either by the SMA saturated fatty chains or by the tris-trimethylsilyl groups from the M3T (co) monomer. Finally, some valuable physical-mechanical parameters of the untreated fabric like air permeability, tensile strength and elongation are not significantly altered in the coated fabrics, showing values very similar to those of the untreated fabric.

Therefore, the fluorine-free finishing agents based on waterborne emulsions of tris-trimethylsilyl and stearyl (co)polymethacrylates will contribute to lower the environmental impact of WOR finishing processes in the textile industry and solvent-water separation sector. In view of these promising results and the urgent need for replacement of fluorochemicals, which are known for bioaccumulation and persistence in the environment, more efforts should be devoted to the design of new polymers based on fluorine-free building blocks that provide advanced surface properties.

Data availability statement

The raw/processed data required to reproduce these findings cannot be shared at this time as the data also forms part of an ongoing study.

CRediT authorship contribution statement

Table 12
Image of drop residues after cleaning (zenith view) on pristine and coated cotton textiles.

Anti-stain performance	water	coffee	red wine	Juice + milk	Olive oil
Untreated fabric					
PM3T (60 g/L)					
PM3T$_{75}$SMA$_{25}$ (60 g/L)					
PM3T$_{50}$SMA$_{50}$ (60 g/L)					
PM3T$_{25}$SMA$_{75}$ (60 g/L)					
PSMA (60 g/L)					
C6 PS (60 g/L)					

Table 13
Values of drop residues on untreated and coated cotton textiles after 5 min.

Anti-stain performance	water	coffee	red wine	Juice + milk	Olive oil
Untreated fabric	0	0	0	0	0
PM3T (60 g/L)	4	4	3	4	2
PM3T$_{75}$SMA$_{25}$ (60 g/L)	4	4	3	4	1
PM3T$_{50}$SMA$_{50}$ (60 g/L)	4	3	2	4	0
PM3T$_{25}$SMA$_{75}$ (60 g/L)	4	3	2	4	0
PSMA(60 g/L)	4	3	2	4	0
C6 PS (60 g/L)	4	4	3	4	4

Table 14
Effiency of n-hexadecane:water separation of the different textiles.

n-hexadecane:water separation efficiency	water initial weight (g)	water final weight (g)	Efficiency (%)
PM3T (60 g/L)	60.1	57.9	96.3
PM3T$_{75}$SMA$_{25}$ (60 g/L)	62.9	61.2	97.3
PM3T$_{50}$SMA$_{50}$ (60 g/L)	60.1	57.5	95.7
PM3T$_{25}$SMA$_{75}$ (60 g/L)	60.1	58.9	98.0
PSMA (60 g/L)	60.6	58.3	96.2
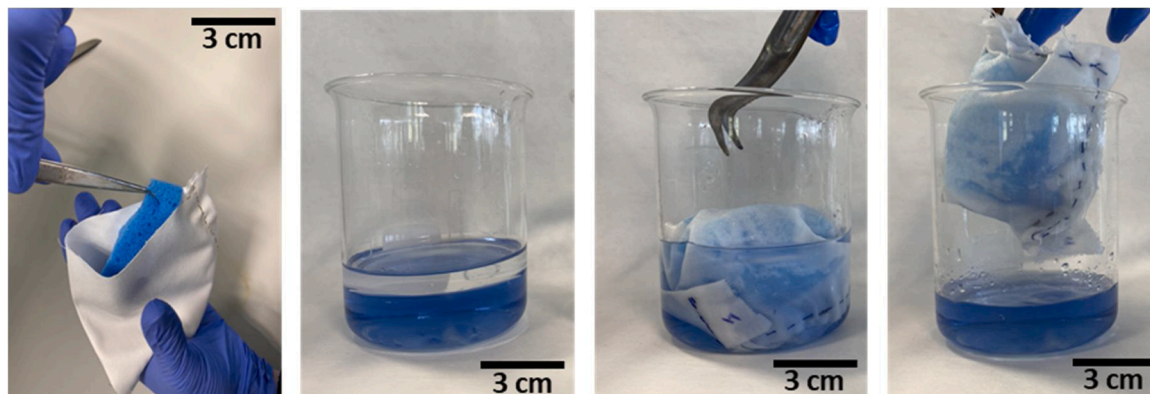
Fig. 13. Pictures of the textile during the n-hexadecane-water separation process for the textile treated with PM3T$_{75}$SMA$_{25}$.

Table 15
Air permeability, tensile strength and elongation of untreated and treated fabrics with PM3T and PM3T$_{75}$SMA$_{25}$.

Properties	Untreated fabric	PM3T (60 g/L)	PM3T$_{75}$SMA$_{25}$ (60 g/L)
Air permeability (mm/s)	119	112	111
Tensile strength (N)	warp: 1039	warp: 1045	warp: 1073
	weft: 544	weft: 589	weft: 570
Elongation (%)	warp: 15.3	warp: 15.7	warp: 15.6
	weft: 13.4	weft: 14.0	weft: 14.3

Declaration of Competing Interest

The authors declare that they have no known competing financial interests or personal relationships that could have appeared to influence the work reported in this paper.

Acknowledgments

Appendix A. Supplementary data

Supplementary material related to this article can be found, in the online version, at doi:https://doi.org/10.1016/j.porgcoat.2020.105968.

References

[1] M. Zahid, G. Mazzon, A. Athanassiou, I.S. Bayer, Environmentally benign non-wettable textile treatments: a review of recent state-of-the-art, Adv. Colloid Interface Sci. 270 (2019) 216–250, https://doi.org/10.1016/j.cis.2019.06.001.

[2] H. Lei, M. Xiong, J. Xiao, L. Zheng, Y. Zhu, X. Li, Q. Zhuang, Z. Han, Fluorine-free low surface energy organic coating for anti-stain applications, Prog. Org. Coat. 103 (2017) 182–192, https://doi.org/10.1016/j.porgcoat.2018.07.036.

[3] M. Ma, Y. Mao, M. Gupta, K.K. Gleason, G.C. Rutledge, Superhydrophobic fabrics produced by electrospinning and chemical vapor deposition, Macromolecules 38 (2005) 9742–9748, https://doi.org/10.1021/ma0511189.

[4] D. Xiong, G. Liu, E.J.S. Duncan, Diblock-copolymer-coated water-and oil-repellent cotton Fabrics, Langmuir 28 (2012) 6911–6918, https://doi.org/10.1021/la300634v.

[5] GORE-TEX garment technology, GORE-TEX brand. https://www.gore-tex.com/technology/original- gore-tex-products/garments.

[6] J.W. Martin, S.A. Mabury, K.R. Solomon, D.C.G. Muir, Progress toward understanding the bioaccumulation of perfluorinated alkyl acids, Environ. Toxicol. Chem. 32 (2013) 2421–2423, https://doi.org/10.1002/etc.2376.

[7] B.J. Apelberg, F.R. Witter, J.B. Herbstman, A.M. Calafat, R.U. Halden, L. L. Needham, L.R. Goldman, Cord serum concentrations of perfluorooctane sulfonate (PFOS) and perfluorooctanoate (PFOA) in relation to weight and size at birth, Environ. Health Perspect. 115 (2007) 1670–1676, https://doi.org/10.1289/ehp.10334.

[8] C. Fei, J.K. McLaughlin, R.E. Tarone, J. Olsen, Perfluorinated chemicals and fetal growth: a study within the Danish national birth cohort, Environ. Health Perspect. 115 (2007) 1677–1682, https://doi.org/10.1289/ehp.10506.

[9] L. Vierke, C. Staude, A. Biegel-Engler, W. Drost, C. Schulte, Perfluorooctanoic acid (PFOA)-main concerns and regulatory developments in Europe from an environmental point of view, Environ. Sci. Eur. 24 (2012) 16, https://doi.org/10.1186/2190-4715-24-16.

[10] K.J. Hansen, L.A. Clemen, M.E. Ellefson, H.O. Johnson, Compound-specific, quantitative characterization of organic fluorochemicals in biological matrices, Environ. Sci. Technol. 35 (2001) 766–770, https://doi.org/10.1021/es001489z.

[11] B. Ballarin, D. Barreca, M.C. Cassani, G. Carraro, C. Maccato, A. Mignanii, D. Lazzari, M. Bertola, Fluoroalkylsilanes with embedded functional groups as building blocks for environmentally safer self-assembled monolayers, Langmuir 31 (2015) 6988–6994, https://doi.org/10.1021/acs.langmuir.5b01416.

[12] S. Nagappan, M.C. Choi, G. Sung, W.K. Lee, C.S. Ha, Highly transparent, hydrophobic fluorinated polymethylsiloxane/silica organic-inorganic hybrids for anti-stain coating, Macromol. Res. 21 (2013) 669–680, https://doi.org/10.1007/s13233-013-1069-7.

[13] E. Bormashenko, R. Grynyov, G. Chaniel, H. Taitelbaum, Y. Bormashenko, Robust technique allowing manufacturing superoleophobic surfaces, Appl. Surf. Sci. 270 (2013) 98–103, https://doi.org/10.1016/j.apsusc.2012.12.124.

[14] J. Williams, Waterproof and Water Repellent Textiles and Clothing, first ed., Elsevier Inc., 2017 https://doi.org/10.1016/C2015-0-06037-3.

[15] A.L. Luz, J.K. Anderson, P. Goodrum, J. Durda, Perfluorohexanoic acid toxicity, part I: development of a chronic human health toxicity value for use in risk assessment, Regul. Toxicol. Pharmacol. 103 (2019) 41–55, https://doi.org/10.1016/j.yrtph.2019.01.019.

[16] J.E. Klaunig, M. Shinohara, H. Iwai, C.P. Chengelis, J.B. Kirkpatrick, Z. Wang, R. H. Bruner, Evaluation of the chronic toxicity and carcinogenicity of perfluorohexanoic acid (PFHxA) in Sprague-Dawley Rats, Toxicol. Pathol. 43 (2015) 209–220, https://doi.org/10.1177/0192623314530532.

[17] Y. Liu, Y. Liu, H. Hu, Z. Liu, X. Pei, B. Yu, P. Yan, f. Zhou, Mechanically induced self-healing superhydrophobicity, J. Phys. Chem. C. 119 (2015) 7109–7114, https://doi.org/10.1021/jp5120493.

[18] K. Sasaki, M. Tenjimbayashi, K. Manabe, S. Shiratori, Asymmetric superhydrophobic/superhydrophilic cotton fabrics designed by spraying polymer and nanoparticles, ACS Appl. Mater. Interfaces 8 (2016) 651–659, https://doi.org/10.1021/acsami.5b09782.

[19] N.F. Attia, M. Moussa, A.M.F. Sheta, R. Taha, H. Gamal, Effect of different nanoparticles based coating on the performance of textile properties, Prog. Org. Coat. 104 (2017) 72–80, https://doi.org/10.1016/j.porgcoat.2016.12.007.

[20] T. Kim, H. Kang, N. Yoon, Synthesis of non-fluorinated paraffinic water repellents and application properties on textile fabrics, Fibers Polym. 18 (2017) 285–289, https://doi.org/10.1007/s12221-017-6469-4.

[21] Q. Zhu, Q. Gao, Y. Guo, C.Q. Yang, L. Shen, Modified silica sol coatings for highly hydrophobic cotton and polyester fabrics using a one-step procedure, Ind. Eng. Chem. Res. 50 (2011) 5881–5888, https://doi.org/10.1021/ie101825d.

[22] M. Zahid, J.A. Heredia-Guerrero, A. Athanassiou, I.S. Bayer, Robust water repellent treatment for woven cotton fabrics with eco-friendly polymers, Chem. Eng. J. 319 (2017) 321–332, https://doi.org/10.1016/j.cej.2017.03.006.

[23] D. Chen, F. Chen, H. Zhang, X. Yin, Y. Zhou, Preparation and characterization of novel hydrophobic cellulose fabrics with polyvinylsilsesquioxane functional coatings, Cellulose 23 (2016) 941–953, https://doi.org/10.1007/s10570-015-0820-y.

[24] Y. Wu, H. Qi, B. Li, Z. Huang, W. Li, S. Liu, Novel hydrophobic cotton fibers adsorbent for the removal of nitrobenzene in aqueous solution, Carbohydr. Polym. 155 (2017) 294–302, https://doi.org/10.1016/j.carbpol.2016.08.088.

[25] J. Li, L. Yan, Y. Zhao, F. Zha, Q. Wang, Z. Lei, One-step fabrication of robust fabrics with both-faced superhydrophobicity for the separation and capture of oil from water, Phys. Chem. Chem. Phys. 17 (2015) 6451–6457, https://doi.org/10.1039/c5cp00154d.

[26] N. Guo, Y. Chen, Q. Rao, Y. Yin, C. Wang, Fabrication of durable hydrophobic cellulose surface from silane-functionalized silica hydrosol via electrochemically assisted deposition, J. Appl. Polym. Sci. 132 (2015) 42733–42739, https://doi.org/10.1002/app.42733.

[27] Q. Liu, J. Huang, J. Zhang, Y. Hong, Y. Wan, Q. Wang, m. Gong, Z. Wu, C.F. Guo, Thermal, waterproof, breathable, and antibacterial cloth with a nanoporous structure, ACS Appl. Mater. Interfaces 10 (2018) 2026–2032, https://doi.org/10.1021/acsami.7b16422.

[28] S. Xu, H. Li, X. Lai, L. Zhang, J. Wang, X.F. Liao, X.R. Zeng, Vapor-liquid sol-gel approach to fabricating highly durable and robust superhydrophobic polydimethylsiloxane@silica surface on polyester textile for oil-water separation, ACS Appl. Mater. Interfaces 9 (2017) 28089–28099, https://doi.org/10.1021/acsami.7b08920.

[29] H. Wang, H. Zhou, S. Liu, H. Shao, S. Fu, G.C. Rutledge, T. Lin, Durable, self-healing, superhydrophobic fabrics from fluorine-free, waterborne, polydopamine/alkyl silane coatings, RSC Adv. 7 (2017) 33986–33993, https://doi.org/10.1039/c7ra04863g.

[30] S. Fu, H. Zhou, H. Wang, J. Ding, S. Liu, Y. Zhao, H. Niu, G.C. Rutledge, T. Lin, Magnet-responsive, superhydrophobic fabrics from waterborne, fluoride-free coatings, RSC Adv. 8 (2018) 717–723, https://doi.org/10.1039/c7ra10941e.

[31] Y. Yin, R. Huang, W. Zhang, M. Zhang, C. Wang, Superhydrophobic-superhydrophilic switchable wettability via TiO2 photoinduction electrochemical deposition on cellulose substrate, Chem. Eng. J. 289 (2016) 99–105, https://doi.org/10.1016/j.cej.2015.12.049.

[32] D. Zhang, B.L. Williams, S.B. Shrestha, Z. Nasir, E.M. Becher, B.J. Lofink, V. H. Santos, H. Patel, X. Peng, L. Sun, Flame retardant and hydrophobic coatings on cotton fabrics via sol-gel and self-assembly techniques, J. Colloid Interface Sci. 505 (2017) 892–899, https://doi.org/10.1016/j.jcis.2017.06.087.

[33] N.D. Tissera, R.N. Wijesena, J.R. Perera, K.M.N. De Silva, G.A.J. Amaratunge, Hydrophobic cotton textile surfaces using an amphiphilic graphene oxide (GO) coating, Appl. Surf. Sci. 324 (2015) 455–463, https://doi.org/10.1016/j.apsusc.2014.10.148.

[34] J.H. Oh, T.J. Ko, M.W. Moon, C.H. Park, Nanostructured fabric with robust superhydrophobicity induced by a thermal hydrophobic ageing process, RSC Adv. 7 (2017) 25597–25604, https://doi.org/10.1039/c7ra03801a.

[35] M. Zhang, J. Pang, W. Bao, W. Zhang, H. Gao, C. Wang, J. Shi, J. Li, Antimicrobial cotton textiles with robust superhydrophobicity via plasma for oily water separation, Appl. Surf. Sci. 419 (2017) 16–23, https://doi.org/10.1016/j.apsusc.2017.05.008.

[36] J. Zhang, Z. Gao, L. Li, B. Li, H. Sun, Waterborne nonfluorinated superhydrophobic coatings with exceptional mechanical durability based on natural nanorods, Adv. Mater. Interfaces 4 (2017) 1700723, https://doi.org/10.1002/admi.201700723.

[37] H. Ye, L. Zhu, W. Li, H. Liu, H. Chen, Simple spray deposition of a water-based superhydrophobic coating with high stability for flexible applications, J. Mater. Chem. A 5 (2017) 9882–9890, https://doi.org/10.1039/C7TA02118F.

[38] X. Zhao, Y. Li, B. Li, T. Hu, Y. Yang, L. Li, J. Zhang, Environmentally benign and durable superhydrophobic coatings based on SiO2 nanoparticles and silanes, J. Colloid Interface Sci. 542 (2019) 8–14, https://doi.org/10.1016/j.jcis.2019.01.115.

[39] W.K. Owens, R.C. Wendt, Estimation of the surface free energy of polymers, J. Appl. Polym. Sci. 13 (1969) 1741–1747, https://doi.org/10.1002/app.1969.0701130815.

[40] D. Saha, M. Hait, M. Patanwar, Ankit Tamrakar, Studies on surface tension of selected juice formulation by drop number method using Traube's stalagmometer technique, Bull.Pharm. Res 1 (2011) 1–3, https://doi.org/10.13140/RG.2.1.1864.0080.

[41] R. Chandan, Dairy Based Ingredients: Practical Guides for the Food Industry, Eagen Press Handbook Series, USA, 1997.

[42] L. Navarini, M. Ferrari, F.S. Liverani, L. Liggieri, F. Ravera, Dynamic tensiometric characterization of espresso coffee beverage, Food Hydrocoll. 18 (2004) 387–393, https://doi.org/10.1016/S0268-005X(03)00126-7.

[43] P. Glampedaki, E. Hatzidimitriou, A. Paraskevopoulou, S. Pegiadou-Koemtzopoulou, Surface tension of still wines in relation to some of their constituents: a simple determination of ethanol content, J. Food Anal. 23 (2010) 373–381, https://doi.org/10.1016/j.jfca.2010.01.006.

[44] Y. Sun, X. Zhao, R. Liu, G. Chen, X. Zhou, Synthesis and characterization of fluorinated polyacrylate as water and oil repellent and soil release finishing agent for polyester fabric, Prog. Org. Coat. 123 (2018) 306–313, https://doi.org/10.1016/j.porgcoat.2018.07.013.

[45] Q. An, W. Xu, L. Hao, L. Huang, Cationic fluorinated polyacrylate core-shell latex with pendant long chain alkyl: synthesis, film morphology, and its performance on cotton substrates, J. Appl. Polym. Sci. 127 (2013) 1519–1526, https://doi.org/10.1002/app.37553.

[46] X. Dong, S. Gao, J. Huang, S. Li, T. Zhu, Y. Cheng, Y. Lai, A self-roughened and biodegradable superhydrophobic coating with UV shielding, solar-induced self-healing and versatile oil-water separation ability, J. Mater. Chem. A 7 (2019) 2122–2128, https://doi.org/10.1039/c8ta10869b.

[47] Y. Deng, D. Han, Y.Y. Deng, Q. Zhang, O. Fu, Facile one-step preparation of robust hydrophobic cotton fabrics by covalent bonding polyhedral oligomeric silsesquioxane for ultrafast oil/water separation, Chem. Eng. J. 379 (2020) 122391, https://doi.org/10.1016/j.cej.2019.122391.

[48] C. Cao, M. Ge, J. Huang, S. Li, S. Deng, S. Zhang, Y. Lai, Robust fluorine-free superhydrophobic PDMS–ormosil@fabrics for highly effective self-cleaning and efficient oil–water separation, J. Mater. Chem. A Mater. Energy Sustain. 4 (2016) 12179–12187, https://doi.org/10.1039/c6ta04420d.

Biobased Waterborne Polyurethane-Urea/SWCNT Nanocomposites for Hydrophobic and Electrically Conductive Textile Coatings

Amado Lacruz [1,2,*], Mireia Salvador [1], Miren Blanco [3], Karmele Vidal [3], Amaia M. Goitandia [3], Lenka Martinková [4], Martin Kyselka [4] and Antxon Martínez de Ilarduya [2]

1   Color Center, S.A. Ptge. Marie Curie 3, Nau 6, 08223 Terrassa, Spain; msalvador@colorcenter.es
2   Departament d'Enginyeria Química, Universitat Politècnica de Catalunya, ETSEIB, Diagonal 647, 08028 Barcelona, Spain; antxon.martinez.de.ilarduia@upc.edu
3   Tekniker, Basque Research and Technology Alliance (BRTA), Surface Chemistry and Nanotechnology Unit, Iñaki Goenaga 5, 20600 Gipuzkoa, Spain; miren.blanco@tekniker.es (M.B.); karmele.vidal@tekniker.es (K.V.); amaia.martinez@tekniker.es (A.M.G.)
4   Inotex spol. s r.o, Stefanikova 1208, 54401 Dvur Kralove n.L., Czech Republic; martinkova@inotex.cz (L.M.); kyselka@inotex.cz (M.K.)
*   Correspondence: amado.lacruz@upc.edu or alacruz@colorcenter.es; Tel.: +34-9378-61113

Abstract: Waterborne polyurethane-urea dispersions (WPUD), which are based on 100% bio-based semi-crystalline polyester polyol and isophorone diisocyanate, have been successfully synthesized and doped with single-walled carbon nanotubes (SWCNT) to obtain a finishing agent that provides textiles with multifunctional properties. The chemical structure of WPUD has been characterized by Fourier-transform infrared spectroscopy (FTIR) and nuclear magnetic resonance (NMR). The thermal properties have been evaluated by differential scanning calorimetry (DSC), thermogravimetric analysis (TGA), and dynamic mechanical thermal analysis (DMTA). Mechanical properties have been studied by tensile stress–strain analysis. Moreover, the particle size, particle size distribution (PSD), and stability of developed waterborne dispersions have been assessed by dynamic light scattering (DLS), Z-potential, and accelerated aging tests (analytical centrifugation). Subsequently, selected fabrics have been face-coated by the WPUD using knife coating method and their properties have been assessed by measuring water contact angle (WCA), water column, fabric stiffness, and air permeability. The electrical conductivity of textiles coated with SWCNT-doped WPUD has been evaluated by EN 1149 standard. Finally, the surface morphologies of uncoated and coated fabrics have been studied by scanning electron microscopy (SEM). All of the synthesized polyurethane-ureas provide the coated substrates with remarkable water-repellency and water column, being therefore a more sustainable alternative to waterproof coatings based on fluoropolymers, such as PTFE. The additivation of the polymeric matrices with SWCNT has led to textile coatings with excellent electrical conductivity, maintaining water column properties, giving rise to multifunctional coatings that are highly demanded in protective workwear and technical textiles.

Keywords: waterproof; water-column; fluorine-free; bio-based; hydrophobic; electrically conductive textiles; nanocomposites; technical textiles; multifunctional fabrics; textile coatings

1. Introduction

Hydrophobicity, permeation-resistance, and electrical conductivity are highly valued functionalities for technical textiles, like medical fabrics, protective workwear, technical garments for extreme outdoor sports, automotive and aeronautical textiles, wearable sensors, smart textiles, etc. Perfluoroalkyl and polyfluoroalkyl substances (PFASs) have been, for several decades valuable, widely used chemicals to coat textile substrates, as they are inert, low surface energy materials, therefore providing coated fabrics with exceptional

durable water and oil repellence (DWOR). PFASs can be divided in two classes: non-polymeric and polymeric PFASs [1]. The most commonly used PFASs in the textile industry fall within the last class. As defined by Buck et al. [1], polymeric PFASs encompasses fluoropolymers, like polytetrafluoroethylene (PTFE) or polyvinylidene fluoride (PVDF), side-chain fluorinated polymers (commonly known in the textile sector as fluorocarbons), and perfluoropolyethers.

It is well established that non-polymeric PFASs, like perfluorooctanoic acid (PFOA) and perfluoroctane sulfonic acid (PFOS), possess harmful effects on health and the environment [2–6]. Shorter homologues, like perfluorohexanoic acid (PFHxA), are currently under study to better understand their environmental and human health effects [7,8], and it is likely that restriction proposals that were recently posted by some EU countries will come into force in the near future. On the other hand, polymeric PFASs are a potential source of non-polymeric PFASs and bioavailable small particles [9,10]. Fluoropolymers, like PTFE and PVDF in the form of emulsions or fine powders, are manufactured using non-polymeric PFASs as processing aids that can be released to the environment during their entire life-cycle, which is, manufacture, application on fabrics (manufacture of finished articles), use, and disposal [11]. Furthermore, many fluoropolymers are commercialized in the form of fine suspensions of low particle size that can give rise to potentially dangerous fluorinated particles and oligomers [12,13]. In addition, side-chain fluorinated polymers can degrade and release non-polymeric PFASs to the environment [14] and, therefore, are considered to be high concern chemicals.

It should be noted that commercial waterproof textiles usually contain multiple types of PFASs susceptible to being released into the environment [15]. For instance, the multiple layered materials used in all-weather clothing are the result of a laminate commonly composed of three layers: outer layer made of polyester or polyamide fibers that are coated by a side-chain fluorinated polymer to confer water and oil repellence, middle layer, which is typically a PTFE or polyurethane membrane that confers hydrostatic pressure, and, finally, an inner layer of hydrophilic nature, which allows the transport of sweat and moisture to the outside. See Figure 1 for a schematic of a typical multi-layered fabric for outdoor clothing. All of the above-mentioned concerns regarding PFASs in textile sector are leading to intensive research and high market demand of fluorine-free alternatives for DWOR finishing [16–18].
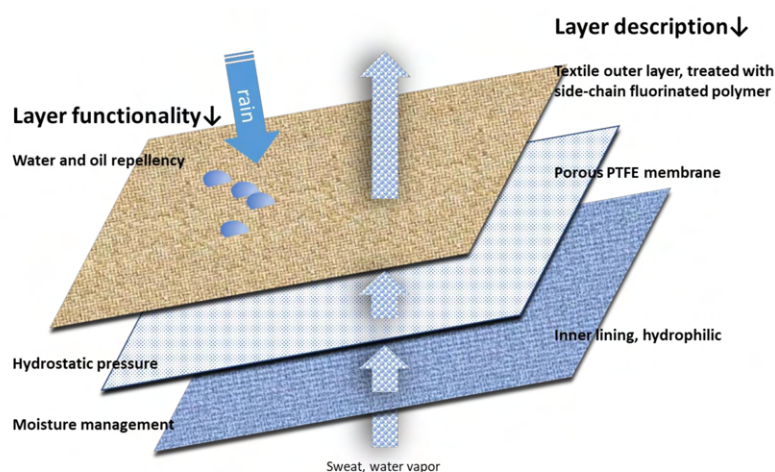
Figure 1. Scheme of a typical multi-layered fabric for outdoor clothing.

On the other hand, providing fabrics with electrical conductivity without affecting the rest of the material's properties is a highly demanded feature. To achieve this goal, polymeric fibers that are made of conductive polymers or polymeric filled nanocomposites have been studied, but this alternative is expensive and the use of high content of fillers can lead to fibers with poor mechanical properties, poor processability, and high cost. Another

alternative is the use of coatings to make conductive textiles. Several technologies, such as layer-by-layer deposition [19], electroless plating [20], or chemical plating [21], among others, have been explored, but with several drawbacks, such as the pollution by heavy metals, time-consuming, and expensive processes [22]. In this context, the development of sustainable conductive coatings, which can be also a reliable alternative regarding PFASs for providing water repellence and water column to the textiles, is an appealing research for the textile industry. Bio-based, waterborne polyurethanes are eco-friendly in nature, avoiding the use of traditional solvents that are toxic and expensive. They also include bio-based building blocks in its composition, and its structure can be tailored to meet specific applications [23–25]. Moreover, they can be modified with different nanofillers to provide them with new properties. Carbonaceous nanostructures, such as carbon nanotubes (CNTs) or graphene, have been reported as a suitable nanofillers for providing conductivity to textile coatings, owing to their unique electrical properties. However, the property improvements can be limited due to the degree of dispersion or poor orientation of the nanomaterial [26]. Different approaches have been reported for improving their dispersion or orienting carbon nanofillers by employing mechanical stretching [27], an electric field [28], or a magnetic field [29], but these approaches are usually difficult to apply at the industrial level.

This work focuses on providing a sustainable and multifunctional alternative to fluoropolymers, like PTFE or petrol-based polyurethanes, which are commonly employed as a membrane to confer water column to multi-layered fabrics for High-Tech applications. Firstly, a series of fluorine-free, waterborne, partially bio-based polyurethane-urea dispersions (WPUD) with remarkable hydrophobicity and good resistance to water permeation (water column or hydrostatic pressure) has been synthesized, characterized, and applied to fabrics by knife coating to form a membrane on its surface. The incorporation of single-walled carbon nanotubes (SWCNT) in the polyurethane-urea matrix by the use of a commercial masterbatch has also been studied as a simple strategy to confer electrical conductivity to the coatings.

The partially bio-based polyurethane-ureas were obtained by the prepolymer method using, as starting building blocks, isophorone diisocyanate (IPDI), 100% bio-based polyester-polyol (Priplast 3294), internal emulsifier dimethylolbutanoic acid (DMBA), and chain extenders bio-1,3-propylene glycol (1,3-PDO) and ethylene diamine (EDA). The experimental design of ternary mixture has been applied as a methodology to explore systematically the ratio between polyol, internal emulsifier and chain extenders.

Structure and properties of the obtained polyurethane-ureas have been assessed by FTIR, NMR, DSC, TGA, DMTA, and stress–strain mechanical tests. Moreover, DLS, Z-potential, and analytical centrifugation have been used to assess particle size distribution and the stability of the developed waterborne dispersions. Subsequently, selected fabrics have been face-coated by the WPUD by knife coating, and their properties have been assessed by measuring water contact angle (WCA), water column, fabric stiffness, and air permeability. The electrical conductivity of the coated textiles with SWCNT-modified WPUD has been evaluated by the EN 1149 standard. Finally, the surface morphologies of uncoated and coated fabrics have been studied by scanning electron microscopy (SEM).

2. Materials and Methods

2.1. Materials

A fully biobased semicrystalline polyester polyol that was based on dimerized fatty acid (Figure 2), commercially known as Priplast 3294 was supplied by Croda Iberica. Priplast 3294 is a highly-hydrophobic, semicrystalline polyester polyol, providing high flexibility at low temperatures, good hydrolytic stability, and enhanced adhesion to dissimilar substrates. This polyol has a M_n of 2000 g mol^{-1}, $f_{(OH)} = 2$, and an average hydroxyl value of 56 mg KOH g^{-1}. Isophorone diisocyanate (IPDI, ≥99.5% purity) was supplied by Evonik Industries GmbH (Vestanat IPDI). 2,2-Bis(hydroxymethyl)butyric acid (DMBA, 99% purity) was supplied by Anhui Sinograce Chemical CO., LTD. 1,3-Propanediol (1,3-PDO,

≥99% purity and 100% biobased) was supplied by DuPont Tate&Lyle BioProducts. Acetone (≥99.5% purity), triethylamine (TEA, 99% purity), and ethylenediamine (EDA, ≥99% purity) were purchased from Sigma-Aldrich. Everchem Specialty Chemicals supplied Bicat 8108 (bismuth neodecanoate 20%).
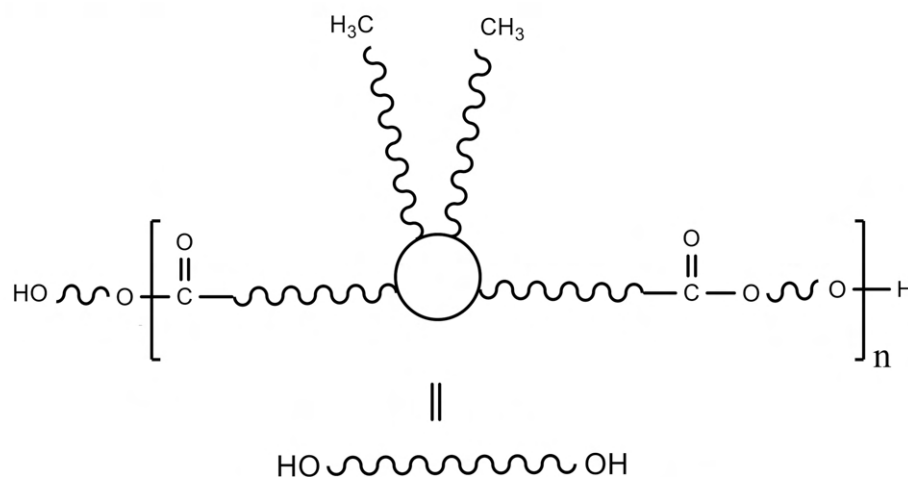
Figure 2. The chemical structure of Priplast 3294.

The additives to formulate the printing pastes were supplied by Color Center, S.A. and are: Defoamer PR (defoamer, mineral oil-based), Complex DG (diethylene glycol-based, runnability improver), DMEA (dimethylethanolamine, neutralizing agent), and Thickener L-120 (polyacrylic acid, associative thickener). A commercial aliphatic polyether-urethane waterborne dispersion from Color Center, S.A., 35% solids, non-biobased, referenced as RD27, has been included in this work as a comparative example.

A masterbatch containing 10 wt. % SWCNT dispersed in a wax matrix, TUBALL MATRIX BETA 302, easily dispersible in waterborne systems, was employed to provide polymeric dispersions with electrical conductivity. The sample was kindly supplied by OCSiAl EUROPE.

Pristine polyester fabric (UPRON) was supplied by HEDVA a.s. and it was used as a substrate to perform the coatings. The main characteristics of the pristine UPRON fabric are summarized, as follows: 100% polyester fabric (PET, polyethylene terephthalate), plain weave, 172 ± 5 g m^{-2}; and, threads per cm^2: warp 32 ± 2, weft 14 ± 1.

2.2. Synthesis of Waterborne Polyurethane-Urea Dispersions

Priplast 3294 was dried under vacuum at 110 °C and 35 mbar for 1 h before use. Priplast 3294 was introduced into a 750 mL five-necked reactor fitted with a mechanical stirrer, an inlet for nitrogen, and a reflux condenser. DMBA internal emulsifier and PDO chain extender were added to the reactor and degassed for 1 h at 80 °C under stirring to complete homogenization. IPDI and Bicat 8108 (25 mg per kg of mixture) were subsequently added to the reactor. The temperature was maintained at 80 °C under nitrogen blanketing until the theoretical value of NCO was reached (measured by titration using the dibuthylamine method). The reaction time for the prepolymer formation was between 2 and 2.5 h. All of the prepolymers were prepared at an isocyanate/hydroxyl ratio (NCO/OH) of 1.62. Afterwards, acetone was added to decrease the viscosity of the prepolymer and facilitate its subsequent dispersion in water (typically 100 g/200 g of prepolymer). The reaction mixture was cooled to 40 °C and TEA was added slowly though a dropping funnel and the mixture maintained for 30 min. under stirring to ensure complete neutralization of the carboxyl groups from DMBA. The reaction system was subsequently cooled to 30 °C and cold deionized water at 8 °C was quickly added with vigorous stirring to promote phase inversion, thus obtaining a milky dispersion of the prepolymer in water. Chain extension agent EDA was stoichiometrically added to react with the free isocyanate groups of the

prepolymer, previously diluted in water to 20%, drop-by-drop by keeping the temperature of the mixture between 15 and 18 °C, gentle stirring for an additional 1 h. Finally, the biobased WPUD was obtained after removing acetone by a rotary evaporator under reduced pressure (250 mbar) at 60 °C. All of the synthesized WPUD were adjusted to a solid content of 35%. It is worth noting that acetone can be readily recovered and recycled.

The ratio between the three diols used in the prepolymer synthesis (Priplast 3294, DMBA, and 1,3-PDO) was systematically varied using the methodology of ternary mixture design of experiments (Figure 3). In our particular case, lower constraints were applied to DMBA and Priplast 3294 because, due to the particularity of the system, it is not possible to study the proportions of the three diols in the full range (from 0 to 100 molar %). For example, the amount of DMBA could not be equal to 0, since then the final polymer would not be dispersible in water; therefore, the lower constraint for DMBA was stablished in 37 molar %. A minimum amount of Priplast was also established, so that all of the prepolymers contain at least a 40 molar % of this polyol.
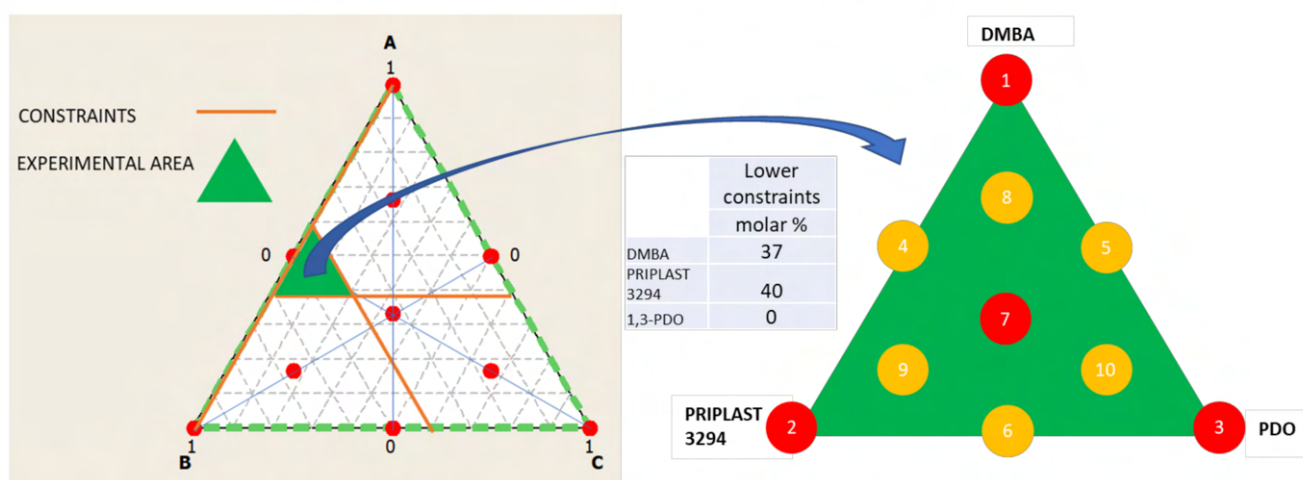
Figure 3. Ternary mixture design of experiments employed to study the proportion between the tree diols that form part of the polymer. (**Left**): in white full design surface area with all the theoretical experimental points marked in red and studied area in green which is delimited by the lower constraints stablished for component A (DMBA) and B (Priplast). Middle: table summarizing the lower constraints stablished for the diols. (**Right**): area studied and experimental points of de simplex design plot (from 1 to 7), experiments marked in red have been performed in this work (1, 2, 3, 7) while experiments that are marked in yellow have not been carried out.

Table 1 shows the overall simplex design table, with all of the experiments that could be done to fully cover the study area of ternary mixture (simplex ternary mixture design). The five columns on the right show the molar % of each polyol employed in the synthesis considering the lower constraints, hard segment content in wt. %, and bio-based content of each experiment in wt. %. The experiments that have been performed in this work have been named starting with 3294IPDI-, and the rest of experiments have not been carried out.

Polyurethane-urea films, suitable for NMR, mechanical, thermal, and swelling characterization were prepared by carefully pouring 20 g of WPUD in a circular Teflon mold, letting the water to evaporate slowly at 40 °C into a vented oven for 48 h to obtain 1 mm thick films that were subsequently cured and dried at 60 °C for 48 h in a vacuum oven.

Table 1. The overall simplex design table. Experiments that have been performed in this work are highlighted in grey.

Experiment	Matrix			Molar %			Hard Segment (wt. %)	Bio-Based Content (wt. %)
	DMBA	Priplast 3294	1,3-PDO	DMBA	Priplast 3294	1,3-PDO		
3294IPDI-1	1	0	0	60.00	40.00	0.00	40.6	59.4
3294IPDI-2	0	1	0	37.00	63.00	0.00	28.0	72.0
3294IPDI-3	0	0	1	37.00	40.00	23.00	38.8	62.6
4	1/2	1/2	0	48.50	51.50	0.00	33.4	66.6
5	1/2	0	1/2	48.50	40.00	11.50	39.7	61.0
6	0	1/2	1/2	37.00	51.50	11.50	32.6	68.0
3294IPDI-7	1/3	1/3	1/3	44.67	47.67	7.67	35.0	65.4
8	2/3	1/6	1/6	52.33	43.83	3.83	37.7	62.5
9	1/6	2/3	1/6	40.83	55.33	3.83	31.2	69.0
10	1/6	1/6	2/3	40.83	43.83	15.33	36.8	64.1

2.3. Additivation of WPUD with SWCNT

The preparation of a WPUD with 0.1% content in SWCNT: 2 g of Tuball Matrix Beta 302 was poured in a cylindrical mixing beaker with a flat bottom and a diameter of 10 cm, 2 g of the selected WPUD were added and then manually dispersed with the help of a glass rod, gently stirred for 15 min. until complete homogenization. Afterwards, 98 g of the same WPUD were added slowly and the mixture was subjected to mechanical stirring with an impeller blade (diameter of 5 cm) and a peripheral speed of 10 m s^{-1} (Heidolph RZR series) for 20 min. Finally, another 100 g of the WPUD were added and the same stirring was continued for 20 min.

To obtain a WPUD with a SWCNT content of 0.05 wt. %, 100 g of the WPUD with 0.1% content in SWCNT were thoroughly mixed with 100 g of the non-additivated WPUD. The mixing procedure was performed using the same beaker and mechanical stirrer discussed above, stirring for 20 min. to ensure complete homogenization.

2.4. Application of WPUD on Fabrics by Coating

The fabrics were coated by the printing pastes that were made of WPUD, water, defoamer, runnability improver, DMEA, and thickener (see Table 2 for the standard printing paste formulation, solid content, and viscosity).

Table 2. Printing paste formulation employed to perform the coating of the fabrics with the WPUDs.

Composition	Printing Paste Formulation (g)
WPUD	85
water	15
Defoamer PR	1
Complex DG	2
DMEA	1
Thickener L-120	Added drop by drop under high shear until viscosity of $18,000 \pm 50$ cPs is reached (Brookfield RV 6/30)
Dry polyurethane-urea content	$30 \pm 1\%$

Knife coating procedure, which is a widely used coating method in the textile sector, was employed to coat all of the fabrics with the corresponding printing pastes. Knife coating was performed using a laboratory coating machine R2R continuous line Werner-Mathis in a coating regime, air knife 90°, followed by drying in vented-oven at 110 °C at a speed of 1 m min.$^{-1}$ and curing at 150 °C at a speed of 0.4 m min.$^{-1}$.

The dry add-on of the coated fabrics was calculated, as follows: a sample cutter James H. Heal model 230/100 was used to cut out regular circular specimens of fixed area (100 cm^2) from the uncoated fabric and all of the coated fabrics. The calculation of weight

per square meter (grammage, G) of a given specimen is performed by multiplying the specimen's weight measured by a balance with a readability of 0.01 g by a factor of 100. Finally, the dry add-on of a coated fabric is calculated using Equation (1), where Gc and Gu are the grammages of the coated and uncoated specimens, respectively.

$$\text{Dry add on} = \text{Gc} - \text{Gu} \qquad (1)$$

2.5. Characterization Techniques

2.5.1. Characterization of Synthesized Polymers and Dispersions

Fourier transform infrared spectroscopy (FTIR) was employed for chemical characterization of the WPUD. The FTIR spectra were obtained using a Perkin Elmer Spectrum Two equipped with transmission accessory. A drop of each waterborne dispersion was spread on a SeZn FTIR window and then dried under IR lamp to evaporate water and to obtain a thin film. Eight scans were taken for each sample in the range of 4000–500 cm^{-1} with a resolution of 4 cm^{-1}.

The structural characterization of all the WPUD casted films was performed by ^{1}H-NMR, using a Bruker AMX-300 spectrometer at 25 °C operating at 300.1 MHz. Samples were dissolved in deuterated chloroform or deuterated tetrachloroethane, and spectra were internally referenced to tetramethylsilane (TMS). Approximately 10 mg of sample dissolved in 1 mL of solvent was used to collect the ^{1}H-NMR spectra. Sixty-four scans were acquired with 32 K data points as well as relaxation delay of 1 s.

Differential scanning calorimetry (DSC) studies of the dry films of all the synthesized WPUD as well as Priplast 3294 have been carried out to determine their melting temperature (T_m), crystallization temperature (T_c), melting enthalpy (ΔH_m), and crystallization enthalpy (ΔH_c), as well as possible second-order transitions such as glass transition temperature (T_g). The samples were heated from −90 to 150 °C at a constant heating rate of 10 °C/min in a Perkin Elmer model Pyris I under nitrogen atmosphere (50 mL/min.), working with 5 mg samples placed in sealed aluminium pans. The T_g values were determined by the StepScan DSC technique that yields enhanced characterization information by separating out the reversible and irreversible thermal events. The measurements were run from −100 °C to 100 °C at heating and cooling rates of 4 and 2 °C/min., respectively, a modulation of amplitude of 1 °C and period of 60 s.

The thermal stability of the synthesized WPUD films has been studied by thermogravimetric analysis (TGA), using a Mettler Toledo TGA2 equipment. The thermogravimetric analysis consisted of recording the weight loss of the samples that were subjected to a temperature gradient from 25 °C to 600 °C at 10 °C min.$^{-1}$ in a furnace with nitrogen atmosphere.

Dynamic Mechanical Thermal Analysis (DMTA) was carried out on rectangular samples 10 × 11.06 × 0.1 mm cut from all of the WPUD films to determine the storage modulus (G') and the loss factor tan δ. The specimens were strained at 0.05% at 1 Hz frequency, using single cantilever clamp TA Instruments DMA Q800 working under tension mode. They were scanned at a heating rate of 3 °C min.$^{-1}$ from 30 °C to 160 °C, previous equilibration at 25 °C for 5 min.

Mechanical properties were determined by stress–strain tensile measurements. The tests were carried out following the BS ISO 37: 2005 standard, using a Zwick/Roell model 500 N equipment. The measurements were carried out on dumbbell shaped Type 4 specimens cut from the WPUD films. Dumbbell dimensions are summarized in Figure S9 of Supporting Information. The test conditions were, as follows: preload 0.1 MPa, preload speed 1 mm min^{-1}, and test speed 50 mm min.$^{-1}$. For each WPUD, at least five samples were taken in different parts of the films and tested. The characteristic parameters measured were: elastic modulus (E), stress at break (σ_b), deformation at break (ε_b), and stress at 100% strain ($\sigma_{100\%}$).

Water-swelling measurements were performed using dumbbell shaped Type 4 specimens cut from the WPUD films. The samples were placed in a closed vial with 20 mL of deionized water at 25 °C for 48 h. Swelling degree was determined by Equation (2), where

w_0 and w were respectively the weight of the initial dried material and this of the swollen material after 48 h. The experiments were carried out in triplicates for each specimen.

$$Swelling\ (\%) = \frac{w - w_0}{w_0} \times 100 \tag{2}$$

The pH of each WPUD was measured with a HACH sensION+ MM378 pH meter that was calibrated with pH = 4 and seven standard solutions.

Moreover, the particle size and particle size distribution (PSD) of developed aqueous polymeric dispersions have been characterized by Dynamic Light Scattering (DLS). The stability of the dispersions has been analyzed by Z-potential measurements. DLS and Z-potential tests were performed on a Malvern Zetasizer ZS equipment at 20 °C. Z-potential measurements were performed after the dilution of the WPUD to 5 wt. % with deionized water buffered at pH 8.2, while the particle size measurements were performed after dilution of the WPUD to 10 wt. % with deionized water.

The WPUD were also subjected to accelerated sedimentation tests using an analytical centrifuge LUMiFuge 110–153.3–12 (LUM GmbH, Berlin, Germany) in order to evaluate long term stability. In each measurement, the suspension was pipetted into a polyamide transparent cell with a path length of 2 mm and 10 mm. Initially, the separation velocity of the WPUD emulsions with the relative centrifugal forces has been analyzed up to $2000 \times g$ (500, 1000, and $2000 \times g$), with changes in the sedimentation boundary not being not observed. Thereafter, measurements were performed at 4 and 40 °C and relative centrifugal force of $2000 \times g$, with a scanning rate of one every 10 s for 5 h. When considering a linear dependency of the WPUD dispersions, the duration of the tests have been optimized to simulate a shelf-life of 14 months, in accordance with ISO/TR13097 [30]. Moreover, a representative sample has been analyzed one year after the synthesis to determine long-term stability.

2.5.2. Characterization of Coated Textiles

The water repellence of the coated fabrics has been tested by measuring the contact angle of a droplet of water placed on the surface of the coated textile. Water contact angle measurements (WCA) were carried out under ambient conditions with a SURFTENS Universal automatic goniometer. Static contact angle measurements and advancing and receding contact angles of the air–water interface were measured on each sample. For each test, an average value of five measurements was adopted as the value of WCA. For the water static contact angle measurement, a drop of deionized water with a volume of 5 μL was placed on the textiles. For the advancing (θ_{Av}) and receding angle (θ_{Re}) measurements, first, a 5 μL of de-ionized (DI) water droplet was placed on the surface using a needle. Next, another 5 μL DI water was pumped into the initial droplet at a constant rate for the advancing contact angle measurement. A contact angle measurement was obtained after inflating the drop with every 0.1 μL. The advancing contact angle value was given as the average of the obtained 51 values. Subsequently, 5 μL DI water at the same speed was removed from the existing droplet to measure the receding contact angle. The receding contact angle was obtained as the average of the 51 values obtained after removing every 0.1 μL from the droplet.

The characterization tests summarized in Tables 3 and 4 were performed according to the indicated standards.

Table 3. Standards employed to evaluate the properties of the coated textiles.

Property	Standard
Determination of resistance to water penetration-Hydrostatic pressure test (water column)	EN 20811:1992
Fabric stiffness	ČSN 80 0858
Determination of the permeability of fabrics to air	ISO 9237:1995

Table 4. The standards employed to evaluate electrostatic properties of the coated textiles and minimum compliance values.

Electrostatic Properties	Standard	Minimum Compliance Values
Surface resistivity & Specific surface resistivity	EN 1149-1	Surface resistance $\leq 2.5 \times 10^9$
Vertical resistance	EN 1149-2	Electrical resistance $> 10^5$
Charge decay (inductive charge)	EN 1149-3, method 2	$t_{50} < 4$ s or S > 0.2 values
Electrostatic properties. Performance requirements and material design.	EN 1149-5	t50 < 4 s or S > 0.2 values; or surface resistance is $\leq 2.5 \cdot 10^9$

The surface morphologies of the relevant coated and uncoated fabrics were studied by scanning electron microscopy (SEM) using an Ultra Gemini-II microscope from Carl Zeiss SMT.

3. Results and Discussion

3.1. Synthesis and Characterization of WPUD

A series of WPUD were synthesized by the prepolymer method, as reported in the experimental section. Once the prepolymer was obtained, the neutralization of the carboxyl groups with triethylamine and subsequent phase inversion in water was carried out. Finally, chain extension by EDA was performed, followed by acetone removal by rotary evaporation and standardization to 35% solid content. The scheme of the synthesis strategy of the WPUD can be seen in Figure 4.
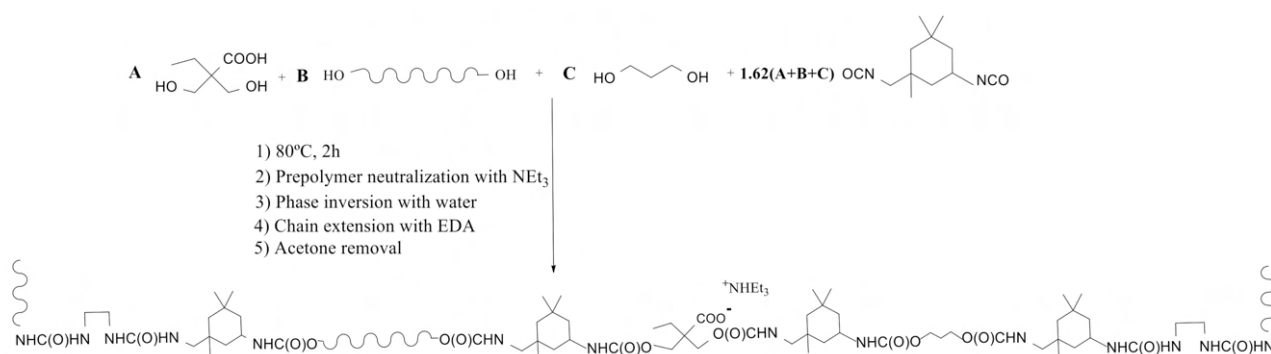
Figure 4. Synthesis scheme of the waterborne polyurethane-urea dispersions.

WPUD were first characterized by FTIR. The infrared spectra of all synthesized polymers showed the complete conversion of isocyanate groups judging by the absence of the characteristic free isocyanate band at 2275 cm^{-1}. By comparing the spectrum of the starting polyol Priplast 3294 with those of the synthesized polyurethane-ureas, the appearance of new bands that are indicative of the formation of urethane/urea bonds can be clearly confirmed (Figure 5). The broad band of NH asymmetrical and symmetrical stretching vibration at 3351 cm^{-1} indicates the great extent of NH established hydrogen bonds with carbonyl groups from urethane, urea, ester, and ionic carboxylate from internal emulsifier DMBA [31]. The zoom in the area of 1500–1600 cm^{-1} shows NHCO stretching and NH bending bands of urethane group at 1550 cm^{-1}, as the hard segment content in the polymer increases, the intensity of this bands also increases; this observation is in good agreement with Poussard et al. [24]. Further enlargement in the area between 1740 and 1600 cm^{-1} shows characteristic C=O stretching bands from DMBA carboxylate, urethane, and urea carbonyl groups at approximately 1661–1700 cm^{-1} region, partially overlapped with the ester band from the polyol at 1739 cm^{-1}. COC(O) stretching bands and NH

out-of-plane bending bands from urethane functional groups at 1242 cm^{-1} and 774 cm^{-1}, respectively, are clearly observed.
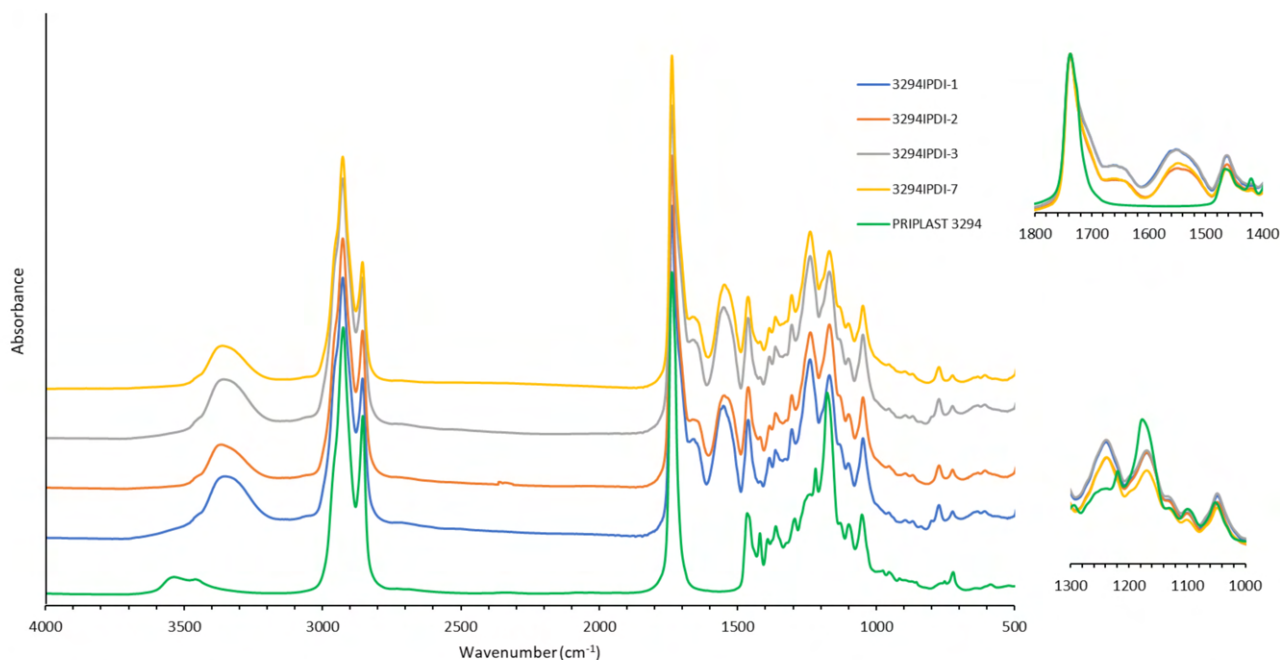
Figure 5. FTIR spectra in the MIR region for synthesized WPUD films. Magnifications of the 1800–1400 cm^{-1} and 1300–1000 cm^{-1} regions.

All of the synthesized WPUD were dried on Teflon plates to obtain the corresponding films. All of the obtained films were transparent and homogenous and were used for NMR, mechanical, thermal, and swelling characterization. Figure 6 shows the appearance of the synthesized WPUD as well as the appearance of casted film from one of the polyurethane-urea dispersions (3294IPDI-2).
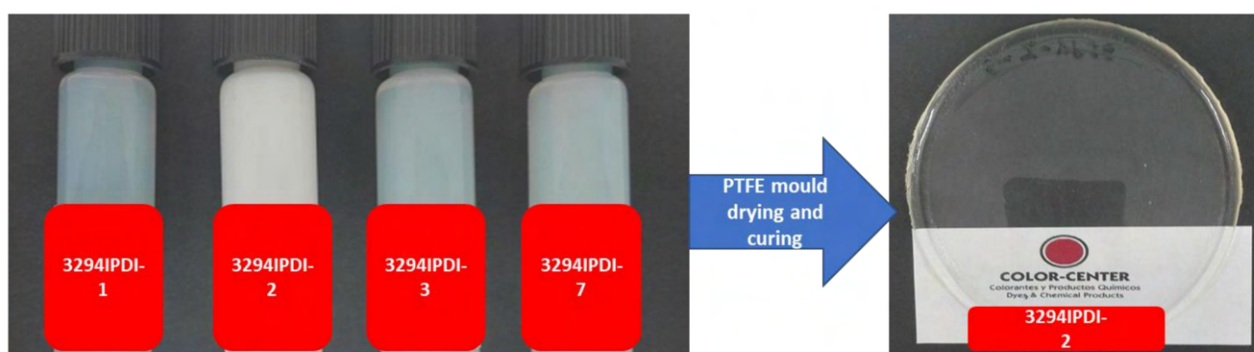
Figure 6. Appearance of the synthesized WPUD (**left**) and appearance of casted film from one of the polyurethane-urea dispersions (3294IPDI-2, **right**).

^{1}H NMR spectra of all polymer films were recorded, thus confirming chemical structure. ^{1}H NMR spectra of all WPUD films are reported in Figure S1 of Supporting Information. Figure 7 depicts the ^{1}H NMR of experiment 3294IPDI-7 and starting Priplast 3294 polyol with peak assignments.
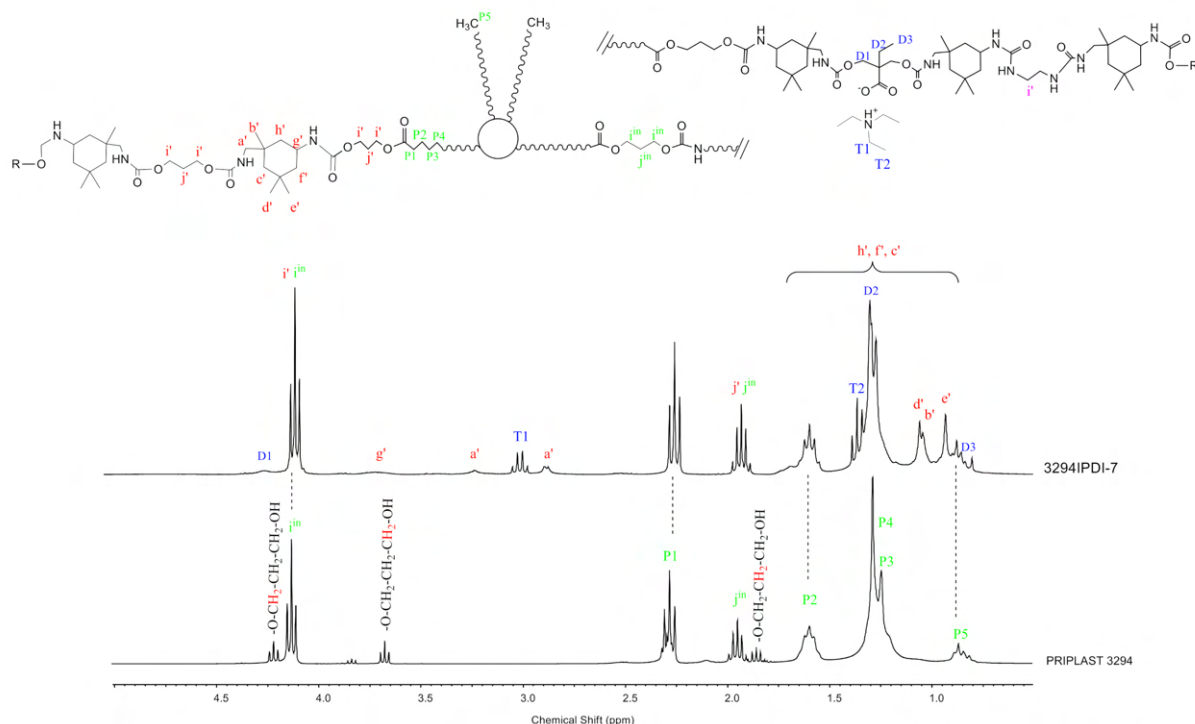
Figure 7. ^{1}H NMR of experiment 3294IPDI-7 and starting polyol Priplast 3294 with peak assignments.

^{1}H NMR spectra provided structural information regarding Priplast 3294 polyol and WPUD films. The main peaks of Priplast 3294 are in good agreement with those reported by Bueno-Ferrer's work [32], showing $CH_2C(O)O$ signal at 2.30 ppm and peaks from $CH_2OC(O)$ and CH_2 in the β position of the ester group at 4.15 and 1.61, respectively.

The CH_2 peaks from the methylene in the α, β, and γ position with respect to free hydroxyl groups ($COO-C_\gamma H_2-C_\beta H_2-C_\alpha H_2-OH$) appear at 3.69, 1.96, and 4.23 ppm, respectively. In the WPUD, the full conversion of hydroxyl groups to form polyurethane segments is confirmed by downfield shifting of the α and β peaks in the polymer spectra.

Commercially available IPDI represents an isomer mixture of approximately 75:25 in favor of the cis- isomer, leading to different reaction mixtures [33] and resulting in complex ^{1}H-NMR spectra. For a better interpretation of the ^{1}H-NMR spectra of the synthesized polyurethane-ureas, they were compared with the ones of model compounds (IPDI:DMBA, IPDI:PDO, IPDI:Priplast 3294, IPDI:EDA, IPDI:EtOH) that were obtained by reacting IPDI with the corresponding building block in a molar ratio of 2:1. Supporting Information (Figures S2–S6) shows the interpretation of the ^{1}H-NMR spectra of these model compounds. This has made it possible to more precisely assign some of the main signals of the polyurethane-ureas under study.

Urethane moieties give the following weak signals:

- IPDI CH_2 in α-position to -NHC(O) group (a'), 3.24 ppm and 2.88 ppm corresponding to trans isomer (25% abundance) and cis isomer (75% abundance), respectively.
- IPDI CH in α-position to -NHC(O) group (g'), 3.73 ppm.

The incorporation of internal emulsifier (DMBA) into the polymer backbone can be assessed by the following signals: DMBA CH_2 in α-position to OC(O) group (D1), 4.26 ppm; DMBA methylene group (D2) attached to methyl, 1.31 ppm; DMBA methyl group (D3), 0.86 ppm.

Triethylammonium salt can be assessed by the peaks at 3.02 (T1) and 1.37 (T2) ppm that correspond to CH_2 and CH_3, respectively, of ethyl group.

The thermal properties of the developed WPUD have been analyzed by DSC and TGA. The non-isothermal DSC thermograms for all of the WPUD films as well as Priplast 3294 have been registered. The DSC thermogram of Priplast 3294 displayed a clear melting peak at 33.0 °C, and a crystallization peak at −6.2 °C, with fusion and crystallization enthalpies of 41.0 and 38.3 J/g, respectively, thus confirming its semicrystalline nature attributed to lamellar packing of methylenes of both paraffinic backbone and side chains (see DSC of Priplast 3294 in Figure S7 of Supporting Information). For the WPUD films, only glass transition temperatures have been detected and determined by DDSC, see Figure 8 and Table 5. The glass transition temperatures (T_g) of the soft segments are very close to the value observed for Priplast 3294 polyester polyol. This is an indication that there is a phase segregation between hard polyurethane-urea segments and polyester soft segments. This phase segregation is enhanced as the content in hard segments increases, and it is reflected by a small decrease in the T_g values observed in the studied series.
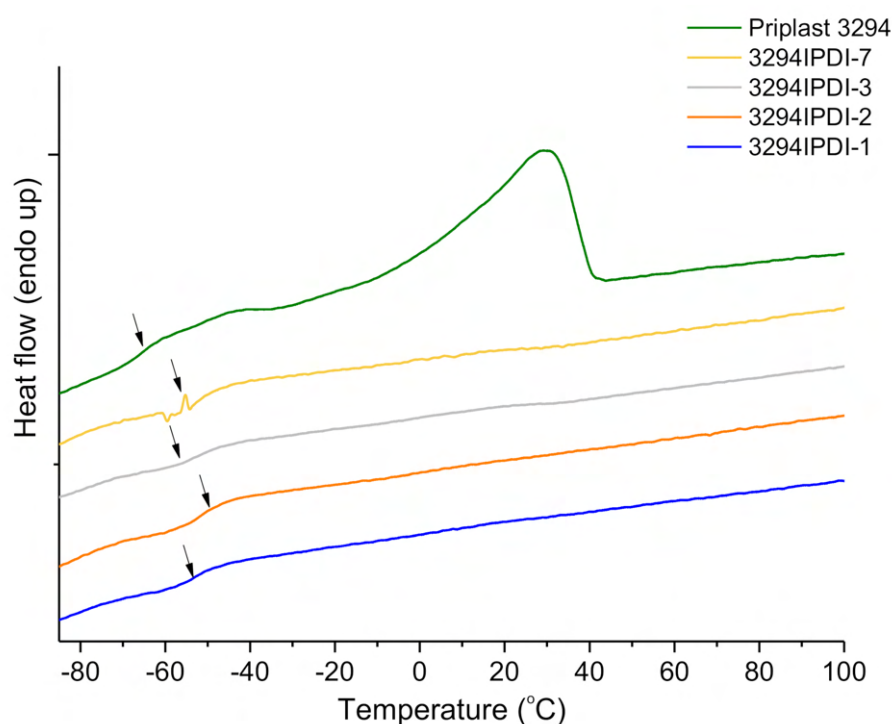
Figure 8. DDSC thermograms of Priplast 3294 and WPUD films. Glass-transition temperatures has been calculated taken as the inflection point of the heating step scan DSC.

Table 5. Thermal properties of WPUD films evaluated by DSC, TGA, and DMTA.

Reference	DSC [a]	TGA [b]				DMTA [c]
	T_g (°C)	$T_{10\%}$ (°C)	T_{dS1} (°C)	T_{dS2} (°C)	T_{dS3} (°C)	T_α (°C)
3294IPDI-1	−53.8	276.5	254.9	326.1	423.2	109.2
3294IPDI-2	−50.8	308.6	263.3	327.2	420.6	68.9
3294IPDI-3	−53.7	297.6	261.1	326.8	422.5	123.5
3294IPDI-7	−51.2	300.1	261.8	326.2	422.7	106.2
Priplast 3294	−66.0	402.7	-	-	414.4	N.D. [d]

[a] T_g values determined by DDSC. [b] TGA characterization of the WPUD films: $T_{10\%}$ is the temperature at which a 10 wt. % loss was observed in the TGA traces recorded at 10 °C min^{-1}; T_{dS1}, T_{dS2}, T_{dS3} are the temperatures of maximum degradation rate for first, second a third degradation stages, respectively. [c] T_α, relaxation temperature calculated from the maximum value of tan δ by DMTA. [d] Data not given on Priplast 3294 due to not appropriate state for DMTA (melts).

The thermal stability of the synthesized WPUD films has been studied by TGA and the curves are collected in Figure 9. The degradation temperatures corresponding to a weight loss of 10% and the temperatures of the maximum degradation rate for each degradation stage are collected in Table 5. All of the (co)polymers have sufficient thermal stability to withstand without degradation the temperature conditions that are required during coating procedures.
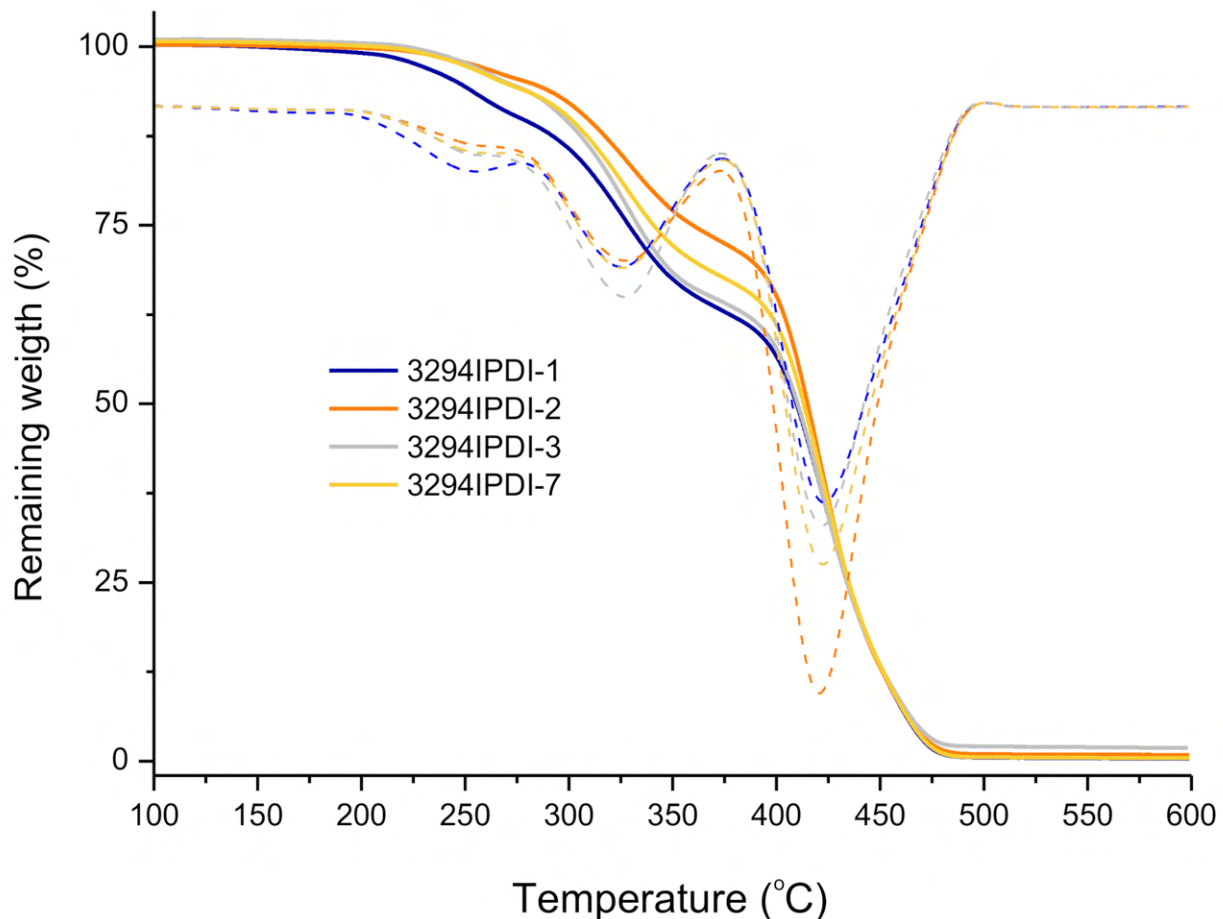
Figure 9. TGA thermograms of synthesized WPUD films. Mass losses (thick lines) and derivative curves (dashed lines).

As can be observed in Figure 9, thermal degradation occurs in three stages, with similar temperatures of maximum degradation rate for all the synthesized WPUD. First step occurs in the temperature range 255–264 °C and could be attributed to volatilization of triethylamine which is in the form of carboxylate salt. Stage 2 around 326 °C corresponds to the degradation of urethane and urea bonds [24]. The remaining weight of WPUD film at this stage is higher for the samples with higher Priplast 3298 content, as can be observed in Figure 9. Finally, stage 3 around 422 °C is related to the degradation of segments of Priplast 3294 biobased polyol (see Figure S8 of Supporting Information). The TGA curve of commercial non-biobased polyether polyurethane film (RD27) has been performed and compared to WPUD 3294IPDI-7, see Figure S8 of Supporting Information. It can be observed that thermal degradation for RD27 also occurs in three stages, and the temperature of maximum degradation rate for the third stage is around 400 °C, thus being 20 °C lower than that observed for 3294IPDI-7. These differences in thermal degradation can be attributed to the different chemical structure of the polyol (polyether vs. polyester).

The dynamomechanical behavior was studied for all of the obtained WPUD films. Figure 10 shows the plots of G′ modulus and tan δ vs. temperature in the range from 30 to 160 °C. The relaxation temperatures (T_α), calculated from the maximum value of

tan δ peak, are reported in Table 5. There is a good agreement between T_α and hard segment content. The highest the hard segment content the highest the T_α value due to the increase in mobility restriction that is induced by urethane and urea groups present in the rigid phase. Thus, T_α for 3294IPDI-2 (28 wt. % hard segment, HS) is the lowest within the experiment set (69.9 °C). while T_α for 3294IPDI-1 and 3294IPDI-3 (41 wt. % HS and 39 wt. % HS, respectively) are the highest within the experiment set (109.2 and 123.5 °C, respectively). From the contour plot of T_α, as in Figure 11, it can be observed that 1,3-PDO also has an important influence in T_α; therefore HS and 1,3-PDO both contribute to the increase of T_α values. It can be inferred from these results that hard segments that are composed of urethane groups generated from 1,3-PDO could interact more strongly by hydrogen bonding than the ones composed of DMBA, most probably due to the steric hindrance caused by the ethyl and carboxylate side groups that are present in the latter.
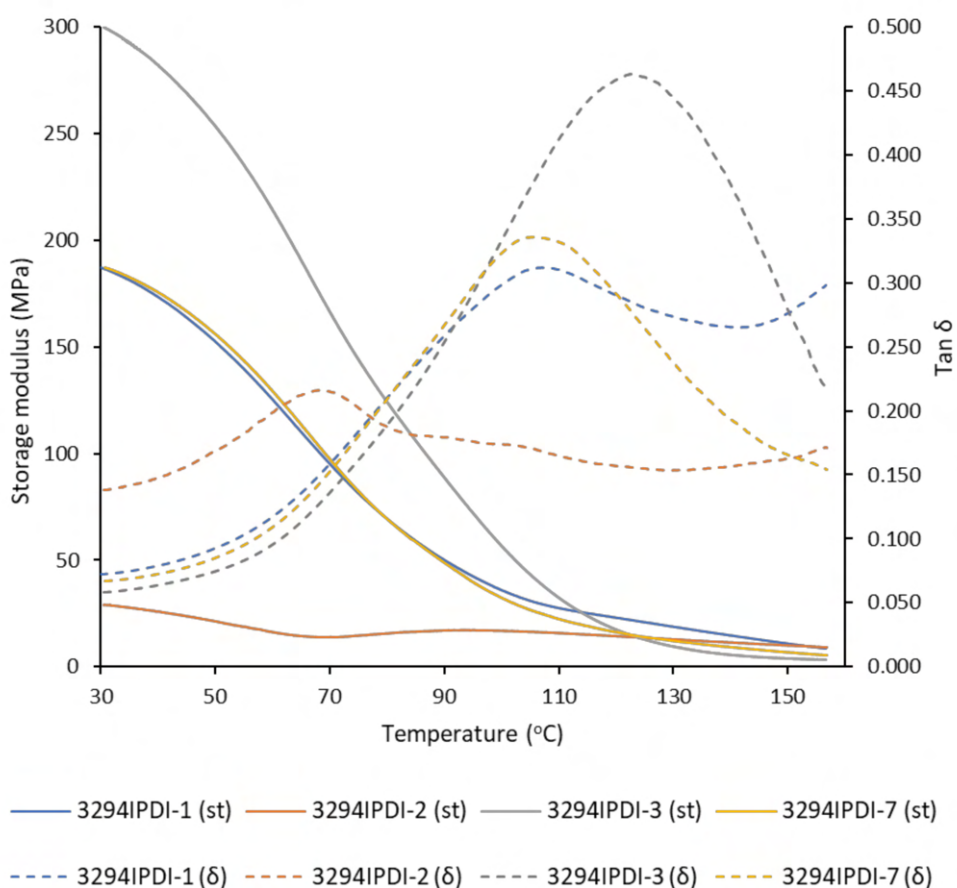
Figure 10. DMTA curves of synthesized WPUD films. Storage modulus (full lines) and tan δ (dashed lines).

Stress–strain tensile experiments were carried out to evaluate the mechanical properties of the synthesized WPUD films. The RD27 film has also been evaluated for comparison purposes. Figure 12 shows the stress–strain curves and Table 6 collects the main mechanical properties of films.
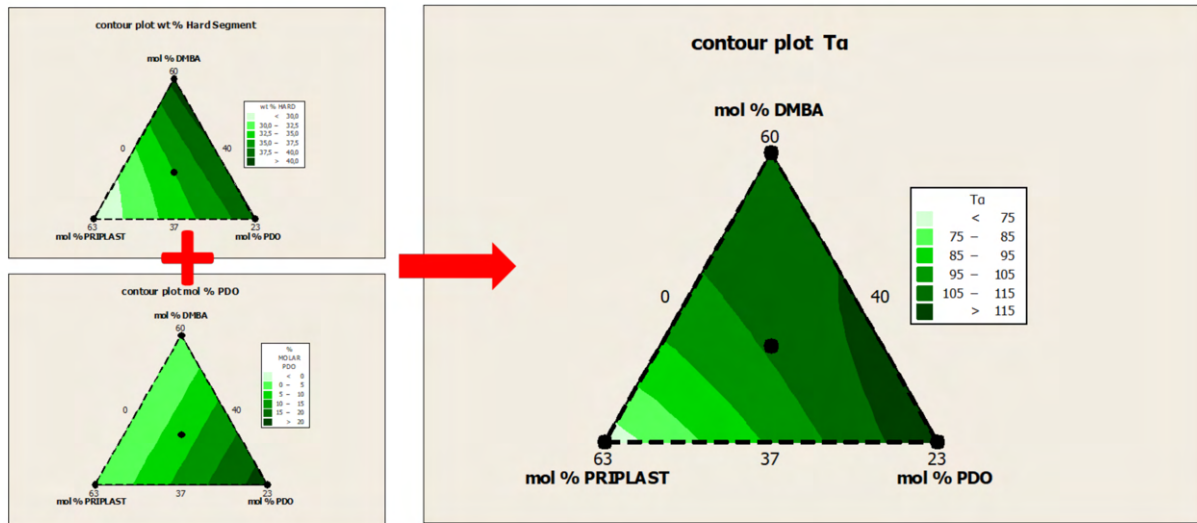
Figure 11. Contour plots obtained by Minitab software from the ternary mixture experimental design. (**Left**) (**up**): contour plot of Hard segment content in wt. %. (**Left**) (**down**): contour plot of 1,3-PDO content in mol %. (**Right**): contour plot of relaxation temperature (T_α).
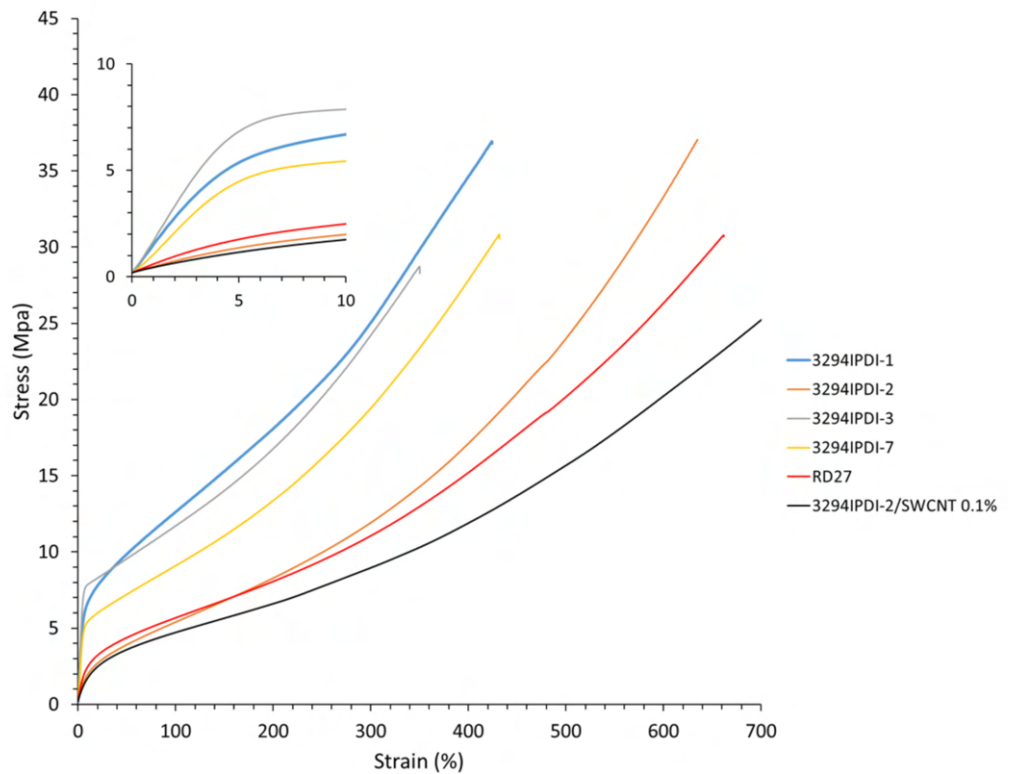
Figure 12. Stress–strain curves of WPUD films. Commercial non-biobased polyurethane (RD27) and polyurethane matrix 3294IPDI-2 additivated with 0.1 wt. % SWCNT (3294IPDI-2/SWCNT 0.1%) has been included for comparison.

Table 6. Mechanical characterization of WPUD and RD27 films.

Reference	E [a] (Mpa)	$\sigma_{100\%}$ [a] (Mpa)	σ_b [a] (Mpa)	ε_b [a] (%)
3294IPDI-1	120.6 ± 4.0	12.5 ± 0.1	35.9 ± 1.2	415.4 ± 11.4
3294IPDI-2	25.1 ± 0.3	5.4 ± 0.0	35.4 ± 1.4	625.4 ± 15.8
3294IPDI-3	161.0 ± 9.3	11.7 ± 0.2	28.4 ± 2.0	347.8 ± 11.9
3294IPDI-7	103.9 ± 6.1	9.1 ± 0.1	28.7 ± 1.3	427.3 ± 8.3
3294IPDI-2/ SWCNT 0.1 wt. % [b]	19.3 ± 1.2	4.8 ± 0.2	25.8 ± 6.1	735.0 ± 6.1
RD27 [b]	35.4 ± 0.4	5.6 ± 0.0	33.4 ± 4.7	700.7 ± 80.5

E [a]: Young modulus, $\sigma_{100\%}$: stress at 100% strain, σ_b: stress at break, ε_b: strain at break. [b] Non-biobased commercial polyurethane (RD27) and 3294IPDI-2 WPUD additivated with 0.1 wt. % SWCNT (3294IPDI-2/SWCNT 0.1 wt. %) have been included for comparison.

The ratio of Priplast 3294, 1,3-PDO and DMBA in the polyol ternary mixture determined polyol composition in each synthesized polymer and, therefore, the hard segment content. There is a reasonably good match between the Young modulus and hard segment content. In general, higher hard segment content showed a higher Young modulus. However, experiment 3294IPDI-3 (39 wt. % HS) led to a slightly higher Young modulus than experiment 3294IPDI-1 (41 wt. % HS), which could be explained by the greater influence of 1,3-PDO on the polymer rigidity caused by stronger hydrogen bonding interactions between urethane groups as compared to DMBA. The concordance between stress at 100% strain ($\sigma_{100\%}$) and hard segment content is even better, as can be seen in the surface plots Figure 13. The strain at break is also very well correlated to the amount of Priplast 3294 (the polyol that provides flexibility), the higher the ratio of Priplast with respect to 1,3-PDO and DMBA, the highest the strain at break, see the contour plots in Figure 14.
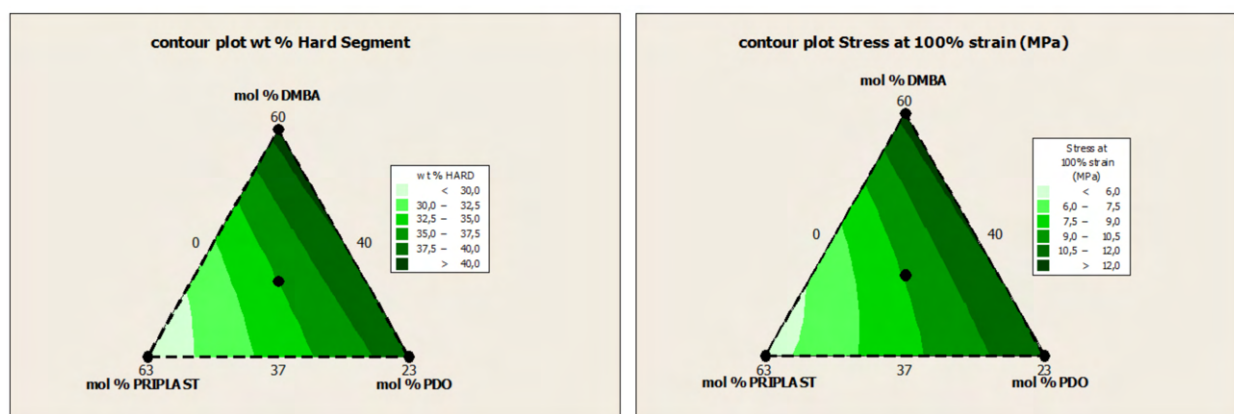
Figure 13. Contour plots obtained by Minitab software from the ternary mixture experimental design. (**Left**): contour plot of Hard segment content in wt. %. (**Right**): contour plot of $\sigma_{100\%}$ (stress at 100% strain).

3294IPDI-2 doped with 0.1% SWCNT leads to lower Young modulus and higher strain at break than the non-doped polymer 3294IPDI-2. This variation in mechanical properties could be caused by the waxes in which the nanotubes are dispersed in TUBALL MATRIX BETA 302, rather than the nanotubes themselves, as far as those waxes would act as plasticizers [34]. Commercial non-biobased polyurethane RD27 has a similar stress–strain profile than 3294IPDI-2 (Figure 12). The use of the ternary mixture experimental design methodology for the production of polyurethanes allows us to explore, in a relatively simple way, different proportions of the building-blocks to obtain WPUD with the desired mechanical properties.
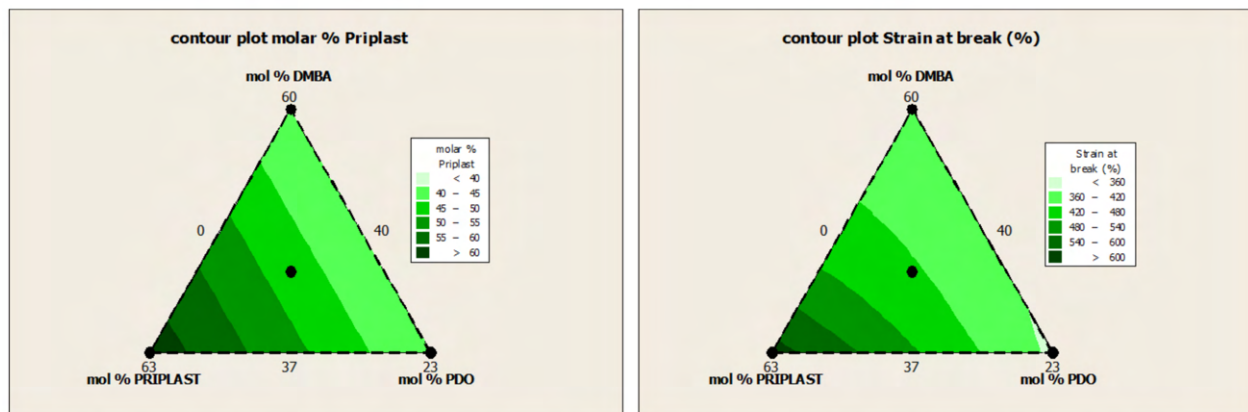
Figure 14. Contour plots obtained by Minitab software from the ternary mixture experimental design. (**Left**): contour plot of Priplast 3294 content in molar %. (**Right**): contour plot of ε_b (strain at break).

Water swelling of the films after 48 h at 25 °C was assessed on all of the WPUD films, as well as the reference sample RD27 for comparison purposes. Figure 15 shows the water swelling values.
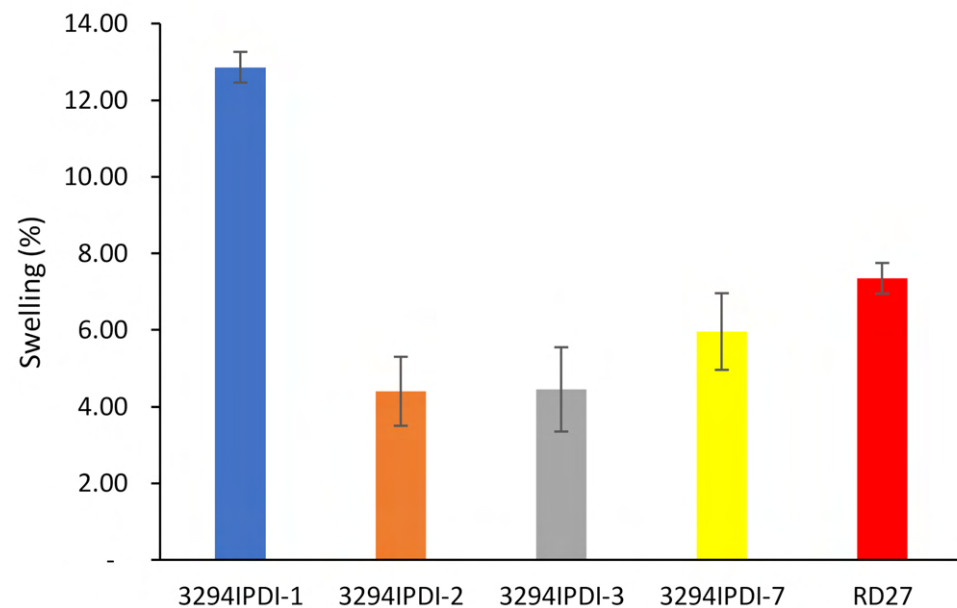
Figure 15. Swelling of WPUD films in water at 25 °C for 48 h.

The swelling values of the films after 48 h are consistent with the increased content of hydrophilic chain extender (DMBA), in agreement with the behavior that was reported by Xu et al. for dimethylol propionic acid (DMPA) [35]. Although the DMBA content seems to be the determining factor in the water absorption of the films, the increasing content of Priplast 3294 (hydrophobic polyol soft segment) also has a notable influence in decreasing water swelling, as can be noted in contour plot from Figure 16 (right).
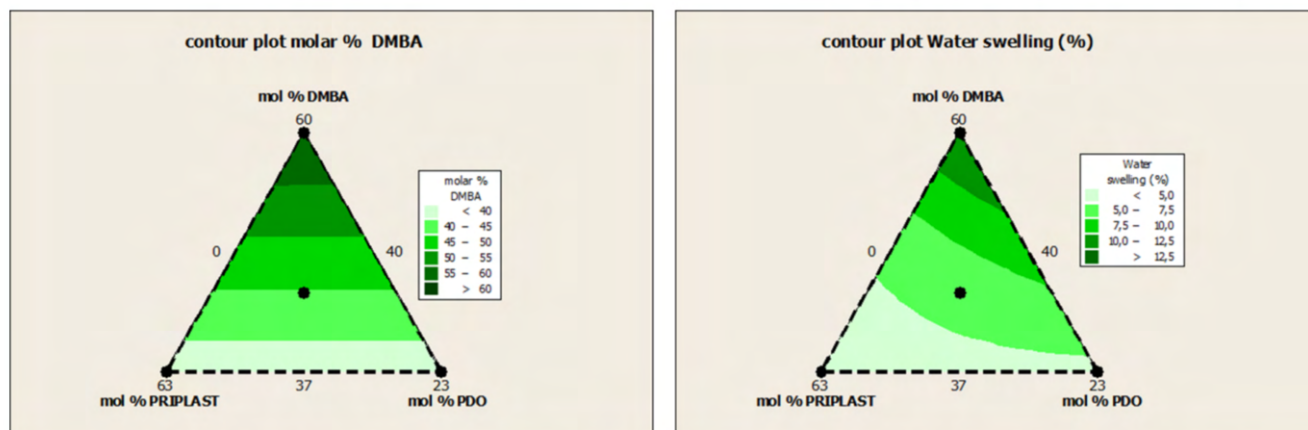
Figure 16. Contour plot of molar % of DMBA (**left**) and Water swelling (**right**) of all the WPUD films from de ternary mixture experimental design.

Finally, the dispersion stability, the particle size, and particle size distribution of WPUD have been investigated. Figure S10 of Supporting Information shows the particle size distribution (PSD) curves of all developed aqueous polymeric dispersions analyzed by DLS. Particle size distribution curves are unimodal for all WPUD. Table 7 summarizes the pH of the WPUD, average particle size, PdI values, and Z-potential. The average particle sizes were around 50 nm for all of the dispersions, except for 3294IPDI-2, which was noticeably higher and around 215 nm. This is consistent with the fact that 3294IPDI-2 has the lower content of DMBA (internal emulsifier) and the highest content on Priplast 3294 (hydrophobic polyol). The polydispersity indexes (PdI) are below 0.2, which indicated that products had satisfactory stability and good dispersibility. The smaller the value of PdI, the better the homogeneity of the dispersion [36].

Table 7. A summary of the particle size and PdI measurements, average particle size, and Z-potential values for synthesized WPUD dispersions.

Reference	pH at 35% of Solid Content	Average Particle Size (nm)	PdI	Z Potential (mV)
3294IPDI-1	8.1	50 ± 7	0.12 ± 0.1	-40.5 ± 6.0
3294IPDI-2	8.2	217 ± 40	0.11 ± 0.1	-38.7 ± 7.9
3294IPDI-3	8.1	49 ± 10	0.20 ± 0.1	-39.8 ± 4.3
3294IPDI-7	8.0	48 ± 15	0.19 ± 0.1	-43.5 ± 4.7

The stability of the dispersions was assessed by measuring the Z potential of each WPUD. The Z potential values are collected in Table 7. For all of the 3294IPDI series, the Z potential presented similar values around -40 mV, indicating that the nanodroplets are negatively charged at the surface due to the presence of carboxylate groups. In addition, Z potential absolute values that are higher than 30 mV are generally considered to represent stable emulsions [37,38].

Accelerated sedimentation tests of WPUD emulsions were also carried out. The analysis of the tested emulsions performed at 40 °C and 4 °C and relative centrifugal force of 2000× *g* are shown in Figures S11 and S12 of Supporting Information, respectively. The first scanning profile obtained is marked in red at the bottom, and the last in green at the top. Only a small clarification is observed at the meniscus area and small sedimentations are observed at the bottom with time, whereas the light transmission of the samples remains constant with time, indicating a good stability of the emulsions. The greater the change in light transmittance during the acceleration of the emulsion, the worse the stability [39].

After one year of storage, WPUD emulsions were evaluated under similar conditions. Figure 17 collects the transmission profile at 470 nm of 3294IPDI-3 sample analyzed with a path length of 2 mm. Similar transmissions are observed in fresh samples and samples measured after one year of storage at room temperature for all the WPUD. The photographs in Figure 18 show the appearance of WPUD for fresh samples and samples after one year of storage, both after being centrifugated to 2000× *g* and 40 °C. No physical changes are observed in the photographs indicating the high long-term stability of the emulsions. The white aspect of 3294IDPI-2 is due to the higher average particle size in the emulsions, being previously observed in DLS measurements.
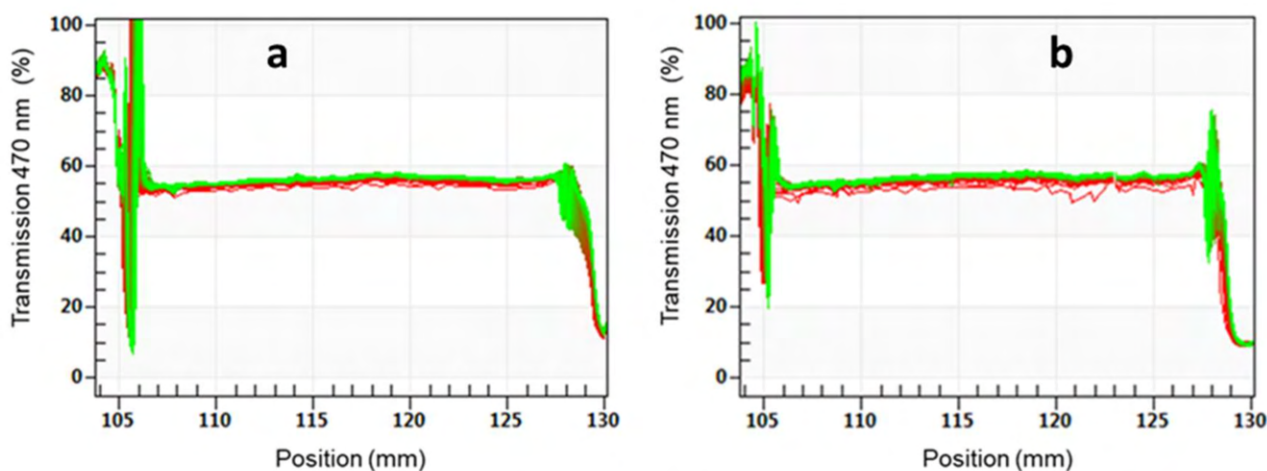
Figure 17. Transmission profiles of 3294IPDI-3 sample subjected to 2000× *g* and 40 °C centrifuge tests using a path length of 2 mm. (**a**) Fresh sample and (**b**) sample after one year of storage.
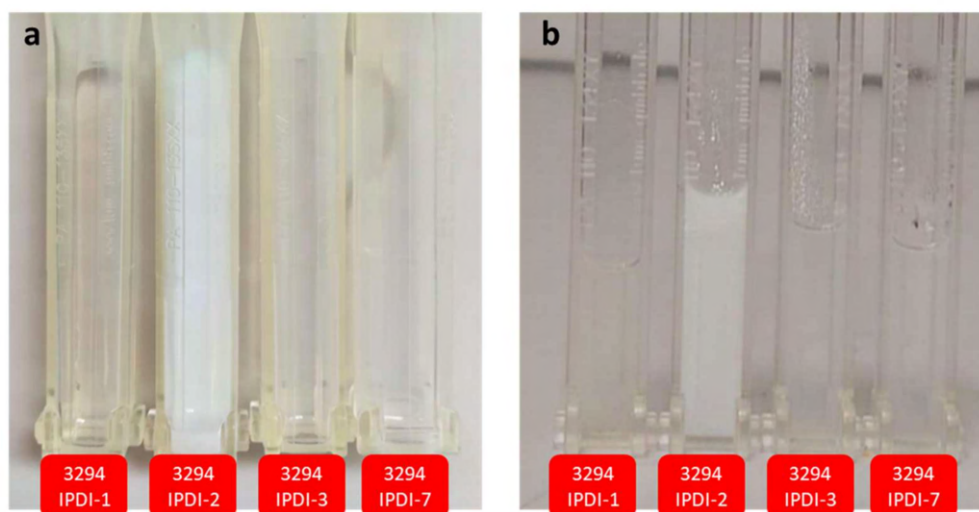
Figure 18. Photographs after centrifugation at 2000× *g* and 40 °C for: (**a**) fresh samples and (**b**) samples after one year of storage.

3.2. Additivation of WPUD with SWCNT

Experiment 3234IPDI-2 was selected as a polymeric matrix to disperse the SWCNT masterbatch. Figure 19 shows the appearance of 3234IPDI-2 before and after Tuball additivation as well as the casted films obtained after drying and curing in Teflon mold.

Figure 19. (a): 3294IPDI-2 WPUD dispersion before and after Tuball additivation. **(b)**: casted films obtained after drying and curing in Teflon mold.

It is important to note how the additivation with SWCNT changes the appearance of the dispersion and the film that become totally black.

3.3. Characterization of Textiles Coated with WPUD

In order to validate the applicability and properties of the polymeric dispersions, all of the synthesized WPUD were formulated in the form of printing pastes and subsequently face-coated on 100% polyester fabrics referenced as UPRON. Knife coating was the method chosen to carry out the coatings, as it is a widely employed method in the textile sector to produce accurate and repeatable coatings, being easily scalable to standard industrial textile machinery. In this way, this work has the purpose of performing the validation of the WPUD in application conditions that are very similar to those that are commonly used at an industrial level in the sector.

Commercial non-bio-based waterborne polyurethane dispersion, referenced as RD27, and dispersions of 3294IPDI-2 doped with 0.05 wt. % and 0.1 wt. % SWCNT have been formulated as printing pastes and face-coated using same conditions than WPUD as a comparative example.

Smooth glass slides have been also coated with all of the above-mentioned printing pastes and WCA measured to establish a comparison between the glass smooth coating substrate and the inherently rough textile substrate (UPRON). The coating procedure on glass slides has been done by a more convenient manual Quadrangular Applicator with a gap of 60 μm, followed by drying at 90 °C for 5 min. and curing at 120 °C for 2 min.

Table 8 lists the values of WCA, advanced angles (θ_{Av}), receding angles (θ_{Re}), and calculated contact angle hysteresis (CAH) of glass slides and UPRON fabrics coated with WPUD, RD27, and SWCNT-doped 3294IPDI-2 printing pastes.

As can be observed, WCAs of coated UPRON fabrics are between 113 and 121° for the synthesized WPUD, which means low water wettability, but not superhydrophobicity (>150°). The incorporation of SWCNT in the emulsions does not affect significantly to the WCA measurements when considering the experimental deviation. Comparative example RD27 gives slightly lower WCAs and, therefore, less performance in terms of water repellence than textiles coated with WPUD and SWCNT-dopped WPUD. It is important to point out that WCAs of coated glass slides are much lower than the WCA of WPUD coated fabrics. Thus, the inherent roughness of the textile substrate contributes to achieving high values of WCA [18]. On the other hand, CAH is an estimator of the degree of imperfection of the surface as the degree of roughness and chemical heterogeneity [40,41], and it can also provide information on solid-liquid adhesion and cohesion forces. According to the low CAH values that are reported in Table 8, it could be inferred that the attractive forces

between the coated fabrics (solid surface) and the water drops are low and that it is a consequence of the chemical nature of the coating.

Table 8. WCA, θ_{Av}, θ_{Re}, and calculated CAH of glass and UPRON substrates coated with WPUD and RD27.

Coating Reference	Substrate							
	Glass Slides				UPRON [a]			
	WCA (°)	θ_{Av} (°)	θ_{Re} (°)	CAH[b] (°)	WCA (°)	θ_{Av} (°)	θ_{Re} (°)	CAH [b] (°)
Uncoated	spreads	-	-	-	wets	-	-	-
3294IPDI-1	98.4 ± 1.3	97.0 ± 3.3	94.8 ± 0.8	2.3 ± 3.4	121.4 ± 1.8	122.7 ± 3.8	119.4 ± 5.1	3.2 ± 1.5
3294IPDI-2	86.0 ± 1.9	91.5 ± 4.5	84.4 ± 5.6	7.1 ± 6.5	119.7 ± 4.0	125.1 ± 4.4	121.6 ± 5.7	2.4 ± 2.2
3294IPDI-3	92.4 ± 2.7	92.9 ± 1.0	87.1 ± 4.5	5.9 ± 4.6	116.3 ± 2.8	117.1 ± 1.1	113.8 ± 1.1	3.3 ± 1.0
3294IPDI-7	86.9 ± 0.6	90.4 ± 2.2	88.2 ± 2.2	2.2 ± 3.1	113.2 ± 7.0	115.3 ± 6.4	111.8 ± 5.7	3.5 ± 1.0
RD27	78.2 ± 1.0	79.4 ± 1.0	77.0 ± 1.3	2.4 ± 1.6	106.8 ± 2.4	111.2 ± 0.4	110.6 ± 0.7	0.6 ± 1.0
3294IPDI-2/ SWCNT 0.05 wt. %	78.3 ± 1.2	90.8 ± 3.6	86.2 ± 1.2	4.6 ± 3.8	111.7 ± 1.4	112.7 ± 3.8	109.4 ± 2.8	3.3 ± 3.2
3294IPDI-2/ SWCNT 0.1 wt. %	89.2 ± 1.6	96.0 ± 3.0	94.3 ± 2.7	1.6 ± 4.1	114.9 ± 5.0	120.5 ± 1.4	115.7 ± 1.6	4.8 ± 0.9

[a] The Dry add-on of the coated UPRON fabrics was 25 ± 2 g m^{-2} for all the coated samples. [b] CAH = $\theta_{Av} - \theta_{Re}$ (°).

The determination of resistance to water penetration measured by hydrostatic pressure test (also known as water column), stiffness and air permeability have been performed on UPRON fabrics face-coated with the printing pastes (Table 9). Printing paste made from experiment 3294IPDI-2 shows the highest water column value of all the 3294IPDI series, which is consistent with the mechanical properties of this experiment, having the highest ε_b of all the 3294IPDI series in addition to the second highest σ_b of all the 3294IPDI series. Therefore, experiment 3294IPDI-2 was chosen to be dopped with the SWCNT and electrostatic properties of UPRON fabrics that were coated with doped and undoped 3294IPDI-2 were measured (Table 10).

Table 9. Stiffness, water column, and air permeability of UPRON fabrics uncoated and coated by knife coating procedure.

Coating Reference	Dry Add-on (g/m2)	Stiffness [mN]		Water Column (cm)	Air Permeability (mm/s)
		Warp	Weft		
Uncoated	-	17.4	9.7	<15 soaked	85.3
3294IPDI-1	23.5	153.0	50.3	26.9	3.7
3294IPDI-2	27.0	127.0	42.2	38.0	0.7
3294IPDI-3	24.9	154.0	50.3	28.9	2.6
3294IPDI-7	26.0	161.0	47.3	29.3	1.8
RD27	22.0	155.0	43.9	34.0	0.4
3294IPDI-2/SWCNT 0.05 wt. %	24.1	124.0	38.9	32.7	4.4
3294IPDI-2/SWCNT 0.1 wt. %	24.0	87.0	31.9	33.8	3.6

From the results shown in Tables 9 and 10, it can be concluded that the multifunctional effect, i.e., water column and antistatic properties, were achieved. From the values in Table 10 (electrostatic properties), it can be concluded that the addition of SWCNT in amount 0.05 wt. % to the WPUD is sufficient for the reliable antistatic effect complying with the standard EN 1149-5 for protective clothing. It is important to note that additivation with SWCNT is essential in ensuring that the fabrics pass the electrostatic properties standard for protective workwear. It must also be emphasized that doping with SWCNT does not substantially modify the water column properties of the coated UPRON fabric; however, the appearance (color) of the coated fabrics is altered, going from being transparent to grey-black (Figure 20). It is also important to mention that air permeability dramatically

decreases and stiffness increases in all of the coated fabrics compared to untreated fabrics. This is logical when considering that we are applying a polymer layer to one of the faces of the fabric. Reduced air permeability can be a positive feature when it comes to outdoor sportswear with wind-stopper functionality. Regarding stiffness, sample 3294IPDI-2 provides the lowest stiffness values, which is consistent with the mechanical properties of this specimen, being the one with the lowest Young's modulus and the highest Strain at break of the entire series. Finally, it is important to underline that all WPUD led to stable coating pastes with good runnability properties with the Werner–Mathis coating machine. Therefore, it is to be expected that the WPUD will lead to good results in later stages of industrial scaling.

Table 10. Summary of electrostatic properties of UPRON fabrics coated with 3294IPDI-2 and 3294IPDI-2 doped with 0.05 and 0.1 wt. % SWCNT.

Coating Reference	Electrostatic Property	Unit	Limit	Value	Requirements EN 1149-5
3294IPDI-2	Surface resistivity	Ω	$\leq 2.5 \times 10^9$	9.2×10^{12}	FAIL
	Charge decay (inductive charging)	s -	$t_{50} < 4$ $S > 0.2$	>30 0.03	
	Vertical resistance	Ω	$>10^5$	$1.1.10^{12}$	
3294IPDI-2/SWCNT 0.05 wt. %	Surface resistivity	Ω	$\leq 2.5 \times 10^9$	3.8×10^6	PASS
	Charge decay (inductive charging)	s -	$t_{50} < 4$ $S > 0.2$	<0.01 0.99	
	Vertical resistance	Ω	$>10^5$	2.8×10^{11}	
3294IPDI-2/SWCNT 0.1 wt. %	Surface resistivity	Ω	$\leq 2.5 \times 10^9$	3.6×10^6	PASS
	Charge decay (inductive charging)	s -	$t_{50} < 4$ $S > 0.2$	<0.01 0.99	
	Vertical resistance	Ω	$>10^5$	3.2×10^{11}	

Figure 20. Appearance of UPRON fabric coated with: (**top**) 3294IPDI-2 and (**bottom**) 3294IPDI-2 dopped with 0.1 wt. % SWCNT.

Figure 21 shows the SEM micrographs of uncoated and coated UPRON fabrics with the printing pastes made from experiments 3294IPDI-2 and SWCNT-doped 3294IPDI-2. The presence of the coating in the fiber's surface can be seen for all of the coated samples. The coatings are not distributed in a completely homogeneous way, as shown by the higher magnification images. The roughness of the surfaces seems to increase with the increase in SWCNT content in the 3294IPDI-2 matrix. In images with higher magnifications, aggregations of SWCNT are clearly observed. The SWCNT-doped coatings covered the fibers of the fabric, thus forming a three-dimensional network that contributes to the electrical conductivity of the textile. The low surface resistivity of the SWCNT coated textiles (see Table 10) is an indication of the proper distribution of SWCNT in the coatings [42]. As observed by other authors [43,44], the continuous structure of fibers in textiles is favorable in forming a conductive path. Moreover, some connections between the SWCNT can be observed.
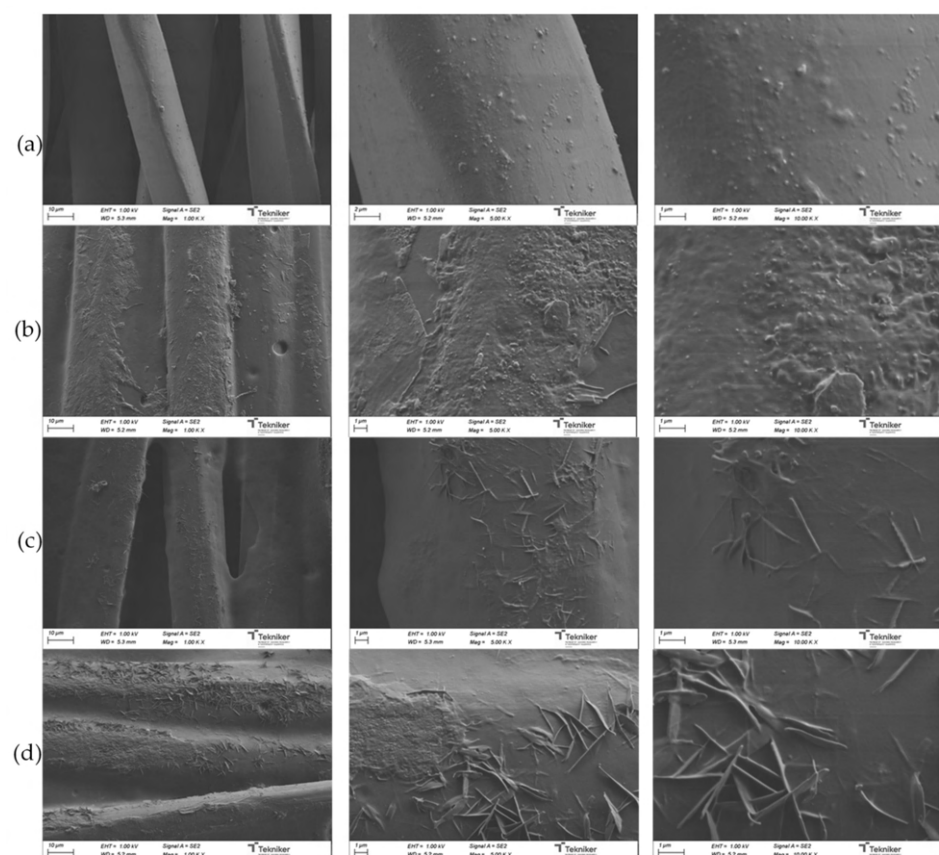
Figure 21. SEM micrographs for (**a**) uncoated UPRON fabric and UPRON fabrics coated with selected printing pastes: (**b**) 3294IPDI-2, (**c**) 3294IPDI-2 doped with 0.05 wt. % SWCNT, and (**d**) 3294IPDI-2 doped with 0.1 wt. % SWCNT.

4. Conclusions

In this work, the synthesis of a series of waterborne polyurethane-urea dispersions (WPUD) has been performed under strict sustainability and Eco-design criteria. For this purpose, the ternary mixture experimental design has been applied as a methodology to systematically explore different proportions between all of the building blocks employed in the synthesis, allowing us to establish a correlation between the structure of polymers and their properties. The WPUD obtained have a bio-based content ranging from 59 to 72%, and are free from tin catalysts and toxic solvents, like alkyl pyrrolidones, presenting a much more favorable carbon footprint and environmental impact than fluoropolymers, like PTFE or conventional petrol-based polyurethanes, which are commonly used in the textile sector as a membrane to confer hydrostatic pressure (water column) to technical-textiles.

The obtained polyurethane-urea coatings offer excellent mechanical and thermal properties with elongations at break above 347.8%, good balance between elasticity and resilience and 10 wt. % loss measured by TGA above 276.5 °C for all of the WPUD series. The stability of the WPUD has been assessed by Z potential measurements and analytical centrifuge tests showing good stability after one year of storage, with no significant destabilization phenomena.

The application properties were also confirmed with good runnability of the coating pastes and proper performance, which, in some cases, equal and exceed those of conventional non-biobased polyurethanes. In this way, the technical feasibility of this type of polymer dispersions is revealed.

The design of experiments of ternary mixture used in this work has allowed for systematically exploring the ratio between the different building-blocks, revealing itself as a good methodology to explore the different characteristics of the designed polymers and establish a correlation between structure and properties that allows the fine-tuning of polymer properties as a function of the relationship between the different components of the mixture.

All of the synthesized polyurethane-ureas provide the coated substrates with remarkable water-repellence (WCA > 112°) and water column ($\geq$26.9 cm), therefore being a more sustainable alternative than waterproof coatings based on fluoropolymers, such as PTFE. In addition to these valuable properties, the additivation of the polyurethane matrix with SWCNT has given rise to textile coatings with advanced functionalities, such as electrical conductivity, which are highly demanded in protective workwear and technical textiles. A surface resistivity as low as 3.6×106 Ω for polyester fabric coated with polymer matrix dopped with 0.1% SWCNT has been achieved, without a significant reduction in the static contact angle measurements or hydrostatic pressure, thus assessing the obtaining of multifunctional fabrics.

Undoubtedly, the synthesis of waterborne polymeric dispersions that were obtained from bio-based building-blocks, tin-free catalysts, and with low volatile organic content (VOC) is a very promising field of research that is gaining importance as the availability in the market of new bio-based building-blocks increases. Thus, it is foreseeable that, in the coming years, the textile-coating's sector will benefit from the advances made in this field, being able to substitute fluoropolymers, like PTFE, or traditional petrol-based polyurethanes or polyacrylates by more sustainable alternatives, like the bio-based WPUD investigated in this work. Therefore, the fluorine-free coating agents based on waterborne dispersions of biobased polyurethane-ureas will contribute to lowering the environmental impact of water-proof finishing processes in the textile industry. In view of these promising results and the urgent need for replacement of fluoropolymers, which are known for its high impact and persistence in the environment, more efforts should be devoted to the design of new polymers based on fluorine-free building blocks that provide advanced barrier to fluids and multifunctional properties.

and 40 °C centrifuge tests using a path length of 10 mm, Figure S12: Transmission profiles of the synthesized WPUD dispersions subjected to 2000× *g* and 4 °C centrifuge test using a path length of 10 mm.

References

1. Buck, R.C.; Franklin, J.; Berger, U.; Conder, J.M.; Cousins, I.T.; De Voogt, P.; Jensen, A.A.; Kannan, K.; Mabury, S.A.; van Leeuwen, S.P.J. Perfluoroalkyl and polyfluoroalkyl substances in the environment: Terminology, classification, and origins. *Integr. Environ. Assess. Manag.* **2011**, *7*, 513–541. [CrossRef] [PubMed]

2. Giesy, J.P.; Kannan, K. Global distribution of perfluorooctane sulfonate in wildlife. *Environ. Sci. Technol.* **2001**, *35*, 1339–1342. [CrossRef] [PubMed]

3. Martin, J.W.; Mabury, S.A.; Solomon, K.R.; Muir, D.C.G. Progress toward understanding the bioaccumulation of perfluorinated alkyl acids. *Environ. Toxicol. Chem.* **2013**, *32*, 2421–2423. [CrossRef] [PubMed]

4. Apelberg, B.J.; Witter, F.R.; Herbstman, J.B.; Calafat, A.M.; Halden, R.U.; Needham, L.L.; Goldman, L.R. Cord serum concentrations of perfluorooctane sulfonate (PFOS) and perfluorooctanoate (PFOA) in relation to weight and size at birth. *Environ. Health Perspect.* **2007**, *115*, 1670–1676. [CrossRef] [PubMed]

5. Fei, C.; McLaughlin, J.K.; Tarone, R.E.; Olsen, J. Perfluorinated chemicals and fetal growth: A study within the Danish national birth cohort. *Environ. Health Perspect.* **2007**, *115*, 1677–1682. [CrossRef]

6. Vierke, L.; Möller, A.; Klitzke, S. Transport of perfluoroalkyl acids in a water-saturated sediment column investigated under near-natural conditions. *Environ. Pollut.* **2014**, *186*, 7–13. [CrossRef]

7. Luz, A.L.; Anderson, J.K.; Goodrum, P.; Durda, J. Perfluorohexanoic acid toxicity, part I: Development of a chronic human health toxicity value for use in risk assessment. *Regul. Toxicol. Pharmacol.* **2019**, *103*, 41–55. [CrossRef] [PubMed]

8. Klaunig, J.E.; Shinohara, M.; Iwai, H.; Chengelis, C.P.; Kirkpatrick, J.B.; Wang, Z.; Bruner, R.H. Evaluation of the chronic toxicity and carcinogenicity of perfluorohexanoic acid (PFHxA) in Sprague-Dawley Rats. *Toxicol. Pathol.* **2015**, *43*, 209–220. [CrossRef]

9. Brusseau, M.L.; Anderson, R.H.; Guo, B. PFAS concentrations in soils: Background levels versus contaminated sites. *Sci. Total Environ.* **2020**, *740*, 140017. [CrossRef]

10. Stoiber, T.; Evans, S.; Naidenko, O.V. Disposal of products and materials containing per- and polyfluoroalkyl substances (PFAS): A cyclical problem. *Chemosphere* **2020**, *260*, 127659. [CrossRef]

11. Lohmann, R.; Cousins, I.T.; DeWitt, J.C.; Glüge, J.; Goldenman, G.; Herzke, D.; Lindstrom, A.B.; Miller, M.F.; Ng, C.A.; Patton, S.; et al. Are Fluoropolymers Really of Low Concern for Human and Environmental Health and Separate from Other PFAS? *Environ. Sci. Technol.* **2020**. [CrossRef] [PubMed]

12. Geiser, M.; Schürch, S.; Gehr, P. Influence of surface chemistry and topography of particles on their immersion into the lung's surface-lining layer. *J. Appl. Physiol.* **2003**, *94*, 1793–1801. [CrossRef]

13. Groh, K.J.; Geueke, B.; Muncke, J. Food contact materials and gut health: Implications for toxicity assessment and relevance of high molecular weight migrants. *Food Chem. Toxicol.* **2017**, *109*, 1–18. [CrossRef] [PubMed]

14. Washington, J.W.; Jenkins, T.M.; Rankin, K.; Naile, J.E. Decades-scale degradation of commercial, side-chain, fluorotelomer-based polymers in soils and water. *Environ. Sci. Technol.* **2015**, *49*, 915–923. [CrossRef] [PubMed]

15. Cobbing, M.; Campione, C.; Kopp, M. *PFC Revolution in the Outdoor Sector*; Greenpeace: Zürich, Switzerland, 2017.

16. Zahid, M.; Mazzon, G.; Athanassiou, A.; Bayer, I.S. Environmentally benign non-wettable textile treatments: A review of recent state-of-the-art. *Adv. Colloid Interface Sci.* **2019**, *270*, 216–250. [CrossRef] [PubMed]

17. Lassen, C.; Jensen, A.A.; Warming, M. *Alternatives to Perfluoroalkyl and Polyfluoroalkyl Substances (PFAS) in Textiles*; The Danish Environmental Protection Agency: Copenhagen, Danish, 2015.

18. Lacruz, A.; Salvador, M.; Blanco, M.; Vidal, K.; Martínez de Ilarduya, A. Development of fluorine-free waterborne textile finishing agents for anti-stain and solvent-water separation based on low surface energy (co)polymers. *Prog. Org. Coat.* **2021**, *150*. [CrossRef]

19. Parsons, G.N.; Atanasov, S.E.; Dandley, E.C.; Devine, C.K.; Gong, B.; Jur, J.S.; Lee, K.; Oldham, C.J.; Peng, Q.; Spagnola, J.C.; et al. Mechanisms and reactions during atomic layer deposition on polymers. *Coord. Chem. Rev.* **2013**, *257*, 3323–3331. [CrossRef]

20. Iwai, Y.; Sameshima, S.; Yonezawa, S.; Katayama, S. Fabrication of conductive cotton by electroless plating method with supercritical carbon dioxide. *J. Supercrit. Fluids* **2015**, *100*, 46–51. [CrossRef]

21. Jiang, S.Q.; Newton, E.; Yuen, C.W.M.; Kan, C.W. Chemical Silver Plating on Cotton and Polyester Fabrics and its Application on Fabric Design. *Text. Res. J.* **2006**, *76*, 57–65. [CrossRef]

22. Trovato, V.; Teblum, E.; Kostikov, Y.; Pedrana, A.; Re, V.; Nessim, G.D.; Rosace, G. Sol-gel approach to incorporate millimeter-long carbon nanotubes into fabrics for the development of electrical-conductive textiles. *Mater. Chem. Phys.* **2020**, *240*, 122218. [CrossRef]

23. Etxaniz, I.; Llorente, O.; Aizpurua, J.; Martín, L.; González, A.; Irusta, L. Dispersion Characteristics and Curing Behaviour of Waterborne UV Crosslinkable Polyurethanes Based on Renewable Dimer Fatty Acid Polyesters. *J. Polym. Environ.* **2019**, *27*, 189–197. [CrossRef]

24. Poussard, L.; Lazko, J.; Mariage, J.; Raquez, J.M.; Dubois, P. Biobased waterborne polyurethanes for coating applications: How fully biobased polyols may improve the coating properties. *Prog. Org. Coat.* **2016**, *97*, 175–183. [CrossRef]

25. Cavallo, D.; Gardella, L.; Soda, O.; Sparnacci, K.; Monticelli, O. Fully bio-renewable multiblocks copolymers of poly(lactide) and commercial fatty acid-based polyesters polyols: Synthesis and characterization. *Eur. Polym. J.* **2016**, *81*, 247–256. [CrossRef]

26. Wu, S.; Ladani, R.B.; Zhang, J.; Bafekrpour, E.; Ghorbani, K.; Mouritz, A.P.; Kinloch, A.J.; Wang, C.H. Aligning multilayer graphene flakes with an external electric field to improve multifunctional properties of epoxy nanocomposites. *Carbon* **2015**, *94*, 607–618. [CrossRef]

27. Wang, Q.; Dai, J.; Li, W.; Wei, Z.; Jiang, J. The effects of CNT alignment on electrical conductivity and mechanical properties of SWNT/epoxy nanocomposites. *Compos. Sci. Technol.* **2008**, *68*, 1644–1648. [CrossRef]

28. Monti, M.; Natali, M.; Torre, L.; Kenny, J.M. The alignment of single walled carbon nanotubes in an epoxy resin by applying a DC electric field. *Carbon* **2012**, *50*, 2453–2464. [CrossRef]

29. Yan, H.; Tang, Y.; Long, W.; Li, Y. Enhanced thermal conductivity in polymer composites with aligned graphene nanosheets. *J. Mater. Sci.* **2014**, *49*, 5256–5264. [CrossRef]

30. Lerche, D.; Sobisch, T. Direct and accelerated characterization of formulation stability. *J. Dispers. Sci. Technol.* **2011**, *32*, 1799–1811. [CrossRef]

31. Poussard, L.; Mecheri, A.; Mariage, J.; Barakat, I.; Bonnaud, L.; Raquez, J.M.; Dubois, P. Synthesis of oligo(butylene succinate)-based polyurethanes: Influence of the chemical structure on thermal and mechanical properties. In *Proceedings of the Journal of Renewable Materials*; Scrivener Publishing LLC: Beverly, MA, USA, 2014; Volume 2, pp. 13–22.

32. Bueno-Ferrer, C.; Hablot, E.; Perrin-Sarazin, F.; Garrigós, M.C.; Jiménez, A.; Averous, L. Structure and Morphology of New Bio-Based Thermoplastic Polyurethanes Obtained From Dimeric Fatty Acids. *Macromol. Mater. Eng.* **2012**, *297*, 777–784. [CrossRef]

33. Lomölder, R.; Plogmann, F.; Speier, P. Selectivity of isophorone diisocyanate in the urethane reaction influence of temperature, catalysis, and reaction partners. *J. Coat. Technol.* **1997**, *69*, 51–57. [CrossRef]

34. Mukherjea, R.N.; Saha, K.K.; Sanyal, S.K. Plasticizing effect of acetylated castor oil on castor oil-based, moisture-cured polyurethane film. *J. Am. Oil Chem. Soc.* **1978**, *55*, 653–656. [CrossRef]

35. Xu, J.; Li, T.; Zhao, W.; Li, P.; Wu, Y. Synthesis and characterization of waterborne polyurethane emulsions based on poly(butylene itaconate) ester. *Des. MonoMers Polym.* **2016**, *19*, 309–318. [CrossRef]

36. Sun, Y.; Zhao, X.; Liu, R.; Chen, G.; Zhou, X. Synthesis and characterization of fluorinated polyacrylate as water and oil repellent and soil release finishing agent for polyester fabric. *Prog. Org. Coat.* **2018**, *123*, 306–313. [CrossRef]

37. Li, D.; Müller, M.B.; Gilje, S.; Kaner, R.B.; Wallace, G.G. Processable aqueous dispersions of graphene nanosheets. *Nat. Nanotechnol.* **2008**, *3*, 101–105. [CrossRef]

38. Sheng, L.; Zhang, X.; Ge, Z.; Liang, Z.; Liu, X.; Chai, C.; Luo, Y. Preparation and properties of waterborne polyurethane modified by stearyl acrylate for water repellents. *J. Coat. Technol. Res.* **2018**, *15*, 1283–1292. [CrossRef]

39. Yuan, F.; Xu, D.; Qi, X.; Zhao, J.; Gao, Y. Impact of High Hydrostatic Pressure on the Emulsifying Properties of Whey Protein Isolate-Chitosan Mixtures. *Food Bioprocess Technol.* **2013**, *6*, 1024–1031. [CrossRef]

40. Gao, L.; McCarthy, T.J. Contact angle hysteresis explained. *Langmuir* **2006**, *22*, 6234–6237. [CrossRef]

41. Baxter, S. Wetting and contact-angle hysteresis. *Nature* **1950**, *165*, 198. [CrossRef]

42. Zhang, R.; Deng, H.; Valenca, R.; Jin, J.; Fu, Q.; Bilotti, E.; Peijs, T. Carbon nanotube polymer coatings for textile yarns with good strain sensing capability. *Sens. Actuators A Phys.* **2012**, *179*, 83–91. [CrossRef]
43. Narkis, M.; Lidor, G.; Vaxman, A.; Zuri, L. New injection moldable electrostatic dissipative(ESD) composites based on very low carbon black loadings. *J. Electrostat.* **1999**, *47*, 201–214. [CrossRef]
44. Dai, M.; Zhai, Y.; Zhang, Y. A green approach to preparing hydrophobic, electrically conductive textiles based on waterborne polyurethane for electromagnetic interference shielding with low reflectivity. *Chem. Eng. J.* **2020**. [CrossRef]

Biobased Waterborne Polyurethane-Ureas Modified with POSS-OH for Fluorine-Free Hydrophobic Textile Coatings

Biobased Waterborne Polyurethane-Ureas Modified with POSS-OH for Fluorine-Free Hydrophobic Textile Coatings

Amado Lacruz [1,2,](#), Mireia Salvador [1], Miren Blanco [3], Karmele Vidal [3], Amaia M. Goitandia [3], Lenka Martinková [4], Martin Kyselka [4] and Antxon Martínez de Ilarduya [2]

1 Color Center, S.A. Ptge. Marie Curie 3, Nau 6, 08223 Terrassa, Spain; msalvador@colorcenter.es
2 Departament d'Enginyeria Química, Universitat Politècnica de Catalunya, ETSEIB, Diagonal 647, 08028 Barcelona, Spain; antxon.martinez.de.ilarduia@upc.edu
3 Tekniker, Basque Research and Technology Alliance (BRTA), Surface Chemistry and Nanotechnology Unit, Iñaki Goenaga 5, 20600 Eibar, Spain; miren.blanco@tekniker.es (M.B.); karmele.vidal@tekniker.es (K.V.); amaia.martinez@tekniker.es (A.M.G.)
4 Inotex Spol. s r.o, Stefanikova 1208, 54401 Dvůr Králové nad Labem, Czech Republic; martinkova@inotex.cz (L.M.); kyselka@inotex.cz (M.K.)
* Correspondence: alacruz@colorcenter.es or amado.lacruz@upc.edu; Tel.: +34-9378-61113

Abstract: Waterborne polyurethane-urea dispersions (WPUD), which are based on fully biobased amorphous polyester polyol and isophorone diisocyanate (IPDI), have been successfully synthesized obtaining a finishing agent that provides textiles with an enhanced hydrophobicity and water column. Grafting of trans-cyclohexanediol isobutyl POSS (POSS-OH) to the biobased polymer backbone has also been investigated for the first time and its properties compared to a standard chain extender, 1,3-propanediol (PDO). The chemical structure of WPUD has been characterized by Fourier-transform infrared spectroscopy (FTIR) and nuclear magnetic resonance (NMR). The thermal properties have been evaluated by differential scanning calorimetry (DSC) and thermogravimetric analysis (TGA). Mechanical properties have been studied by tensile stress–strain analysis. Moreover, the particle size, particle size distribution (PSD), and stability of developed waterborne dispersions have been assessed by dynamic light scattering (DLS), Z-potential, storage aging tests, and accelerated aging tests by analytical centrifuge (LUM). Subsequently, selected fabrics have been face-coated by the WPUD using the knife coating method and their properties have been assessed by measuring the water contact angle (WCA), oil contact angle (OCA), water column, fabric stiffness, air permeability, and water vapor resistance (breathability). Finally, the surface morphology and elemental composition of uncoated and coated fabrics have been studied by scanning electron microscopy (SEM) and energy-dispersive X-ray spectroscopy (EDS), respectively. All of the synthesized polyurethane-ureas provided the coated substrates with a remarkable hydrophobicity and water column, resulting in a more sustainable alternative to waterproof coatings based on fluoropolymers, such as PTFE. Grafting POSS-OH to the polymeric backbone has led to textile coatings with enhanced hydrophobicity, maintaining thermal, mechanical, and water column properties, giving rise to multifunctional coatings that are highly demanded in protective workwear and technical textiles.

Keywords: waterproof; water-column; fluorine-free; bio-based; hydrophobic; hybrid POSS; technical textiles; multifunctional fabrics; textile coatings

1. Introduction

Our current society relies predominantly on fossil resources such as oil, natural gas, or coal to meet all the needs of modern life. In addition, advanced textile properties such as repellency to liquids or a water column currently require chemicals that are considered of high concern, like fluorochemicals that dominate the water- and oil-repellent textile finishing market because of their excellent performance. However, fluorinated chemicals release harmful substances, giving rise to serious damage to ecosystems worldwide [1,2].

This is not a sustainable situation, and therefore a transition to a less harmful and biobased solution is necessary [3].

Accordingly, sustainability is nowadays an important topic not only for the chemical industry but also for other industrial sectors as well as governments and society itself. Renewable resources derived from plants can be used to produce building blocks suitable for obtaining partially or fully biobased high-performance polymeric materials. Nevertheless, much work remains to be done in this field through innovation and joint efforts involving industries, universities, research centers, and governments. Biobased polymers are a group of materials that are totally or partially derived from biomass. They try to fulfill global trends toward environmentally friendly solutions in the field of electronics, packaging, automobiles, textiles, etc. At present, thanks to the growing supply of commercially available biobased building blocks [4], a great opportunity opens up for the synthesis of sustainable high-performance polymers offering highly demanded features like outstanding mechanical properties, barrier properties, hydrophobicity, and stability against oxidation, hydrolysis, heat, or UV radiation. Biobased polyurethanes are an important group of materials that is attracting growing interest from industry and research groups [5,6]. Chemical, mechanical, and barrier properties of these types of materials can be precisely modulated from the appropriate selection of the starting building blocks and the synthesis strategy [7,8].

In this work, the commercial fully biobased amorphous polyester polyol Priplast 3238 has been combined with IPDI, internal emulsifier DMBA, and chain extenders 1,3-propanediol (PDO), trans-cyclohexanediol isobutyl POSS (POSS-OH), and ethylenediamine (EDA) to obtain a series of waterborne polyurethane-urea dispersions (WPUD). These WPUD have been specifically designed as sustainable fluorine-free coating agents for technical textiles where hydrophobic and liquid barrier finishes are required. A ternary mixture experimental design methodology has been used as a systematic approach to explore the relationship between the polymer structure and the properties of the obtained polymer films and coated fabrics.

Despite reactive polyhedral oligomeric silsesquioxanes having been previously reported in the literature as a building block for polyurethanes [9,10], we describe for the first time the grafting of POSS-OH to a biobased polyurethane-urea. POSS-OH is a hybrid molecule with an inorganic silsesquioxane at the core, organic isobutyl groups attached at seven corners of the cage, and a trans-cyclohexanediol group on the eighth corner that allows its incorporation as a co-monomer in the polyurethane-urea chain. Its structure is displayed in Figure 1. The bulky and highly hydrophobic heptaisobutyl silsesquioxane group is able to confer enhanced hydrophobicity without noticeably affecting the mechanical and thermal properties of the coatings.
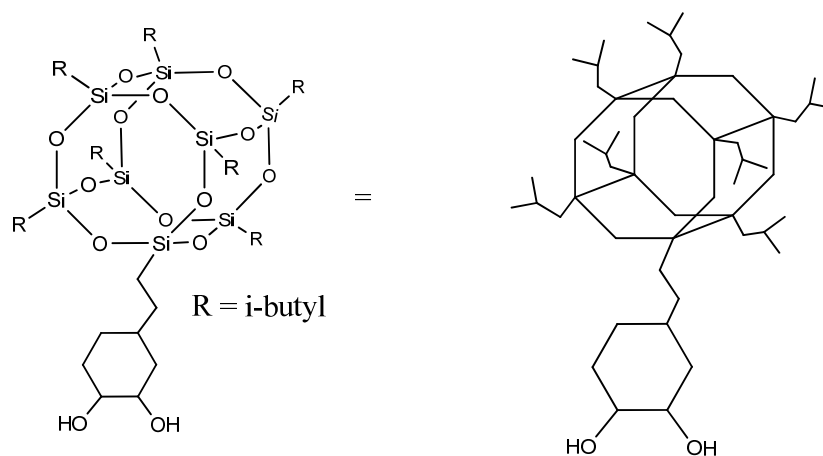
Figure 1. Cyclohexanediol isobutyl POSS (POSS-OH).

2. Materials and Methods

2.1. Materials

Fully biobased amorphous polyester polyol based on dimerized fatty acids (Figure 2), commercially known as Priplast 3238 and supplied by Croda Iberica, S.A. (Barcelona, Spain), was used as a main biobased polyol for the synthesis of all of the polyurethane-ureas. Priplast 3238 is a highly hydrophobic, amorphous polyester polyol providing high flexibility at low temperatures, good hydrolytic stability, and enhanced adhesion to dissimilar substrates. This polyol has a M_n of 2000 g mol^{-1}, f(OH) = 2 and an average hydroxyl value of 56 mg KOH g^{-1}. Isophorone diisocyanate (IPDI, ≥99.5% purity) was supplied by Evonik Industries GmbH (Essen, Germany). 2,2-Bis(hydroxymethyl)butyric acid (DMBA, 99% purity) was supplied by Anhui Sinograce Chemical CO., LTD (Hefei, People's Republic of China). 1,3-Propanediol (PDO, ≥99% purity and fully biobased) was supplied by DuPont Tate & Lyle BioProducts (Loudon, TN, USA). Trans-cyclohexanediol isobutyl POSS (POSS-OH) was supplied by Hybrid Plastic Co. Inc. (Hattiesburg, MS, USA) Acetone (≥99.5% purity), triethylamine (TEA, 99% purity), and ethylenediamine (EDA, ≥99% purity) were purchased from Sigma-Aldrich (Darmstadt, Germany). Everchem Specialty Chemicals (Media, PA, USA) supplied Bicat 8108 (bismuth neodecanoate 20%).
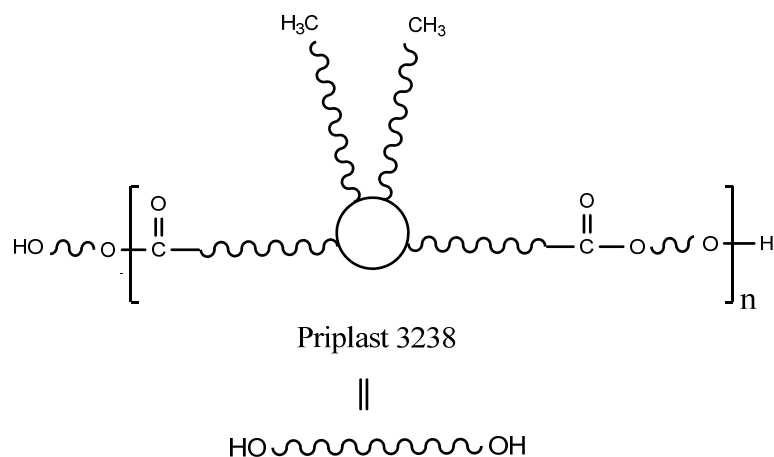
Figure 2. The chemical structure of Priplast 3238.

The additives to formulate the printing pastes were supplied by Color Center, S.A. (Terrassa, Spain) and are: Defoamer PR (defoamer, mineral oil-based), Complex DG (diethylene glycol-based, runnability improver), DMEA (dimethylethanolamine, neutralizing agent), and Thickener L-120 (polyacrylic acid, associative thickener).

Pristine polyester fabric (UPRON) was supplied by HEDVA a.s. (Moravská Třebová, Czech Republic) and was used as a substrate to perform the coatings. The main characteristics of the pristine UPRON fabric are summarized as follows: 100% polyester fabric (PET, polyethylene terephthalate), plain weave, 172 ± 5 g m^{-2}; threads per cm: warp 32 ± 2, weft 14 ± 1.

2.2. Synthesis of Waterborne Polyurethane-Urea Dispersions (WPUD)

Priplast 3238 was dried in a vacuum at 110 °C and 35 mbar for 1 h before use. It was introduced into a 750 mL five-necked reactor equipped with a mechanical stirrer, an inlet for nitrogen, and a reflux condenser. DMBA internal emulsifier and POSS-OH or PDO were added to the reactor and degassed for 1 h at 80 °C under stirring to complete homogenization. IPDI and Bicat 8108 catalyst (25 mg per kg of mixture) were subsequently added to the reactor. The temperature was maintained at 80 °C under nitrogen blanketing until the theoretical value of NCO was reached (measured by titration using the dibutylamine method). The reaction time for the prepolymer formation was between 2 and 2.5 h. All of the prepolymers were prepared at an isocyanate/hydroxyl ratio (NCO/OH) of 1.62. Afterward, acetone was added to decrease the viscosity of the prepolymer and facilitate

its subsequent dispersion in water (typically 100 g/200 g of prepolymer). The reaction mixture was cooled to 40 °C and TEA was added slowly through a dropping funnel and the mixture maintained for 30 min under stirring to ensure complete neutralization of the carboxyl groups from DMBA. The reaction system was subsequently cooled to 30 °C and cold deionized water at 8 °C was quickly added with vigorous stirring to promote phase inversion, thus obtaining a milky dispersion of the prepolymer in water. Chain extension agent EDA was stoichiometrically added to react with the free isocyanate groups of the prepolymer, previously diluted in water to 20%, drop-by-drop, by keeping the temperature of the mixture between 15 and 18 °C along with gentle stirring for an additional 1 h. Finally, the biobased WPUD was obtained after removing acetone by a rotary evaporator under reduced pressure (250 mbar) at 60 °C. All of the synthesized WPUD were adjusted to a solid content of 35%. It is worth noting that acetone can be readily recovered and recycled.

The ratio between the three diols used in the prepolymer synthesis (Priplast 3238, DMBA, and POSS-OH or PDO) was systematically varied using the methodology of ternary mixture design of experiments (Figure 3). In our particular case, two experimental designs were established, in the first design the ternary mixture of DMBA, Priplast 3238 and POSS-OH was investigated and in the second design the ternary mixture of DMBA, Priplast 3238 and PDO was investigated. Experiments 1 and 2 were common to both experimental designs as they did not contain PDO or POSS-OH. Lower constraints were applied to DMBA and Priplast 3238 because, due to the particularity of the system, it is not possible to study the proportions of the three diols in the full range (from 0 to 100 molar%). For example, the amount of DMBA could not be equal to 0, since then the final polymer would not be dispersible in water; therefore, the lower constraint for DMBA was established in 37 molar%. A minimum amount of Priplast 3238 was also established so that all of the prepolymers contained at least a 40 molar% of this biobased polyol.
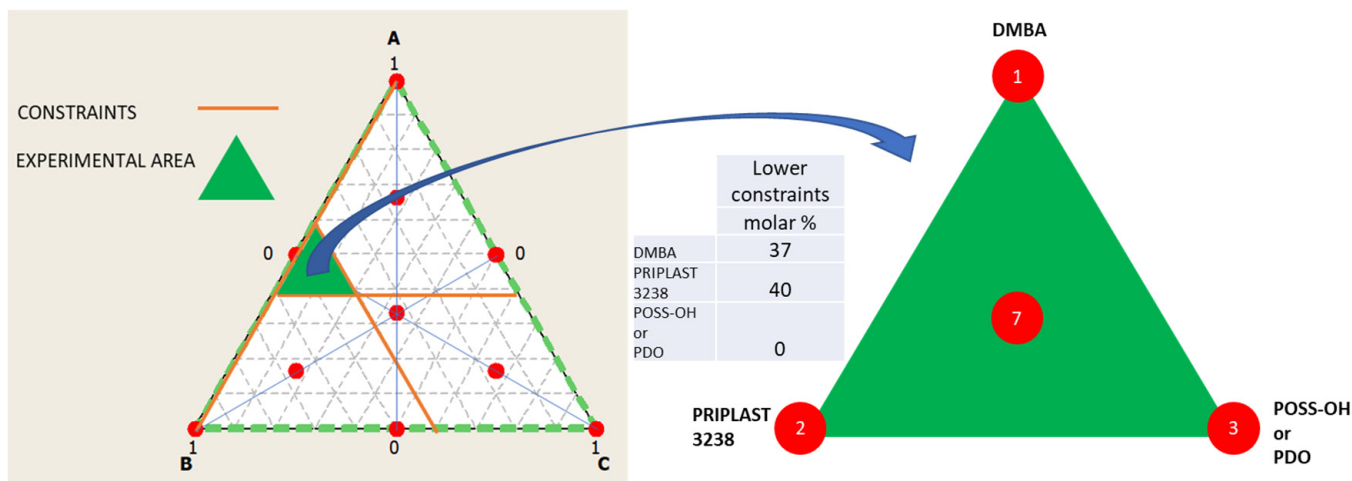
Figure 3. Ternary mixture design of experiments employed to study the proportion between the tree diols that form part of the polymer. **Left**: full design surface area in white with all the theoretical experimental points marked in red and studied area in green, which is delimited by the lower constraints stablished for component A (DMBA) and B (Priplast 3238). Middle: table summarizing the lower constraints stablished for the diols. **Right**: area studied and experimental points of the simplex design plot (1, 2, 3, 7).

Table 1 shows the simplex design table with all of the performed experimental points from the simplex ternary mixture design. The six columns on the right show the molar% of each polyol employed in the synthesis considering the lower constraints, hard segment content in wt.%, and bio-based content of each experiment in wt.%, respectively.

Table 1. The simplex design table with experiments carried out in this work.

Experiment	Matrix				Molar%				Hard Segment (wt.%)	Biobased Content (wt.%)
	DMBA	Priplast 3238	POSS-OH	PDO	DMBA	Priplast 3238	POSS-OH	PDO		
3238-1	1	0	0	0	60.00	40.00	0.00	0.00	40.6	59.4
3238-2	0	1	0	0	37.00	63.00	0.00	0.00	28.0	72.0
3238-3POSS	0	0	1	0	37.00	40.00	23.00	0.00	47.0	53.0
3238-3PDO	0	0	0	1	37.00	40.00	0.00	23.00	38.8	62.6
3238-7POSS	1/3	1/3	1/3	0	44.67	47.67	7.67	0.00	37.9	62.1
3238-7PDO	1/3	1/3	0	1/3	44.67	47.67	0.00	7.67	35.0	65.4

Polyurethane-urea films suitable for NMR, mechanical, thermal, and swelling characterization were prepared by carefully pouring 20 g of WPUD in a circular Teflon mold, allowing the water to evaporate slowly at 40 °C into a vented oven for 48 h to obtain 1-mm thick films that were subsequently cured and dried at 60 °C for 48 h in a vacuum oven.

2.3. Application of WPUD on Fabrics by Coating

The fabrics were coated by printing pastes that were made of WPUD, water, defoamer, runnability improver, DMEA, and thickener (see Table 2 for the standard printing paste formulation, solid content, and viscosity).

Table 2. Printing paste formulation employed to perform the coating of the fabrics with WPUD.

Composition	Printing Paste Formulation (g)
WPUD	85
Water	15
Defoamer PR	1
Complex DG	2
DMEA	1
Thickener L-120	Added drop-by-drop under high shear until viscosity of 18,000 ± 50 cPs is reached (Brookfield RV 6/30)
Dry polyurethane-urea content	30 ± 1%

The knife coating procedure, which is a widely used coating method in the textile sector, was employed to coat all of the fabrics with the corresponding printing pastes. Knife coating was performed using a laboratory coating machine R2R continuous-line Werner Mathis in a coating regime, air knife at 90 °, followed by drying in a vented oven at 110 °C at a speed of 1 m per min^{-1} and curing at 150 °C at a speed of 0.4 m per min^{-1}. The coating procedure on glass slides has been done by a more convenient manual Quadrangular Applicator with a gap of 60 μm, followed by drying at 90 °C for 5 min and curing at 120 °C for 2 min.

The dry add-on of the coated fabrics was calculated as follows: a sample cutter James H. Heal model 230/100 was used to cut out regular circular specimens of a fixed area (100 cm^2) from the uncoated fabric and all of the coated fabrics. The calculation of weight per square meter (grammage, G) of a given specimen was performed by multiplying the specimen's weight measured by a balance with a readability of 0.01 g by a factor of 100. Finally, the dry add-on of a coated fabric was calculated using Equation (1), where Gc and Gu are the grammages of the coated and uncoated specimens, respectively.

$$Dry\ add\ on = Gc - Gu \tag{1}$$

2.4. Characterization Techniques

2.4.1. Characterization of Synthesized Polymers and Dispersions

Fourier-transform infrared spectroscopy (FTIR) was employed for chemical characterization of the WPUD. The FTIR spectra were obtained using a Perkin Elmer Spectrum

Two spectrometer (Madrid, Spain) equipped with transmission accessory. A drop of each waterborne dispersion was spread on a SeZn FTIR window and then dried under an IR lamp to evaporate water and to obtain a thin film. Eight scans were taken for each sample in the range of 4000–500 cm^{-1} with a resolution of 4 cm^{-1}.

The structural characterization of all the WPUD casted films was performed by ^{1}H-NMR using a Bruker AMX-300 spectrometer (Billerica, MA, USA) at 25 °C operating at 300.1 MHz. Samples were dissolved in deuterated chloroform or deuterated tetrachloroethane, and spectra were internally referenced to tetramethylsilane (TMS). Approximately 10 mg of sample dissolved in 1 mL of solvent was used to collect the ^{1}H-NMR spectra. Sixty-four scans were acquired with 32 K data points as well as a relaxation delay of 1 s.

Differential scanning calorimetry (DSC) studies of the dry films of all the synthesized WPUD as well as Priplast 3228 were carried out to determine first- and second-order thermal transitions. T_g and T_m values were determined by heating the sample from −90 to 200 °C at a constant heating rate of 10 °C min^{-1} in a Mettler-Toledo DSC1 module (Gießen, Germany) equipped with an intracooler and previously calibrated with high purity indium and zinc standards. Experiments were conducted in a dry atmosphere, under a nitrogen constant flow of 50 mL/min, working with around 10 mg samples and using microperforated aluminum pans.

The thermal stability of the synthesized WPUD films was studied by thermogravimetric analysis (TGA) using a Mettler-Toledo TGA2 module (Columbus, OH, USA). The thermogravimetric analysis consisted of recording the weight loss of the samples that were subjected to a temperature gradient from 25 °C to 600 °C at 10 °C min^{-1}. TGA curves were recorded under nitrogen and air atmospheres.

Mechanical properties were determined by stress–strain tensile measurements. The tests were carried out following the BS ISO 37: 2005 standard using a Zwick/Roell model 500 N (Ulm, Germany). The measurements were carried out on dumbbell-shaped Type 4 specimens cut from the WPUD films. The test conditions were as follows: preload 0.1 MPa, preload speed 1 mm min^{-1}, and test speed 50 mm min^{-1}. For each WPUD, at least five samples were taken in different parts of the films and tested. The characteristic parameters measured were: elastic modulus (E), stress at break (σ_b), deformation at break (ε_b), and stress at 100% strain ($\sigma_{100\%}$).

Water-swelling measurements were performed using dumbbell-shaped Type 4 specimens cut from the WPUD films. The samples were placed in a closed vial with 20 mL of deionized water at 25 °C for 48 h. Swelling degree was determined by Equation (2), where w_0 and w were respectively the weight of the initial dried material and of the swollen material after 48 h. The experiments were carried out in triplicate for each specimen.

$$\text{Swelling } (\%) = \frac{w - w_0}{w_0} \times 100 \tag{2}$$

Moreover, the particle size and particle size distribution (PSD) of developed aqueous polymeric dispersions were characterized via dynamic light scattering (DLS). The stability of the dispersions was analyzed using Z-potential measurements. DLS and Z-potential tests were performed on a Malvern Zetasizer ZS at 20 °C. Particle size and Z-potential measurements were performed after the dilution of the WPUD to 1 wt.% with deionized water buffered at pH 8.2. Storage stability was assessed for all of the WPUD stored in sealed glass vials and kept for 6 months at 4 °C and 40 °C, respectively. Finally, the WPUD specimens were subjected to accelerated sedimentation tests using an analytical centrifuge, LUMiFuge 110–153.3–12 (LUM GmbH, Berlin, Germany), in order to evaluate long-term stability. In each measurement, the suspension was pipetted into a polyamide transparent cell with a path length of 2 mm. Thereafter, a transmission profile at 470 nm of the samples was analyzed at 4 °C and 40 °C and a relative centrifugal force of 2000× *g* with a scanning rate of once every 60 s for 5 h.

2.4.2. Characterization of Coated Textiles

The water and oil repellence of the coated fabrics was tested by measuring the contact angle of a droplet of water and a droplet of olive oil placed on the surface of the coated textile, respectively. Water contact angle (WCA) and oil contact angle (OCA) measurements were carried out under ambient conditions with a SURFTENS Universal automatic goniometer (OEG GmbH, Frankfurt, Germany). Static contact angle of the air–liquid interface was measured on each coated fabric. The volume of each liquid droplet was 5 μL and the average value of five measurements, made at different positions of the textile surface, was adopted as the value of WCA or OCA.

Hydrostatic pressure, fabric stiffness, air permeability, and water vapor resistance were evaluated according to the indicated standards in Table 3.

Table 3. Standards employed to evaluate the properties of the coated textiles.

Property	Standard
Determination of resistance to water penetration-Hydrostatic pressure test (water column)	EN 20811:1992
Fabric stiffness	ČSN 80 0858
Determination of the permeability of fabrics to air	ISO 9237:1995
Water vapor resistance under steady-state conditions (sweating guarded hotplate test)	ISO 11092:2014

In ISO 11092, the water vapor resistance of the fabric (R_{et}) refers to the ratio of the water vapor pressure difference on both sides of the fabric (P1, P2) to the heat flux evaporated vertically (Q) per unit area of the fabric (S). The units of R_{et} are square meters pascal per watt, $m^2 \cdot Pa \, W^{-1}$.

$$Ret = \frac{S \, (P1 - P2)}{Q} \tag{3}$$

Finally, the surface morphologies of the relevant coated and uncoated fabrics were studied via scanning electron microscopy (SEM) using an Ultra Gemini-II microscope from Carl Zeiss SMT (LLC, Thornwood, NY, USA), also equipped with energy-dispersive X-ray spectroscopy (EDS), which was employed for element analysis on textile surfaces.

3. Results and Discussion

3.1. Synthesis and Characterization of WPUD

A series of WPUD were synthesized using the prepolymer method, as reported in the experimental section. Once the prepolymer was obtained, the neutralization of the carboxyl groups with triethylamine and subsequent phase inversion in water was carried out. Finally, chain extension via EDA was performed, followed by acetone removal by rotary evaporation and standardization to 35% solid content. The scheme of the synthesis strategy of the WPUD can be seen in Figure 4.

WPUD were first characterized by FTIR. The infrared spectra of all synthesized polymers showed the complete conversion of isocyanate groups judging by the absence of the characteristic free isocyanate band at 2275 cm^{-1}. By comparing the spectrum of the starting polyol Priplast 3238 with those of the synthesized polyurethane-ureas, the appearance of new bands that are indicative of the formation of urethane/urea bonds could be clearly confirmed (Figure 5). The broad band of NH asymmetrical and symmetrical stretching vibration at 3351 cm^{-1} indicated the great extent of NH established hydrogen bonds with carbonyl groups from urethane, urea, ester, and ionic carboxylate from internal emulsifier DMBA [11]. The region of 1500–1600 cm^{-1} showed NH-CO stretching and NH bending bands of the urethane group at 1548 cm^{-1}. The region between 1740 and 1600 cm^{-1} showed characteristic C=O stretching bands from DMBA carboxylate, urethane, and urea carbonyl groups at approximately the 1661–1700 cm^{-1} region, partially overlapped with the ester band from the polyester polyol at 1739 cm^{-1}. COC(O) stretching bands and NH

out-of-plane bending bands from urethane functional groups at 1242 cm^{-1} and 775 cm^{-1}, respectively, were clearly observed. On the other hand, the pure POSS-OH showed strong bands at 1108, 743, and 480 cm^{-1} that corresponded to the Si-O-Si asymmetric stretching, symmetric stretching, and bending mode, respectively. The pure POSS-OH also showed a band at 1039 cm^{-1} that, according to [9], can be attributed to Si-isobutyl. 3238-3PDO, 3238-1, 3238-2, 32387PDO showed all the aforementioned characteristic polyurethane-urea bands while 3238-3POSS and 3238-7POSS showed the same bands plus the characteristic silsesquioxane peaks.
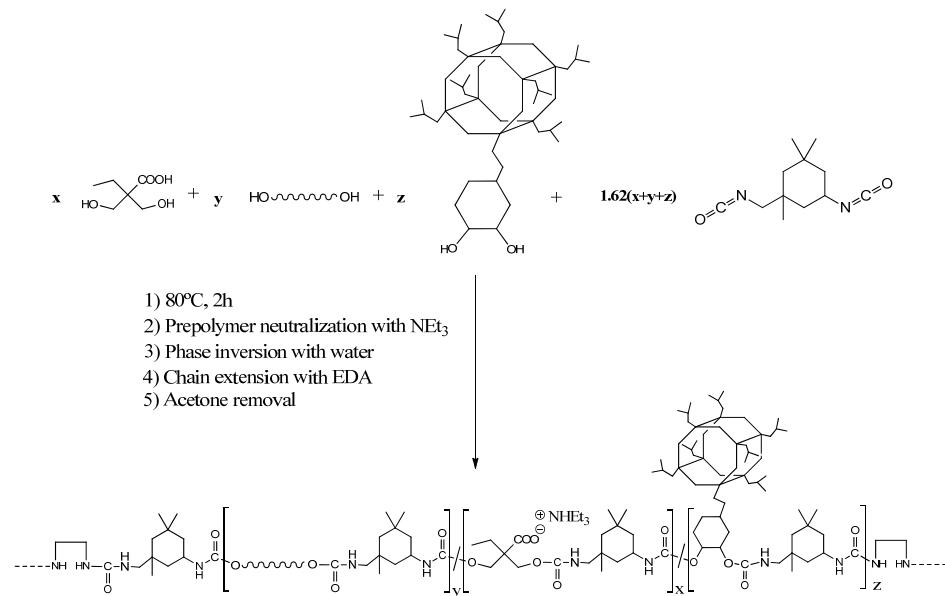
Figure 4. Synthesis scheme of the waterborne polyurethane-urea dispersions using POSS-OH as a co-polyol.
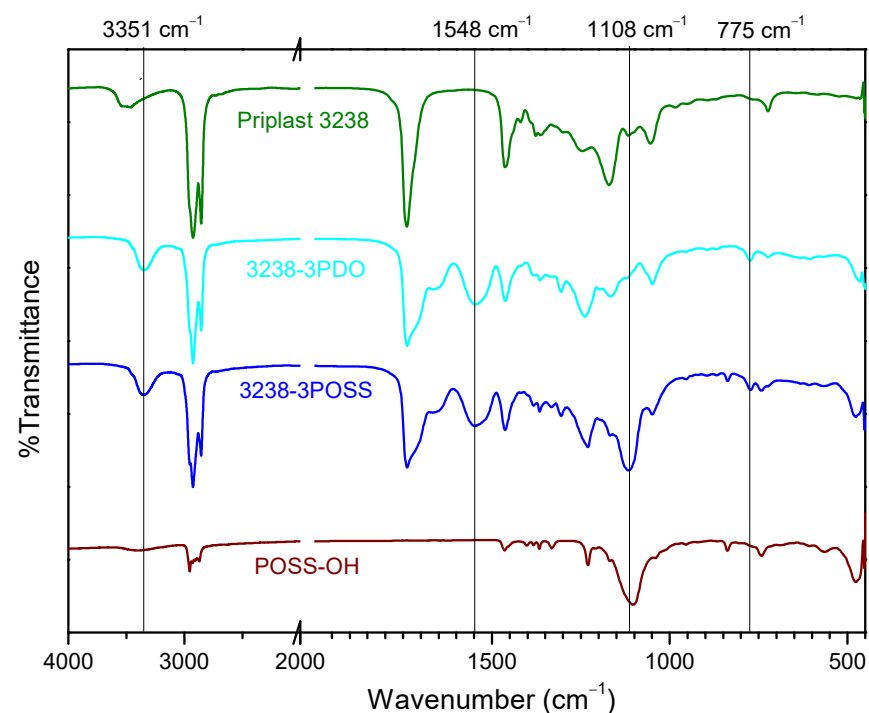
Figure 5. FTIR spectra of (from top to bottom): Priplast 3238, 3238-3PDO, 3238-3POSS, and pure POSS-OH.

All of the synthesized WPUD were dried on Teflon plates to obtain the corresponding films. All of the obtained films were transparent (except the ones containing POSS that were not completely clear) and homogenous and were used for NMR, mechanical, thermal, and swelling characterization. Figure 6 shows the appearance of the synthesized WPUD as well as the appearance of casted film from two of the polyurethane-urea dispersions (3238-7POSS and 3238-7PDO).

Figure 6. Appearance of the synthesized WPUD (**top**) and casted films (**bottom**) from two of the polyurethane-urea dispersions (3238-7POSS and 3238-7PDO).

^{1}H NMR spectra of all polymer films were recorded, thus confirming chemical structure. Figures 7 and 8 depict the ^{1}H NMR spectra of 3238-3PDO and starting Priplast 3238 polyol and 3238-3POSS and starting POSS-OH, respectively, with peak assignments.
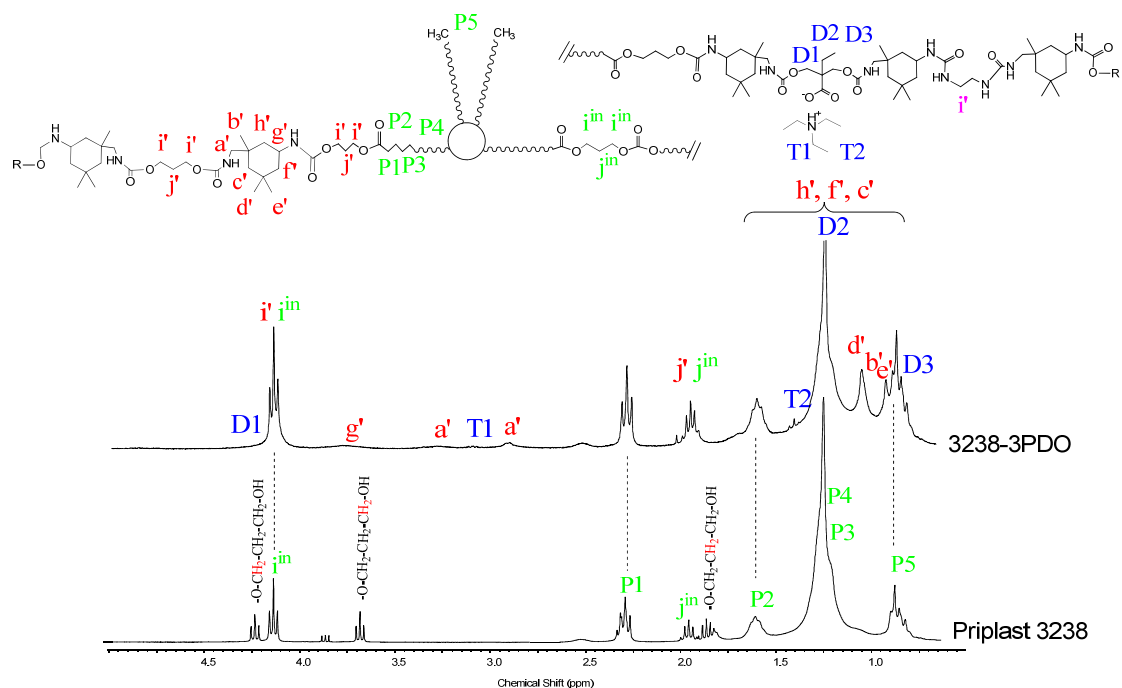
Figure 7. ^{1}H NMR of experiment 3238-3PDO and starting polyol Priplast 3238 with peak assignments.
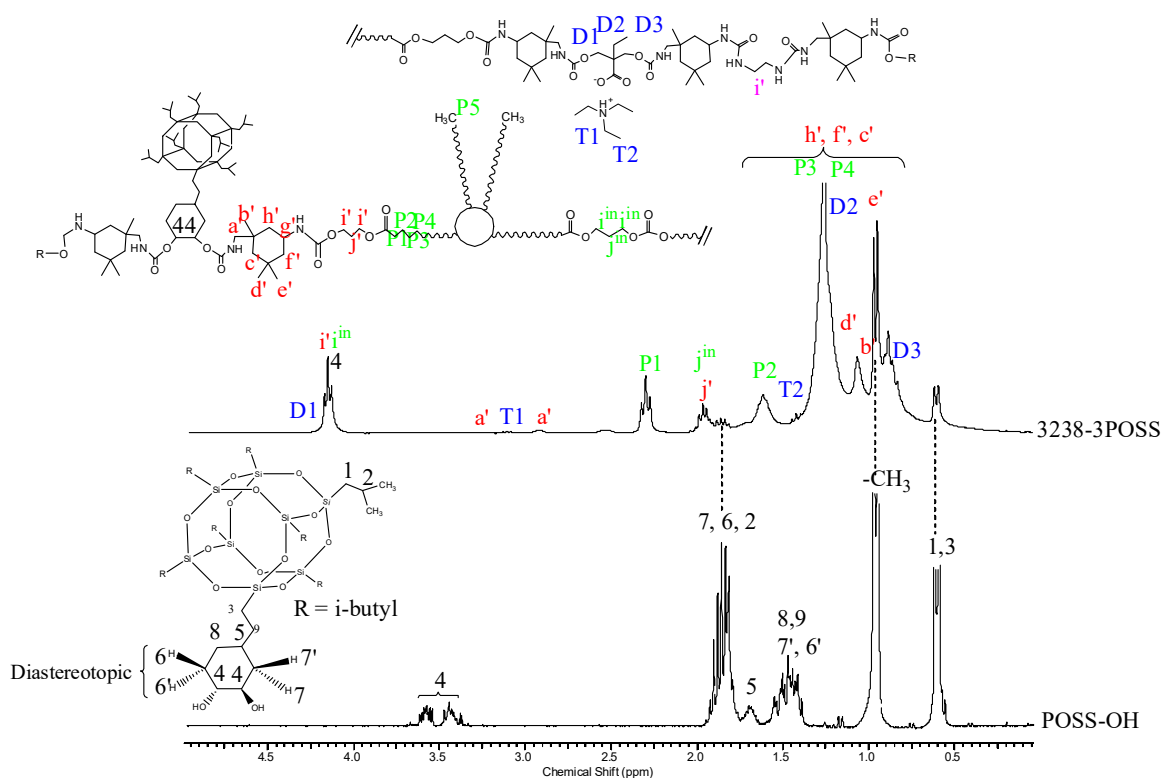
Figure 8. ^{1}H NMR of experiment 3238-3POSS and pure POSS-OH with peak assignments.

^{1}H NMR spectra provided structural information regarding Priplast 3238 polyol, pure POSS-OH, and WPUD films. The main peaks of Priplast 3238 were in good agreement with those reported by Bueno-Ferrer's work [12], showing a $CH_2C(O)O$ signal at 2.30 ppm and peaks from $CH_2OC(O)$ and CH_2 in the β position of the ester group at 4.15 and 1.61, respectively (Figure 7).

The CH_2 peaks from the methylene in the α, β, and γ position with respect to free hydroxyl groups ($COO-C_\gamma H_2-C_\beta H_2-C_\alpha H_2-OH$) appeared at 3.69, 1.96, and 4.23 ppm, respectively. In the WPUD, the full conversion of hydroxyl groups to form polyurethane segments was confirmed by downfield shifting of the α and β peaks in the polymer spectra (Figure 7).

Commercially available IPDI consists of an isomer mixture of approximately 75:25 in favor of the cis-isomer, leading to different reaction mixtures [13] and resulting in complex ^{1}H-NMR spectra. For a better interpretation of the ^{1}H-NMR spectra of the synthesized polyurethane-ureas, they were compared with the ones of model compounds reported in our previous work [14] (IPDI:DMBA, IPDI:PDO, IPDI:EDA, IPDI:EtOH) that were obtained by reacting IPDI with the corresponding building blocks in a molar ratio of 2:1. This made it possible to more precisely assign some of the main signals of the polyurethane-ureas under study.

Urethane moieties gave the following weak signals:

- IPDI CH_2 in α-position to -NHC(O) group (a'), 3.24 ppm and 2.88 ppm corresponding to the trans-isomer (25% abundance) and cis-isomer (75% abundance), respectively.
- IPDI CH in α-position to -NHC(O) group (g'), 3.73 ppm.

The incorporation of internal emulsifier (DMBA) into the polymer backbone could be assessed by the following signals: DMBA CH_2 in α-position to OC(O) group (D1), 4.26 ppm; DMBA methylene group (D2) attached to methyl, 1.31 ppm; DMBA methyl group (D3), 0.86 ppm.

Triethylammonium salt could be assessed by the peaks at 3.02 (T1) and 1.37 (T2) ppm that correspond to CH_2 and CH_3, respectively, of the ethyl group.

Figure 8 depicts the ^{1}H NMR spectra of sample 3238-3POSS and pure POSS-OH with peak assignments. Hydrogens 6, 6′ and 7, 7′ from the cyclohexyl ring were diastereotopic and therefore appeared at different chemical shifts. In pure POSS-OH, the signals from the methine hydrogens directly bonded to the hydroxyl groups appeared in the form of complex multiplets at 3.58 and 3.44 ppm. In all the WPUD containing POSS-OH as a building block, the full conversion of hydroxyl groups from POSS-OH to form polyurethane segments was confirmed by downfield shifting of the -CH-O- signals from the cyclohexyl ring in the polymer spectra (Figure 8).

The thermal properties of the developed WPUD were analyzed by DSC and TGA. The non-isothermal DSC thermograms for all of the WPUD films as well as Priplast 3238 were registered. DSC curves of the synthesized WPUD performed at a heating rate of 10 °C min^{-1} are shown in Figure 9 and thermal transition temperatures for all of the WPUD are summarized in Table 4.
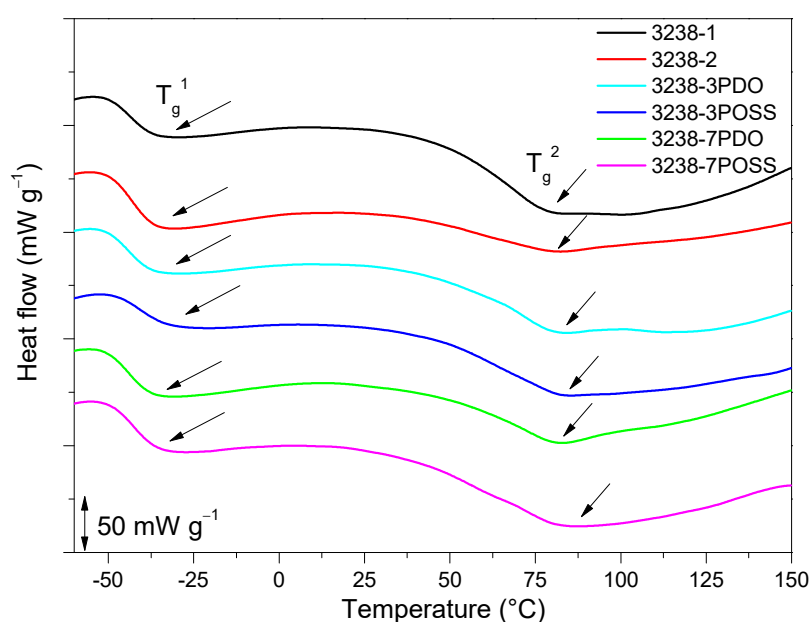
Figure 9. DSC thermogram of all of the synthesized WPUD. Glass-transition temperatures were calculated as the inflection point of the heating step scan DSC.

Table 4. Thermal properties of WPUD films evaluated by DSC, TGA, and DMTA.

Reference	DSC [a]				TGA [b]			
	T_g^1 (°C)	T_g^2 (°C)	T_m (°C)	ΔH_m (J/g)	$T_{10\%}$ (°C)	T_{dS1} (°C)	T_{dS2} (°C)	T_{dS3} (°C)
3238-1	−43	70	153	4.4	284	242	309	416
3238-2	−43	88	148	1.0	308	247	307	418
3238-3POSS	−40	77	149	3.1	306	255	333	423
3238-3PDO	−44	73	170	3.9	298	252	328	432
3238-7POSS	−43	74	144	2.3	308	263	332	430
3238-7PDO	−44	90	155	2.5	298	243	307	416
Priplast 3238	−59	-	-	-	403	-	-	414

[a] T_g, T_m, and ΔH_m values determined by DSC. [b] TGA characterization of the WPUD films under N$_2$ atmosphere: $T_{10\%}$ is the temperature at which a 10 wt.% loss was observed in the TGA traces recorded at 10 °C min^{-1}; T_{dS1}, T_{dS2}, and T_{dS3} are the temperatures of maximum degradation rate for first, second. and third degradation stages, respectively.

Two T_g values were detected for all of the synthesized WPUD, T_g^1 and T_g^2, which corresponded to soft segment and hard segment phases, respectively. The T_g^1 of the soft segment phase was close to the value observed for Priplast 3238 polyester polyol. This is an indication that there was a phase segregation between hard polyurethane-urea

segments and polyester soft segments. All of the WPUD showed T_g2 values between 70 and 90 °C, corresponding to the softening of hard segments. Melting temperatures and small enthalpies associated with the melting of crystallized hard segments were also detected in the range of 144–170 °C and data collected from these thermograms are shown in Table 4.

The thermal stability of the synthesized WPUD films was studied via TGA under N_2 and air atmospheres and the curves of experiments 3238-3POSS and 3238-3PDO are shown in Figure 10. The degradation temperatures under the N_2 atmosphere corresponding to a weight loss of 10% and the temperatures of the maximum degradation rate for each degradation stage are collected in Table 4 for all of the WPUD. All of the (co)polymers had sufficient thermal stability to withstand, without degradation, the temperature conditions that are required during coating procedures.
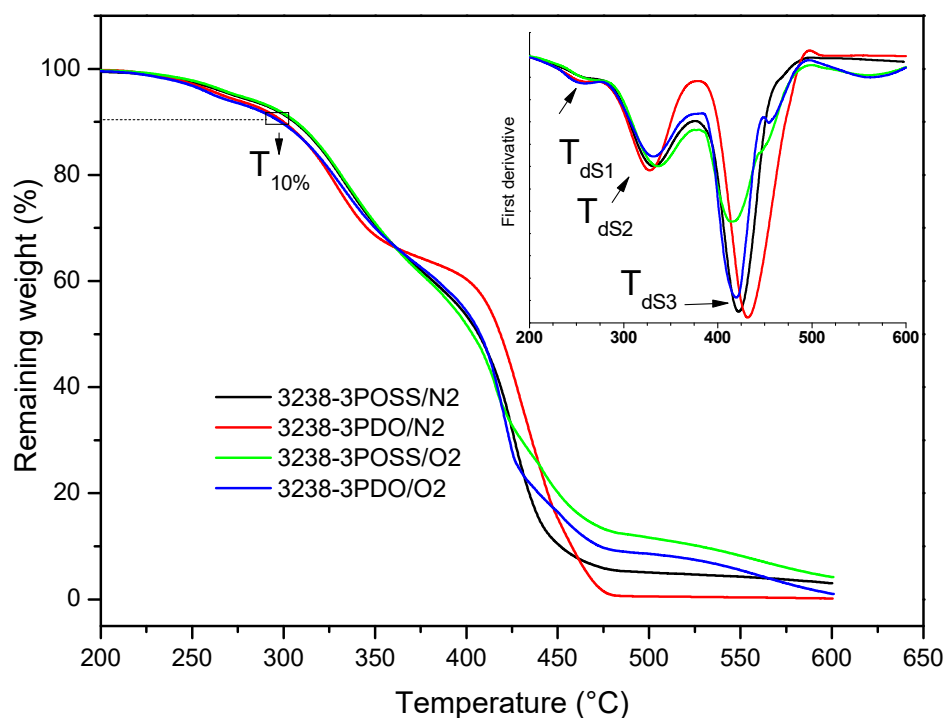
Figure 10. TGA thermograms of experiments 3238-3POSS and 3238-3PDO under a nitrogen atmosphere (/N2) and under an air atmosphere (/O2). DTGA curves are shown in inset graph.

As can be observed in Figure 10 and Table 4, under N_2 conditions thermal degradation occurred in three stages, with similar temperatures of maximum degradation rate for all the synthesized WPUD. The first step occurred in the temperature range of 242–263 °C and could be attributed to the volatilization of triethylamine, which was in the form of carboxylate salt. Stage 2 took place in the temperature range of 307–332 °C and corresponded to the degradation of urethane and urea bonds [8,14]. Finally, Stage 3, between 416 and 432 °C, was related to the degradation of segments of Priplast 3238 polyol as far as the TGA curve of this pure polyol showed a single degradation step under an N_2 atmosphere at a maximum degradation rate of 414 °C. Thermal degradation profiles under N_2 and air atmospheres were quite similar except for the fact that a fourth degradation step around 550 °C could be detected under oxidative conditions due to the complete decomposition to CO_2. It is also worth noting that polymers containing POSS-OH in their structure left a residual weight that corresponded with silicon dioxide (Figure 10).

Stress–strain tensile experiments were carried out to evaluate the mechanical properties of the synthesized WPUD films. Figures 11 and 12 display the stress–strain curves from the experimental designs that included POSS-OH and PDO in the tertiary mixture, respectively, and Table 5 displays the main mechanical properties of films.
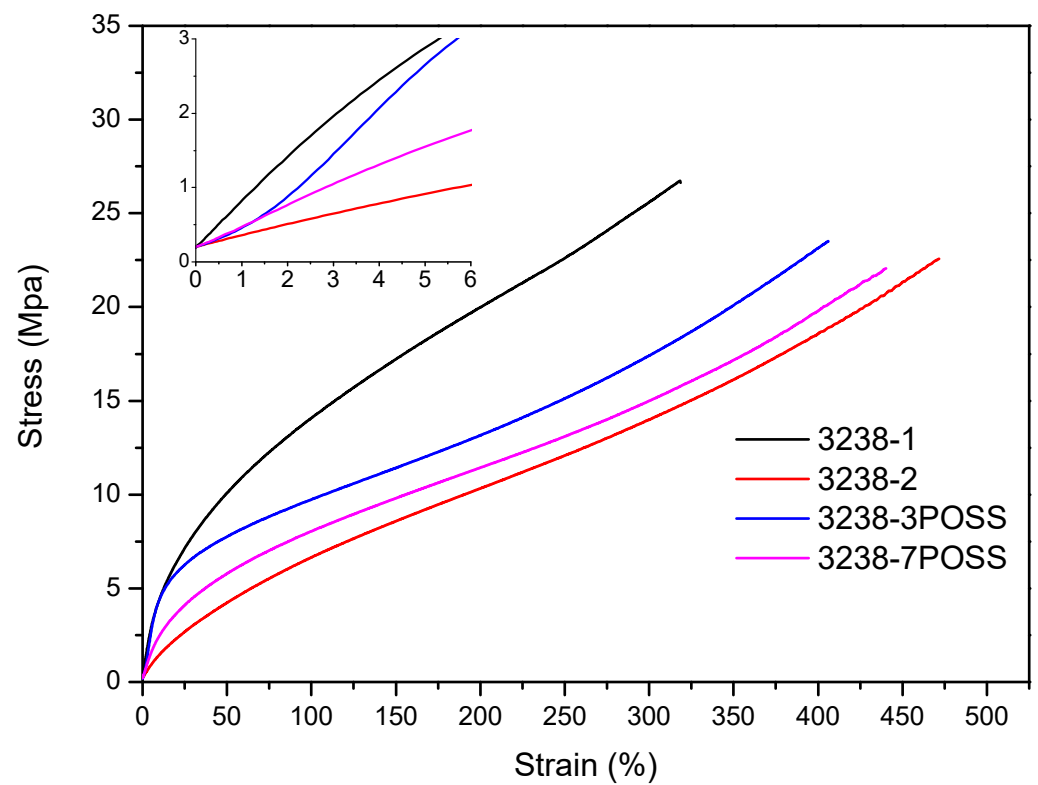
Figure 11. Stress–strain curves of WPUD films from experimental design that included POSS-OH in the ternary mixture.
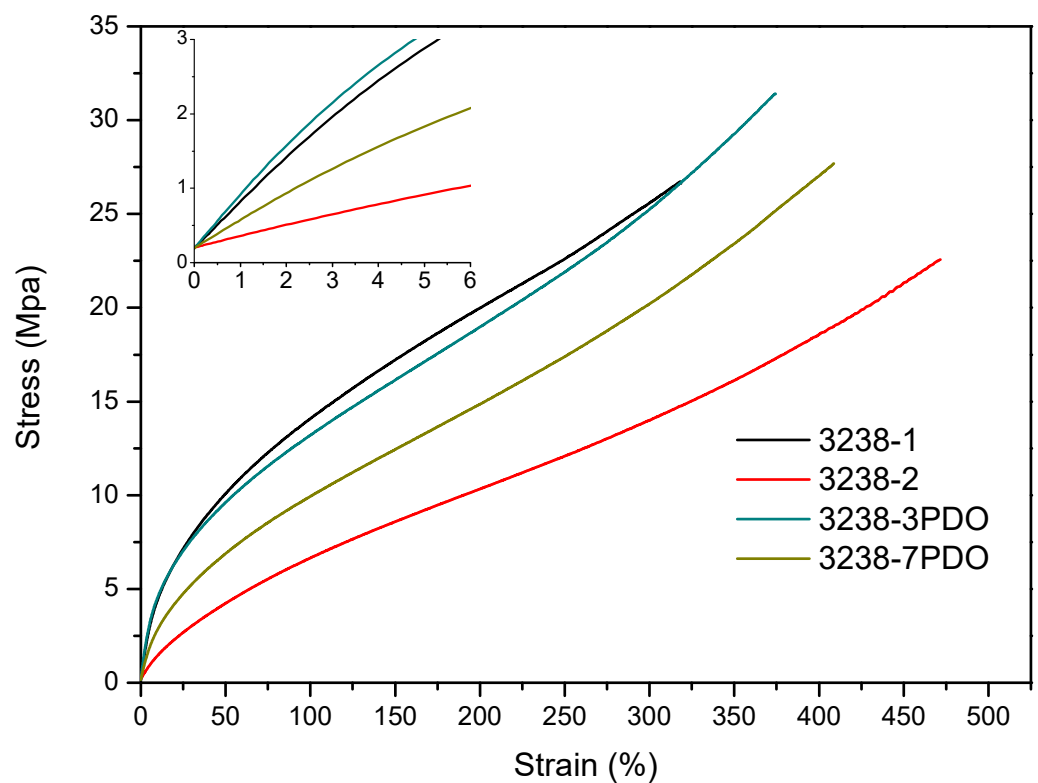
Figure 12. Stress–strain curves of WPUD films from experimental design that included PDO in the ternary mixture.

Table 5. Mechanical characterization of WPUD films.

Reference	E [a] (Mpa)	$\sigma_{100\%}$ [a] (Mpa)	σ_b [a] (Mpa)	ε_b [a] (%)
3238-1	59.0 ± 1.4	14.1 ± 0.2	27.5 ± 1.2	335.0 ± 13.0
3238-2	14.8 ± 0.3	6.6 ± 0.1	23.6 ± 1.8	490.0 ± 22.7
3238-3POSS	39.7 ± 4.9	9.6 ± 0.2	22.7 ± 1.1	391.8 ± 9.6
3238-3PDO	64.2 ± 1.3	13.3 ± 0.3	29.4 ± 1.6	352.7 ± 23.6
3238-7POSS	29.1 ± 0.4	8.0 ± 0.1	22.1 ± 0.5	443.0 ± 9.5
3238-7PDO	35.2 ± 1.6	9.8 ± 0.4	27.9 ± 1.7	422.3 ± 14.5

[a] E: Young modulus, $\sigma_{100\%}$: stress at 100% strain, σ_b: stress at break, ε_b: strain at break.

The ratio of Priplast 3238, DMBA, and PDO or POSS-OH in the polyol ternary mixture determined the polyol composition in each synthesized polymer and, therefore, the hard segment content. There was a reasonably good match between the Young modulus and hard segment content. In general, higher hard segment content showed a higher Young modulus. However, experiment 3238-3PDO (38.8 wt.% HS) led to a slightly higher Young modulus than experiment 3238-1 (40.6 wt.% HS), which could be explained by the greater influence of PDO on the polymer rigidity caused by stronger hydrogen bonding interactions between urethane groups as compared to DMBA. Experiment 3238-3POSS (47.0 wt.% HS) led to a lower Young modulus than experiment 3238-1 (40.6 wt.% HS) due to the bulkiness of the heptaisobutyl POSS groups and the consequent reduction of hydrogen bonding interactions. The concordance between stress at 100% strain ($\sigma_{100\%}$) and hard segment content was even better, as can be seen in the surface plots in Figure 13. The strain at break was also very well correlated to the amount of Priplast 3238 (the polyol that provides flexibility); the higher the ratio of Priplast with respect to PDO or POSS-OH and DMBA, the higher the strain at break (see the contour plots in Figure 14).
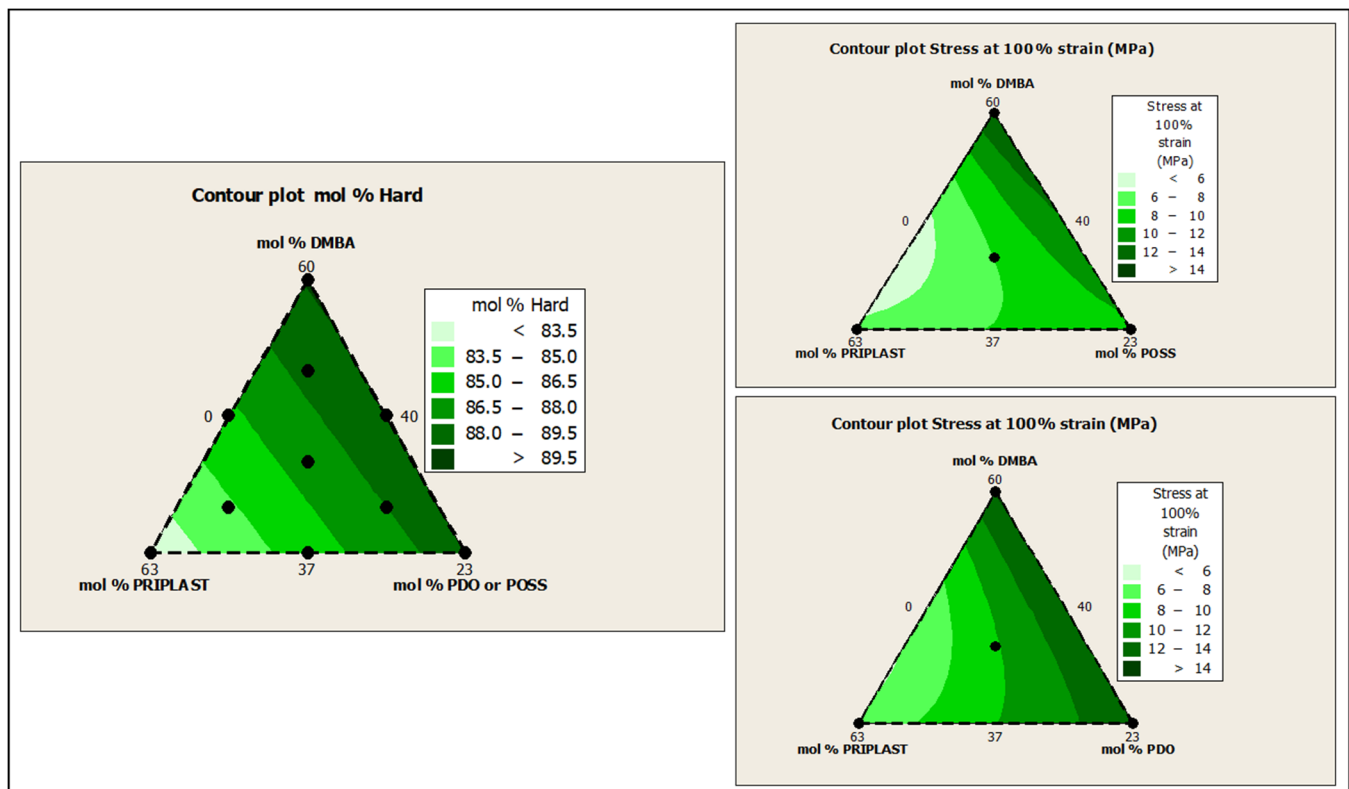
Figure 13. Contour plots obtained using the Minitab software from the ternary mixture experimental design. **Left**: contour plot of hard segment content in mol%. **Upper right**: contour plot of $\sigma_{100\%}$ (stress at 100% strain) for the ternary mixture design with POSS-OH. Bottom right: contour plot of $\sigma_{100\%}$ for the ternary mixture design with PDO.
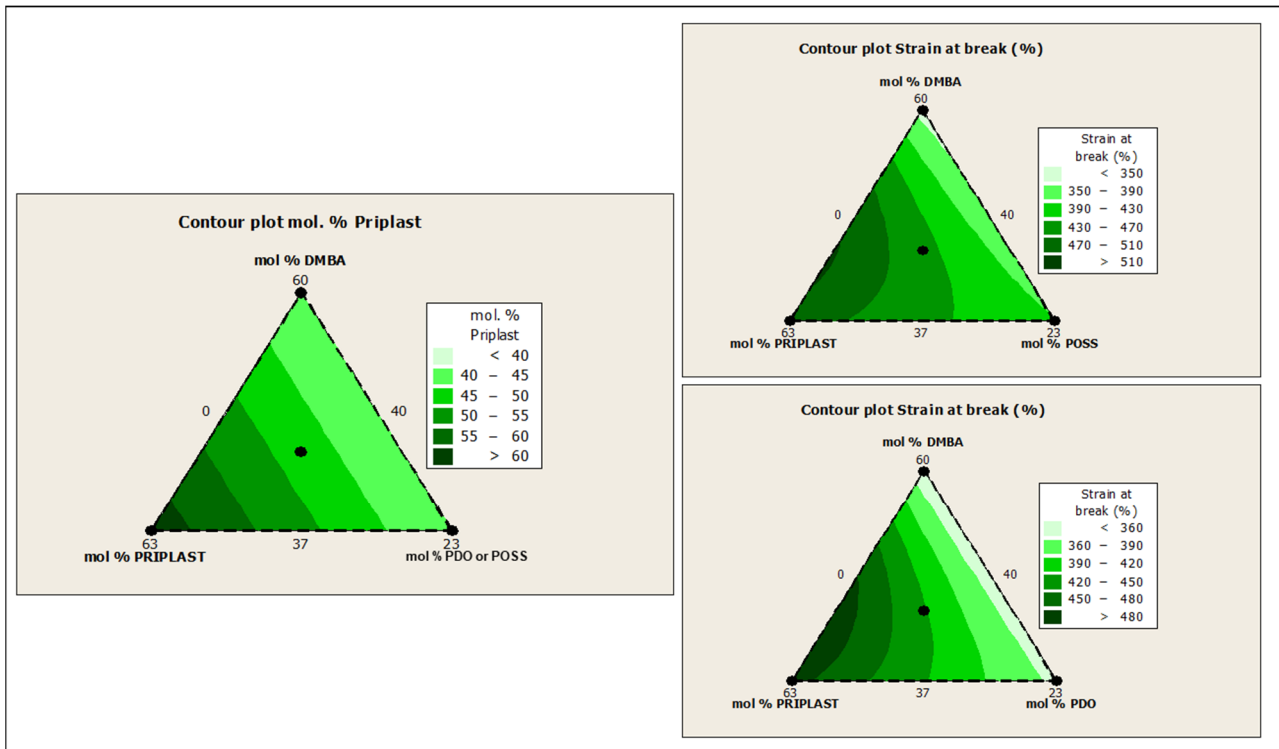
Figure 14. Contour plots obtained using the Minitab software from the ternary mixture experimental design. **Left**: contour plot of Priplast content (soft segment) in mol%. **Upper right**: contour plot of ε_b (strain at break) for the ternary mixture design with POSS-OH. Bottom right: contour plot of ε_b for the ternary mixture design with PDO.

Water swelling of the films after 48 h at 25 °C was assessed on all of the WPUD films. Figure 15 shows the water swelling values. The swelling values of the films after 48 h were consistent with the increased content of hydrophilic chain extender (DMBA), in agreement with the behavior that was reported by Xu et al. for waterborne polyurethane emulsions using dimethylol propionic acid (DMPA) as an internal emulsifier [15]. Contour plots from the ternary mixture experimental designs clearly confirm the relationship between DMBA content and water swelling in Figure 16.
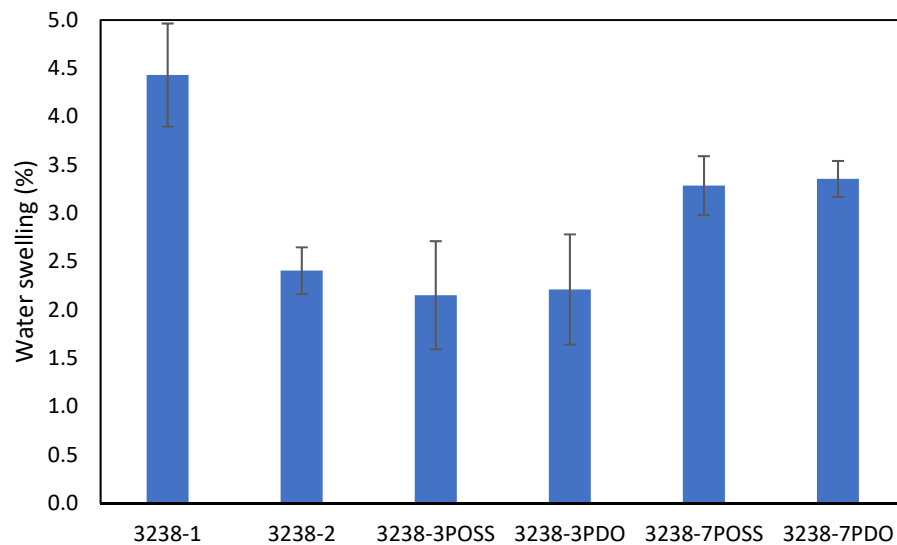
Figure 15. Swelling of WPUD films in water at 25 °C for 48 h.
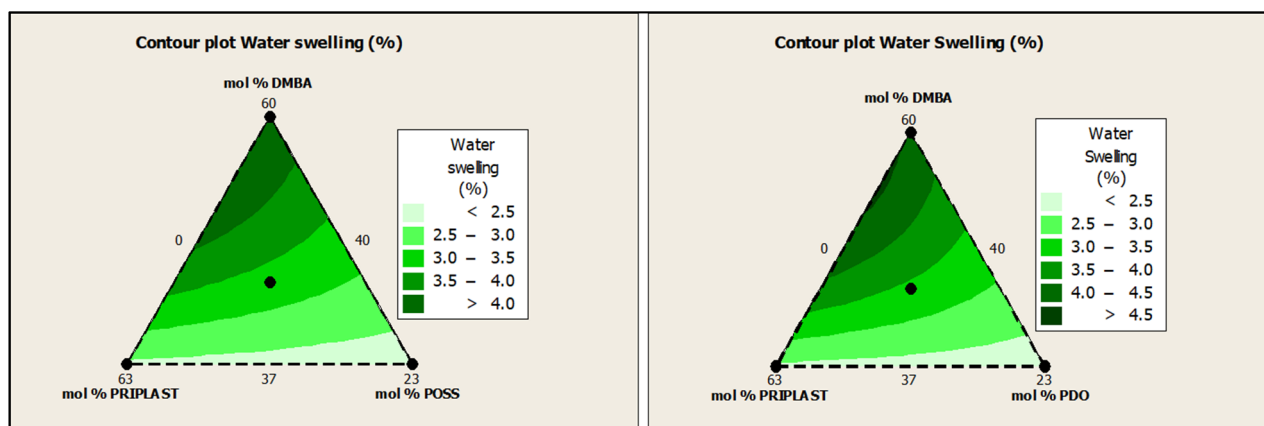
Figure 16. Contour plots of water swelling in wt.% of ternary mixture experimental design with POSS-OH (**left**) and PDO (**right**).

Dispersion stability, particle size, and particle size distribution of WPUD were also investigated. Figure S1 (Supplementary Material) shows the particle size distribution (PSD) curves of all developed aqueous polymeric dispersions analyzed by DLS. Particle size distribution curves are unimodal for all WPUD. Table 6 summarizes average particle size of all of the WPUD, PdI values, and Z-potential. Low particle size values ranging from 57 to 66 nm were observed for the dispersions with the lowest molar% of Priplast 3238, namely, 3238-1, 3238-3PDO, and 3238-3POSS. This is consistent with the fact that Priplast 3238 is a highly hydrophobic polyol of high Mw. Logically, the WPUD with the highest particle size was 3238-2 (203 nm) because it had the highest Priplast 3238 content. The dispersions with intermediate content in Priplast 3238 (3238-7PDO and 3238-7POSS) displayed intermediate particle size values. It is also worth mentioning that those WPUD with the same composition but having POSS-OH instead of PDO, for instance 3238-7POSS vs. 3238-7PDO, showed higher particle size, probably because POSS-OH provides more hydrophobicity than PDO and has a higher molecular weight. The polydispersity indexes (PdI) were below 0.2, which indicated that products had satisfactory stability and good dispersibility. The smaller the value of PdI, the better the homogeneity of the dispersion [16].

Table 6. Summary of the average particle size, PdI, and Z-potential values for synthesized WPUD dispersions.

Reference	Average Particle Size (nm)	PdI	Z Potential (mV)	Storage Stability [a]	
				4 °C	40 °C
3238-1	63 ± 21	0.15 ± 0.01	-23 ± 11	Good	Good
3238-2	203 ± 73	0.16 ± 0.01	-34 ± 7	Good	Good
3238-3POSS	66 ± 22	0.08 ± 0.01	-51 ± 19	Good	Good
3238-3PDO	57 ± 20	0.10 ± 0.01	-22 ± 10	Good	Good
3238-7POSS	158 ± 80	0.14 ± 0.01	-58 ± 12	Good	Good
3238-7PDO	99 ± 43	0.15 ± 0.01	-56 ± 16	Good	Good

[a] Good storage stability means that sealed glass vials stored at the indicated temperature for 6 months did not show sedimentation, creaming of visible alteration of the original dispersion appearance.

The stability of the dispersions was assessed by measuring the Z-potential of each WPUD. The Z-potential values are shown in Table 6. For all of the 3238 series, the Z-potential presented values ranging from -58 to -22 mV, indicating that the nanodroplets were negatively charged at the surface due to the presence of carboxylate groups. Most of the Z-potential absolute values were higher than 30 mV and were generally considered to represent stable emulsions [17,18]. However, 3238-1 and 3238-3PDO showed Z-potential absolute values below 30 mV. Despite this fact, the appearance of all of the WPUD emul-

sions stored at 4 °C and 40 °C for 6 months was good and there were no visual signs of instability such as phase separation, gelling, sedimentation, or creaming.

Finally, accelerated sedimentation tests of WPUD emulsions were also carried out. The analysis of the tested emulsions performed at 4 °C and 40 °C and relative centrifugal force of $2000 \times g$ is shown in Figures S2 and S3 (Supplementary Material). The first scanning profile obtained is indicated in red at the bottom, and the last in green at the top. Only a small clarification was observed at the meniscus area and small sedimentations were observed at the bottom with time, whereas the light transmission of the samples remained constant with time, indicating a good stability of the emulsions. The greater the change in light transmittance during the acceleration of the emulsion, the worse the stability [14].

3.2. Characterization of Textiles Coated with WPUD

In order to validate the applicability and properties of the polymeric dispersions, all of the synthesized WPUD were formulated in the form of printing pastes and subsequently face-coated on 100% polyester fabrics referenced as UPRON. Knife coating was the method chosen to carry out the coatings, as it is a widely employed method in the textile sector to produce accurate and reproducible coatings, being easily scalable to standard industrial textile machinery. In this way, this work has the purpose of performing the validation of the WPUD in application conditions that are very similar to those that are commonly used at an industrial level.

Smooth glass slides were also coated with all of the above-mentioned printing pastes, and WCA and OCA were measured to establish a comparison between the glass smooth coating substrate and the inherently rough textile substrate (UPRON).

Table 7 lists the values of WCA and OCA measured on glass slides and UPRON fabrics coated with WPUD printing pastes.

Table 7. WCA and OCA of glass and UPRON substrates coated with WPUD.

	Substrate			
Coating Reference	**Glass Slides**		**UPRON [a]**	
	WCA (°)	**OCA (°)**	**WCA (°)**	**OCA (°)**
Uncoated	Spreads	Spreads	Wets	Wets
3238-1	85 ± 2	22 ± 2	117 ± 1	37 ± 1
3238-2	90 ± 1	25 ± 1	112 ± 1	37 ± 1
3238-3POSS	93 ± 1	32 ± 2	135 ± 1	33 ± 1
3238-3PDO	84 ± 1	30 ± 1	108 ± 1	35 ± 2
3238-7POSS	97 ± 1	29 ± 1	132 ± 1	33 ± 1
3238-7PDO	84 ± 1	26 ± 1	117 ± 1	32 ± 2

[a] The dry add-on of the coated UPRON fabrics was 26 ± 3 g m^{-2} for all the coated samples.

As could be observed, WCAs of coated UPRON fabrics were between 108 and 135° for the synthesized WPUD, which means low water wettability, but not superhydrophobicity (>150°). The incorporation of POSS-OH in the polymer increased significantly the WCA of the coated fabrics. It is important to point out that the WCAs of coated glass slides were much lower than the WCAs of WPUD coated fabrics. Thus, the inherent roughness of the textile substrate contributed to achieving high values of WCA [19]. The OCA values of the coated surfaces were low. However, it is worth noting that in the case of coated fabrics the oil droplets, while not maintaining their spherical shape, did not penetrate the coating either. This is an indication that the coatings exerted a remarkable barrier effect against olive oil.

The determination of resistance to water penetration measured by hydrostatic pressure tests (also known as water column), stiffness, air permeability, and water vapor resistance were performed on UPRON fabrics face-coated with the printing pastes (Table 8). Printing paste made from experiment 3238-2 showed the highest water column value of all the experiments, which is consistent with the mechanical properties of this sample, having

the highest ε_b of all the samples. It is also worth noting that incorporation of POSS-OH in the polymer structure did not significantly alter water column properties with respect to polyurethane-ureas obtained without using POSS-OH as a co-polyol. Water column values higher than 30 cm were achieved by all of the coated fabrics, thus being in the same range as fossil-based coatings reported in our previous work [14].

Table 8. Stiffness, water column, and air permeability of UPRON fabrics uncoated and coated by knife coating procedure.

Coating Reference	Dry Add-On (g/m²)	Stiffness [mN]		Water Column (cm)	Air Permeability (mm/s)	Water Vapor Resistance (R_{et} [m² Pa W⁻¹])	
		Warp	Weft			Face	Back
Uncoated	-	17.4	9.7	<15 soaked	85.3	3.6	3.6
3238-1	24.9	133.5	38.0	34.1	1.3	150.0	160.0
3238-2	28.9	122.0	36.3	36.2	0.8	841.0	760.0
3238-3POSS	24.0	110.0	37.5	31.0	1.3	184.0	190.0
3238-3PDO	25.5	132.5	44.0	31.3	1.2	292.0	274.0
3238-7POSS	27.1	110.0	44.1	31.7	0.5	469.0	448.0
3238-7PDO	24.0	124.7	41.4	35.3	0.7	631.0	667.0

Air permeability dramatically decreased and stiffness increased in all of the coated fabrics compared to untreated fabrics. This is logical when considering that we applied a polymer layer to one of the faces of the fabric. Reduced air permeability can be a positive feature when it comes to outdoor sportwear with wind-stopper functionality.

The standard ISO 11092 uses the sweating guarded hotplate method (skin model method), to simulate the heat and moisture transfer process close to the human skin and to test the thermal resistance and water vapor resistance of textiles under steady-state conditions to evaluate the comfort of textiles. The lower the water vapor resistance (R_{et}), the higher the breathability. In this work, R_{et} was assessed for all of the coated fabrics on the coated face ("face") and on the uncoated face ("back") with no significant differences between "face" and "back". However, it should be noted that the greater the soft segment content, the greater the water vapor resistance, as can be clearly seen in contour plots from Figure 17. Although the R_{et} values obtained for all of the coatings were quite high (>150 m² Pa W⁻¹) and denoted low perspiration breathability and therefore low comfort, we can conclude that coating breathability decreased for those polymers with higher amounts of Priplast 3238. On the other hand, for a given mol.% of Priplast 3238 and DMBA, R_{et} decreased when we replaced PDO for POSS-OH (Ret 3238-3PDO > Ret 3238-3POSS, Ret 3238-7PDO > Ret 3238-7POSS). This observation made us think that the incorporation of bulky heptaisobutyl POSS as a pendant side group in the polymer chain prevented close packing of adjacent chains, thus favoring water molecule diffusion.
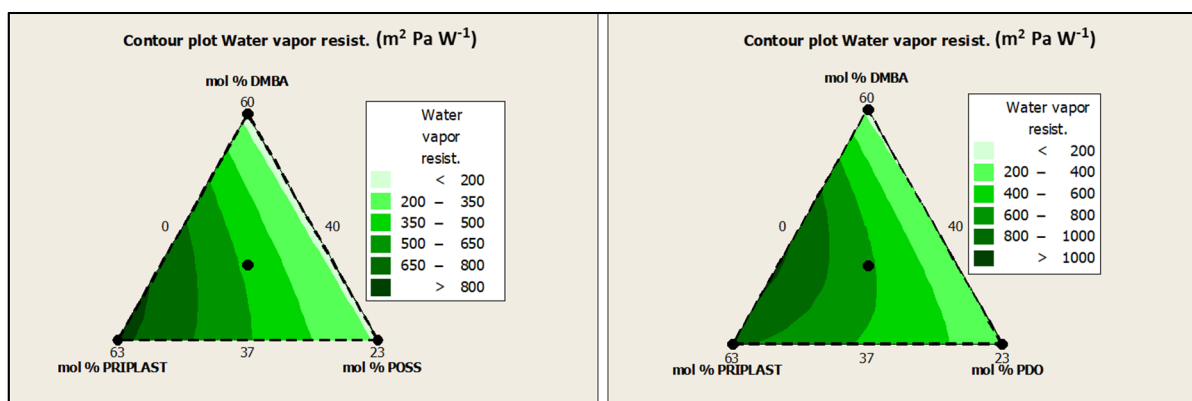
Figure 17. Contour plots of R_{et} for experimental design with POSS-OH (**left**) and experimental design with PDO (**right**).

Figure 18 shows the SEM micrographs of uncoated and coated UPRON fabrics with the printing pastes made from experiments 3238-3PDO and 3238-3POSS. The presence of the coating in the fiber's surface could be seen for coated samples. The coatings were not distributed in a completely homogeneous way. The roughness of the surfaces seemed to increase with the presence of the POSS-OH.
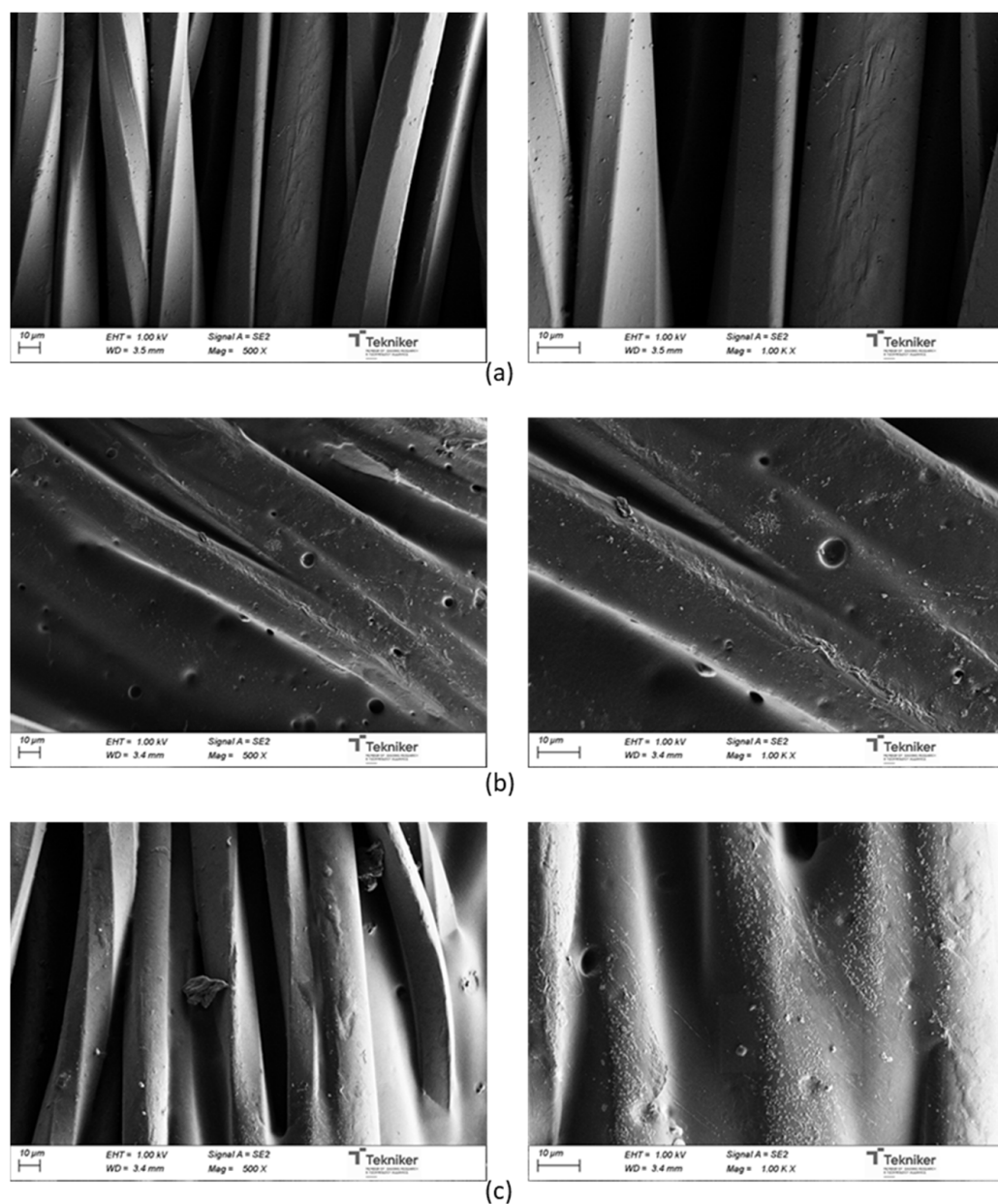
Figure 18. SEM micrographs for: (**a**) untreated UPRON and fabrics coated with (**b**) 3238-3PDO and (**c**) 3238-3POSS.

The presence of the element Si in the surface could be clearly observed in the fabrics coated with WPUD containing heptaisobutyl POSS functional groups, as can be observed in the EDS spectra (Figure 19).
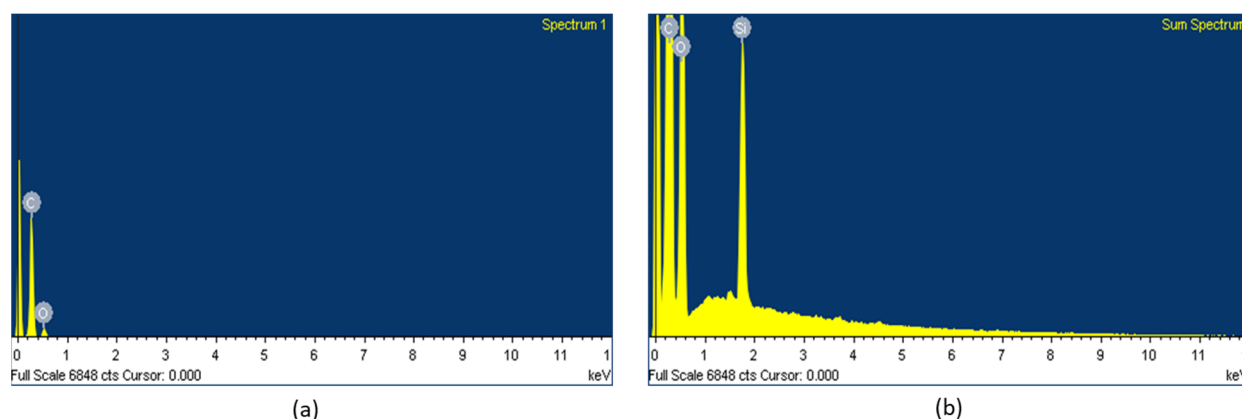
Figure 19. EDS spectra of fabrics coated with (**a**) 3238-3PDO and (**b**) 3238-3POSS.

Finally, it is important to underline that all WPUD led to stable coating pastes with good runnability properties with the Werner Mathis coating machine. Therefore, it is to be expected that the WPUD would lead to good results in later stages of industrial scaling.

4. Conclusions

In this work, waterborne partially biobased polyurethane-urea dispersions have been developed, with a biobased content ranging from 53 to 72 wt.%. All the obtained WPUD were fluorine-free, low VOC, and showed proper mechanical and thermal properties that make them perfectly viable to be used as a coating for textile industry, providing coated fabrics with hydrophobic properties and a water column. Water contact angles close to 140° have been achieved by incorporating trans-cyclohexanediol isobutyl POSS into the polymer chain, a hybrid nanomaterial that has provided an important improvement in the hydrophobicity of the coatings without altering the mechanical, thermal or applicative properties of polyurethane-ureas. The characterization by FTIR and NMR showed that trans-cyclohexanediol isobutyl POSS has been covalently fixed in the polymer chain and therefore none of the known drawbacks are expected when working with discrete nanomaterials (bioavailability, toxicity, leachate, and liberation in the environment). Water column values higher than 30 cm have been achieved by all of the coated fabrics, thus being in the same range as fossil-based coatings reported in our previous work.

References

1. Luz, A.L.; Anderson, J.K.; Goodrum, P.; Durda, J. Perfluorohexanoic acid toxicity, part I: Development of a chronic human health toxicity value for use in risk assessment. *Regul. Toxicol. Pharmacol.* **2019**, *103*, 41–55. [CrossRef] [PubMed]
2. Knight, E.R.; Bräunig, J.; Janik, L.J.; Navarro, D.A.; Kookana, R.S.; Mueller, J.F.; McLaughlin, M.J. An investigation into the long term binding and uptake of PFOS, PFOA and PFHxS in soil–plant systems. *J. Hazard. Mater.* **2021**, *404*, 124065. [CrossRef] [PubMed]
3. Schellenberger, S.; Hill, P.J.; Levenstam, O.; Gillgard, P.; Cousins, I.T.; Taylor, M.; Blackburn, R.S. Highly fluorinated chemicals in functional textiles can be replaced by re-evaluating liquid repellency and end-user requirements. *J. Clean. Prod.* **2019**, *217*, 134–143. [CrossRef]
4. Chinthapalli, R.; Skoczinski, P.; Carus, M.; Baltus, W.; De Guzman, D.; Käb, H.; Raschka, A.; Ravenstijn, J. Biobased Building Blocks and Polymers-Global Capacities, Production and Trends, 2018–2023. *Ind. Biotechnol.* **2019**, *15*, 237–241. [CrossRef]
5. Coates, G.W.; Hillmyer, M.A. A Virtual Issue of Macromolecules: "Polymers from Renewable Resources". *Macromolecules* **2009**, *42*, 7987–7989. [CrossRef]
6. Santamaria-Echart, A.; Fernandes, I.; Barreiro, F.; Corcuera, M.A.; Eceiza, A. Advances in Waterborne Polyurethane and Polyurethane-Urea Dispersions and Their Eco-friendly Derivatives: A Review. *Polymers* **2021**, *13*, 409. [CrossRef]
7. Cavallo, D.; Gardella, L.; Soda, O.; Sparnacci, K.; Monticelli, O. Fully bio-renewable multiblocks copolymers of poly(lactide) and commercial fatty acid-based polyesters polyols: Synthesis and characterization. *Eur. Polym. J.* **2016**, *81*, 247–256. [CrossRef]
8. Poussard, L.; Lazko, J.; Mariage, J.; Raquez, J.M.; Dubois, P. Biobased waterborne polyurethanes for coating applications: How fully biobased polyols may improve the coating properties. *Prog. Org. Coat.* **2016**, *97*, 175–183. [CrossRef]
9. Lai, Y.S.; Tsai, C.W.; Yang, H.W.; Wang, G.P.; Wu, K.H. Structural and electrochemical properties of polyurethanes/polyhedral oligomeric silsesquioxanes (PU/POSS) hybrid coatings on aluminum alloys. *Mater. Chem. Phys.* **2009**, *117*, 91–98. [CrossRef]
10. Madbouly, S.A.; Otaigbe, J.U.; Nanda, A.K.; Wicks, D.A. Rheological Behavior of POSS/Polyurethane-Urea Nanocomposite Films Prepared by Homogeneous Solution Polymerization in Aqueous Dispersions. *Macromolecules* **2007**, *40*, 4982–4991. [CrossRef]
11. Poussard, L.; Mecheri, A.; Mariage, J.; Barakat, I.; Bonnaud, L.; Raquez, J.M.; Dubois, P. Synthesis of oligo(butylene succinate)-based polyurethanes: Influence of the chemical structure on thermal and mechanical properties. *J. Renew. Mater.* **2014**, *2*, 13–22. [CrossRef]
12. Bueno-Ferrer, C.; Hablot, E.; Perrin-Sarazin, F.; Garrigós, M.C.; Jiménez, A.; Averous, L. Structure and Morphology of New Bio-Based Thermoplastic Polyurethanes Obtained From Dimeric Fatty Acids. *Macromol. Mater. Eng.* **2012**, *297*, 777–784. [CrossRef]
13. Lomölder, R.; Plogmann, F.; Speier, P. Selectivity of isophorone diisocyanate in the urethane reaction influence of temperature, catalysis, and reaction partners. *J. Coat. Technol.* **1997**, *69*, 51–57. [CrossRef]
14. Lacruz, A.; Salvador, M.; Blanco, M.; Vidal, K.; Goitandia, A.M.; Martinková, L.; Kyselka, M.; de Ilarduya, A.M. Biobased Waterborne Polyurethane-Urea/SWCNT Nanocomposites for Hydrophobic and Electrically Conductive Textile Coatings. *Polymers* **2021**, *13*, 1624. [CrossRef] [PubMed]
15. Xu, J.; Li, T.; Zhao, W.; Li, P.; Wu, Y. Synthesis and characterization of waterborne polyurethane emulsions based on poly(butylene itaconate) ester. *Des. Monomers Polym.* **2016**, *19*, 309–318. [CrossRef]
16. Sun, Y.; Zhao, X.; Liu, R.; Chen, G.; Zhou, X. Synthesis and characterization of fluorinated polyacrylate as water and oil repellent and soil release finishing agent for polyester fabric. *Prog. Org. Coat.* **2018**, *123*, 306–313. [CrossRef]
17. Li, D.; Müller, M.B.; Gilje, S.; Kaner, R.B.; Wallace, G.G. Processable aqueous dispersions of graphene nanosheets. *Nat. Nanotechnol.* **2008**, *3*, 101–105. [CrossRef] [PubMed]
18. Sheng, L.; Zhang, X.; Ge, Z.; Liang, Z.; Liu, X.; Chai, C.; Luo, Y. Preparation and properties of waterborne polyurethane modified by stearyl acrylate for water repellents. *J. Coat. Technol. Res.* **2018**, *15*, 1283–1292. [CrossRef]
19. Lacruz, A.; Salvador, M.; Blanco, M.; Vidal, K.; Martínez de Ilarduya, A. Development of fluorine-free waterborne textile finishing agents for anti-stain and solvent-water separation based on low surface energy (co)polymers. *Prog. Org. Coat.* **2021**, *150*. [CrossRef]

Poliuretano-ureas bio-basados en dispersión acuosa para el sector de recubrimientos textiles

Autores: Amado Lacruz Cruz[1,2,*], Mireia Salvador Ibáñez[1], Josep Aliaga Parera[1], Jan Camps Ubach[1], Antxon Martínez de Ilarduya[2].

[1] Color Center, S.A., Ptge. Marie Curie 3, 08223 Terrassa (España); msalvador@colorcenter.es (M.S.); tecnico@colorcenter.es (J.A.); regulatory@colorcenter.es (J.C.)

[2] Departament d'Enginyeria Química. Universitat Politècnica de Catalunya, ETSEIB, Diagonal 647, 08028 Barcelona, España; antxon.martinez.de.ilarduia@upc.edu (A.M.d.I.)

[*] alacruz@colorcenter.es (A.L.)

Resumen

El presente trabajo es un resumen de las líneas de investigación llevadas a cabo en la empresa Color Center, S.A. para el desarrollo de poliuretano-ureas sostenibles en dispersión acuosa y su aplicación en el sector de los recubrimientos textiles. Tras seleccionar diversos precursores biobasados se procedió a la síntesis de los polímeros y su posterior dispersión en agua. Las dispersiones poliméricas obtenidas se utilizaron para recubrir distintos substratos textiles con el objetivo de conferirles propiedades de alto valor añadido como hidrofobia, columna de agua y conductividad eléctrica. Dichas líneas de investigación siguieron estrictos criterios de sostenibilidad y eco-diseño, evitando la utilización de substancias per- y polifluoradas (PFASs), catalizadores basados en metales pesados y minimizando la presencia de compuestos orgánicos volátiles (VOCs). De esta forma se pone de manifiesto la viabilidad y el enorme potencial de los polímeros biobasados en el campo de los recubrimientos para textiles técnicos.

Palabras clave: poliuretanos, recubrimientos textiles, bio-basado, tejidos multifuncionales, hidrofobia, columna de agua, presión hidrostática.

.

Supporting Information

Development of fluorine-free waterborne textile finishing agents for anti-stain and solvent-water separation based on low surface energy (co)polymers.

Amado Lacruz[a,c]*, Mireia Salvador[a]

Miren Blanco[b], Karmele Vidal[b]

Antxon Martínez de Ilarduya[c]

[a] Color Center, S.A. Ptge. Marie Curie 3, Nau 6, 08223, Terrassa, Spain.

[b] Tekniker, Basque Research and Technology Alliance (BRTA), Surface Chemistry and Nanotechnology Unit, Iñaki Goenaga 5, 20600, Gipuzkoa, Spain.

[c] Departament d'Enginyeria Química, Universitat Politècnica de Catalunya, ETSEIB, Diagonal 647, 08028 Barcelona, Spain.

(Co)polymers of M3T and SMA have been synthesized by emulsion polymerization using water as a polymerization media. FTIR spectra of the monomers, emulsifier and catalyst employed in the synthesis are reported in Figure S1 and Figure S2, respectively.
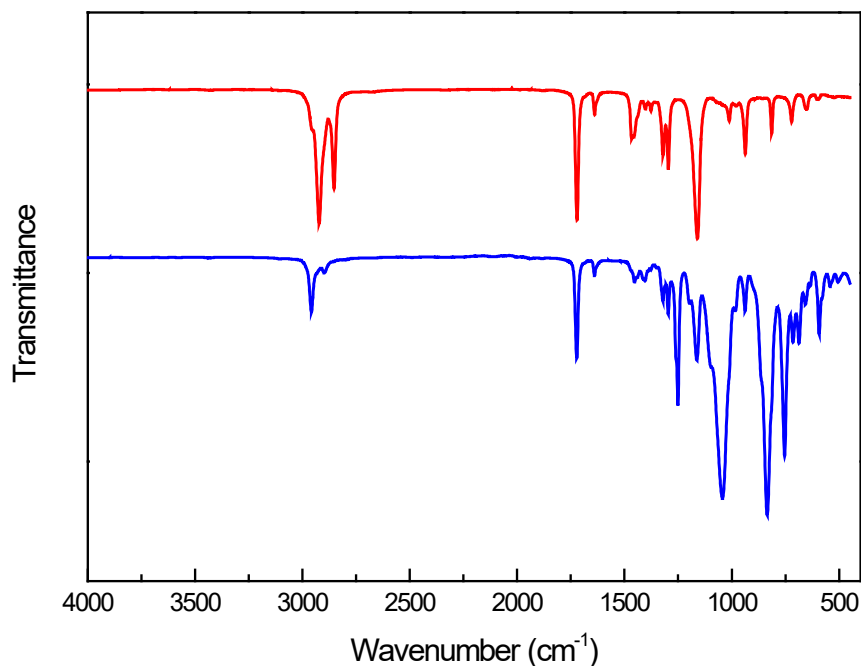
Figure S1. FTIR spectra in the MIR region for the monomers: Stearyl methacrylate (top, red) and M3T (bottom, blue)
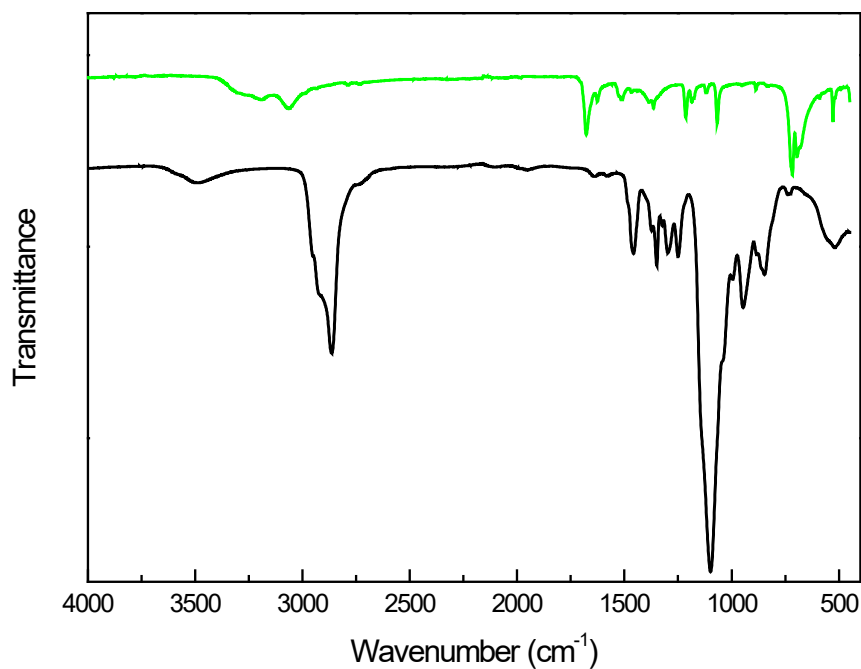
Figure S2. FTIR spectra in the MIR region for the catalyst (top, green) and IAEO (bottom, black)

Structural characterization of the developed $PM3T_xSMA_y$ (co)polymethacrylates was performed by nuclear magnetic resonance. Figure S3 shows 1H NMR spectrum of PM3T50SMA50 copolymer over 0-7 ppm range. No signals were detected in the 5.0-6.5 ppm region which allows to confirm the absence of any residual monomer in the copolymer obtained. Formulas used for the determination of copolymer composition are embedded in the same figure.
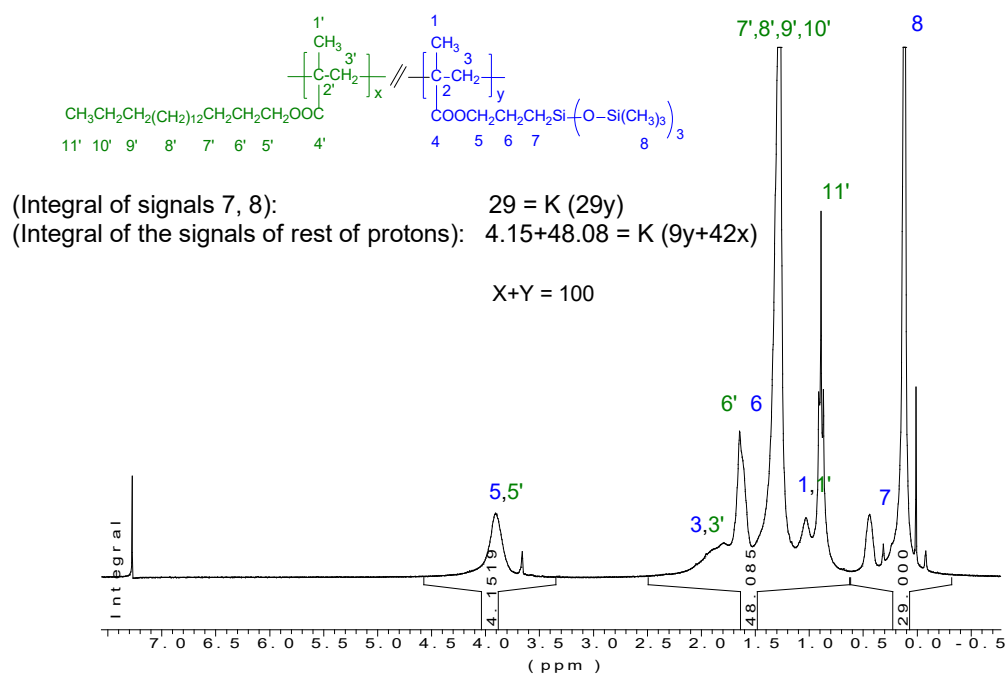
Figure S3. ^{1}H NMR spectrum of PM3T$_{50}$SMA$_{50}$ with peak assignments and formulas used for the determination of copolymer composition

^{1}H NMR (Figure S4) and ^{13}C NMR (Figure S5) spectra confirmed chemical structure, tacticity and final (co)polymer composition.
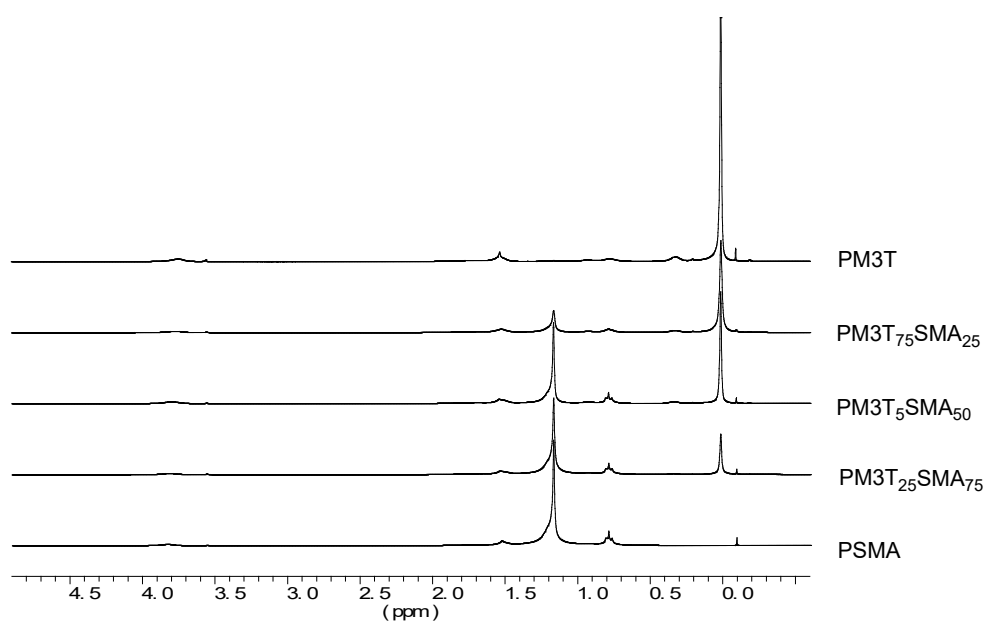
Figure S4. ^{1}H NMR spectra of PM3T, PSMA and M3T-containing copolymethacrylates recorded in CDCl$_3$
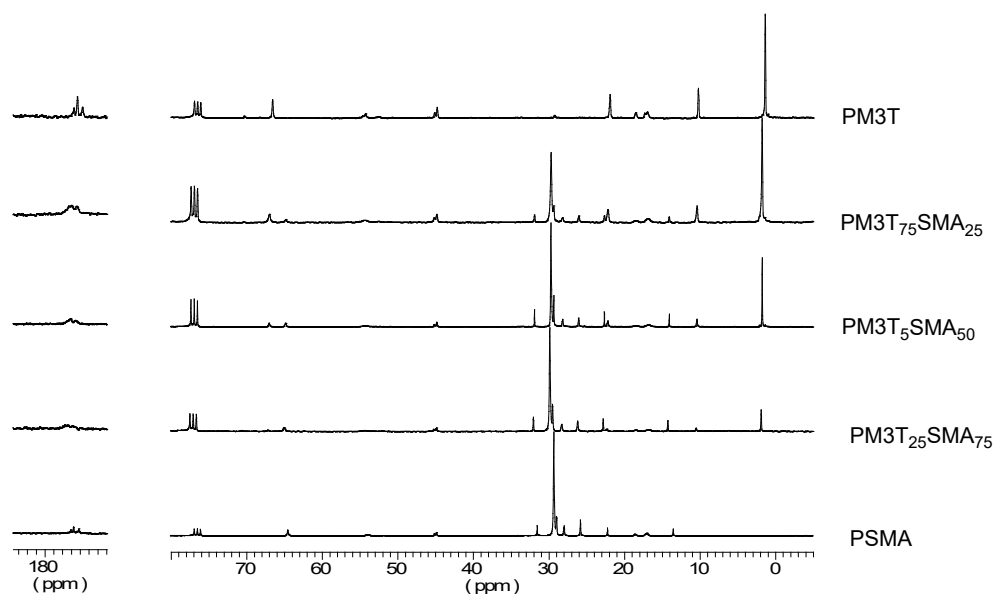
Figure S5. ^{13}C *NMR spectra of PM3T, PSMA and M3T-containing copolymethacrylates recorded in CDCl₃*

The thermal properties of the developed (co)polymers have been analysed by differential scanning calorimetry (DSC) and thermogravimetric analysis (TGA). The StepScan non-isothermal DSC thermograms for PM3T and PM3T₇₅SMA₂₅ are shown in Figure S6. PM3T showed a second order transition at 2.0 ºC, and PM3T₇₅SMA₂₅ at -31 ºC ascribed to T_g.
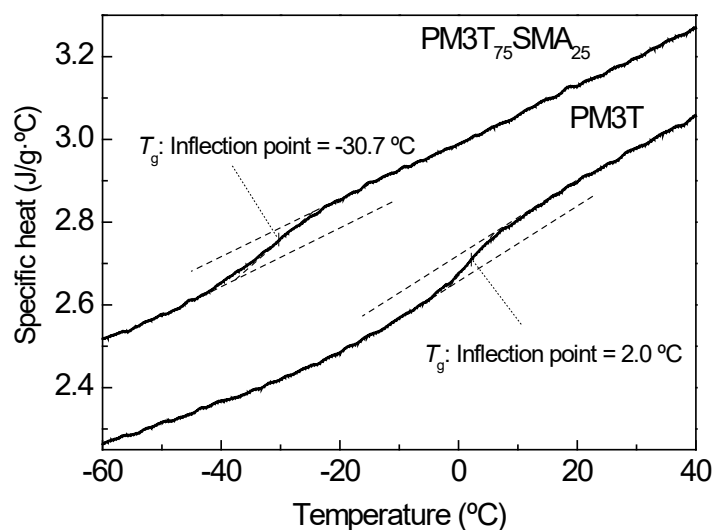
Figure S6. StepScan non-isothermal DSC thermograms for PM3T (bottom) and PM3T₇₅SMA₂₅ (top)

The thermal stability of the synthetized (co)polymers has been studied by TGA under nitrogen and air atmospheres (Figure S7). The thermograms exhibit only slight changes with copolymer composition, with maximum degradation rates observed at 324-343 ºC and 287-332 ºC for thermograms recorded under nitrogen and air circulation respectively. Among them, PM3T homopolymer and $PM3T_{25}SMA_{75}$ copolymer showed the best thermal stability under nitrogen circulation, while copolymer with the highest content of M3T ($PM3T_{75}SMA_{25}$) showed de lowest thermal stability. On the other hand, the temperature of the maximum degradation rate under air atmosphere was observed to increase with the content of SMA in the copolymer. Concluding, all the (co)polymers have sufficient thermal stability to withstand without degradation the temperature conditions that are required to be applied on the fabrics both under inert or air atmospheres (drying at 120ºC followed by curing at 160ºC for 1 minute).
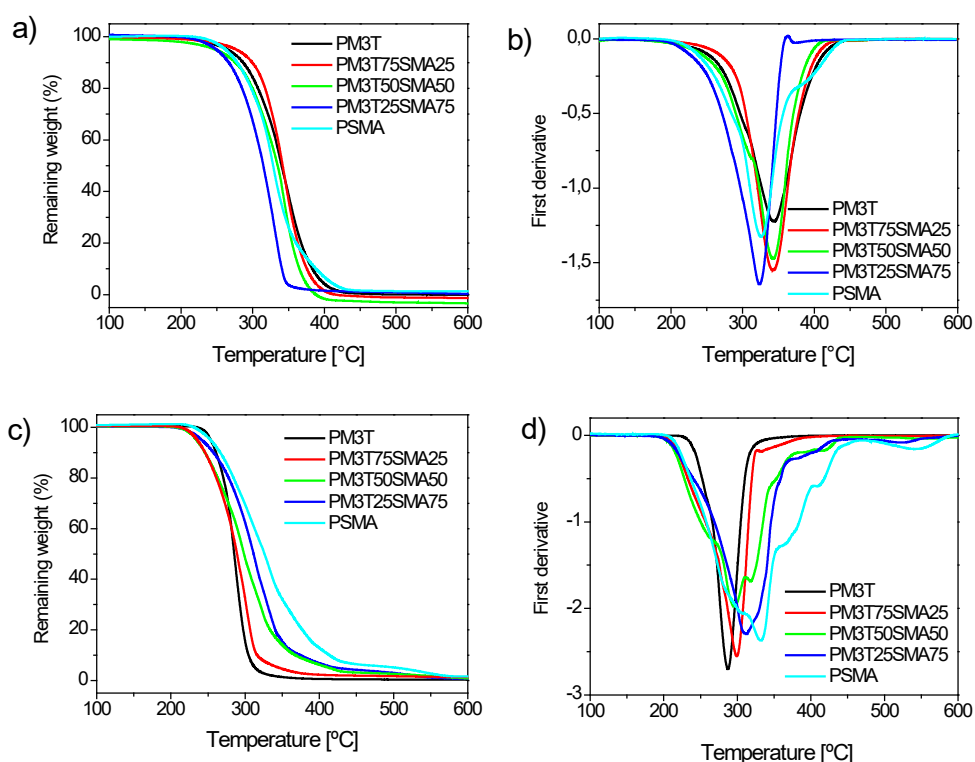
Figure S7. (a,c) TGA and (b,d) DTGA curves for PM3T, M3T-containing copolymethacrylates under nitrogen (a,b) and air (c,d) atmospheres

The emulsion stability, the particle size and particle size distribution of emulsions derived from M3T-containing copolymethacrylates have been investigated. Particle size distribution (PSD) curves of all developed aqueous polymeric emulsions analysed by LDS are shown in Figure S8.
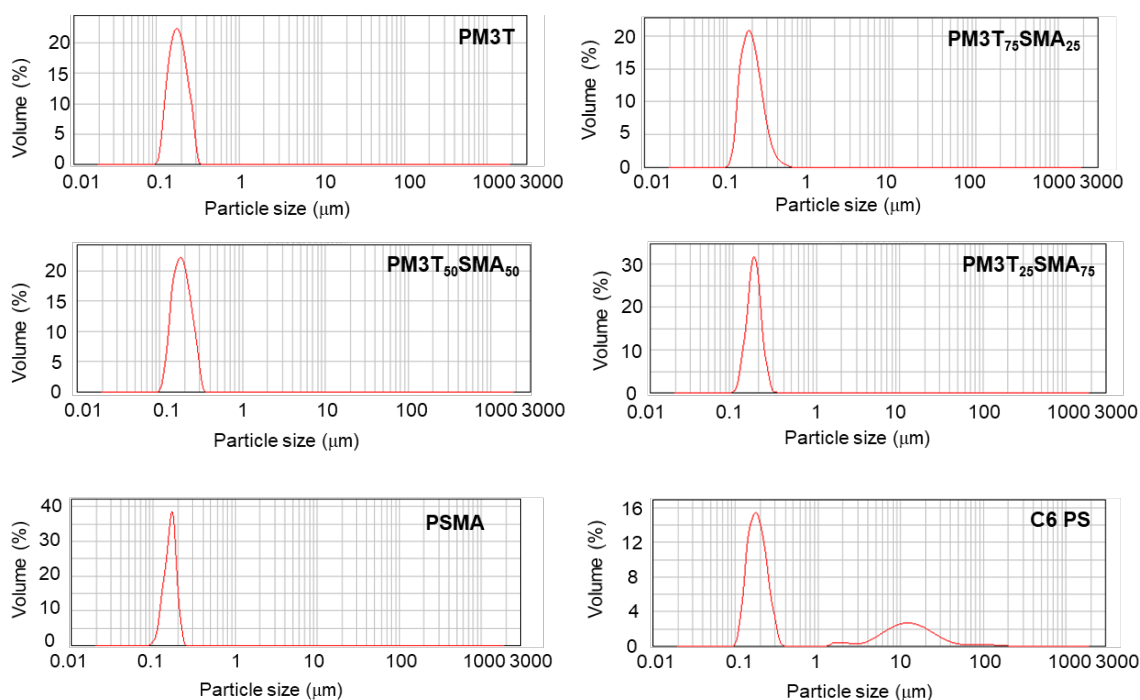
Figure S8. Particle size distribution obtained by LDS for PM3T, PSMA, M3T-containing copolymethacrylates and reference C6 fluorocarbon

Figure S9 shows the Z potential curves of the samples along with Z potential values. Measurements have been carried out using diluted samples (40 g/L).
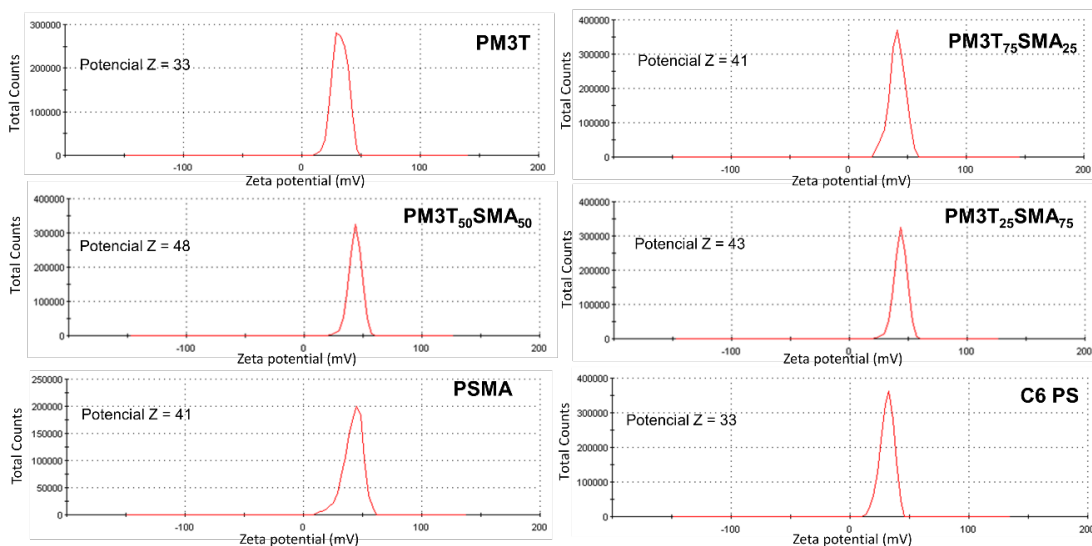
Figure S9. Zeta potential for PM3T, M3T-containing copolymethacrylates and reference C6 fluorocarbon

All the textiles showed good chloroform-water separation capacity. As example, a video has been recorded showing the performance of a cotton fabric coated with PM3T$_{75}$SMA$_{25}$ at 60 g/L.
(see Video: https://www.sciencedirect.com/science/article/pii/S0300944020311796).

Biobased Waterborne Polyurethane-Urea/SWCNT Nanocomposites for Hydrophobic and Electrically Conductive Textile Coatings

SUPPORTING INFORMATION

Amado Lacruz [1,2,*], Mireia Salvador [1], Miren Blanco [3], Karmele Vidal [3], Amaia M. Goitandia [3], Lenka Martinková [4], Martin Kyselka [4], and Antxon Martínez de Ilarduya [2]

[1] Color Center, S.A. Ptge. Marie Curie 3, Nau 6, 08223 Terrassa, Spain; alacruz@colorcenter.es (A.L.); msalvador@colorcenter.es (M.S.)

[2] Departament d'Enginyeria Química, Universitat Politècnica de Catalunya, ETSEIB, Diagonal 647, 08028 Barcelona, Spain; antxon.martinez.de.ilarduia@upc.edu (A.M.d.I.)

[3] Tekniker, Basque Research and Technology Alliance (BRTA), Surface Chemistry and Nanotechnology Unit, Iñaki Goenaga 5, 20600 Gipuzkoa, Spain; miren.blanco@tekniker.es (M.B.); karmele.vidal@tekniker.es (K.V.); amaia.martinez@tekniker.es (A.M.G.)

[4] Inotex spol. s r.o, Stefanikova 1208, 54401 Dvur Kralove n.L., Czech Republic; martinkova@inotex.cz (L.M.); kyselka@inotex.cz (M.K.)

* Correspondence: Amado Lacruz (amado.lacruz@upc.edu). Phone number: +34 937861113

Table of Contents

1 NMR
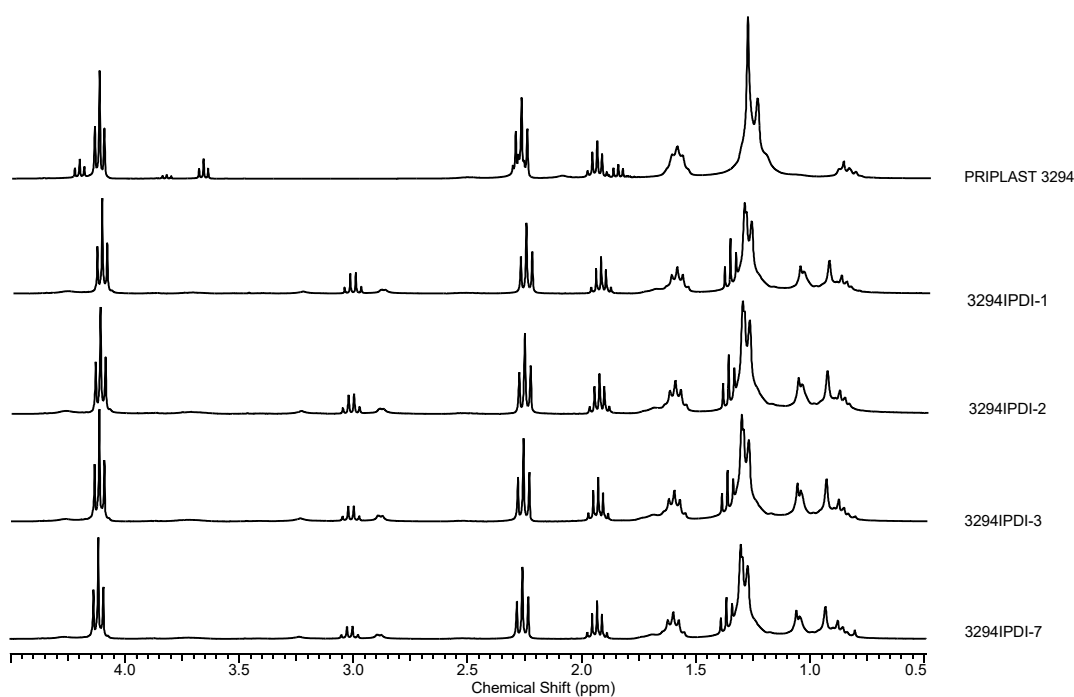
Figure S1. ¹H NMR spectra of starting polyol Priplast 3294 and all the synthesized WPUD.
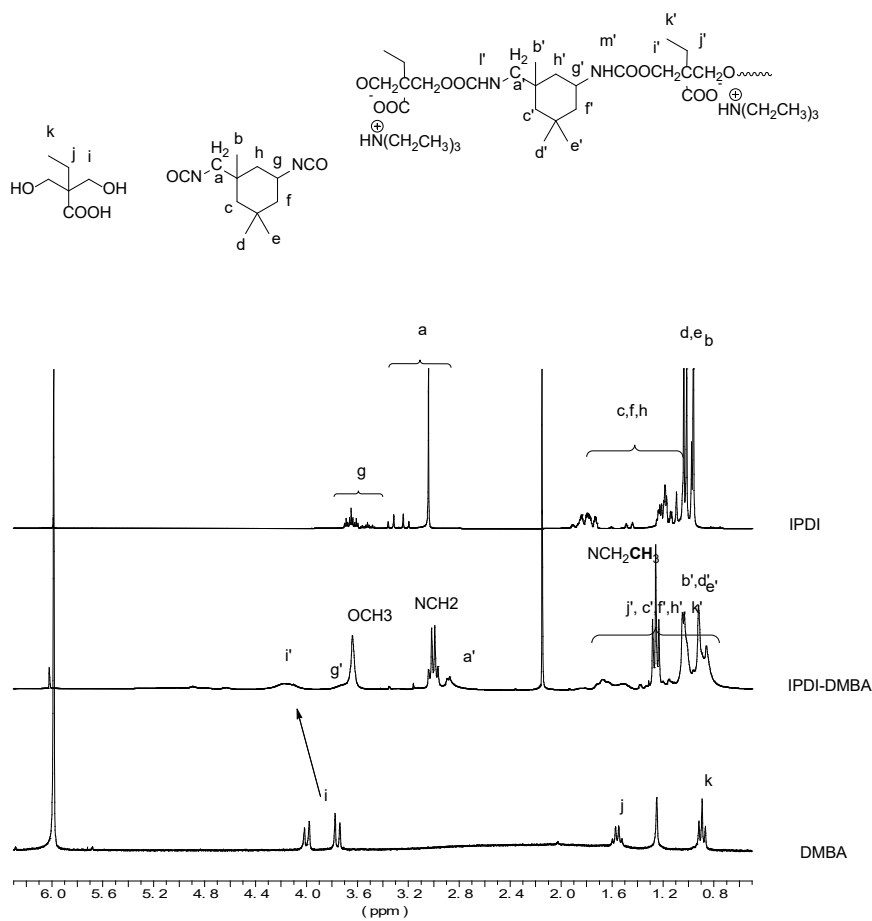
Figure S2. ¹H NMR spectra of model compound IPDI:DMBA (molar ratio 2:1).
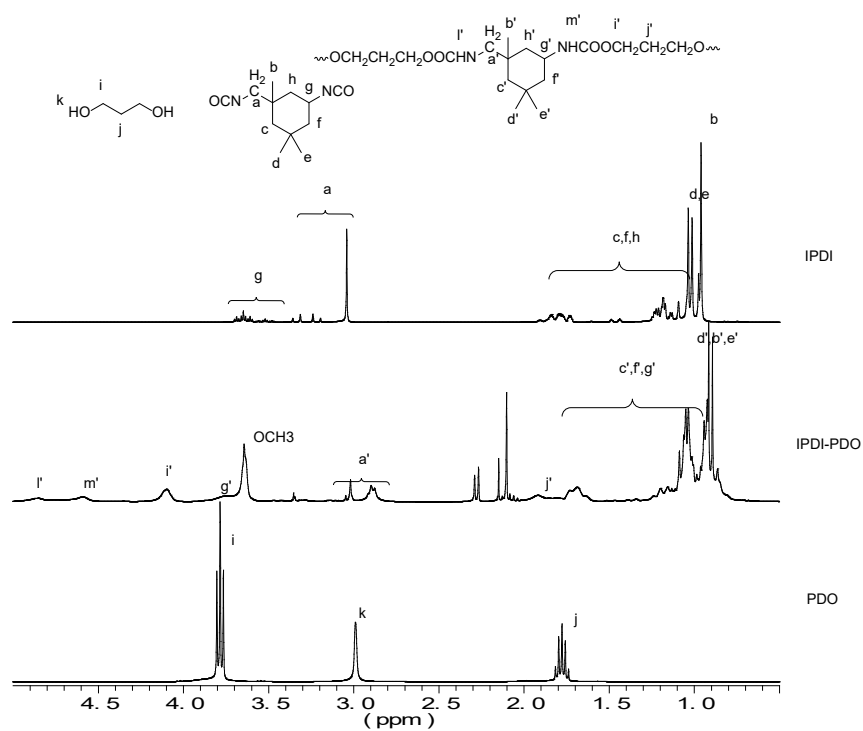
Figure S3. ¹H NMR spectra of model compound IPDI:PDO (molar ratio 2:1).
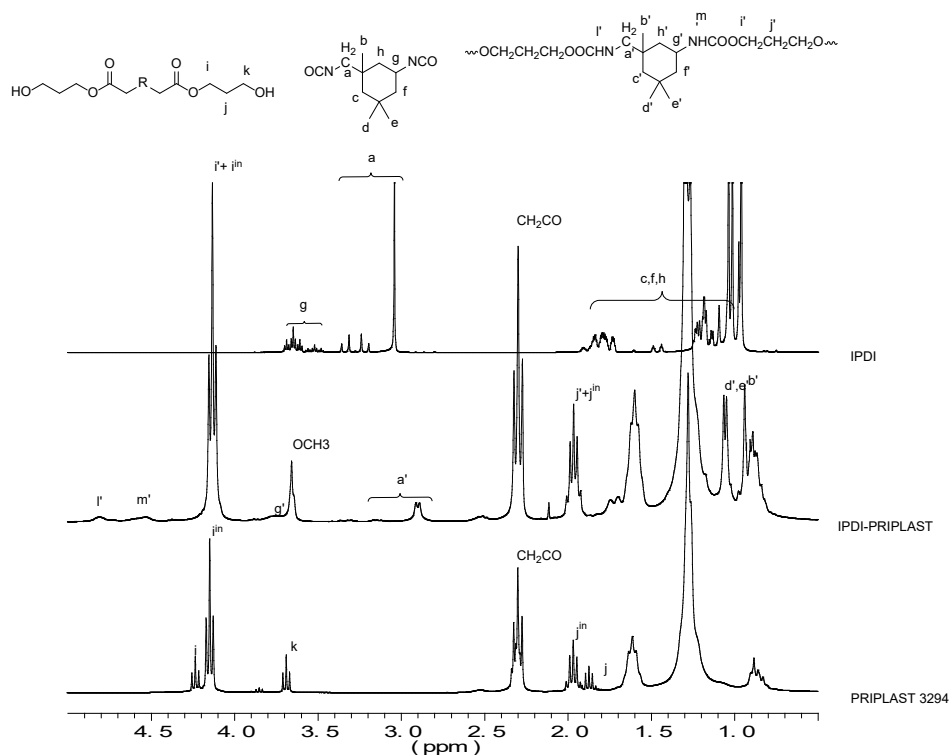
Figure S4. ^1H NMR spectra of model compound IPDI:Priplast 3294 (molar ratio 2:1).
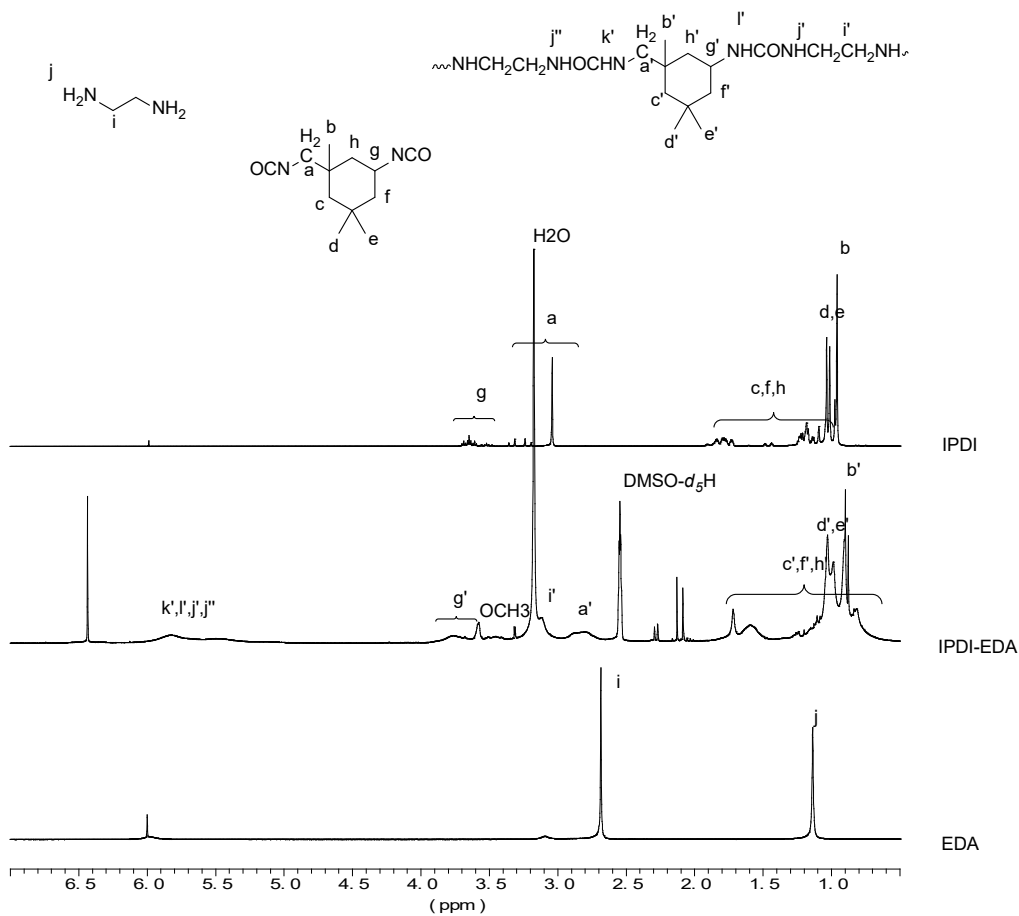
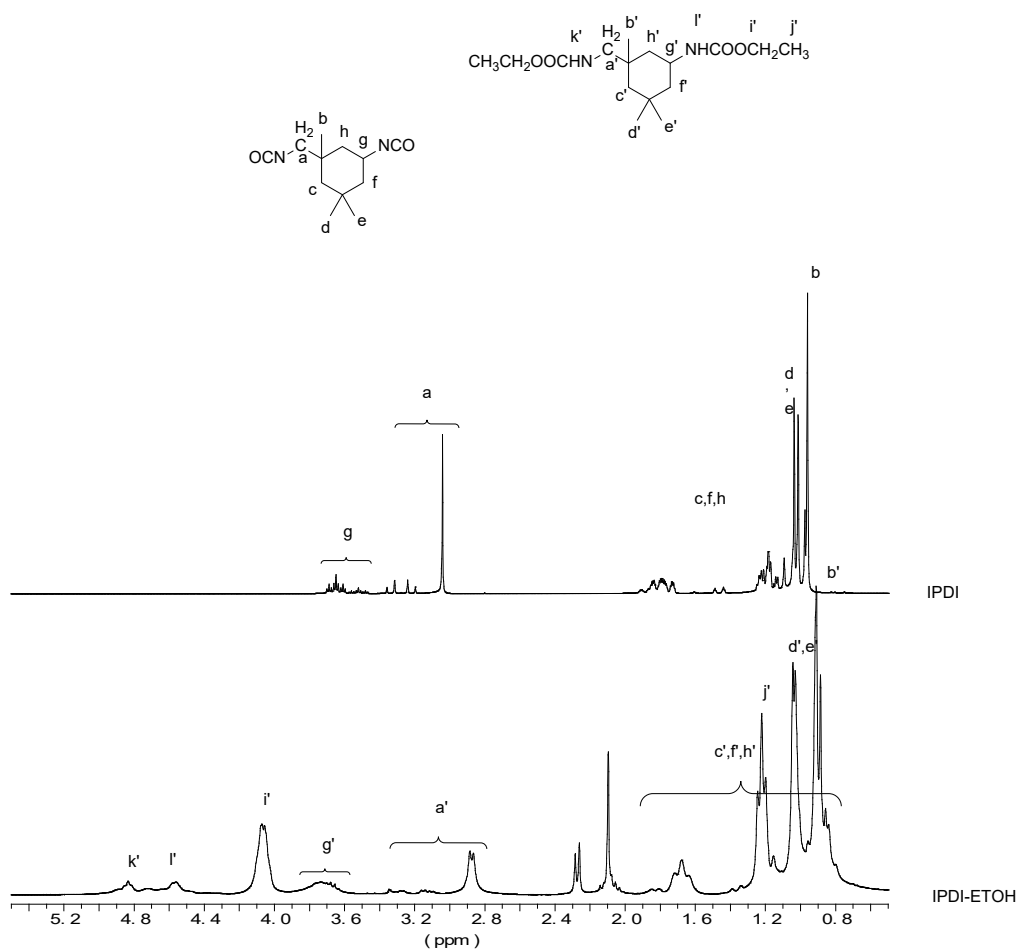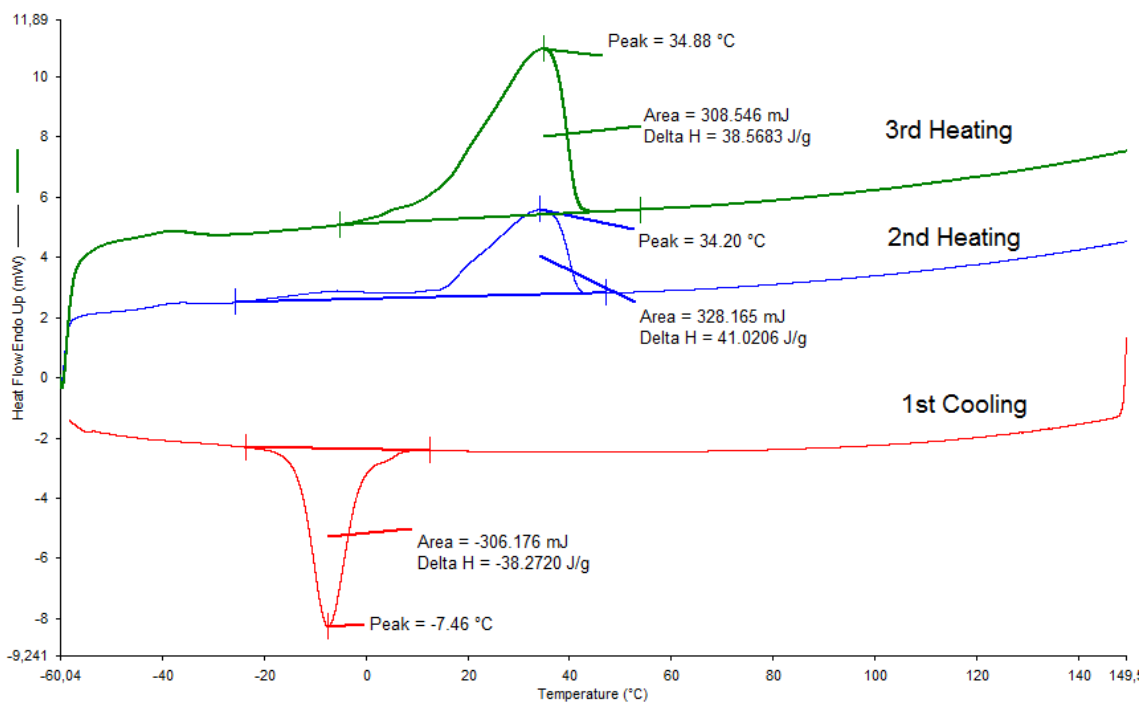Figure S5. ^1H NMR spectra of model compound IPDI:EDA (molar ratio 2:1).

S4

Figure S6. ¹H NMR spectra of model compound IPDI:EtOH (molar ratio 1:3).

2 DSC

Figure S7. DSC of Priplast 3294 were T_m, ΔH_m and T_c, ΔH_c have been determined during second heating and cooling, respectively.

3 TGA
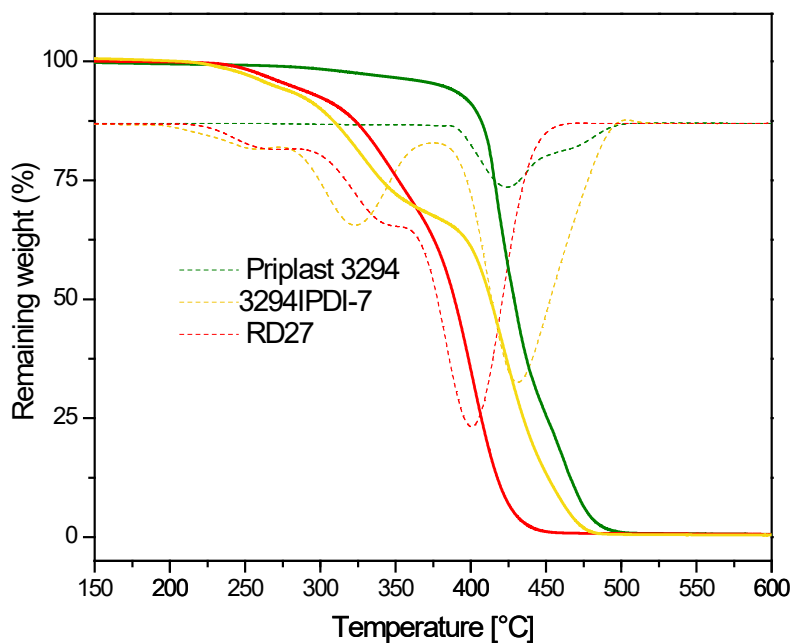
Figure S8. TGA curves of starting polyol Priplast 3294, commercial non-biobased polyurethane RD27 (polyether polyurethane) and WPUD 3294IPDI-7. Mass losses (thick lines) and derivative curves (dashed lines).

4 MECHANICAL PROPERTIES
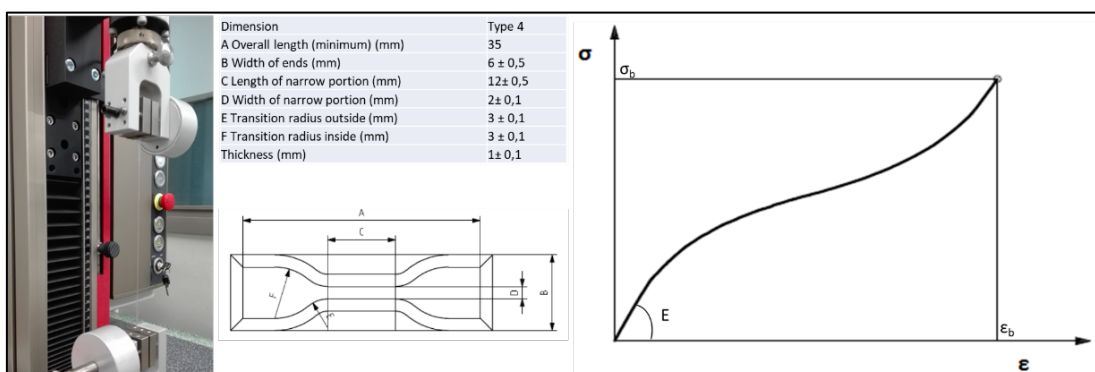
Figure S9. Left, equipment used to perform stress-strain measurements. Center, dimensions of the dumbbell type 4 specimens used in this test. Right, generic stress-strain graph with characteristic parameters (elastic modulus, stress at break, strain at break).

5 PSD
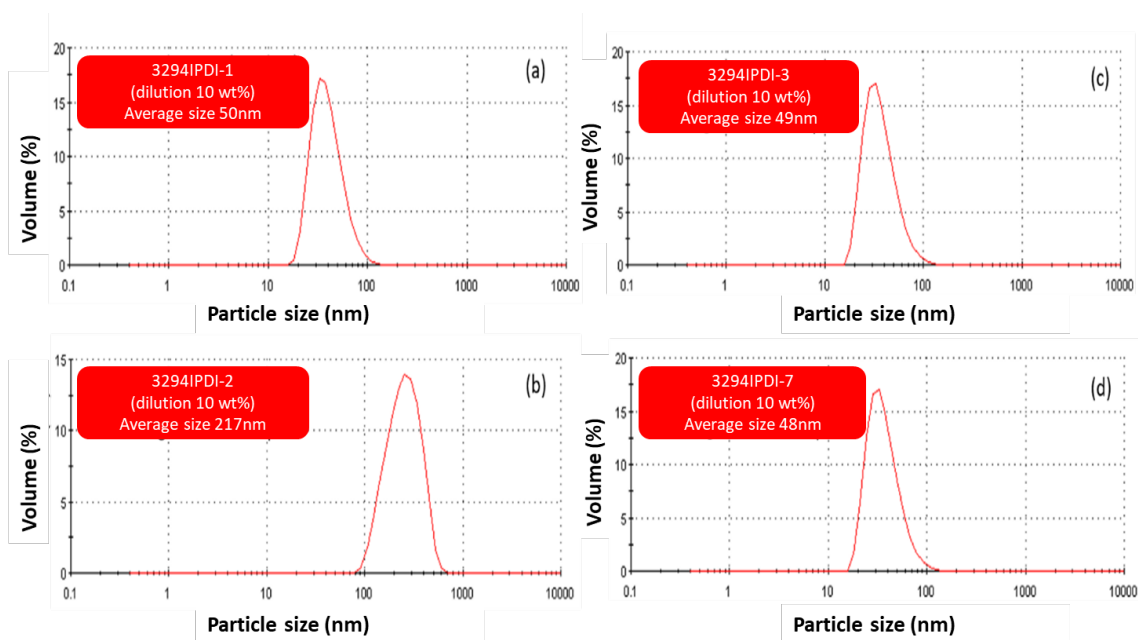
Figure S10. Particle size distribution measured by DLS.
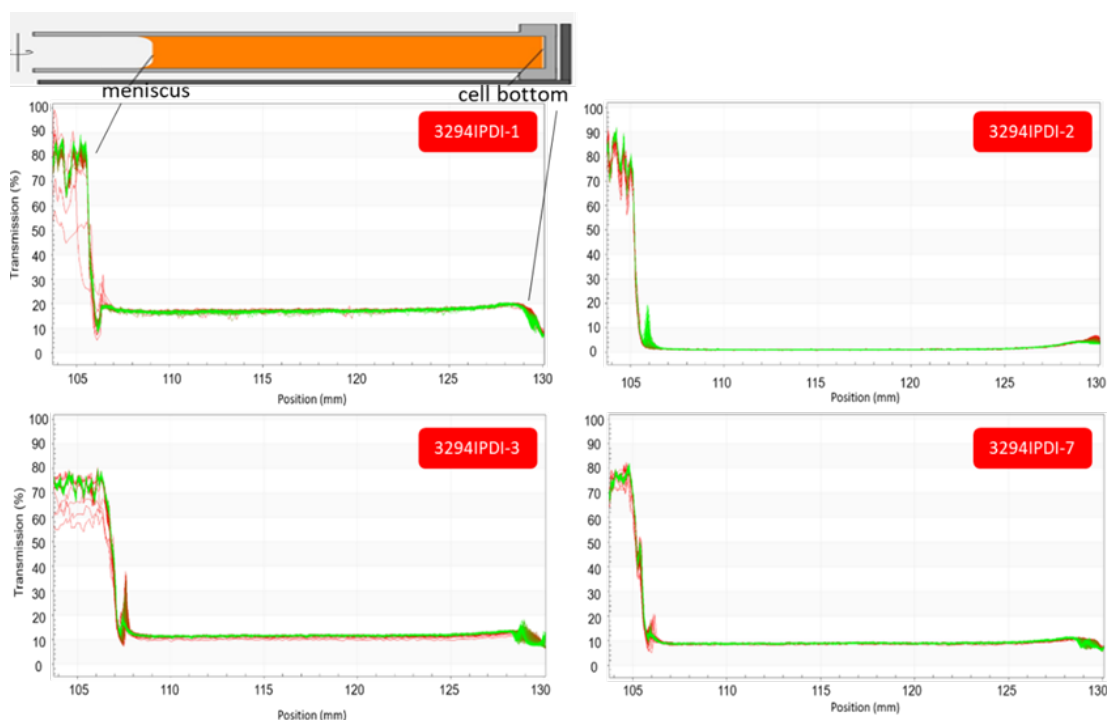
6 ANALYTICAL CENTRIFUGUE

Figure S11. Transmission profiles of the synthesized WPUD dispersions subjected to 2000 g and 40 ℃ centrifuge tests using a path length of 10 mm.
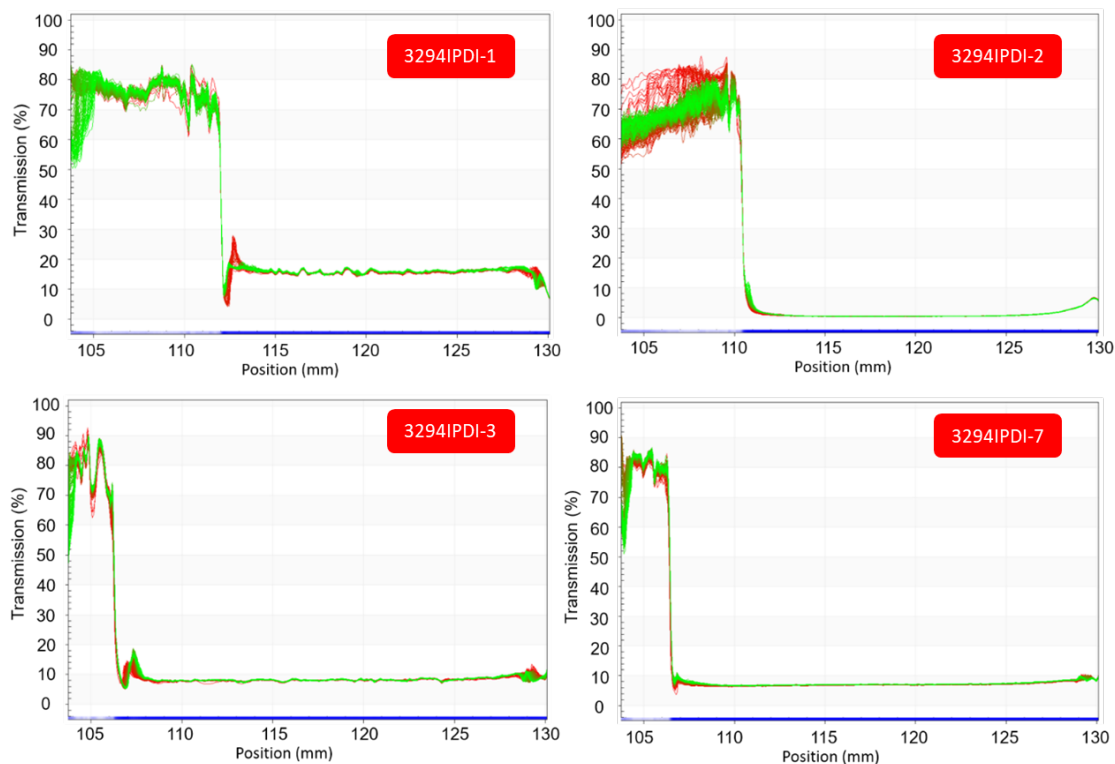

Figure S12. Transmission profiles of the synthesized WPUD dispersions subjected to 2000 g and 4 ℃ centrifuge test using a path length of 10 mm.

Supplementary Material: Biobased Waterborne Polyurethane-ureas Modified with POSS-OH for Fluorine-free Hydrophobic Textile Coatings

Amado Lacruz, Mireia Salvador, Miren Blanco, Karmele Vidal, Amaia M. Goitandia, Lenka Martinková, Martin Kyselka, and Antxon Martínez de Ilarduya
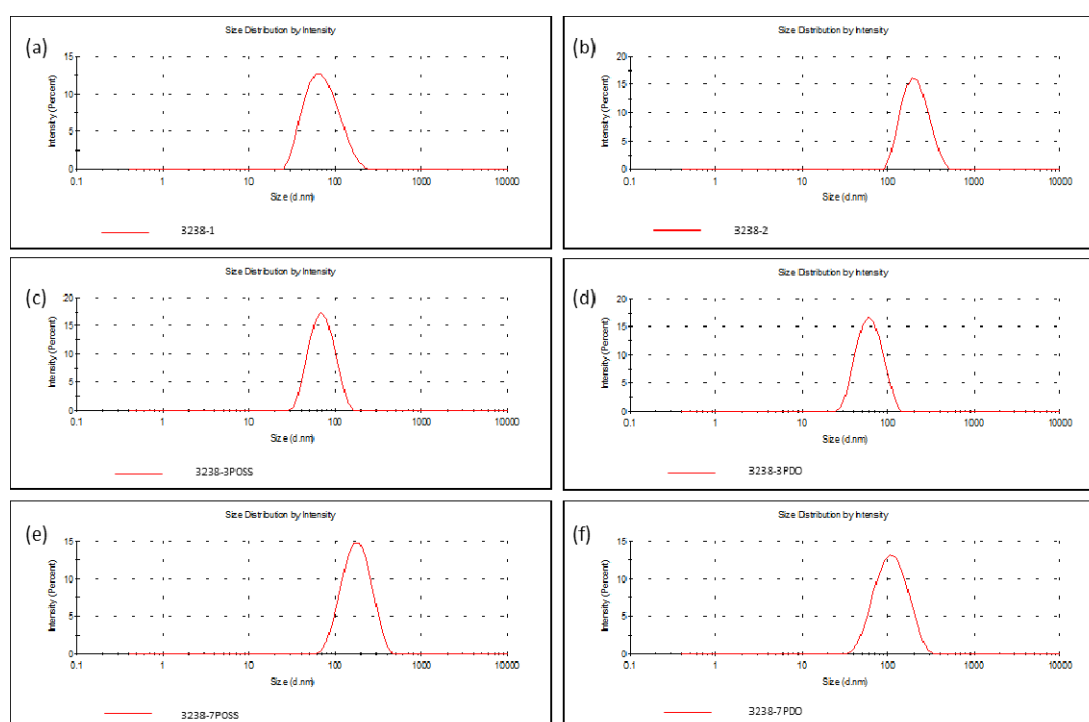
1. Particle size distribution of WPUD

Figure S1. Particle size distribution of WPUD measured by DLS, (**a**) 3238-1, (**b**) 3238-2, (**c**) 3238-3POSS, (**d**) 3238-3PDO, (**e**) 3238-7POSS, (**f**) 3238-7PDO.
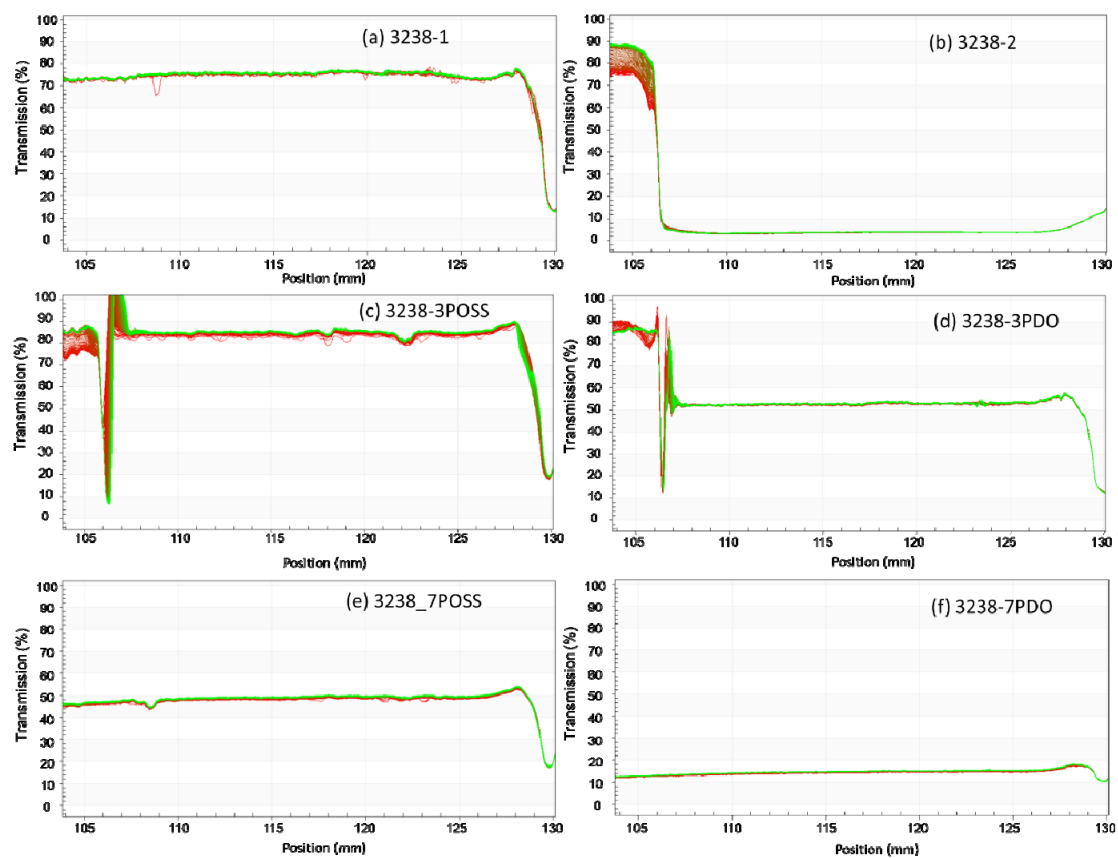
2. LUM measurements of WPUD

Figure S2. LUM transmission profiles of WPUD measured at 470 nm, 4 °C, Relative acceleration force (RCA) 2000 x g (3900 R.P.M.). (**a**) 3238-1, (**b**) 3238-2, (**c**) 3238-3POSS, (**d**) 3238-3PDO, (**e**) 3238-7POSS, (**f**) 3238-7PDO.
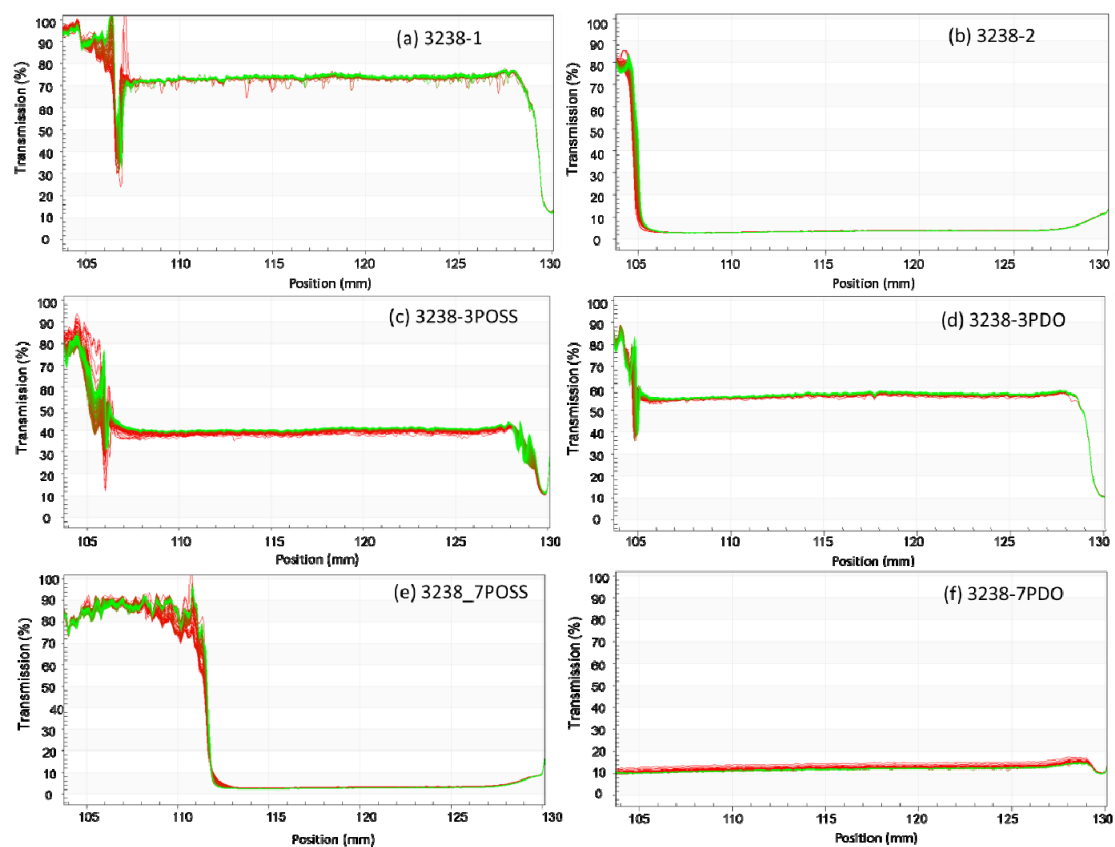
Figure S3. LUM transmission profiles of WPUD measured at 470 nm, 40 °C, Relative acceleration force (RCA) 2000 x g (3900 R.P.M.). (**a**) 3238-1, (**b**) 3238-2, (**c**) 3238-3POSS, (**d**) 3238-3PDO, (**e**) 3238-7POSS, (**f**) 3238-7PDO.